Max Nein / PS02
SA08 - 33893 FR 1

(NASA-CR-170758) FEASIBILITY STUDY OF AN OPTICALLY COHERENT TELESCOPE ARRAY IN SPACE Final Report, 19 May 1980 - 31 Dec. 1982 (Smithsonian Astrophysical Observatory) 236 p HC A11/MF A01 CSCL 20F G3/74

N83-25545

Unclas
11760

FEASIBILITY STUDY OF AN OPTICALLY COHERENT TELESCOPE ARRAY IN SPACE

CONTRACT NAS8-33893

Final Report
and
Technical Report No. 2
For the period 19 May 1980 to 31 December 1982

Dr. Wesley A. Traub
Principal Investigator

February 1983

Prepared for
National Aeronautics and Space Administration
Marshall Space Flight Center
Alabama 35812

Smithsonian Institution
Astrophysical Observatory
Cambridge, Massachusetts 02138

The Smithsonian Astrophysical Observatory
and the Harvard College Observatory
are members of the
Center for Astrophysics

The NASA Technical Officer for this contract is Mr. Max Nein, Deputy Director, Advanced Systems Office, Marshall Space Flight Center, Alabama 35812.

FEASIBILITY STUDY OF AN OPTICALLY COHERENT TELESCOPE ARRAY IN SPACE

CONTRACT NAS8-33893

Final Report

and

Technical Report No. 2

For the period 19 May 1980 to 31 December 1982

Principal Investigator
Dr. Wesley A. Traub
Smithsonian Astrophysical Observatory
60 Garden Street
Cambridge, MA 02138
(617) 495-7406; (FTS: 830-7406)

Associate Director for
Optical and Infrared Astronomy
Dr. David W. Latham

Coinvestigators
Dr. Nathaniel P. Carleton, SAO
(617) 495-7405 (FTS: 830-7405)

Dr. Giuseppe Colombo, SAO
(617) 495-7261

Dr. Herbert Gursky
Space Science Division
Naval Research Laboratory
Code 4100
Washington, DC 20375

Smithsonian Institution
Astrophysical Observatory
Cambridge, Massachusetts 02138

Director: Dr. Irwin I. Shapiro   Deputy Director: Mr. John G. Gregory

The Smithsonian Astrophysical Observatory
and the Harvard College Observatory
are members of the
Center for Astrophysics

ORIGINAL PAGE IS
OF POOR QUALITY

TABLE OF CONTENTS

1. Introduction

This report summarizes the second stage of work done at the Smithsonian Astrophysical Observatory on a feasibility study of a coherent optical system of modular imaging collectors, or COSMIC. This report is also submitted as the Final Report. Considerable progress was made since the submission of Technical Report #1 in November 1981. We believe that the work done to date will form a solid base on which to build for subsequent progress.

The 3 publications that appeared during this period are reprinted in sections A, B, and C. Supportive details as well as developments on a number of as-yet unpublished topics are included directly as 7 internal working papers. One of these, the notes by W. F. Davis, is a continuation of the series which appeared in the preceding Technical Report No. 1. These latter notes contain suggestions for a number of image reconstruction techniques which should be tested in future programs.

Coherent optical system of modular imaging collectors (COSMIC) telescope array: astronomical goals and preliminary image reconstruction results

Wesley A. Traub, Warren F. Davis
Harvard-Smithsonian Center for Astrophysics
60 Garden Street, Cambridge, Massachusetts 02138

Abstract

We are developing numerical methods of image reconstruction which can be used to produce very high angular resolution images at optical wavelengths of astronomical objects from an orbiting array of telescopes. The engineering design concept for COSMIC (coherent optical system of modular imaging collectors) is currently being developed at Marshall S.F.C., and includes four to six telescope modules arranged in a linear array. Each telescope has a 1.8 meter aperture, and the total length of the array is about 14 meters. This configuration, when controlled to fractional wavelength tolerances, will yield a diffraction pattern with an elongated central lobe about 4 milli-arc-sec wide and 34 milli-arc-sec long, at a wavelength of 0.3 microns, and correspondingly larger at longer wavelengths. The goal of image reconstruction is to combine many images taken at various aspect angles in such a way as to reconstruct the field of view with 4 milli-arc-sec angular resolution in all directions. We are developing a Fourier transform method for extracting from each individual image the maximum amount of information, and then combining these results in an appropriately weighted fashion to yield an optimum estimate of the original scene. The mathematical model is discussed, and the results of preliminary numerical simulations of data are presented.

Introduction

We have recently developed a method of image reconstruction which makes efficient use of the individual images received by an orbiting linear array of telescopes, and allows the reconstruction of a conventional image of the scene which is equivalent to that which would be recorded by a large circular aperture of diameter equal to the longest dimension of the linear array. Our previous papers[1,2,3] on the concept of a coherent, linear array of telescopes in space alluded to the likelihood that such a reconstruction scheme should be possible, but at that time we were not able to suggest an appropriate procedure. Now, however, we are able to present: first, an optimized algorithm for image combination; second, a suggestion of the direction in which we are currently moving to develop an optimum noise filtering technique; and third, a series of numerical examples of image reconstruction using hueristic noise filters which demonstrate the effects of noise and optical imperfections, and also demonstrate the initial coherent alignment procedure.

Astronomical goals

The preceding paper in this volume[4] discusses a first-stage COSMIC with an effective length of about 14 m, and a second-stage of about 35 m, corresponding to angular resolution limits at 0.3 micron of about 4 and 1.6 milli-arc-sec, respectively. This unprecedented capability means that we will be exploring a new domain, so our scientific expectations must necessarily be relatively general and open-ended. However, by analogy with the spectacular results from the VLA and VLBI radio instruments as well as the x-ray images from Einstein, we should anticipate a dramatic increase in our ability to understand the visible universe. COSMIC in fact should have an angular resolution in the optical region which will match VLA and VLBI images.

A sampling of projects which have recommended themselves on the basis of a simple extrapolation from present knowledge includes the following: investigate the nature of the diffuse emission seen around certain quasars, to see if it represents an underlying galaxy, and if so, what type; probe the structure of the region surrounding the nuclei of Seyfert galaxies, down to the equivalent of about a light-year in size, i.e. the scale on which broad-line spectral variations are seen; study the nuclei of ordinary galaxies with suspected massive black hole centers to see if the gravitational potential is truly point-like; make detailed comparisons of the several images produced by a gravitational lens, to probe more fully the gravity field of the lens; examine the as-yet unresolvable central regions of globular clusters for evidence of mass distributions indicative of either black holes or simply self-gravitation; image the actual motion and excitation of material around a recent nova; measure diameters, limb and polar darkening, and spots of nearby stars; directly image reflected light from circumstellar shells or discs; image stellar surfaces in very narrow spectral bands, as is done for hydrogen or calcium on the sun; directly image nearby asteroids to measure rotation and search for

ORIGINAL PAGE IS
OF POOR QUALITY

companions; resolve cometary nuclei and follow the evolution of the coma and jet-like activity; search for Jupiter-like planets around nearby stars by detecting position variations using localized astrometric techniques.

Telescope concept

The basic idea of the rotating linear array is indicated schematically in Figure 1 where we see a plan view of 7 telescope primaries with a beam-combiner telescope (BCT) at one end. To fit into the Shuttle bay, the length of the collecting area is limited to about 14 m. Although it is, of course, extremely desirable to have available all 7 mirrors, in principle one can still achieve the same resolution if a minimum redundency array is used, i.e., only mirrors 1, 2, 5, and 7; the discussion in this paper is applicable in either case. As the array rotates about the line of sight, it sweeps out an area of diameter D_1, as shown. We will show in the following sections that the final image, which can be reconstructed while the array is rotating through 180° and simultaneously recording instantaneous images, is equivalent in angular resolution to that obtained with a single large mirror D_1. The power of the array is further increased by adding a second colinear stage, and possibly two perpendicular stages, as indicated by the dotted elements and the final equivalent diameter D_2.

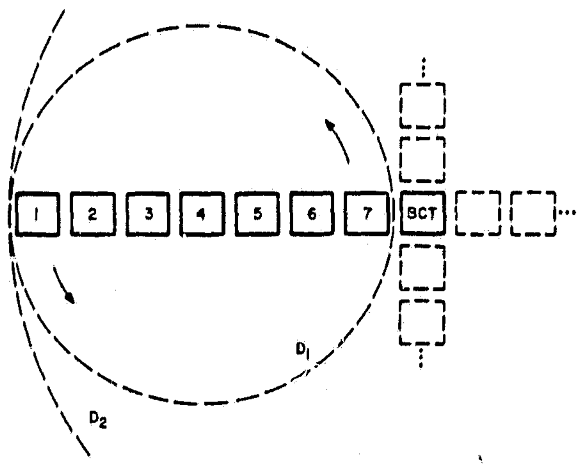

Figure 1. Linear array of 7 telescopes, plus beam combiner telescope.

Motivation

The image produced by a linear coherent array will exhibit non-uniform resolution as a function of direction in the image plane. Specifically, the diffraction-limited resolution in the direction colinear with the array will exceed that normal to the array in the same ratio as the aperture aspect ratio L/W. If the array width is decreased to zero, resolution in the normal direction will also become zero (normal diffraction limit becomes infinite).

The situation is analogous to the CAT scan in medical imaging in which the ability to resolve along the beam path is zero. In the latter technique views are taken from a number of directions around the subject and the results combined in such a way that the favorable resolution capability across the beam path is exhibited in all directions in the final image. This suggests that a similar technique might be possible in the case of the linear coherent array. The array would be rotated slowly about the optical axis and the intermediate images combined in such a way that the more favorable colinear resolution would obtain in all directions in the image plane.

In fact such a technique is possible as we will show. An important distinction is that, due to the finite array or aperture width, the normal resolution of the coherent array is not zero as it is along the CAT beam path. Consequently, the appropriate reconstruction algorithm differs somewhat from the CAT but, not surprisingly, goes over to the CAT algorithm in the limit as the aperture width goes to zero. This will be demonstrated. The image reconstruction algorithm appropriate to the rotating linear coherent array is, then, a generalization of the CAT algorithm familiar from medical applications[6]. As is the case in CAT analysis, Fourier techniques yield an exact reconstruction algorithm and provide a deep insight into the nature of the process. Fourier techniques are used in the derivation which follows.

Concepts

The starting point of the derivation of the reconstruction algorithm is the integral representation of the effect of the telescope aperture on the incident wave field. See Figure 2.

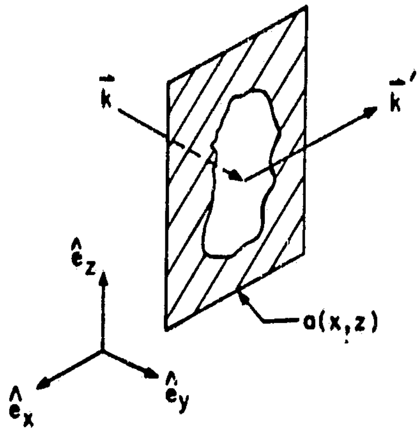

Figure 2. Diffraction by an aperture a(x,z).

$\vec{k}$ and $\vec{k}'$ are the incident and outgoing wave vectors.

$$\vec{k} = k_x\hat{e}_x + k_y\hat{e}_y + k_z\hat{e}_z \tag{1}$$

$$k = |\vec{k}| = \omega/c = 2\pi/\lambda$$

The aperture a(x,z) which is, in general, a complex function is assumed to lie in the x,z-plane. To simplify the notation, vectors confined to the x,z-plane will be denoted by a subscript zero. Thus, for example,

$$a(x,z) \equiv a(\vec{r}_0) \tag{2}$$

$$\vec{r}_0 \equiv x\hat{e}_x + z\hat{e}_z$$

We assume that $u(\vec{k})$ represents the amplitude of the incoming E-field as a function of direction. By formally representing the outgoing field as a superposition of plane waves (Fraunhofer diffraction), we are led to the result that[5]

$$I(\vec{k}') = \int_{-\infty}^{+\infty}\int_{-\infty}^{+\infty} dk_x dk_z \; |u(\vec{k})|^2 \; |A[(k_x'-k_x),(k_z'-k_z)]|^2 \tag{3}$$

where $I(\vec{k}')$ is the time-averaged intensity of the outgoing component in the $\vec{k}'$ direction, and $A(\vec{k})$ is the Fourier transform of the aperture defined by

$$A(\vec{k}) = \frac{1}{(2\pi)^2}\int_{-\infty}^{+\infty} d^2\vec{r}_0 \; a(\vec{r}_0) \; e^{-i\vec{k}\cdot\vec{r}_0} \tag{4}$$

ORIGINAL PAGE IS
OF POOR QUALITY

In words, (3) says that the outgoing intensity distribution is given by the convolution of the squared magnitude of the Fourier transform of the aperture with the incoming intensity function.

Consider now the Fourier transform of the intensity $I(\vec{k})$.

$$\mathcal{I}(\vec{\nu}) = \int_{-\infty}^{+\infty}\int_{-\infty}^{+\infty} dk_x dk_z \; I(\vec{k}) \; e^{-2\pi i\vec{k}\cdot\vec{\nu}}$$

$$\vec{\nu} = \nu_x\hat{e}_x + \nu_z\hat{e}_z \qquad (5)$$

We find from evaluation of (5) using (3) that

$$\mathcal{I}(\vec{\nu}) = U(\vec{\nu})\mathcal{A}(\vec{\nu}) \qquad (6)$$

where

$$U(\vec{\nu}) = \int_{-\infty}^{+\infty}\int_{-\infty}^{+\infty} dk_x dk_z \; |u(\vec{k})|^2 \; e^{-2\pi i\vec{k}\cdot\vec{\nu}} \qquad (7)$$

$$\mathcal{A}(\vec{\nu}) = \int_{-\infty}^{+\infty}\int_{-\infty}^{+\infty} dk_x dk_z \; |A(\vec{k})|^2 \; e^{-2\pi i\vec{k}\cdot\vec{\nu}} \qquad (8)$$

Result (6) is just the familiar Borel convolution theorem applied to (3). $U(\vec{\nu})$ given by (7) is the Fourier transform of the incoming intensity function. $\mathcal{A}(\vec{\nu})$ given by (8) can be related to the aperture function by substituting (4) into (8) and evaluating to get

$$\mathcal{A}(\vec{\nu}) = \int_{-\infty}^{+\infty} d^2\vec{r}_0 \; a(2\pi\vec{r}_0) \; a^*[2\pi(\vec{r}_0+\vec{\nu})] =$$

$$= \int_{-\infty}^{+\infty} d^2\vec{r}_0 \; a^*(2\pi\vec{r}_0) \; a[2\pi(\vec{r}_0-\vec{\nu})] \qquad (9)$$

Result (9) is the generalized autocorrelation of the aperture function and represents a second application of Borel's convolution theorem to the product $A(\vec{k})A^*(\vec{k})$.

The results derived so far state that the Fourier transform of the image intensity is equal to the product of the Fourier transform of the incoming, unmodified intensity distribution and the generalized aperture autocorrelation function in suitable coordinates.

It is useful to think of the aperture autocorrelation as providing a "window" onto the true (unmodified by the instrument aperture) image Fourier plane. As the aperture rotates, so does the aperture autocorrelation. At each orientation only a portion of the Fourier plane can be "seen" through the window. By piecing together glimpses of the Fourier plane provided by a set of distinct aperture orientations, a measure of $U(\vec{\nu})$ can be built up over a region corresponding to the union of the areas covered by the individual autocorrelations. From (9) it is seen that

$$\mathcal{A}(-\vec{\nu}) = \mathcal{A}^*(\vec{\nu}) \qquad (10)$$

so that after one-half revolution of the aperture it is possible to map out a circular region of the $\vec{\nu}$-plane whose radius $L/2\pi$ is given by the largest value of $|\vec{\nu}|$ for which $\mathcal{A}(\vec{\nu})$ is non-zero. Depending on the geometry, there may be annular regions within this radius which can not be mapped because $\mathcal{A}(\vec{\nu}) = 0$ there.

Such a circular region corresponds to the autocorrelation of a circular aperture of diameter L. In this way we see the possibility of synthesizing from the rotating linear aperture of length L an image equivalent in resolution to that obtainable from a full circular aperture of diameter L. In particular, the resolution in all directions in the synthesized image plane will be equivalent to that attainable from the greatest dimension across the aperture, L.

ORIGINAL PAGE IS
OF POOR QUALITY

Relationship to CAT algorithm

Imagine now that the aperture width W is reduced to zero. In this case the aperture autocorrelation too reduces to a line of width zero, and length L/π. The corresponding image resolution normal to the array also goes to zero. For each angular orientation of the aperture, the autocorrelation "window" permits determination of the image Fourier transform only along a line through the origin of $\vec{\nu}$-space at the orientation angle.

This process matches precisely the Fourier description of the computer-assisted tomography (CAT) algorithm in which the one-dimensional Fourier transforms of the individual ray projection functions are mapped onto $\vec{\nu}$-space at angles equal to the projection angles.[6] The inverse transform yields the reconstructed image. Just as the instantaneous image resolution of the telescope is zero normal to the aperture, so too is the resolution of the CAT scanner along the beam and, hence, normal to the projection. Thus our present algorithm contains the CAT algorithm as a special case.

Image combination

Each orientation of the aperture "exposes" part of $U(\vec{\nu})$ in the Fourier domain, weighted by the aperture autocorrelation according to (6). A given point in the $\vec{\nu}$-plane may be exposed, with a different weight, by each of several aperture orientations. The question is how to combine optimally the information about the value of $U(\vec{\nu})$ implicit in each exposure. In particular, a real instrument will produce images contaminated by noise so that the true value of $U(\vec{\nu})$ can only be estimated.

Let us assume that a set of images, N in number, has been formed corresponding to various aperture orientations. We use a subscript to denote a specific member of the set. Let us also assume that signal-independent noise has been added to the spatial domain images. Because of the linearity of the transform, the noise will be additive also in the Fourier domain. Thus, we write for the measured signal at a specific point $\vec{\nu}$ in the n-th image transform,

$$y_n = U\mathcal{A}_n + \epsilon_n \tag{11}$$

where ϵ_n represents the noise. Explicit reference to $\vec{\nu}$ has been dropped to ease the notation.

Let us assume that the ϵ_n are statistically independent, have zero mean, and variance $\sigma_{\epsilon n}^2$

$$E\{\epsilon_n\} = avg(\epsilon_n) = 0 \tag{12a}$$

$$E\{\epsilon_n\epsilon_m^*\} = 0 \qquad (n\neq m) \tag{12b}$$

$$= var(\epsilon_n) \equiv \sigma_{\epsilon n}^2 \qquad (n=m) \tag{12c}$$

In this formulation the variance of the noise at a given $\vec{\nu}$ is a function of the image member index. This might be the case, for example, if unequal times are spent observing at the various aperture orientations. To estimate U let us form a weighted sum of the measurements y_n over the set of images.

$$\sum_{n=1}^{N} g_n y_n = U\sum_{n=1}^{N} g_n\mathcal{A}_n + \sum_{n=1}^{N} g_n\epsilon_n \tag{13}$$

where g_n are weights to be determined. The estimated value of U is, from (13),

$$\hat{U} = \sum_{n=1}^{N} g_n y_n \Big/ \sum_{n=1}^{N} g_n\mathcal{A}_n = U + \sum_{n=1}^{N} g_n\epsilon_n \Big/ \sum_{n=1}^{N} g_n\mathcal{A}_n \tag{14}$$

where $\hat{U}$ is defined only where $\mathcal{A}(\vec{\nu}) \neq 0$. If the noise goes to zero, the estimate $\hat{U}$ goes over to the true value U.

ORIGINAL PAGE IS
OF POOR QUALITY

The proper value for the weights g_n is found by demanding that the variance of $\hat{U} - U$ be minimum.

$$E\{|\hat{U}-U|^2\} = minimum \tag{15}$$

A straightforward calculation leads to the conclusion that

$$g_n = \mathcal{A}_n^* / \sigma_{\epsilon n}^2 \tag{16}$$

so that

$$\hat{U} = \sum_{n=1}^{N}\left[\frac{\mathcal{A}_n^* y_n}{\sigma_{\epsilon n}^2}\right] / \sum_{n=1}^{N}\left[\frac{|\mathcal{A}_n|^2}{\sigma_{\epsilon n}^2}\right] = U + \sum_{n=1}^{N}\left[\frac{\mathcal{A}_n^* \epsilon_n}{\sigma_{\epsilon n}^2}\right] / \sum_{n=1}^{N}\left[\frac{|\mathcal{A}_n|^2}{\sigma_{\epsilon n}^2}\right] \tag{17}$$

It is easy to show that the variance of $\hat{U}$ about the true value U will be

$$\sigma_{\hat{U}}^2 = E\{|\hat{U}-U|^2\} = \left[\sum_{n=1}^{N}\frac{|\mathcal{A}_n|^2}{\sigma_{\epsilon n}^2}\right]^{-1} \tag{18}$$

The aperture autocorrelation $\mathcal{A}_n$ can be determined from the geometry or, using (6), from a test image with good signal-to-noise ratio whose transform $U(\vec{\nu})$ is known. Assuming white noise, the variance $\sigma_{\epsilon n}^2$ is probably best estimated by considering those parts of the n-th $\vec{\nu}$-plane which are not "exposed" by the autocorrelation window. There, in the absence of noise, the image transform should be zero. Any non-zero contribution can be assumed to be due to noise or other image contaminant. In this way, using (16), the weights which minimize the variance of the estimate of U (17) can be determined.

Equation (17) represents the optimum combination, in the sense of minimum variance of U, of information from the Fourier transforms of the individual images formed with the aperture at different orientations. Discounting the need to deal with the effects of noise, the desired spatial image is, by (7), the inverse Fourier transform of (17). Equation (18) shows that in general the variance of the estimate of U will not be constant over the $\vec{\nu}$-plane. In particular, the variance will increase in those regions in which the magnitude of the aperture autocorrelation decreases. Thus, the noise associated with the weighted combination of the individual image transforms will be non-stationary over $\vec{\nu}$.

Equation (14) expresses the estimate of U which is to be optimized in the weighted combination of images. Direct implementation of (14), or (17), in a practical image reconstruction application would suffer from the effective amplification of noise, attributable to the second term, in regions where the magnitude of the aperture autocorrelation is small. We have already described this effect in terms of the non-stationarity of the noise in the $\vec{\nu}$-plane. To recover satisfactory images in the presence of noise, a filtering operation, to be discussed in the next section, must generally follow the image-combining step. Image combination according to the criterion of least variance of $\hat{U}$ and the subsequent filtering operation are separate and distinct steps in the overall processing.

Noise filtering

A frequently applied method for dealing with noise is Wiener filtering[7,8]. In this technique the noisy function is filtered (weighted) by another function which is inversely proportional to the noise variance. To be effective it is important that regions in which most of the signal information is contained do not coincide with regions in which the noise variance is greatest. The noisy function is, thereby, attenuated most where the noise is greatest, and least where the signal is greatest.

In the case at hand the variance of the noise associated with the estimate of U may be greatest, due to the geometry of the aperture, in regions where U is also most significant. Intuitively, it is undesirable to apply a filtering function which simply attenuates (biases downward) the estimate of U in such regions. Rather, it would be preferable to adopt a strategy which utilizes information from adjacent areas where the noise variance is less, as well as averaging within the relatively noisy areas, to provide a filtered estimate of U which is everywhere unbiased.

We are currently investigating a technique, which may be described as weighted multiple regression, which yields such an unbiased filtered estimate. The results of this work will be presented elsewhere.

Resolution

The limiting resolution, in the absence of noise, inherent in the image combination scheme described above is twice that of an aperture of comparable dimensions according to the usual laws of passive optics. That is, without Fourier-domain processing. This is most easily seen by considering a one-dimensional example.

Assume that a point source is observed in the absence of noise. The magnitude of its Fourier transform $U(\vec{\nu})$ will be constant over $\vec{\nu}$. Let the aperture be unity over a span of length L, and zero elsewhere. The one-dimensional aperture autocorrelation will be a "tent" function centered on $\nu = 0$ which spans an interval L/π.

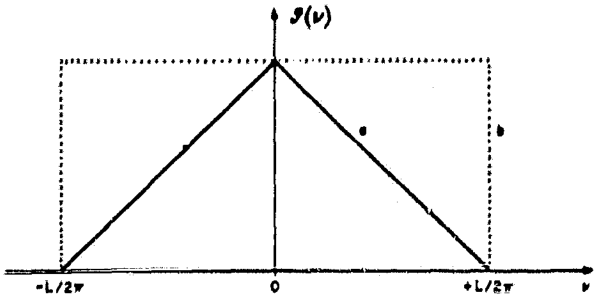

Figure 3. (a) Image transform $\mathcal{J}(\nu)$ for a point source. (b) Effective point-source image transform from eqn. (17) with no noise.

Since the transform of the source is a constant, the image transform (6) given by the product with the aperture autocorrelation will also have the form of a "tent" function in ν of width L/π. The inverse Fourier transform of this tent is, within a scale factor,

$$L\left[\frac{\sin(kL/2)}{kL/2}\right]^2$$

which has its first zeros at

$$k = \pm 2\pi/L \tag{19}$$

For small angles θ the normal component of $\vec{k}$ is $(2\pi/\lambda)\theta$ so that (19) is equivalent to

$$\theta = \pm\lambda/L \tag{20}$$

which is the result familiar from elementary optics.

Result (17), which divides-out the magnitude of the autocorrelation, recovers the underlying uniform source transform in the interval $-L/2\pi < \nu < +L/2\pi$. The inverse transform of the resulting pedestal of width L/π is, within a scale factor,

$$L\left[\frac{\sin(kL)}{kL}\right] \tag{21}$$

which has its first zeros at

$$k = \pm\pi/L \rightarrow \theta = \pm\lambda/2L \qquad (22)$$

Thus the resolution of the proposed image combination scheme is, in the absence of noise, twice that expected from elementary optics. In the presence of noise resolution will necessarily be degraded from this ideal because of the requirement to suppress noise amplification in regions where the aperture autocorrelation is small.

Sampling

The results derived so far have been in terms of integral representations. Digital implementation necessarily involves manipulation of sampled functions. The relevant expressions can be converted to discrete summations amenable to computer processing by introducing a series of Dirac delta functions under the integral signs.

$$\sum_{m=-\infty}^{\infty}\delta(x-mX) \leftrightarrow \frac{2\pi}{X}\sum_{n=-\infty}^{\infty}\delta[2\pi(\nu-n/X)] \qquad (23)$$

In relation (23), which is applicable to one dimension, $\leftrightarrow$ indicates that the two sides are Fourier transform pairs. x and ν represent the two domains; X, the sampling interval in the x-domain, is a constant to be determined. 1/X is the corresponding sampling interval in the ν-domain.

Sampling of the aperture at intervals X will, by (9), cause the aperture autocorrelation, and hence $\mathcal{J}(\vec{\nu})$, to be sampled at intervals $X/2\pi$ in $\vec{\nu}$. From the convolution theorem and (23) the corresponding image domain representation will be given by the convolution of the continuous reconstructed image with a series of Dirac delta functions at intervals $\vec{k} = 2\pi/X$. That is, the continuous image will be replicated at intervals $2\pi/X$ in $\vec{k}$.

Suppose that the field of view (FOV) is k_o. Suppose also that we demand that the point-source image response given by (21) be attenuated by a factor α at the point at which such a source at the lower (upper) FOV edge enters the upper (lower) FOV edge due to the sampling-induced image replication. That is, we require from (21) that the separation of the upper and lower edges of the FOV in the replicated images be

$$k \geq \alpha/L$$

Allowing also for the FOV k_o, the image domain periodicity must be at least $k_o + \alpha/L$. Therefore, the required aperture sampling interval is

$$X \leq \frac{2\pi}{k_0 + \alpha/L} = \frac{\lambda}{\theta_0 + \lambda\alpha/2\pi L} \qquad (24)$$

where θ_o is the FOV in radians.

The reconstruction simulations which follow employ discrete Fourier techniques (FFTs) with sampling intervals over the aperture based on the above considerations.

Numerical image reconstruction: examples

We imagine the detector (CCD or equivalent) to be fixed in inertial space, while the telescope array is rotated, so the center of each star image will not move with respect to the detector, but the diffraction pattern will rotate about each bright point source. To display the various stages in a calculation, we will first discuss what happens when a conventional circular telescope aperture is used to image a point source. In the following figures we will display the apertures, functions, or images as points on a 64 by 64 grid, with contour levels at either 5 or 9 equispaced intervals between the maximum and minimum values. Above each contour diagram there is a plot displaying a slice through the same data, from left to right; the slice is positioned to include the peak data point.

In Figure 4a we show a single large telescope mirror which is circular to within the discrete limits of our grid, and has unity transmission and no phase delay within this circle. The mirror diameter is 31 units. From eqn. (8) we find the autocorrelation of the aperture, $\mathcal{A}(\nu)$, as a function of spatial frequency ν across the detector, and display this in Figure 4b. The corresponding conventional, diffraction-limited image I(k) is obtained from the real part of the inverse transform of eqn. 5, and is shown in

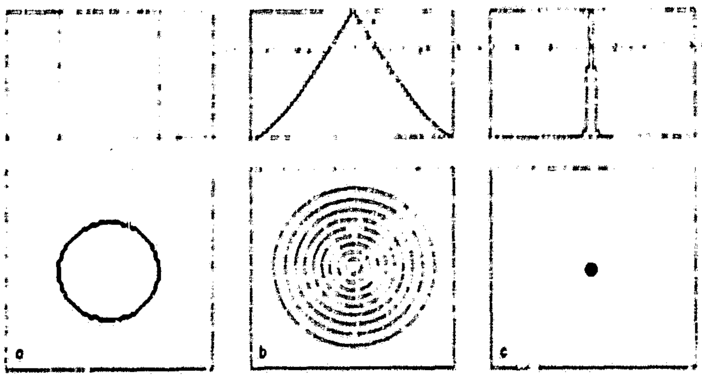

Figure 4. (a) Telescope aperture $a(x,z)$, diameter = 31 units. (b) Autocorrelation of aperture $\mathcal{A}(\vec{v})$. (c) Image of point source $I(\vec{k})$.

Figure 4c for the case of a single, point-like star centered in the FOV. For contrast, we show in Figure 5 the same sequence for a mirror with diameter 7 units; as expected, the smaller mirror samples fewer of the spatial high frequencies, and therefore produces a broader star image.

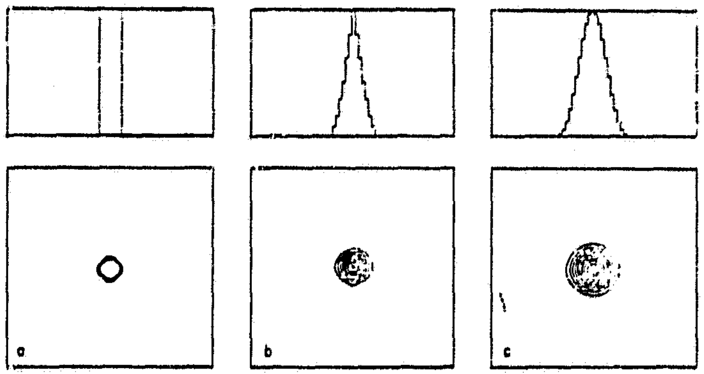

Figure 5. (a) Telescope aperture $a(x,z)$, diameter = 7 units. (b) Autocorrelation of aperture $\mathcal{A}(\vec{v})$. (c) Image point source $I(\vec{k})$.

The imaging properties of a coherent linear array of telescopes will now be sketched in a way that attempts to clarify the relationship between a circular aperture and a rotating linear aperture. This discussion also applies to rectangular single mirror segments, since it is the overall shape of the aperture, not the details of construction, that matters here. In Figure 6a we show an aperture which is 3 by 15 units; the autocorrelation of the aperture in Figure 6b extends to high frequencies in the direction parallel to the long axis of the aperture. Figure 6c shows the effect of this aperture on a star field which consists of 3 stars of equal intensity; 2 of the stars are completely unresolved with this viewing angle. In Figure 7 we show the case where the aperture has rotated by 45 degrees.

From eqn. (17) we see that an appropriately weighted sum over all angles of Fourier transforms of snapshot images will yield a reconstructed image. However, as was pointed out above, eqn. (17) also tends to produce highly amplified noise, and appropriate filtering must be applied to control this effect. We have done numerical experiments with various types of filters, and have found that, although we do not yet have in hand an optimally derived filter, it is relatively easy to generate filters which perform quite well. One such ad hoc filter we have tried is to multiply eqn. (17) by

$$\sum_{n=1}^{N} |\mathcal{A}_n|^2 \Big/ \sum_{n=1}^{N} \mathcal{A}_n \qquad (25)$$

or equivalently, simply to replace $|\mathcal{A}_n|^2$ in the denominator of (17) by $\mathcal{A}_n$; in all our cases we assume equal noise variance and equal exposure time at each angle snapshot, so the σ^2 terms drop out.

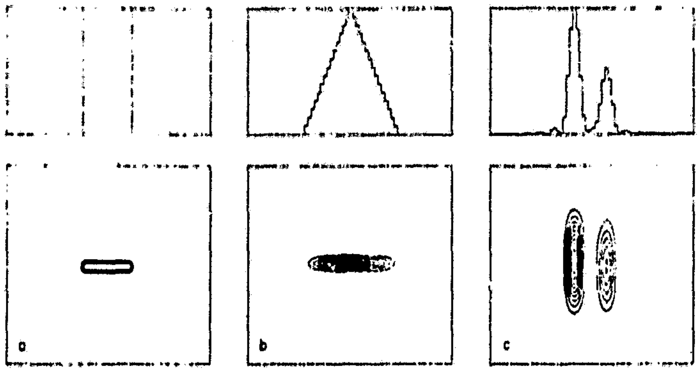

Figure 6. (a) Linear aperture at 0 degrees, 3 by 15 units. (b) Autocorrelation. (c) Snapshot image.

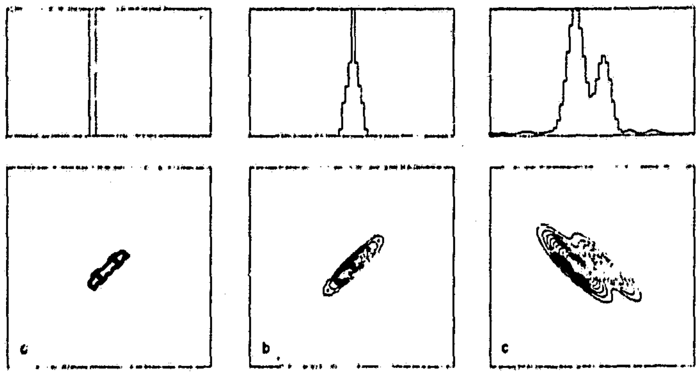

Figure 7. (a) Linear aperture at 45 degrees, 3 by 15 units. (b) Autocorrelation. (c) Snapshot image.

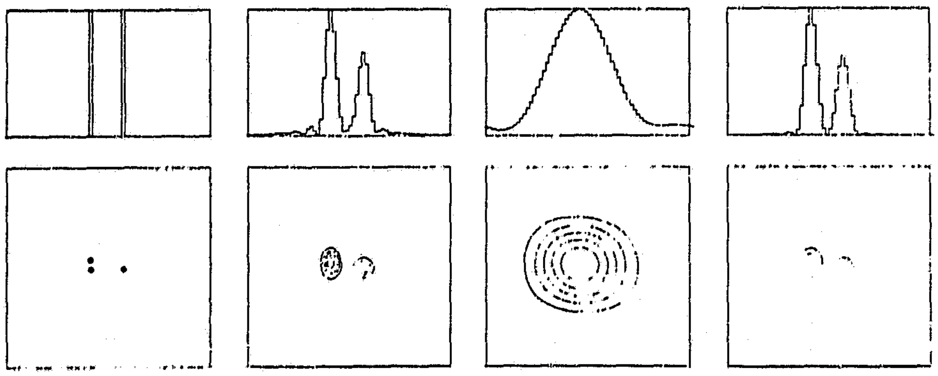

From left to right:
Figure 8. Three point-like stars.
Figure 9. Image reconstruction, using 16 angle views and a 3 by 15 telescope.
Figure 10. Snapshot image using a 3 by 3 telescope.
Figure 11. Snapshot image using a 15 unit circular aperture.

For reference we show in Figure 8 the input star field which was used to generate Figures 6c and 7c. Carrying out the reconstruction for 16 angle views between 0 and 180 degrees, in the noise-free case, we find the result shown in Figure 9; note the clean separation of the wide-spaced components and the clear elongation of the close-spaced stars. For comparison we show what the star field would look like if we used a small telescope with a 3 by 3 aperture (Figure 10), and a large telescope with a round aperture 15 units in diameter (Figure 11). Note that Figure 9 is quite similar to Figure 11, but

ORIGINAL PAGE IS
OF POOR QUALITY

with slightly stronger sidelobes. In comparing these figures, note that the diffraction FWHM of a 15 pixel circular mirror is 4.4 pixels, and the star separations shown are 3 and 10 pixels center-to-center, so the close pair is expected to be unresolved.

Effects of noise and misalignment

To test the robustness of the algorithm to noise, we have added to each pixel in each snapshot random noise values with relative peak-to-peak levels of 0.1 and 1.0, with the results shown in Figures 12 and 13. The algorithm clearly is stable.

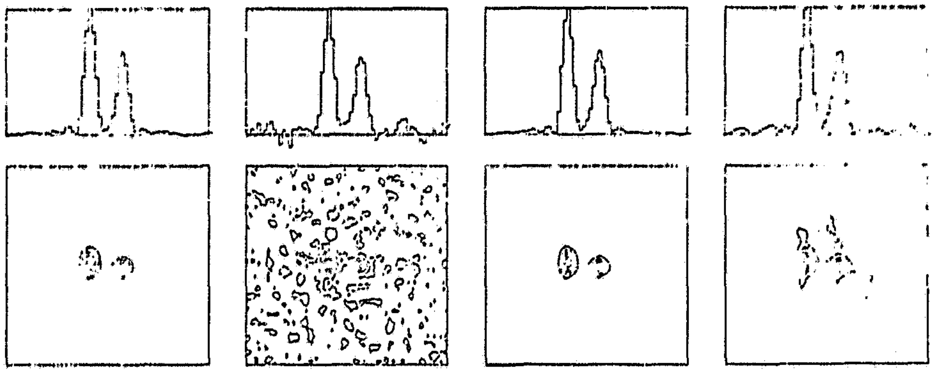

From left to right:
Figure 12. Image reconstruction with relative noise = 0.1.
Figure 13. Image reconstruction with relative noise = 1.0.
Figure 14. Image reconstruction with phase error = λ/4 peak-to-peak.
Figure 15. Image reconstruction with phase error = λ/2 peak-to-peak.

The mirror train between the incident wavefront and the detector will undoubtedly include various types of imperfections. Here we model random small-scale piston errors distributed over the pixels which represent the mirrors, with peak-to-peak phase shifts uniformly distributed over the range of 90 and 180 degrees (i.e. λ/4 and λ/2), in Figures 14 and 15, respectively. If we take λ/4 as an upper limit on the phase variation, and we have 7 mirrors in the optical path, the surface quality on each mirror must be roughly $(1/2)/7^{1/2}$ times better, or λ/20, which is well within the limits of conventional optical polishing technology.

We conclude the numerical results with a brief description of tip-tilt and (large scale) piston errors as applied to individual telescope primaries and their optical trains. This is essentially an exercise in initial alignment of the array, from a non-coherent to a coherent state. We start by blocking the beams from all but two of the telescopes. Taking these two to be adjacent, we will initially see two sets of star images in the focal plane. The telescopes can now be focussed to that each one produces images which are as small in diameter as is possible. If we look at a portion of this field of view, we will have a situation similar to that shown in Figure 16a, where a single star appears double because the mirrors are tilted with respect to one another. Here the wavefront tilt in each of two directions is λ/D, where D is the width of each primary, and for convenience we have scaled each mirror to be 7 by 7 units in size. Removing the tilt on one axis gives us the situation in Figure 16b, where we see significant interference developing in the overlap region. A final tip brings us to Figure 16c, perfect alignment. Intermediate tilts (not shown) demonstrate that 0.125 λ/D is virtually indistinguishable from perfect alignment, and that even 0.25 λ/D is quite good; these may be taken as preliminary upper limits on tip-tilt.

Monochromatic piston errors between two adjacent telescopes are illustrated in Figure 17a, where one of the two 7 by 7 unit primaries is displaced by 0.5 λ toward the star; the image bifurcation is an artifact produced by the exact cancellation of amplitudes at the position where the star should ideally have been imaged. Reducing the piston error to 0.25 λ yields Figure 17b, where one of the images grows at the expense of the other, and the peak intensity shifts toward the expected star position. Zero error simply returns us to Figure 16c. Polychromatic piston correction requires the leverage of several different wavelength bands, and is an extension of the technique just discussed.

Conclusion

The preliminary results presented here have demonstrated that image reconstruction for a rotating linear array of coherent telescopes in space is both theoretically and practically a tractable problem. Nevertheless it is clear that there are many avenues yet

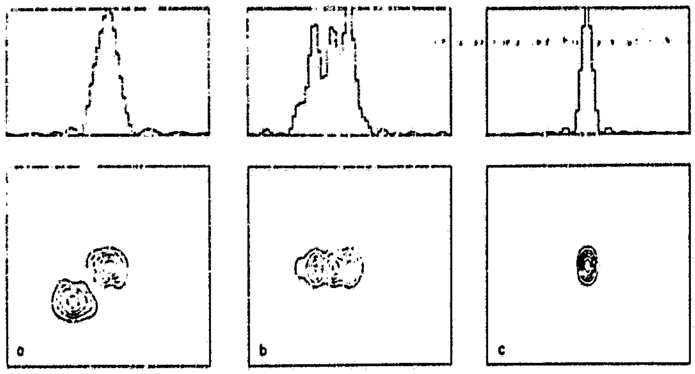

Figure 16. Snapshot images of a single star, using two adjacent 7 by 7 telescopes, with tip-tilt errors. (a) Wavefront tip = λ/D, tilt = λ/D. (b) Wavefront tip = 0, tilt = λ/D. (c) Wavefront tip = 0, tilt = 0.

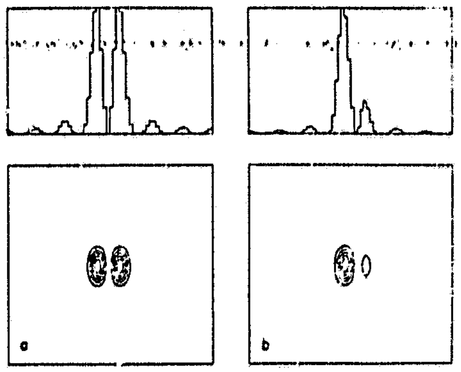

Figure 17. Snapshot images of a single star, using two adjacent 7 by 7 telescopes, with piston errors. (a) Wavefront piston error = 0.5 λ. (b) Wavefront piston error = 0.25 λ.

to be explored, including for example the definition of an optimum filter function, the question of limiting magnitude, the effect of signal-dependent noise, the effect of varying pointing of the spacecraft, the handling of a rotating detector instead of an inertially fixed detector, the sensitivity of the image to optical imperfections, and many other points. We are continuing active study of these problems, meanwhile also addressing the related question of maintaining optical alignment of the array.

As a result of these efforts, it is becoming increasingly clear that it would be extremely helpful to build in the next few years a balloon-borne version of COSMIC, perhaps at half scale. A balloon-borne COSMIC would be especially valuable because it would allow key engineering questions to be addressed at an early stage. Such an instrument would be capable of investigating a small but significant number of scientifically rewarding questions, much in the spirit of the pioneering Stratoscope flights of two decades ago.

Acknowledgements

This work was supported by NASA, through MSFC contract NAS 8-33893. We are grateful to M. Nein and his colleagues at MSFC for their preliminary engineering studies which have encouraged our recent image reconstruction work. We gratefully acknowledge many fruitful conversations with our collaborators H. Gursky and N. P. Carleton.

References

1. Gursky, H. and Traub, W. A., "Use of coherent arrays for optical astronomy in space," in Space Optics, SPIE vol. 183, pp. 188-197, 1979.
2. Traub, W. A. and Gursky, H., "Coherent arrays for optical astronomy in space," in Optical and Infrared Telescopes for the 1990's, vol. I, ed. A. Hewitt, KPNO, pp. 250-262, 1980.
3. Traub, W. A. and Gursky, H., "Coherent optical arrays for space astronomy," in Active Optical Devices and Applications, SPIE vol. 228, pp. 136-140, 1980.
4. Nein, M. E. and Davis, B., "Conceptual design of coherent optical system of multiple imaging collectors (COSMIC)", this vol., 1982.
5. Born, M. and Wolf, E., Principles of Optics, section 9.5.2, Pergamon Press, 1965.
6. Brooks, R. A. and Di Chiro, G., "Principles of Computer Assisted Tomography (CAT) in Radiographic and Radioisotopic Imaging," Phys. Med. Biol., Vol. 21 (5), pp. 689-732, 1976.
7. Pratt, W. K., Digital Image Processing, section 15.1, John Wiley and Sons, 1978.
8. Brault, J. W. and White, O. R., "The Analysis and Restoration of Astronomical Data via the Fast Fourier Transform," Astron. and Astrophys., Vol. 13(2), pp. 169-189, 1971.

Conceptual design of a coherent optical system of modular imaging collectors (COSMIC)

Max E. Nein, Billy G. Davis
NASA/Marshall Space Flight Center, Alabama 35812

Abstract

A concept is presented for a phase-coherent optical telescope array which may be deployed in orbit by the Space Shuttle in the 1990's. The system would start out as a four-element linear array with a 12 m baseline. The initial module is a minimum redundant array with a photon-collecting area three times larger than Space Telescope and a one-dimensional resolution of better than 0.01 arc seconds in the visible range. Thermal structural requirements for the optical bench are assessed, and major subsystem concepts are identified.

Introduction

A vigorous and comprehensive astronomical program in the 1990's and beyond must provide for the increased spatial resolution and large apertures which will be required to address the questions raised but not answered by the Space Telescope. These needs derive, on the one hand, from the fact that the large cosmological distances over which light must travel reduce the number of photons available to be recorded by Space Telescope (ST) to fewer than 1/sec for many objects of interest. On the other hand, understanding the details of the fundamental interaction of matter and energy in the most energetic objects in the universe depends on recording the spectral characteristics of photons over small physical volumes, a fact which dictates high angular resolution for the large distances involved.

Scientific investigations that will be pursued in the 1990's and beyond will require imaging resolutions of 10^{-3} arc-sec. To meet these requirements, a comprehensive program must be formulated that makes use of the Space Transportation System, the advanced technology inherent in the Space Telescope Program, and new technology as it can be foreseen and developed in order to produce a phased, cost-effective set of astrophysics payloads with a wide spectrum of capabilities.

One such program which is currently being studied is a phase-coherent optical telescope array for launch on the Space Shuttle in the 1990's. The scientific goals for such an instrument and the initial results of image reconstruction analyses are discussed in a companion paper during this conference by W. A. Traub and W. F. Davis of the Harvard-Smithsonian C nter for Astrophysics.

Coherent Optical System of Modular Imaging Collectors (COSMIC)

The COSMIC Program will meet the needs of increased resolution and aperture by the development of phase-coherent arrays which will be progressively combined to form a large equivalent aperture imaging complex capable of achieving 10^{-3} arc-sec imaging resolution.

The study objective for COSMIC is to investigate the feasibility of developing a modular phase-coherent array which may achieve at least an order-of-magnitude increase in capability over the Space Telescope, through a single Shuttle launch. Later additions to the linear array module would then further build up the capability of the telescope facility. Figure 1 shows an artist's concept of COSMIC and the envisioned evolutionary construction of a large cruciform array. The initial linear array contains four Afocal Interferometric Telescopes (AIT) with a Beam Combining Telescope (BCT) at one end. The COSMIC spacecraft module pivots from its launch position at the end of the BCT to its deployed position below the BCT. The solar arrays deploy from stowed positions alongside the telescope module. The scientific instruments are placed

ORIGINAL PAGE
BLACK AND WHITE PHOTOGRAPH

in the focal plane of the BCT, and sunshades are extended above the telescope apertures. Telemetry antennas will pivot into position for communication and data transmission.

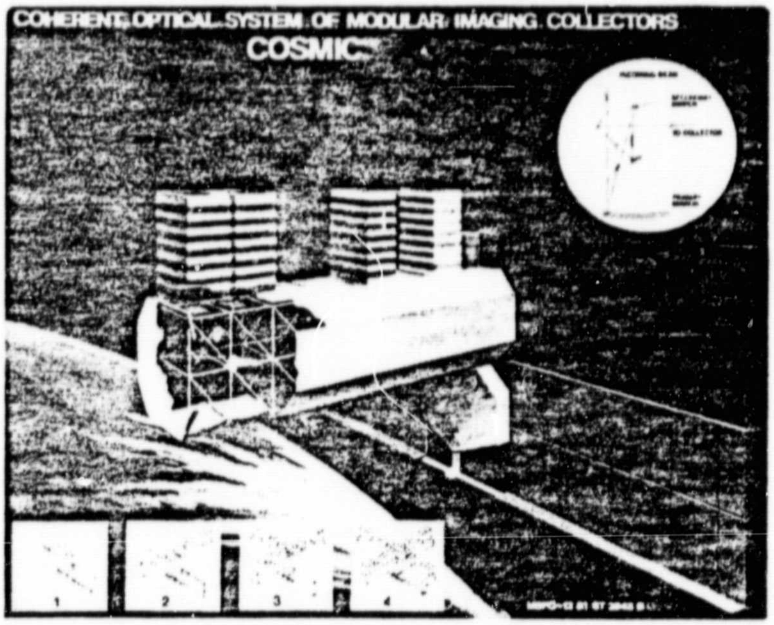

Figure 1. Initial COSMIC Module and Evolutionary Buildup

COSMIC Configuration

Optics

The key to high angular resolution is that light remains coherent over large distances. Diffraction-limited performance of an array of telescopes requires coherence of all participating wave fronts. Such a method has been used successfully to study radio sources at high resolution (0.001 arc-sec) by using data from simultaneously observing radiotelescopes on baselines stretching over the diameter of the Earth. Theoretically, the same resolution can be achieved at optical wavelengths by devices one hundred thousand times smaller in scale. Since the spatial coherence of widely separated beams of visible light is nearly destroyed by passing through the atmosphere, investigations of interesting faint sources of small angular size must be performed in space.

The concept of a minimum redundancy array of telescopes is borrowed from radio astronomy and has been applied by the Smithsonian Astrophysical Observatory to optical systems, as illustrated by the linear four-element array shown in Figure 2. The AIT's are identical and all feed through fold flats, which compensate for the staggered spacings, to the BCT. The four AIT's are located at positions (0, 1, 4, 6), giving the effect of simultaneously having mirror separations of 0, 1, 2, 3, 4, 5, and 6 units.

It is required that the array be rotated about its target axis so that two-dimensional images can be constructed that have the full resolution of a single large mirror with a diameter equal to the length of the array. The requirement for maintaining all the optical path lengths equal to within 1/4 wavelength peak to valley is the traditional Rayleigh criterion for near-diffraction imagery. It is an overly simplistic criterion in this case, but it adequately scopes the required dimensional stability at

ORIGINAL PAGE IS
OF POOR QUALITY

this conceptual stage. To minimize the complexity of an already beyond-the-state-of-the-art adaptive optics control problem, the primary mirrors were restricted to a size that would retain their figure quality passively and be packaged within the Shuttle payload bay constraints.

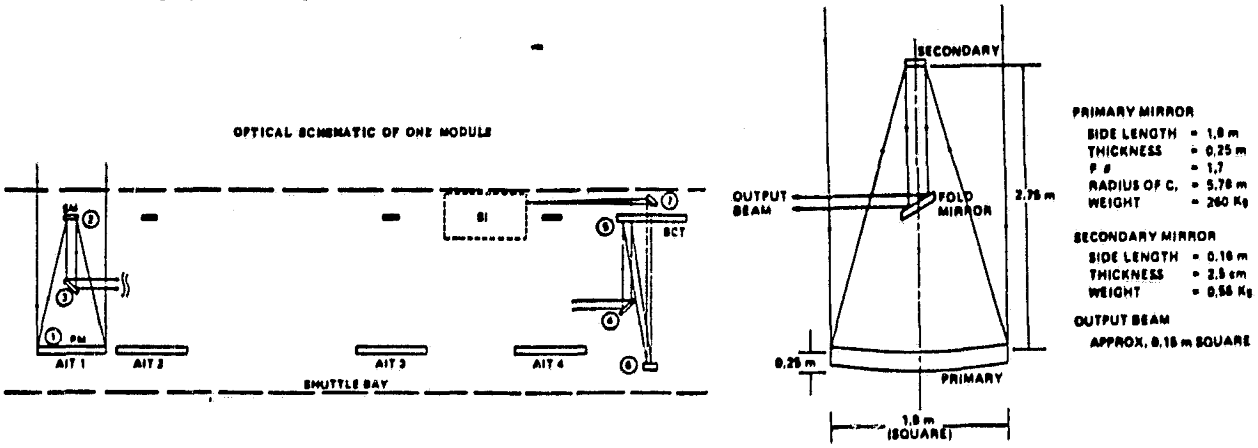

Figure 2. Linear Four Element Array Optical Schematic and AIT Mirror Definition

The 1.8 m square mirrors selected for COSMIC are lightweight mirrors of the Space Telescope class. Figure 2 shows the AIT optical schematic and mirror definition.

Active alignment of all secondary mirrors is essential, but probably will only require occasional intermittent adjustment as in the case of Space Telescope. Conversely, it is almost certain that one or more beam-steering fold mirrors and some sort of active path length adjustment will be required in each leg.

The beam from AIT 1 is directed into the BCT in a direct path. The beam from AIT 2, however, must be folded in an indirect manner (optical delay line) so that the total path length is the same as for AIT 1. AIT 3 and AIT 4, which are even closer to the BCT, must have proportionately longer folded paths so that all wave fronts from the four AIT's arrive in phase at the BCT entrance aperture. The large number of reflections, a minimum of seven for AIT 1, from entrance aperture to focus is an inherent drawback to the COSMIC concept. At visible and infrared wavelengths where very low-loss reflective coatings are achievable, the drawback is minimal, but the uv throughput will be significantly attenuated.

With about 3 sq m of collecting area per AIT for a total of 12 sq m, COSMIC has three times the collecting area of the Space Telescope. This, coupled with the factor of ten increase in angular resolution, means that COSMIC will have a faint-object-detectivity advantage over Space Telescope comparable to the advantage Space Telescope has over ground-based observatories.

Although it is an objective of this study to develop a system which can provide meaningful science with one Shuttle flight, the design concepts which were considered are based on the eventual coupling of several linear arrays to form a cross configuration. For this reason, the beam combiner telescope was placed at the end of the linear array to accommodate additional modules (Figure 1).

Thermal Structural Concept

Two major factors were design drivers for COSMIC: (1) The structural members and structural/thermal approach must produce an optical system with dimensional stability in all directions. In most telescopes, the structure holding the mirrors in relative alignment must be designed to focus the beam on a specified point with very little deviation caused by disturbances which act on the system. But in COSMIC, both relative alignment between individual telescope mirrors and between AIT's and the BCT must be maintained. Although the coherent beam combination requirement will be met by an active control system, the structural/thermal design for COSMIC must still meet more stringent criteria than previously designed optical systems such as Space Telescope.

(2) The beams from individual telescopes must be combined to form a coherent wave front to approximatey one-tenth wavelength RMS. Thus, dimensional stability of the structure and/or active path-length control must be better than 0.1 micrometer RMS. COSMIC has an overall line-of-sight aspect determination goal of 0.0005 arc-sec RMS.

Figures 3 and 4 show the structure of COSMIC. The telescopes and instruments are mounted in or on the optical bench, which is mounted inside an aluminum structure.

Since active path-length control of the optical components has been ground-ruled, the overall dimensional stability does not depend entirely on the metering structure. A tradeoff exists between the stability of the metering structure and the range over which the active control system must compensate. However, since the structural stability has not been budgeted, the approach was to determine the best metering structure using Space Telescope technology.

Ideally, the metering structure material should have a coefficient of thermal expansion (CTE) of zero. However, to postulate a zero CTE would not be practical. Based on results of very precise measurements of Space Telescope metering truss members, a CTE value of about 4×10^{-8} in/in°F was chosen for the structural members of the graphite epoxy truss.

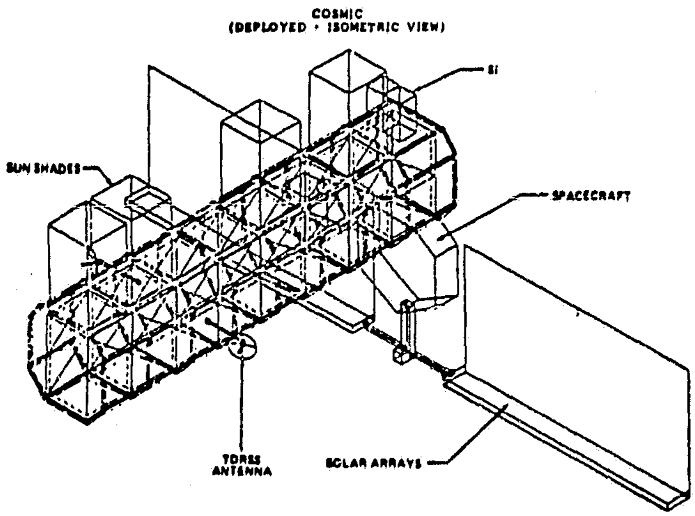

Figure 3. COSMIC - Isometric View of Interior Structure

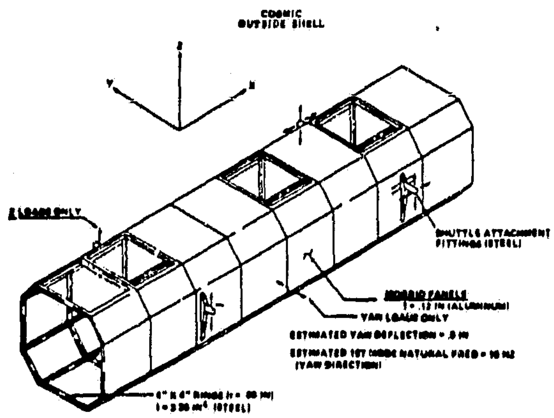

Figure 4. Exterior Shell Structure

A relatively high natural frequency is desirable to have adequate separation between the structure and attitude control bandwidth during on-orbit operations. For the launch or return phase, the observatory should be designed to prevent coupling with the Shuttle's 16 Hz critical frequency. Since the truss weight increases rapidly with increasing frequencies, a lower frequency of 15 Hz was selected as a basis for the truss design.

The metering structure is supported at many redundant points along the outside shell structure during launch. The redundant attach points are subsequently released for on-orbit operations so that thermal deflections are not transmitted from the outside shell to the metering structure.

The mirrors are attached directly to the metering structure by flexure joints similar to the ST mirror supports. Launch loads are taken directly to the outside shell.

To obtain a truss structure with minimum elongation and bore-sighting deflections resulting from temperature gradients in the metering truss, a thermally stable optical bench structure was designed to support the mirrors. The truss is thermally isolated by an outer shell covered with a Multiple Layer Insulation (MLI) having a low α/ϵ ratio. This thermal configuration results in a temperature bias, causing energy to be continuously lost from the bench. Thermal conditions are maintained by replacing the lost energy with energy supplied by electric heaters which are controlled by a microprocessor. This power is estimated to be 200 watts. Other thermal control requirements are estimated to be approximately four times that of Space Telescope, as shown in Figure 6.

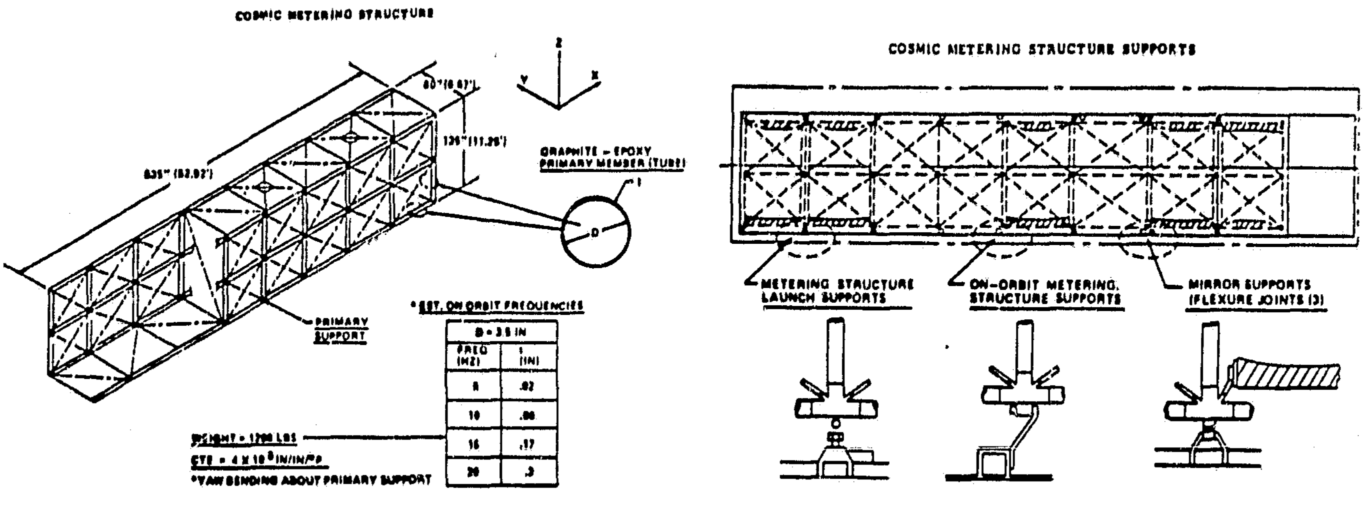

Figure 5. Metering Structure and Supports

THERMAL CONTROL BUDGET (W)

COMPONENT	ST	COSMIC
PMA	35	175
SMA	13	65
MRA	43	~ 200*
FPS	105	105
	196	545

PMA = PRIMARY MIRROR ASSEMBLY
SMA = SECONDARY MIRROR ASSEMBLY
MRA = METERING REFERENCE ASSEMBLY
FPS = FOCAL PLANE STRUCTURE
MLI = MULTILAYER INSULATION
q = HEAT LOSS

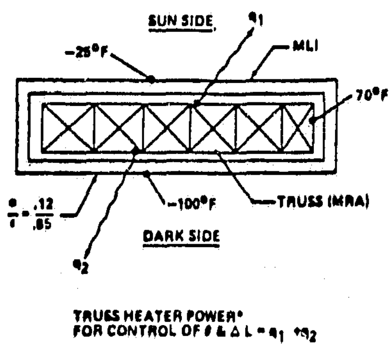

Figure 6. Thermal Control Budget and Truss Thermal Control Approach

Application of classical beam bending equations for an unconstrained configuration led to expressions for bore sighting and elongation. Truss elongation and boresighting values as functions of temperature changes are shown in Figure 7 and 8 for various CTE values.

ORIGINAL PAGE IS
OF POOR QUALITY

Based on ST performance obtained in extensive thermal vacuum testing of the ST metering structure, COSMIC requirements for elongation control to 0.1 μm can be met with a CTE of 4×10^{-8} in/in°F. The bore-sighting error, however, exceeds the allowable requirement by a factor of two. The results imply that the active optical correction mechanism must be capable to span this range.

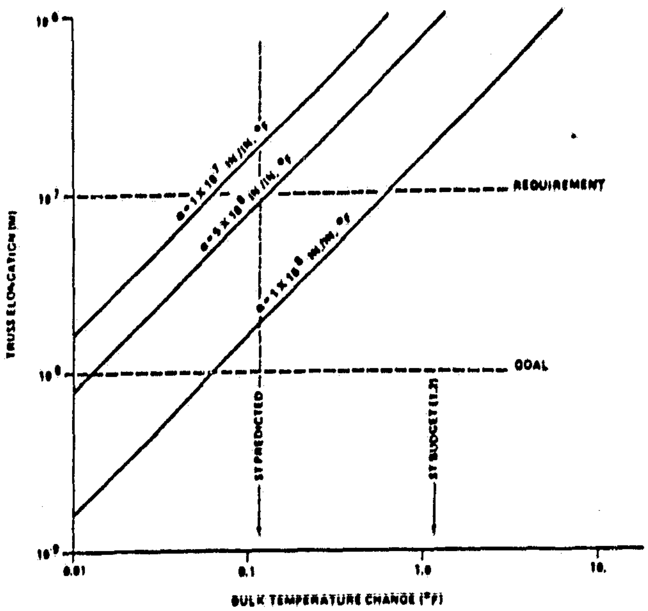

Figure 7. Influence of Bulk Temperature Change on Truss Elongation

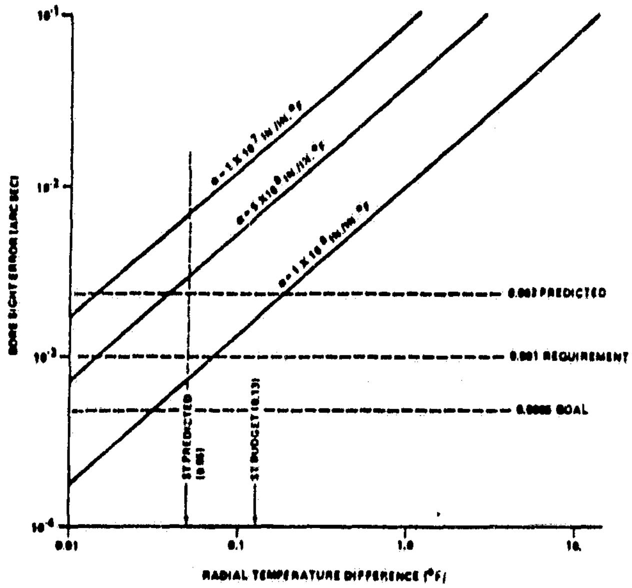

Figure 8. Bore-Sighting Error as a Function of Radial Temperature Difference

Avionics

The avionics subsystems consisting of the Attitude Control System (ACS), Fine Guidance System (FGS), Communications and Data Management System (CDMS), Electrical Power System (EPS), and the Propulsion Systems (PS) were analyzed. This paper concentrates on the Attitude Control and Fine Guidance Systems because of their role in establishing feasibility.

It was assumed that COSMIC should permit viewing any source on the celestial sphere at any time, subject to constraints such as the sun, moon, and the Earth's limb viewing interference.

Since COSMIC will view a target for periods up to hours and then maneuver to another selected target, the maneuver rate should be rapid to optimize total viewing time. In addition, COSMIC must be rotated about its line-of-sight (LOS) to build up a total high resolution image with the data being digitally reconstructed on the gound.

While attitude-holding against environmental forces, the ACS must point the COSMIC LOS within 0.2 arc-sec of the target and be stable to 0.001 arc-sec per sec while data is being taken. These requirements are similar to those of the Space Telescope. However, COSMIC uses photon-counting science detectors with continuous readout; therefore, long-term stability (slow drift) has little meaning in contrast with Space Telescope. However, in reconstructing the data on the ground, the location of the source viewed must be determined relative to the guide stars used for inertial reference to an accuracy of 0.001 arc-sec or better (0.0005 arc-sec goal).

The ACS actuators must be sized to provide control authority during all mission phases from Shuttle deployment to Shuttle revisit for repair or retrieval.

Since COSMIC is unbalanced both in mass distribution and surface areas, large gravity gradient, 0.46 ft-lb, and aerodynamic torques, 0.17 ft-lb, will result at the operational orbit altitude of 500 km. As a minimum sizing criterion, the Reaction Wheel Assembly (RWA) or Control Moment Gyros (CMG's) must be sized to counteract the cyclic momentum and have some reserve capacity for failure modes and to prevent saturation during the peaks of each cycle. With 50 percent contingency, approximately 18 of the Space Telescope's 200 ft-lb-s RWA's would be needed.

Obviously, new and larger torque devices must be provided. It appears that four single gimbal control moment gyros of an existing design (Sperry 1200) can provide sufficient control authority. To prevent the momentum exchange system from saturating, the secular momentum buildup is continuously reacted against the Earth's magnetic field by utilizing three Space Telescope magnetic torquer bars per control axis.

Several design approaches for the Fine Guidance System were investigated (see Figure 9). Option 1 was selected for COSMIC. In this approach, the FGS uses part of the field from one AIT that has its total field enlarged to obtain the required probability of guide star acquisition. Fixed solid-state detectors are positioned around the perimeter of the square field of the AIT. Several Charge Transfer Devices (CTD's) are needed to cover the field required for a high star acquisition probability. Option 1 appears viable for the 0.001 arc-sec resolution requirement. Thermal control of the detector is critical. Currently we assume an operational temperature of -20°C.

OPTION 1: USE AIT FIELD

- APPROACH: SEVERAL FIXED CTD IN THE FGS FIELD
- ASSESSMENT: VIABLE FOR 0.001 ARC-SEC REQUIREMENT

OPTION 2: TELESCOPE WITH FIXED FIELD

- APPROACH: FOV FOR STAR ACQUISITION WITH FIXED CTD TO COVER THE FIELD
- ASSESSMENT: VIABLE FOR 0.001 ARC-SEC REQUIREMENT
- PROBLEM OF ALIGNMENT WITH AIT

OPTION 3: SCAN MECHANISMS TO COVER FIELD

- APPROACH: DEDICATED TELESCOPE WITH CTD AND SCAN MECHANISMS
- ASSESSMENT: OPTICAL GAIN MUST BE BETTER THAN ST VIABLE FOR 0.0005 ARC-SEC GOAL

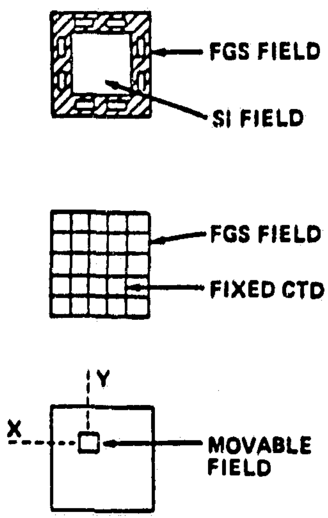

Figure 9. Fine Guidance System Options

Advanced Technology

Several areas for advanced technology were examined that should increase the probability that COSMIC can meet its mission objectives, especially for the full cross configuration. The structural members for the metering structure must be designed using very low Coefficient of Thermal Expansion (CTE) materials to meet the one-tenth wavelength criterion over the long length of COSMIC. Materials, manufacturing techniques, and ways of joining members should be examined in detail.

ORIGINAL PAGE IS
OF POOR QUALITY

The large and difficult-to-control COSMIC configuration will require new attitude control actuators that have the precision of Space Telescope, but are several times larger than Space Telescope actuators. At the shorter wavelengths and for the cruciform, the expected resolution will require that the subsystems and structure be designed for the 0.0005 arc-sec stability goal. Improvements in sensing for the fine guidance and aspect determination will require development of more accurate rate gyros and star trackers with less noise than those currently available.

While devices for measuring and correcting the optical path distances from each collecting telescope to the science instruments were not addressed during this study, emphasis should be placed in this general technology area. Optical devices for correcting both the path length and focal point must be examined in more depth to determine the operational range required.

COSMIC uses photon-counting detectors on the science instruments whose output is telemetered to Earth for image reconstruction. The COSMIC subsystems selection and permissible performance ranges must be related to image quality and/or complexity of data reconstruction, currently under investigation. A greater understanding of those relationships could lead to a relaxation of spacecraft pointing and structural stability requirements.

Conclusions

Overall system concepts for COSMIC were developed, and the primary subsystems, such as thermal control, attitude control, fine guidance, communication and data management, and electrical power, were analyzed.

The initial engineering work concentrated primarily on achieving a very stable optical bench structure by selectively utilizing low thermal expansion materials in conjunction with structural heaters. The design approach results in a structure which is sufficiently stable to allow fine tuning of the optical train via active beam steering devices.

Although current technology should suffice in development of many of the systems, advanced technology will be required in areas where COSMIC systems exhibit specific sensitivity to technological advances, such as in the active optical path length control and alignment, and fine pointing and control of the spacecraft.

Acknowledgements

We gratefully acknowledge the advice and engineering analyses provided by the members of the COSMIC Study Team at the Marshall Space Flight Center and the invaluable review comments by the Smithsonian Astrophysical Observatory. The encouragement and support of Dr. George Newton, Manager, Advanced Programs and Technology, Office of Space Science and Applications, NASA Headquarters, is also greatly appreciated.

Bibliography

1. Gursky, H., Traub, W. A., and Colombo, G., Proposal for a Feasibility Study of an Optically Coherent Telescope Array in Space, Smithsonian Institution Astrophysical Observatory, Cambridge, Massachusetts, May 1979.

2. Astrophysics Long Term Program, Project Concept Summary: COSMIC, NASA, October, 1980.

3. Rosendhal, J. D., Space Astronomy to the Year 2000: A Preview of the Possibilities Society of Photo Optical Instrumentation Engineers, Proceedings, Volume 228, 1980.

4. A Conceptual Definition Study of "Coherent Optical System of Modular Imaging Collectors" (COSMIC), Program Development Directorate, NASA/George C. Marshall Space Flight Center, Alabama, December 1981.

ORIGINAL PAGE IS
OF POOR QUALITY

Reprinted from a Bound Collection of Technical Papers

AIAA 82-1851-CP
Concepts for Large Interferometers in Space

S.H. MORGAN, M.E. NEIN,
B.G. DAVIS, E.C. HAMILTON,
D.H. ROBERTS and W.A. TRAUB

AIAA/SPIE/OSA TECHNOLOGY
FOR SPACE ASTROPHYSICS CONFERENCE:
The Next 30 Years

October 4-6, 1982/Danbury, Connecticut

82-1851

CONCEPTS FOR LARGE INTERFEROMETERS IN SPACE

S. H. Morgan
M. E. Nein
B. G. Davis
E. C. Hamilton
Program Development
George C. Marshall Space Flight Center
National Aeronautics and Space Administration
Huntsville, Alabama

D. H. Roberts
Brandeis University
Waltham, Massachusetts

W. A. Traub
Smithsonian Astrophysical Observatory
Cambridge, Massachusetts

Abstract

Very high angular resolution can be achieved in optical and radio astronomy through interferometers in space. Evolutionary approaches and required technological advances are presented. In the optical region a phase-coherent array (COSMIC) starting as a four-element linear array is discussed. Combining several modules results in greatly improved resolution with a goal of combining images to obtain a single field of view with 0.004 arcsecond resolution. The angular resolution, detail and temporal coverage of radio maps obtained by ground-based Very Long Interferometry (VLBI) can be greatly improved by placing one of the stations in Earth orbit. An evolutionary program leading to a large aperture VLBI observatory in space is discussed.

Introduction

During the 1980's Space Astronomy will, without doubt, make discoveries and raise questions that require the use of more powerful astronomical instruments in order for us to understand the diverse astrophysical phenomena that will be unveiled. Detailed structural studies of objects ranging from nearby planets and small bodies to distant quasars will be required during the final decades of this century and into the next. To meet these needs, large astronomical facilities with greatly improved angular resolution and larger collecting areas will be placed in space above the absorbing and distorting interference of the Earth's atmosphere.

Frontier problems in astrophysics during the next 30 years will require angular resolution approaching 10^{-3} arcseconds in the UV/visible spectral region. This high resolving power coupled with large flux collectors will lead to great advances in our understanding of objects within our solar system, stars, galactic nuclei and other objects as well as offering new avenues to cosmological studies.

At the longer (radio) wavelengths milliarcsecond resolution has already been surpassed with intercontinental VLBI. However, in most objects, there remains spatial structure that is unresolved. For example, virtually every active galactic nucleus has angular structure that cannot be resolved, even with the best VLBI network currently available (offering a resolution of 10^{-4} arcsec). VLBI measurements have reached the limits imposed by the size of the Earth.

The capability to assemble large structures in space and the existence of advanced technology for maintaining precise baselines and accurate pointing of large systems will make possible interferometers in space. Two such concepts currently under study by the Marshall Space Flight Center (MSFC) are the orbiting VLBI and a phase-coherent UV/visible telescope array. Each concept is considered to be evolutionary in nature, progressing from simpler to more complex configurations. The concepts, program approach and technological readiness of the required systems are discussed in the following sections.

Extending VLBI To Space

Radio interferometry observations of celestial sources are routinely performed on Earth by using atomic frequency standards to synchronize radio telescopes that may be separated by as much as intercontinental distances. Angular resolution better than a milliarcsecond, four orders of magnitude superior to that of Earth-based optical telescopes, has been achieved. By placing one or more of the observing elements in Earth orbit and making observations in concert with those on the ground, significant advantages over purely ground-based systems may be obtained. Among these advantages are improved angular resolution, improved coverage of the celestial sphere, more accurate radio maps, and more rapid mapping.(1)

Scientific Advances with Space VLBI

With orbiting VLBI we will be able to study in detail the structure of many astrophysical objects. For example, we will be able to investigate the superluminal phenomenon in quasars (expansion of different portions of quasars that apparently exceed the velocity of light), the structure of the interstellar masers that are often associated with the star-formation process, active binary systems, radio stars and other objects.

The famous quasar 3C273 provides an interesting example of the dramatic improvements that we will achieve with orbiting VLBI. It has become evident that highly unusual physical processes are occurring within quasars and galactic nuclei. Very large amounts of energy are being produced within compact structures. The map resolution and quality required to study these compact sources surpasses the capabilities of our current ground-based instruments. In particular, for a low declination source such as 3C273, the North-South resolution is poor. This limitation is caused by the location of present radio telescopes in the temperate zone of the Northern Hemisphere.

Figures 1 and 2 are computer simulations illustrating the advantages of a VLBI terminal in space. Observations are of 3C273 at 18 cm. Figure 1(a) shows the synthesized beam from a conventional ground-based network consisting of stations at Haystack (Mass.), NRAO Green Bank (W.Va.), Owens Valley (Calif.) and Bonn (W. Germany). Figure 1(b) adds a space-based terminal in low-Earth orbit to a three-station ground-based network. By comparing Figures 1(a) and 1(b), one notes the dramatic improvement in resolution obtained by adding a single space-based station.

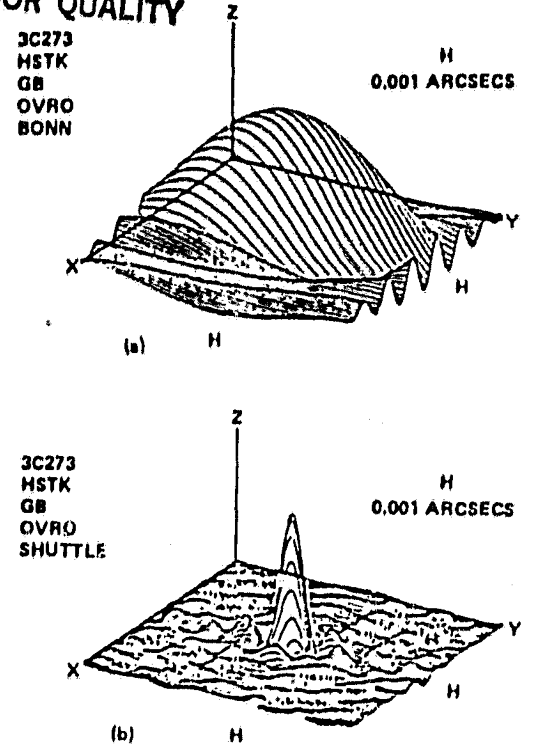

Figure 1. Comparison of Synthesized Beams from VLBI Observatories

Figure 2 shows the Fourier (u-v) coverage for the two cases shown in Figure 1. The u-v plane is normal to the vector to the source being studied; u and v are the East-West and North-South components of the baseline joining a pair of antennas, as seen from the source. As the elements of the VLBI network move in space due to the Earth's rotation or the orbital motion, the apparent baselines joining the stations change. When the entire set of baselines from all network stations are plotted in the u-v plane, the result is equivalent to the synthesized telescope aperture. The extent and completeness of u-v coverage determines the resolution and quality of the radio image constructed from the data. Note from Figure 2(b) both the density and extent of the Fourier coverage is greatly improved by adding a terminal in space.

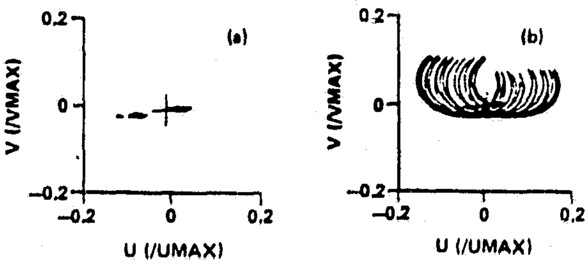

Figure 2. Comparison of Fourier Coverage from VLBI Observatories

A Space VLBI Program

The Astronomy Survey Committee of the National Academy of Sciences has recommended that a space VLBI antenna be launched in low Earth orbit during this decade.[2] To achieve a permanent VLBI system in space, three natural phases can be identified (see Figure 3). Each phase utilizes the expected evolution in the capabilities of space systems.

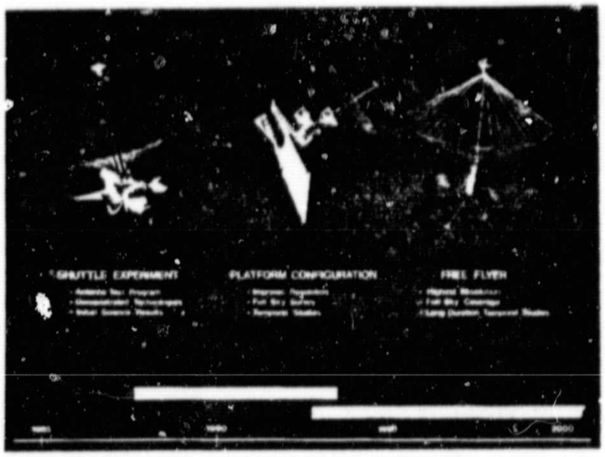

Figure 3. An Evolutionary Space VLBI Program

An initial step would be to utilize the capability of the Space Shuttle to demonstrate orbiting VLBI by deploying a large retrievable antenna attached to the Shuttle. This mission could be part of the Large Deployable Antenna Flight Experiment that has been under active study by MSFC and aerospace contractors during the past several years.[3,4] This flight would provide an on-orbit test of a large (~ 50 meter) antenna system (which also has potential applications in defense, communications and Earth observations among others). An artist's concept of one possible antenna is shown in Figure 4. During the mission about three days would be devoted to VLBI observations. Figure 5 is a block diagram of the system with probable locations of the various subsystems indicated in Figure 6. An alternative system now under study at MSFC is a 15 meter antenna aboard the Shuttle that could later be used on the Space Platform or perhaps on an Explorer class mission. Although a larger aperture

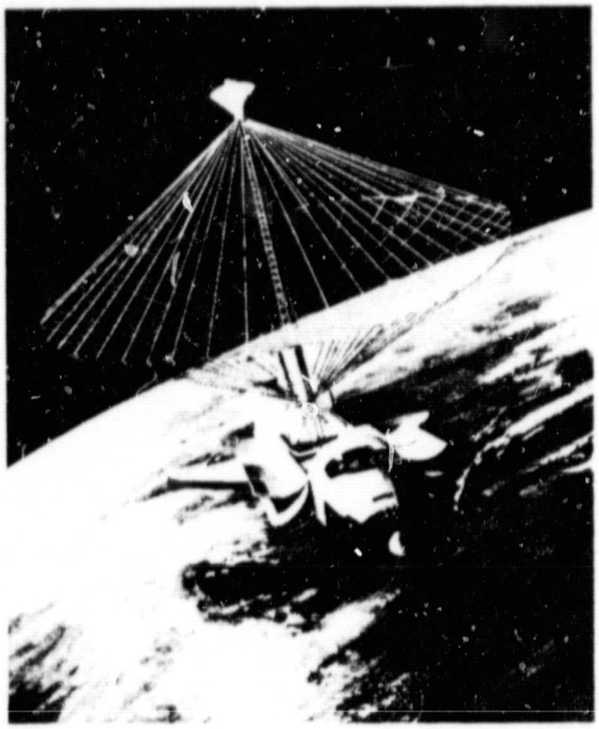

Figure 4. 50 Meter Deployable Antenna

antenna is desirable, an important set of bright sources could be observed with a space antenna as small as 5 to 10 meters in diameter.

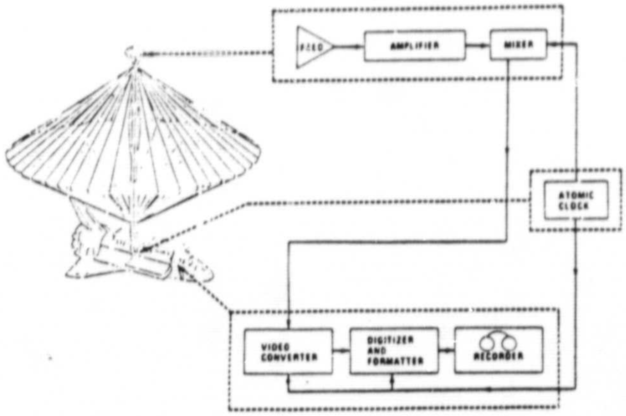

Figure 5. Block Diagram of a Space VLBI System

ORIGINAL PAGE IS
OF POOR QUALITY

ORIGINAL PAGE
BLACK AND WHITE PHOTOGRAPH

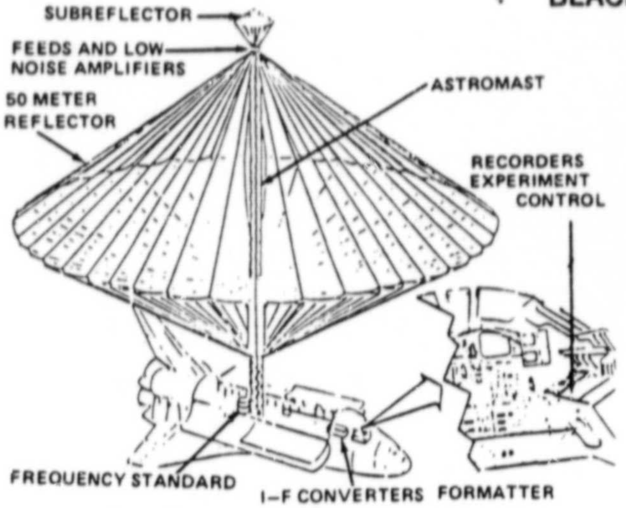

Figure 6. Shuttle VLBI Flight System

The Space Platform could be available by the end of this decade. A VLBI terminal aboard a Space Platform (or Space Station) could carry out observations for extended periods using essentially the same science package previously demonstrated on the Shuttle. Figure 7 illustrates the Platform concept with a 15 meter VLBI antenna attached to one of the ports. A Platform mission would yield a high-resolution survey of the entire sky and temporal studies of the most important sources.

During this time frame an alternative or perhaps concurrent flight configuration might be a 15 meter free flyer in the Explorer class but placed at a higher (5000 km) altitude. Ultimately a large aperture antenna aboard a high altitude free flyer would be desirable.

Both Platform and free flyer VLBI observations are naturally complementary to a dedicated ground-based VLBI array. A single space VLBI terminal improves both the resolution and density of u-v coverage by large factors and significantly increases the sky coverage available.

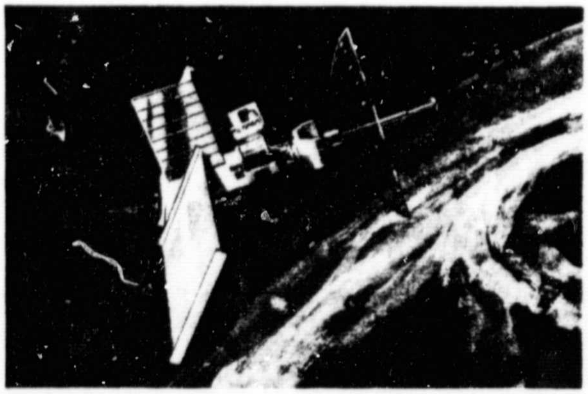
Figure 7. Orbiting VLBI: Platform Configuration

Technology Requirements

The technology readiness for orbiting VLBI depends upon the availability of space versions of the same systems that are used for ground observations. These major systems include antenna, receiver, frequency standards, IF to digital electronics and data handling systems. Each of these will be discussed briefly below. The mission and system parameters for the Shuttle mission are shown in Table 1.

Antennas

Two major parameters determine the antenna contribution to the signal-to-noise ratio of the received signal: diameter and efficiency. The first is the more important of the two. The largest civilian space antenna was the 9 meter ATS-6 reflector that was flown in 1974. During the past decade antenna technology has progressed significantly, however a 50 meter antenna operating up to about 8 GHz will probably require demonstration in space.

The antenna efficiency depends on the mesh size and surface irregularities with the latter the more difficult to control. Predicted values of the ratio of antenna diameter to rms surface irregularity for the 50 meter Shuttle antenna is estimated to be about 2×10^4 which should allow good performance up to about 10 GHz.

A final important consideration is the antenna pointing. It is essential that the antenna be pointed to within the half power beamwidth (i.e., approximately λ/D where λ is the observing wavelength and D the antenna dameter). For $\lambda = 3.6$ cm and $D = 50$ m the pointing requirement is about 0.04 degrees. The pointing can be achieved using several steps.

For the Shuttle mission the following three steps could be used:
(1) the Shuttle points the antenna to within 0.5 degrees of the celestial target.
(2) An optical or RF sensor is used to drive a movable subreflector to place the target within the 3 dB beamwidth of the antenna.
(3) Knowledge of pointing is recorded from the above sensor to later correct for any residual mispointing of the antenna. This knowledge will permit a posteriori corrections for amplitude loss during mispointing.

As part of the Shuttle VLBI mission study the C. S. Draper Laboratory performed a brief study of the dynamics and control of the Shuttle attached antenna.[5] Initial finite elements simulations have indicated that the antenna structure that was considered is quite stable during various Shuttle motions.

	SURFACE ACCURACY	FREQ. (GHz)	BEAM TYPE	POLARIZATION	RECEIVER BANDWIDTH	SYSTEM NOISE TEMPERATURE
ANTENNA SYSTEM	$> \frac{\lambda}{30}$ @ 1.4 GHz	1.66 2.3 8.4	SINGLE	ONE SENSE – CIRC. POL. TO BE DETECTED	100 MHz	160^{o}K @ FEEDPOINT

	ELECTRICAL AXIS	ANT. TRACKING/ POINTING SUBSYS.	KNOWLEDGE OF POINTING	SLEW RATE	INTEG. TIME
POINTING REQUIRE-MENTS OF ANTENNA SYSTEM*	POINTED TO WITHIN 1/2 BEAMWIDTH OF TARGET 1.66 GHZ – 0.25^{o} 2.3 – 0.18^{o} 8.4 – 0.05^{o}	$\pm 0.025^{o}$	$\pm 0.01^{o}$	3^{o} /MIN	60 SEC (REQUIRED TO TRACK SOURCE FOR 60 SEC WITHOUT VRCS FIRING)

	ALTITUDE	INCLINATION	POSITION KNOWLEDGE	VELOCITY KNOWLEDGE
ORBIT REQUIRE-MENTS	MINIMUM: 350 km	$40^{o} \leq i \leq 57^{o}$	± 10km	± 1 m/SEC

* ANTENNA SYSTEM POINTING INCLUDES: ORBITER, ANTENNA STRUCTURE, MOVABLE FEED/SUBREFLECTOR AND BEAM STEERING TO REACH REQUIRED ACCURACIES.

Table 1 VLBI Demonstration Experiment Parameters

Receivers

Gallium arsenide field effect transistor (GaAs FET) receivers are very suitable for orbiting VLBI. Through radiative cooling, system temperatures of 70°K at 2 GHz and 160°K at 8 GHz are probably possible. The long cooldown time of radiative cooling systems may preclude their use for the Shuttle mission. However, Peltier devices may be used. Performance can be considerably improved by cryogenic cooling.

Frequency Standards

The local oscillator frequency standard must be stable over the data integration periods to a small fraction of a cycle of RF phase. A hydrogen maser flown in 1976 as part of the sub-orbital Gravity Probe-A (Redshift) rocket flight achieved a level of stability of $\Delta f/f \approx 3\times10^{-14}$. This is sufficient for a 100 second coherent integration at frequencies as high as 22 GHz.

IF to Digital Electronics and Data Handling

The signal from the receiver is mixed with the local oscillator and converted to an IF signal. It is then converted to a video signal and digitized (See Figure 3). The standard for ground-based observations is the Mark III system. The electronic modules of this system could be repackaged and qualified for space.

The data recording equipment for a space mission will depend upon the data storage and transmission capability of the particular mission. For the Shuttle mission one could use several cassette tape recorders each of which would record one 4 Mbits /s channel. The tapes would then be returned to the central correlator site to be combined with the recorded data from the ground-based radio telescopes.

VLBI systems aboard a platform, space station or free flyer would periodically return data via the TDRSS system. High altitude free flyers having long term communication with the Deep Space Network could send data directly to the ground for recording.

Summary of VLBI Technology Readiness

In general, the subsystems required to support orbiting VLBI missions are technologically ready. Antennas as large as 50 meters appear to be technologically feasible; however testing in space is probably required.

The program for orbiting VLBI discussed in this paper is driven by the availability of the space systems described and the continued interest in extending the capability to utilize space. The technology is available. Only the opportunity remains for us to enter into the exciting era of space VLBI.

Space Based Coherent Optical System of Modular Imaging Collectors (COSMIC)

At microwave wavelengths large ground-based interferometers are routinely employed for high resolution astronomical observations. However, the difficulties of dealing with wavelengths 5 orders of magnitude smaller than microwave have made this a less attractive technique for achieving similar advances with ground-based observations at UV/visible wavelengths. In addition, ground-based problems of atmospheric absorption and seeing fundamentally limit the possible advances. Space will overcome these barriers as well as providing the necessary undisturbed environment.

The capability to construct large systems in space and the development of advanced optical control technology to maintain accurate baselines and alignments will allow the development of an array of coherent optical telescopes - the optical analog of radio VLBI. This program, called COSMIC, will meet the needs of increased resolution and larger aperture through the development of phase-coherent arrays which are progressively combined to form a large equivalent aperture imaging complex. Images with angular resolution in the milliarcsecond range can be achieved.(6-8)

Scientific Prospects with COSMIC

There are a large number of unique astronomical observations which would be possible with an orbiting telescope having both a large collecting area and an angular resolution in the milliarcsecond range. COSMIC will be able to resolve the nucleus of many comets, to detect the splitting of a nucleus, and to study the activity of the inner core. At Jupiter, COSMIC will be able to obtain images down to 5 km resolution, comparable to some of the best images obtained by Voyager 2. Detailed studies of the large scale features of nearby main sequence stars will also be made. Correlations with VLBI measurements of the H_2O and SiO maser emissions in the atmospheres of super giant stars will be possible.

COSMIC will be unique in being able to resolve the highly condensed cores of globular clusters. As an illustration we show in Figure 8 a series of images of the globular cluster M3 as it would appear if it were removed from our own galaxy to a much more remote distance, in the galaxy M87. The first panel in Figure 1 is a long-exposure photograph of M87 which shows the many globular clusters surrounding this galaxy. The next three panels show respectively the appearance of M3 (taken from a CCD image) as it would appear at the distance of M87 from the Space Telescope, then from a first stage COSMIC (14m in length) and finally a second stage COSMIC (35m in length).

COSMIC will be able to resolve the central regions of active galactic nuclei to help us understand what powers these very bright and condensed regions.

Because such a telescope will be able to solve outstanding astrophysical problems such as these, the Astronomy Survey Committee of the National Academy of Sciences has recommended "the study and development of the technology required to place a very large telescope in space early in the next century."(2)

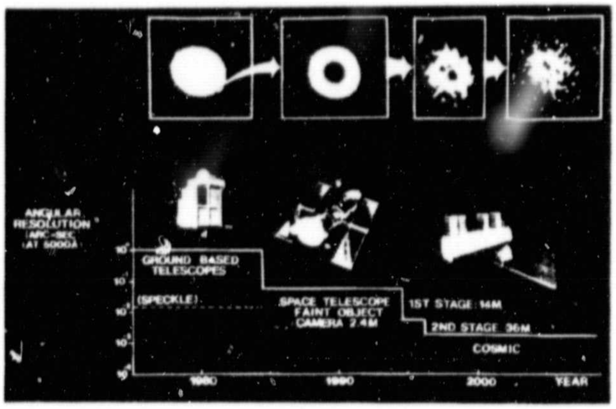

Figure 8. Advances in Telescope Resolution

The COSMIC Configuration

Figure 9 shows an artist's concept of COSMIC and the evolutionary construction of a large cruciform array. The initial

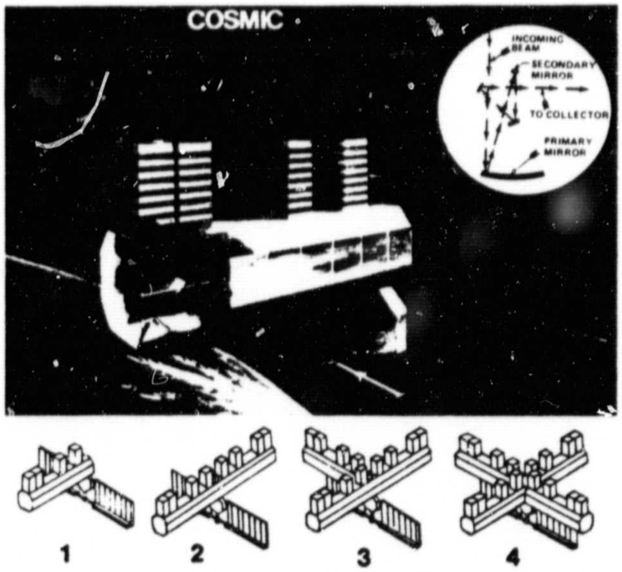

Figure 9. Coherent Optical System of Modular Imaging Collectors

linear array contains four Afocal Interferometric Telescopes (AIT) with a Beam Combining Telescope (BCT) at one end. The COSMIC spacecraft module pivots from its launch position at the end of the BCT to its deployed position below the BCT. The solar arrays deploy from stowed positions alongside the telescope module. The scientific instruments are placed in the focal plane of the BCT, and sunshades are extended above the telescope apertures. Telemetry antennas will pivot into position for communication and data transmission.

Optics

The concept of a minimum redundancy array of telescopes is borrowed from radio astronomy and applied to optical systems, as illustrated by the linear four-element array shown in Figure 10. The AIT's are identical and all feed through fold flats, which compensate for the variations in the optical path lengths to the BCT. The four AIT's are located at positions (0,1,4,6), giving the effect of simultaneously having mirror separations of 0,1,2,3,4,5, and 6 units.

The instantaneous diffraction-limited image of a point source is narrow along the array's major axis only, but by using an already demonstrated image reconstruction technique it will be easy to build up fully resolved images after a 180 degree rotation of the array, even in the presence of noise and optical imperfections.

The requirement for maintaining all the optical path lengths equal to within 1/4 wavelength peak to valley is the traditional Rayleigh criterion for near-diffraction imagery. It is an overly simplistic criterion in this case, but it adequately scopes the required dimensional stability at this conceptual stage. To minimize the complexity of an adaptive optics control problem that is already beyond-the-state-of-the-art, the primary mirrors were restricted to a size that would retain their figure quality passively and be packaged within the constraints of the Shuttle payload bay.

Active alignment of all secondary mirrors is essential, but probably will only require occasional adjustment as in the case of the Space Telescope. Conversely, it is almost certain that one or more beam-steering fold mirrors and an active path length adjustment will be required in each leg.

Optical Schematic of One Module

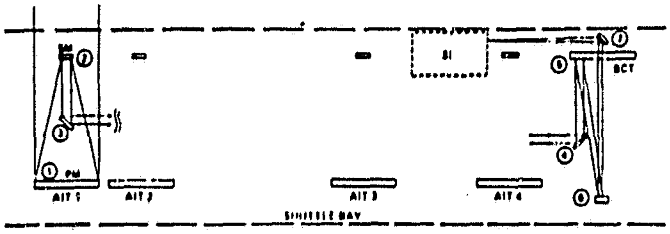

Optical Schematic of Afocal Interferometric Telescope

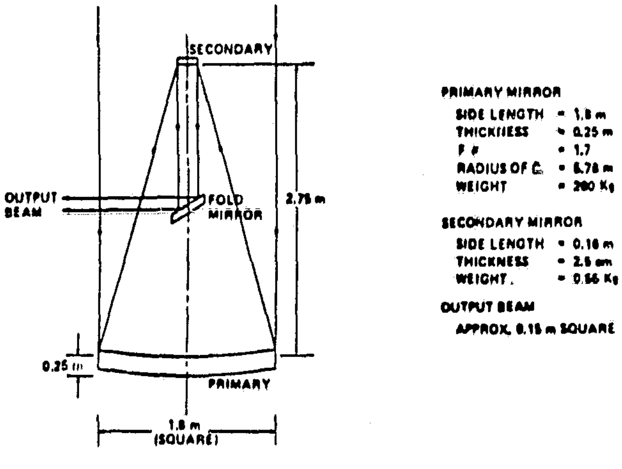

Figure 10. Linear Four Element Array Optical Schematic and AIT Mirror Definition

The beam from AIT 1 is directed into the BCT in a direct path. The beam from AIT 2, however, must be folded in an indirect manner (optical delay line) so that the total path length is the same as for AIT 1. AIT 3 and AIT 4, which are even closer to the BCT, must have proportionately longer folded paths so that all wave fronts from the four AIT's arrive in phase at the BCT entrance aperture.

A collecting area of about $3m^2$ per AIT gives the initial COSMIC configuration three times the collecting area of the Space Telescope. This, coupled with a factor of six increase in angular resolution, means that COSMIC will have a faint-object-detectivity advantage over Space Telescope comparable to the advantage Space Telescope has over ground-based observatories.

Image Reconstruction

The image produced by a linear coherent array will exhibit non-uniform resolution as a function of direction in the image plane. Specifically, the diffraction-limited resolution in the direction colinear with the array will exceed that normal to the array in the same ratio as the aperture aspect ratio. The image formed in the focal plane is the convolution of the aperture autocorrelation function and the "ideal" sky which falls in the several telescopes' common field of view. If we consider the focal plane two-dimensional detector (such an as intensified CCD) to be fixed in inertial space, while the linear telescope rotates about the line of sight, then it is useful to think of the aperture autocorrelation as providing a "window" onto the true (unmodified by the instrument aperture) image Fourier plane. As the aperture rotates, so does the aperture autocorrelation. At each orientation only a portion of the Fourier plane can be "seen" through the window. By piecing together glimpses of the Fourier plane provided by a set of distinct aperture orientations, a measure of the Fourier transform of the sky can be built up over a region corresponding to the union of the areas covered by the individual autocorrelations.

We have begun computer simulations of the image reconstruction process and have been able to investigate the effects of additive noise as well as optical system imperfections.[9] Noise is strongly rejected in this technique, since in the Fourier-plane summing operation, we are able to exploit natural opportunity to suppress noise from non-information bearing frequencies. The images are also very stable against optical imperfections up to about one-quarter wavelength, peak-to-peak. Finally, no artifacts have been found to be generated; this should not be at all surprising because the reconstruction process is in fact very close to being a "selective addition" process wherein we simply save and then add together the "good" parts of each image; there is no amplification whatsoever of weak signals, so artifacts and instabilities are completely avoided.

Structural Concept

Two major factors were design drivers for COSMIC: (1) The structural members and structural/thermal approach must produce an optical system with dimensional stability in all directions. In most telescopes, the structure holding the mirrors in relative alignment must be designed to focus the beam on a specified point with very little deviation caused by disturbances. But in COSMIC, both relative alignment between individual telescope mirrors and between AIT's and the BCT must be maintained. Although the coherent beam combination requirement will be met by an active control system, the structural/thermal design for COSMIC must still meet more stringent criteria than previous optical systems such as Space Telescope; (2) The beams from individual telescopes must be combined to form a coherent wave front to approximately one-tenth wavelength rms. Thus, dimensional stability of the structure coupled with active path length control must be better than 0.03 micrometer rms. COSMIC has an overall line-of-sight aspect determination goal of 0.0005 arcsec rms.

Figures 11 and 12 illustrate the structure of COSMIC. The telescopes and instruments are mounted in or on the optical bench, which is mounted inside an aluminum structure.

Since active path length control of the optical components has been assumed the overall dimensional stability does not depend entirely on the metering structure. A tradeoff exists between the stability of the metering structure and the range over which the active control system must compensate. However, since the structural stability has not been budgeted, the approach used was to determine the best metering structure using Space Telescope technology.

Ideally, the metering structure material should have a zero coefficient of thermal expansion (CTE). However, to postulate a zero CTE would not be practical. Based on results of very precise measurements of Space Telescope metering truss members, a CTE value of about 4×10^{-8} in/in°F was chosen for the structural members of the graphite epoxy truss. This will allow elongation control to $0.1\ \mu m$. The boresighting error which exceeds the allowable requirements by a factor of two must be corrected with an active optical compensation mechanism.

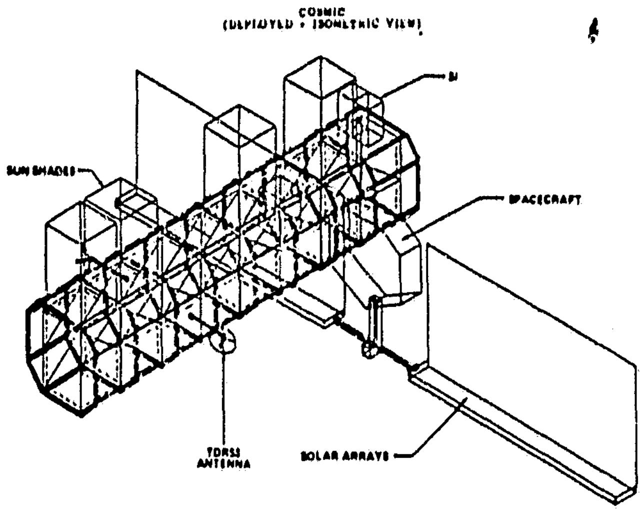

Figure 11. COSMIC - Isometric View of Interior Structure

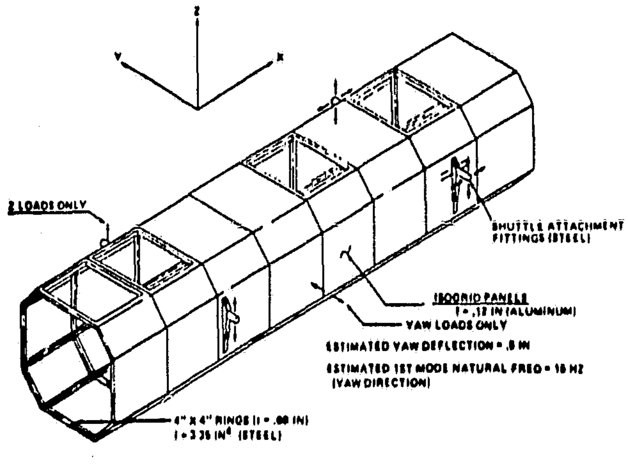

Figure 12. Exterior Shell Structure

The metering structure is supported at many redundant points along the outside shell structure during launch. The redundant attach points are subsequently released for on-orbit operations so that thermal deflections are not transmitted from the outside shell to the metering structure. The mirrors are attached directly to the metering structure by flexure joints similar to the Space Telescope mirror supports.

Avionics

The avionics subsystems consisting of the Attitude Control System (ACS), Fine Guidance System (FGS), Communications and Data Management System, Electrical Power System, and the Propulsion Systems were analyzed.

While attitude-holding against environmental forces, the ACS must point the COSMIC line-of-sight within 0.2 arcsec of the target and be stable to 0.001 arcsec per sec while data is being taken. These requirements are less restrictive than those of the Space Telescope. Since COSMIC will use photon-counting detectors with continuous readout, long-term stability (slow drift) has little meaning in contrast with Space Telescope. However, in reconstructing the data on the ground, the location of the source viewed must be determined relative to the guide stars used for inertial reference to an accuracy of 0.001 arcsec or better (0.0005 arcsec goal).

Since COSMIC is unbalanced both in mass distribution and surface areas, large gravity gradient and aerodynamic torques will be present at the operational orbit altitude of 500 km. Approximately 18 of the Space Telescope's 200 ft·lb·s Reaction Wheels would be needed to counteract these torques.

Obviously, new and larger torque devices must be provided. It appears that four single gimbal control moment gyros of an existing design can provide sufficient control authority. To prevent the momentum exchange system from saturating, the secular momentum buildup is continuously reacted against the Earth's magnetic field by utilizing three magnetic torquer bars per control axis.

Several design approaches for the FGS were investigated. We selected an FGS which uses part of the field from one AIT that has its total field enlarged to obtain the required probability of guide star acquisition. This system is capable of meeting the 0.001 arcsec resolution requirements.

Summary of COSMIC Technology Readiness

Several areas of advanced technology were examined that should increase the probability that COSMIC can meet its mission objectives, especially for the full cross configuration. The structural members for the metering structure must be designed using very low Coefficient of Thermal Expansion materials to meet the one-tenth wavelength criterion over the long length of COSMIC. Materials, manufacturing techniques, and methods of joining members should be examined in detail.

The large COSMIC configuration will require new attitude control actuators that have the precision of Space Telescope, but are several times larger than Space Telescope actuators. At the shorter wavelengths and for the cruciform configuration the expected resolution will require that the subsystems and structure be

ORIGINAL PAGE IS
OF POOR QUALITY

designed for the 0.0005 arcsec stability goal. Improvements in sensing for the fine guidance and aspect determination will require development of more accurate rate gyros and star trackers with less noise than those currently available.

While devices for measuring and correcting the optical path distances from each collecting telescope to the science instruments were not addressed, emphasis should be placed in this general technology area.

COSMIC uses photon-counting detectors on the science instruments with outputs telemetered to Earth for image reconstruction. The COSMIC subsystems selection and permissible performance ranges must be related to image quality and/or complexity of data reconstruction, currently under investigation. A greater understanding of those relationships could lead to a relaxation of spacecraft pointing and structural stability requirements.

Conclusion

Results from preliminary studies of two large interferometers in space have been presented that would lead to major advances in capabilities for astrophysics during the next 30 years.

At radio wavelengths the technology is generally available to place a VLBI station in Earth orbit. However, large (~50 m) aperture deployable antennas will probably require demonstration in space.

For UV/visible spectral coverage COSMIC is a very attractive approach that is both theoretically and practically feasible. Although major technology barriers have not been identified in our studies thus far, one must recognize that the development of the large systems presented here poses formidable tasks in orbital assembly and servicing, maintenance of optical coherency, pointing and stability of the spacecraft and thermal control.

For current systems the accepted approach is to verify performance through extensive ground testing. However, the new generation of large aperture instruments which have structural frequencies as low as a few Hertz can only be adequately tested as functional systems in space. It is thus imperative that considerable space demonstration work precede any commitment to a specific design of a long duration space system. Since the space demonstration capability would lead the design of the final system by several years, it would actually establish many of the technology requirements.

Acknowledgement

The authors wish to thank Professor Bernard Burke (MIT), Dr. Frank Jordan (JPL), Dr. Robert Preston (JPL), and Lester Sackett (Draper Lab), members of a NASA-sponsored VLBI working group. The VLBI concepts discussed in this paper are based on studies conducted by this working group. We would also like to thank Dr. Herbert Gursky (NRL), Dr. Nathaniel Carleton (SAO), and Dr. Warren Davis (SAO) who have made significant contributions to the COSMIC studies.

References

1. Shuttle VLBI Experiment: Technical Working Group Summary Report, NASA TM-82491 (Samuel H. Morgan and D. H. Roberts, eds.), NASA, G. C. Marshall Space Flight Center, July 1982.

2. Field, G. et al., Astronomy and Astrophysics for the 1980's, Report by the Astronomy Survey Committee, National Academy of Sciences, National Academy Press, Washington, DC, 1982.

3. Deployable Antenna Flight Experiment Definition Study, Final Report, Grumman Aerospace Corp., Bethpage, NY, March 1982.

4. Deployable Antenna Flight Experiment Definition Study, Final Report, Harris Government Electronics Systems Division, Melbourne, FL, March 1982.

5. L. L. Sackett and C. B. Kirchwey, Dynamic Interaction of the Shuttle On-Orbit Flight Control System with Deployable Flexible Payloads, AIAA Symposium on Guidance and Control, Paper No. 82-1535-CP, San Diego, CA, August 1982.

6. W. A. Traub and H. Gursky, "Coherent Arrays for Optical Astronomy in Space," in <u>Optical and Infrared Telescopes for the 1990's</u>, Vol. 1, ed. A. Hewitt, Kitt Peak National Observatory, pp. 250-262, 1980.

7. M. E. Nein and B. G. Davis, "Conceptual Design of a Coherent Optical System of Modular Imaging Collectors (COSMIC)," in Advanced Technology Optical Telescopes, SPIE Vol. to appear in 1982.

8. W. A. Traub, N. P. Carleton and G. Colombo, Feasibility Study of an Optically Coherent Telescope Array in Space, Technical Report No. 1, Smithsonian Institution Astrophysical Observatory, Cambridge, MA, November 1981.

9. W. A. Traub and W. F. Davis, "The COSMIC Telescope Array: Astronomical Goals and Preliminary Image Reconstruction Results," Advanced Technology Optical Telescopes, SPIE Vol. to appear in 1982.

ORIGINAL PAGE IS
OF POOR QUALITY

D1

Center for Astrophysics

Harvard College Observatory
Smithsonian Astrophysical Observatory

MEMORANDUM

To: Distribution — December 16, 1981

From: W. A. Traub WAT

Subject: First results from a crude image reconstruction computer program.

The theoretical work that Warren Davis has been doing during the past three months has led to a better understanding of the image reconstruction problem for COSMIC (OCTAS), and has suggested a simple computer technique which will be illustrated in this memo. Part of the motivation for writing this computer program was to gain some experience with the practical aspects of generating an image, doing fast Fourier transforms with the array processor, and displaying the results in a meaningful way. The program also provides a simple reconstruction technique as a baseline against which more refined methods can be compared later. The name of this program, CRUDE, is intended to convey a sense of its current state of sophistication. In fact, only a very few of the theoretical constructs which appear in Davis' notes on this subject have been used in the current computer program; many as yet untouched areas must be explored before we can claim to be able to extract the full amount of information from the individual images produced by a linear array of coherent telescopes.

Consider a single image of a small region of the sky as formed by an ideal, diffraction-limited telescope having an aperture which is essentially a long, narrow slit. The diffraction pattern in the focal plane which corresponds to a point source in the sky will also be elongated, but at a right angle to the aperture slit. This image clearly contains the maximum available amount of high-resolution information in one spatial direction, but little information in the orthogonal direction. We can demonstrate this by taking the two-dimensional Fourier transform of the image: we will find many more Fourier coefficients going out in the high-resolution direction than we will in the low-resolution direction. Suppose we save these coefficients.

Now we imagine the detector to be fixed in inertial space, while the telescope array is rotated, so the center of each star image will not move with respect to the detector, but the diffraction pattern will rotate about each bright point source. An image with such a rotated aperture will have high-resolution information in a different direction, so Fourier-transforming the new image and combining this result with the original will start to fill in the frequency plane. Clearly some low-frequency points will be represented in both views and they will be disproportionally represented unless we allow for this multiple counting; a weight function of some sort can easily be used which essentially will keep track of the degree to which each frequency point has been sampled by the various rotated slit apertures. After all views have been added, this weight can be used to normalize each frequency point. The inverse Fourier transform will then be a representation of the star field which contains essentially all measured high-spatial-frequency components in all directions. This reconstructed star field should be essentially the same as could have been obtained with a single large mirror having a diameter equal to the length of the slit-aperture telescope, and this is indeed true, as we shall show below.

1. Conventional telescope apertures. To illustrate these concepts and to show how program CRUDE can be used to display the various stages in a calculation, we will first discuss what happens when a conventional circular telescope aperture is used to image a point source. In the following figures we will display various 2-dimensional objects, functions, or images as points on a 64 by 64 grid, with contour levels drawn at either 9 intervals (ie, 10, 20, ..., 90 percent) or at 5 intervals (ie, 16, 33, 50, 67, 83 percent). Above each contour diagram there is plot displaying a slice through the same data, from left to right; the slice is positioned to include the peak data point. In Fig. 1a we show a single large telescope mirror which is circular to within the discrete limits of our grid, and has unity transmission within this circle. The mirror diameter is 31 units.

For photons of a given wavelength, the diffraction pattern of a telescope is conveniently given by the Fourier transform of the auto-correlation of the aperture transmission, as described in Davis' notes (eqn. 26). The autocorrelation can be calculated either by stepping the aperture across itself and multiplying a total of 64 x 64 times, or more conveniently by calculating the Fourier transform, taking the square magnitude, and again Fourier transforming (eqns. 24 and 25). Using the latter technique, we calculate the autocorrelation shown in Fig. 1b, where the lower left-hand corner point is the origin, ie., the point which corresponds to zero relative displacement between the multiplied apertures. This figure and all others are periodic modulo 64 points, so the plane should be considered to be tiled with such figures, making it clear that the four filled corners of Fig. 1b can be looked upon as offset segments of circles centered on the origin. The total extent of these circles is just one point less than twice the telescope diameter, as expected (Davis' eqn. 197). Again, viewing Fig. 1b as the Fourier transform of the diffraction pattern of the aperture, we see that the origin corresponds to the zero-frequency or DC point, and that higher spatial frequencies correspond to points farther from the origin. Those points beyond 64/2 = 32 points in either direction are aliased, and the values in these 3 quadrants should be considered to be translated to the left by 64 points so as to surround the origin.

The image of a single point-like star, as seen by the telescope in Fig. 1a, is shown in Fig. 1c. This image was calculated by first setting up a single (1 pixel) star, then calculating the Fourier transform of the star (in this case a complex vector with unity magnitude everywhere in the frequency plane), multiplying by Fig. 1b, inverse Fourier transforming, and displaying the real part as seen in Fig. 1c.

Continuing the illustration, we show in Figs. 2 and 3 the corresponding apertures, autocorrelations, and star images from circular mirrors with diameters of 15 and 7 pixels respectively. As expected, smaller mirrors sample fewer of the spatial high frequencies, and therefore produce broader star images.

With these three images before us, it is of interest to attach an absolute scale to the figures and make a comparison with standard measures of resolution. Interpolating between the discrete data points shown in the upper parts of Figs. 1c, 2c and 3c, we find values for the full-width at half-maximum (FWHM) of 2.18, 4.43, and 9.67 pixels, respectively. Referring to Davis' eqn. 172, we find that the field-of view, ie. the width of Fig. 1c, 2c, or 3c, is given by $\lambda/\Delta\chi$ where λ is the wavelength and $\Delta\chi$ is the sample interval across the mirror, ie. the pixel size in Fig. 1a, 2a, or 3a. If we choose a visible wavelength $\lambda = 0.5$ micron, and a telescope scale factor of $\Delta\chi = 1$ meter per pixel, we find a field-of-view of 0.103 arc-sec, which for 64 pixels gives a scale factor of 1.61 milli-arc-sec per pixel. The mirrors in Figs 1a, 2a, and 3a are then 31, 15, and 7 meters in diameter, and the stars have FWHM = 3.5, 7.1, and 15.6 milli-arc-sec, respectively.

To compare this with the classical equation for the intensity distribution given by $[2\, J_1(z)/z]^2$, where z is a distance scaled by $\pi\lambda/D$ and D is the telescope diameter, we find that this function has a FWHM of 1.03 λ/D and a distance to the first zero of 1.22 λ/D. This predicts values of FWHM = 3.4, 7.1, and 15.2, all of which are close enough to the hand-measured values that the differences can be attributed to uncertainties in the linear interpolation process, and the discrete approximation to a circular mirror (which biases the perimeter to be less than or equal to a specified diameter, so the diffraction pattern is always wider than predicted by the classical formula).

2. Linear apertures. The imaging properties of a coherent linear array of telescopes will now be sketched in a way that attempts to clarify the relationship between a circular aperture and a rotating linear aperture. This discussion also applies to rectangular single mirror segments, since it is the overall shape of the aperture, not the details of construction, that matters here. In Fig. 4a we show an aperture which is 3 by 15 pixels, or 3 by 15 meters using our previous scaling for the sake of concreteness. The autocorrelation of the aperture appears in Fig. 4b, where the lower left-hand corner is the zero spatial-frequency point. Note that the orientation of the aperture is important, since the higher spatial frequencies are sampled in a direction parallel to the long axis of the aperture. In Fig. 4c we show the effect of this aperture on a star field which consists of 3 stars of equal intensity; 2 of the stars are completely unresolved with this viewing angle. (In this and the following, only 5 contour levels appear in the figures.)

If we now imagine the detector to stay fixed with respect to inertial space, while the aperture is rotated by 45 degrees, we have the situation shown in Fig. 5. Note that the rather simple technique which is employed to rotate the discrete 3 by 15 aperture sometimes produces edge distortions and even gaps in the rotated array, both of which are seen in the aperture drawn in Fig. 5a. The effects of these edge distortions and gaps on the final image are relatively minor however, since the overall shape of the aperture is not strongly affected. The frequency plane coverage is shown in Fig. 5b, and the star field image appears in Fig. 5c.

To complete the present example we show in Fig. 6 the case where the rotation has reached 90 degrees. Here the 3 stars have been completely smeared into one feature. In the next section we show how these snapshots can be combined and an image reconstructed.

3. Image reconstruction. The key idea behind our present image reconstruction scheme is given by Davis' eqn. 35, namely that we consider a stack of frequency planes and that we simply add these planes together, with a suitable filtering function if desired. This sum should be properly normalized to account for the greater number of low frequency measurements with respect to samples at the rotating high frequency end of the autocorrelation function. The real part of the inverse Fourier transform then is the desired image. This method is very general, as can be seen from the fact that in the limit of very long and narrow apertures, the calculation yields just the computer-assisted-tomographic (CAT) scan reconstruction (see Davis, pp. 9-11).

The entire simulation procedure which was used can be outlined as follows:

A. Set up real stars within the basic 64 by 64 pixel field-of-view.

B. Calculate FT of stars and save.

C. Set up an "ideal" aperture shape by assigning real 1's to the 3 by 15 aperture and 0's elsewhere.

D. Rotate the aperture to the nearest discrete grid points available for a specified rotation angle.

E. Set up a "noisy" aperture by following C and D, except that the 1's are replaced by exp (ix) where x is a real random number between +X/2 and -X/2 and X is the peak-to-peak phase error assigned to each mirror element.

F. For the "ideal" aperture, calculate the FT, find the magnitude squared at each point, and calculate a second FT; this is the autocorrelation function.

G. For the "noisy" aperture, follow step F.

H. Set up background noise, by filling the 64 by 64 field-of-view with real random numbers y, where y is between +Y/2 and -Y/2 and Y is the peak-to-peak background noise assigned to each pixel in the field of view, from CCD read-out noise, cosmic rays, etc.

I. Calculate the FT of the background noise.

J. Calculate the effect of image smearing and added noise by forming (B x G) + I.

K. Calculate a filter function according to whether filter number 0, 1, or 2 is desired:
Filter 0 = real 1's filling 64 by 64;
Filter 1 = real 1's where the magnitude of F is essentially non-zero;
Filter 2 = magnitude of F.

L. Filter the image FT by forming J x K, and add this to previously formed stack, if any.

M. Calculate the current contribution to the normalizing function by adding K into a separate stack.

N. If there are more angles to contribute to the final image, return to step C, and repeat this until the desired number of images has been added, typically 1, 8, or 16.

P. For the summed data now, calculate the normalized, weighted image FT by forming L/M.

Q. Find the final image by calculating the inverse FT of P and keeping the real part.

The above reconstruction procedure differs from that discussed by Davis (eqn. 56) in that Davis' normalizing factor includes an extra multiplicative aperture term; in the noise-free case this term will enhance the angular resolution substantially, but when noise is included the algorithm becomes unstable. The present method of reconstruction has not yet been theoretically analyzed to optimize the filtering (K) or the normalization (M), and should be regarded as being purely exploratory.

For reference we show in Fig. 7 the input star field (step A above) which was used to generate Figs. 4, 5, and 6. Carrying out the full reconstruction as outlined above, in the noise-free case and using filter type 2, we have tried both 8 and 16 angle views (between 0 and 180 degrees) with the results shown in Fig. 8 and 9a, respectively. Except for an improved baseline, the two reconstructions are quite similar. Both show a clean separation of the wide-spaced components, and a clear elongation of the close-spaced stars. For comparison, we show what this star field would look like if we used a small telescope with a 3 by 3 aperture (Fig. 9b), and a large telescope with a round aperture 15 pixels in diameter (Fig. 9c). Note that Fig. 9a is quite similar to Fig. 9c, but with slightly stronger sidelobes (see also Fig. 4c). In comparing these figures, note that the diffraction FWHM of a 15 pixel circular mirror is 4.4 pixels, and the star separations shown are 3 and 10 pixels, so the close pair is expected to be unresolved.

4. Background noise and filters. We now present a catalog of images showing the effects of adding background noise as described in section 3H. At present the noise level is not clearly related to the amplitudes of the stars; this will have to be clarified in later versions of the program. For now, amounts of noise with peak-to-peak parameters of 0.0, 0.1, and 1.0 have been tried, and the effects of the 3 filter schemes have been examined. In Fig. 10 we show the results of using filter types 0, 1, and 2 with no noise. Figs. 11 and 12 are similar, but with noise levels of 0.1 and 1.0 respectively. Several points can be made from these figures. First, filter type 0 gives large, extended wings and relatively poor noise rejection, as could be expected from adding unweighted and unfiltered data. Second, filter types 1 and 2 are roughly comparable in their effects, with type 1 apparently giving somewhat better smoothing of the noise; this is surprising because by design filter type 2 smoothly rolls off the higher frequencies within the passband, whereas type 1 keeps all frequency components right out to the edge of the passband and then cuts off sharply. Future work will be needed to better define useful filters which will deliver optimum resolution at a given noise level.

5. Optical phase fluctuations. The mirror train which lies between the incident wavefront and the detector will undoubtedly include various types of imperfections. We assume here that there are no gross tip-tilt errors in the alignment of the combining wavefronts, but that there is a residual, random piston error distributed over the pixels which represent the mirrors. In Fig. 13 we show the effect of introducing piston errors with peak-to-peak phase shifts uniformly distributed over the ranges of 36, 90, 180, and 360 degrees, corresponding to amplitudes of $\lambda/10$, $\lambda/4$, $\lambda/2$, and λ. The rms values are about 4 times smaller than the peak-to-peak values. We see from Fig. 13b in particular that an acceptable upper limit on the phase variation is probably somewhat greater than $\lambda/4$, assuming that we require a signal-to-noise of about 100 in the image. If there are 7 mirrors in the optical path, the surface quality on each mirror must be roughly $7^{1/2}$ times better, or $\lambda/10$. This is certainly within the limits of conventional optical polishing technology and should not be too expensive to achieve. This value should be only tentatively entertained however until further computer simulations have been completed, using more pixels across each mirror, and including some tip-tilt errors as well.

WAT:jv

Distribution:
- N. P. Carleton
- W. F. Davis
- H. Gursky, NRL
- M. Nein, MSFC
- R. Taylor

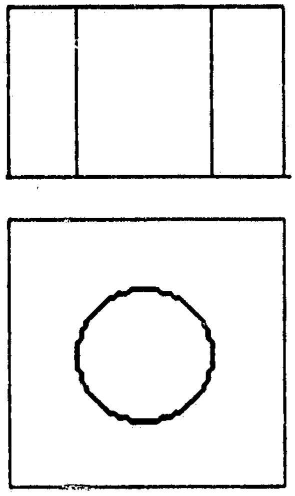

Fig. 1a Mirror, diameter = 31 units

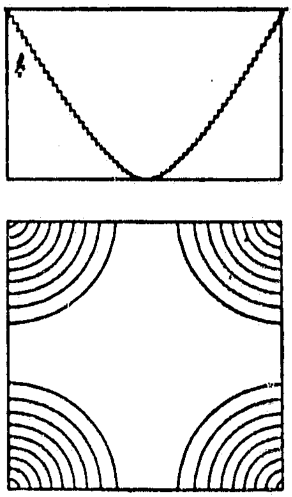

Fig. 1b Autocorrelation.

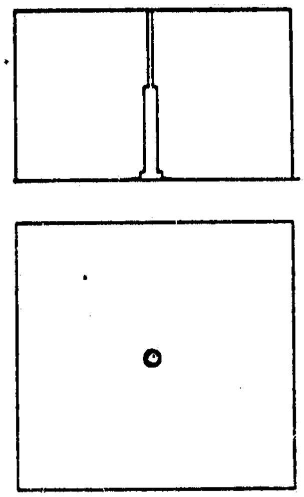

Fig. 1c Image

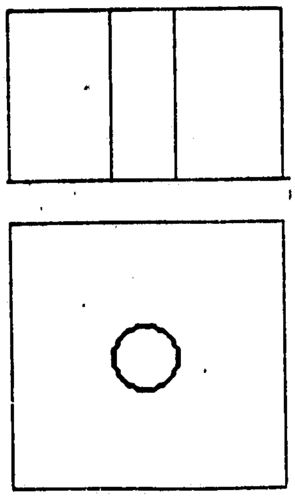

Fig. 2a Mirror, diameter = 15 units

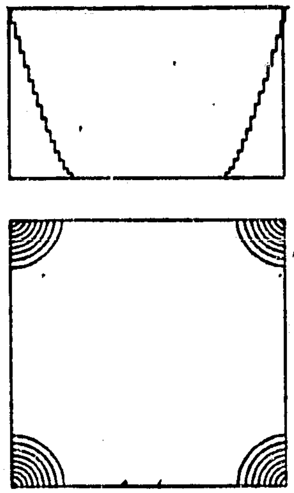

Fig. 2b Autocorrelation

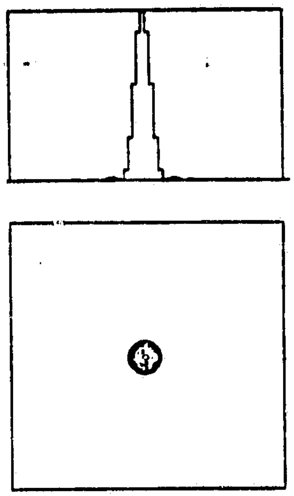

Fig. 2c Image

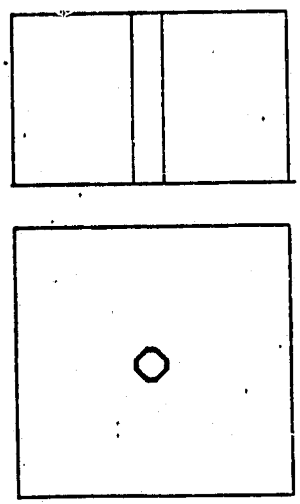

Fig. 3a Mirror, diameter = 7 units

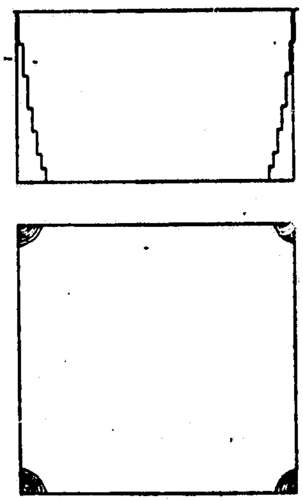

Fig. 3b Autocorrelation

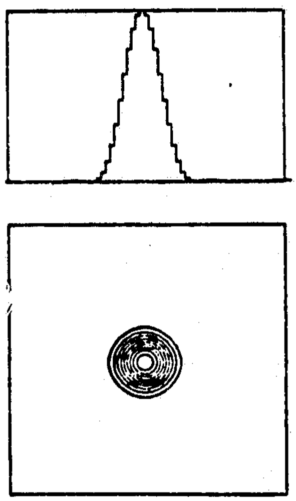

Fig. 3c Image

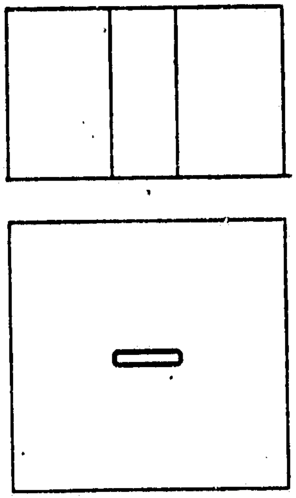

Fig. 4a Linear aperture at 0 degrees

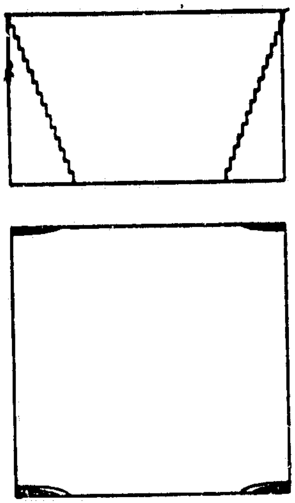

Fig. 4b Autocorrelation

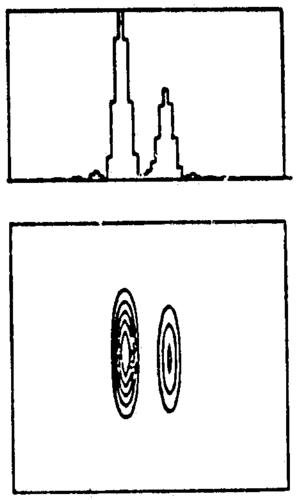

Fig. 4c Snapshot image

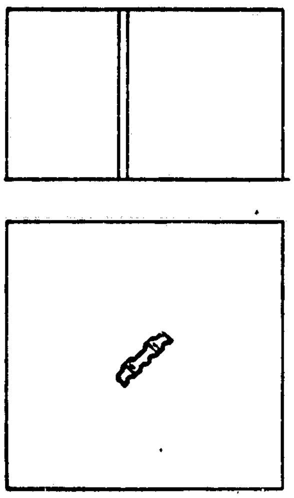

Fig. 5a Linear aperture at 45 degrees

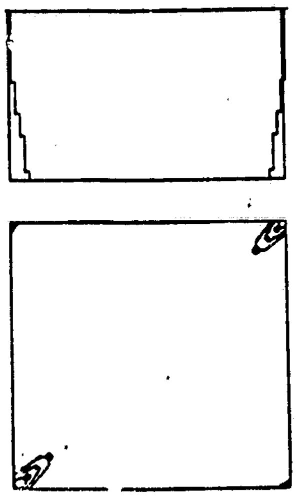

Fig. 5b Autocorrelation

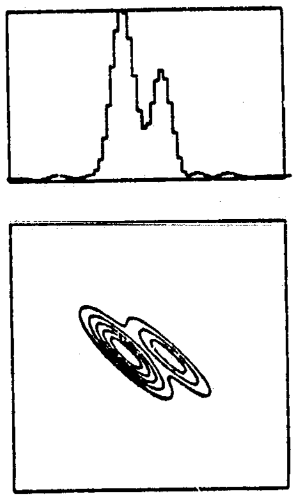

Fig. 5c Snapshot image

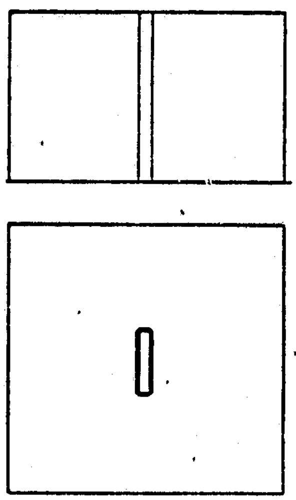

Fig. 6a Linear aperture at 90 degrees

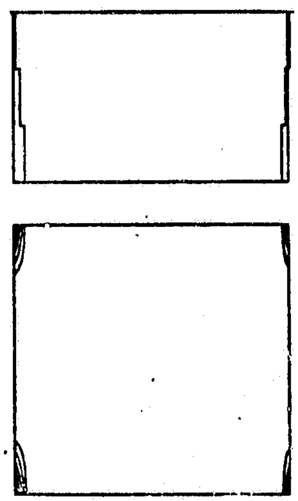

Fig. 6b Autocorrelation

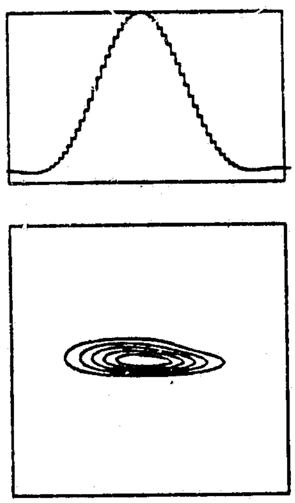

Fig. 6c Snapshot image

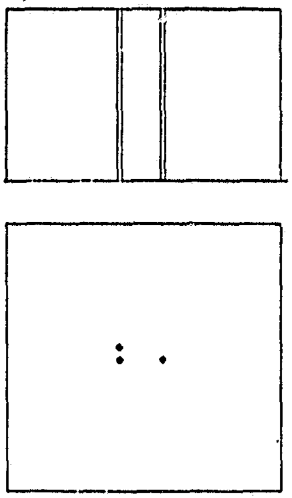

Fig. 7 Three point-like stars

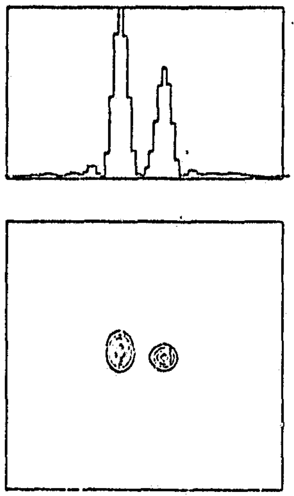

Fig. 8 Reconstruction using 8 angle views and a 3 x 15 array

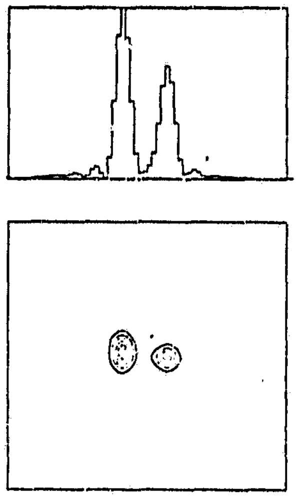

Fig. 9a Reconstruction using 16 angle views, and a 3 x 15 telescope

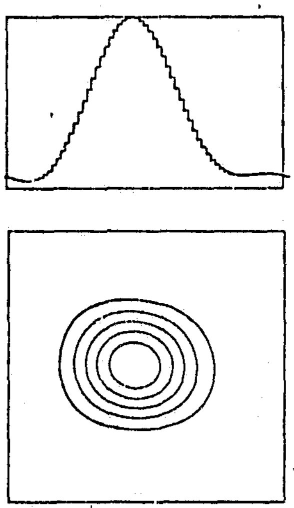

Fig. 9b Single image using one 3 x 3 telescope aperture

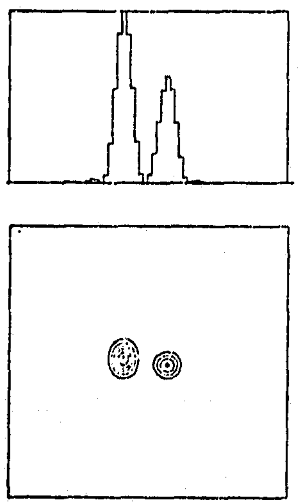

Fig. 9c Single image using one round 15 pixel aperture

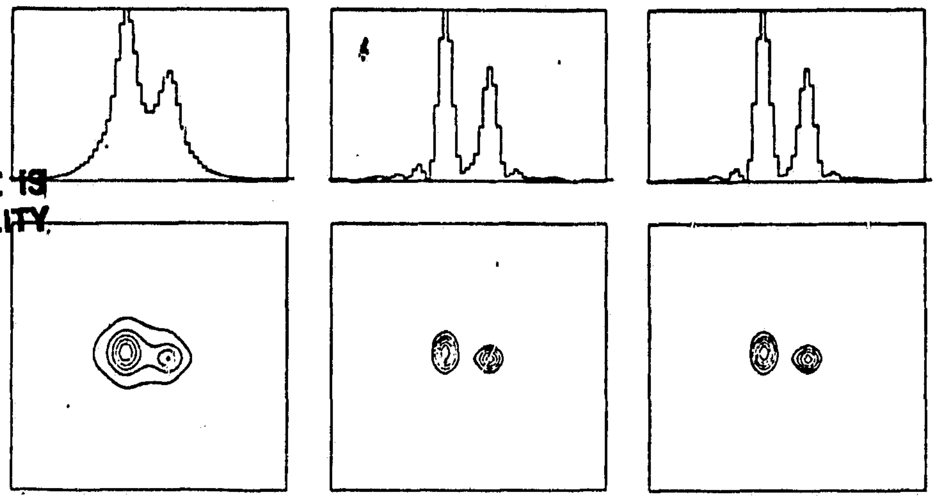

Fig. 10a Filter 0 Fig. 10b Filter 1 Fig. 10c Filter 2
Noise level = 0.0 in each case.

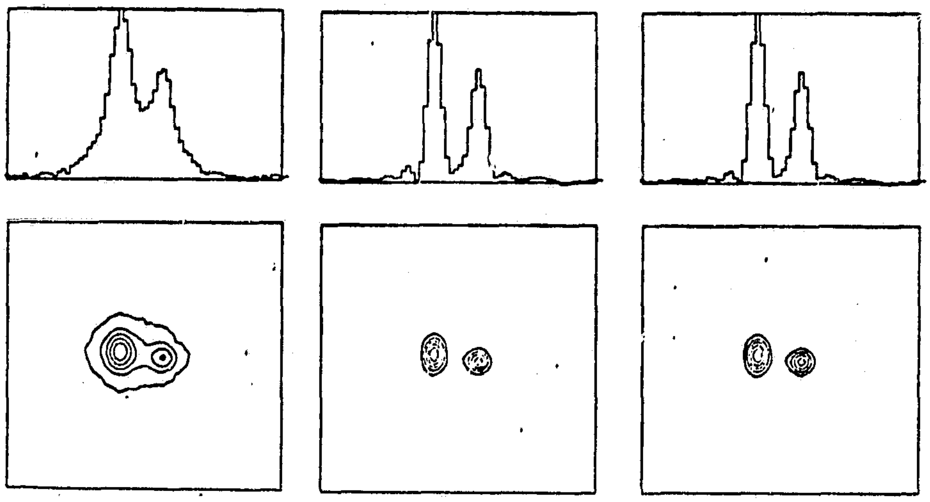

Fig. 11a Filter 0 Fig. 11b Filter 1 Fig. 11c Filter 2
Noise level = 0.1 in each case.

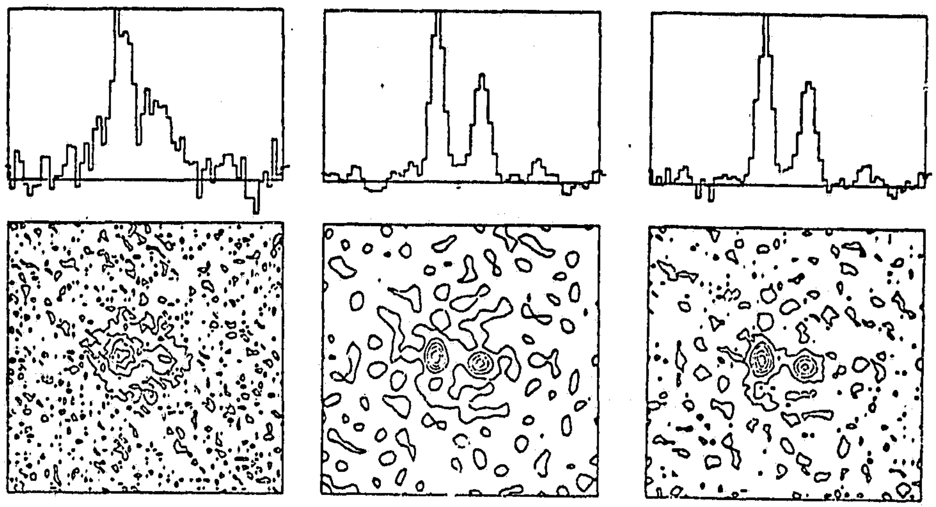

Fig. 12a Filter 0 Fig. 12b Filter 1 Fig. 12c Filter 2
Noise level = 1.0 in each case.

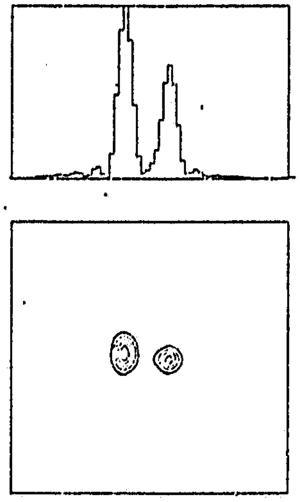

Fig. 13a Phase errors = $\lambda/10$ peak-to-peak

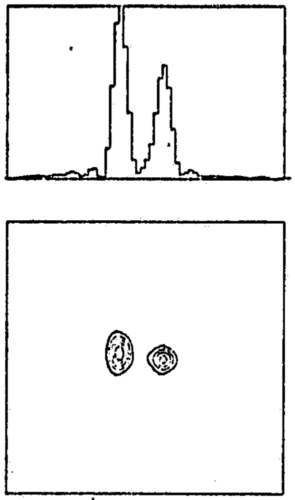

Fig. 13b Phase error = $\lambda/4$ p-p

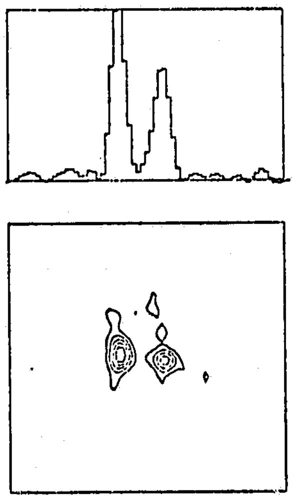

Fig. 13c Phase error = $\lambda/2$ p-p

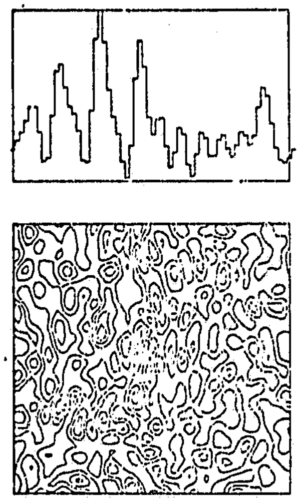

Fig. 13d Phase error = λ p-p

ORIGINAL PAGE IS
OF POOR QUALITY

Center for Astrophysics

Harvard College Observatory
Smithsonian Astrophysical Observatory

MEMORANDUM

18 January 1982
(revised version)

To: Distribution

From: W. A. Traub

Subject: Computer demonstration of the initial coherent alignment of COSMIC

1. Introduction. This memo is an illustrated demonstration of the technique by which the COSMIC telescope array can be easily aligned using a small or distant star. To start, we assume that each independent telescope module is essentially optically ideal, and that the recombination optics and detector are likewise ideal. Initially, however, these ideal telescopes are assumed to be mutually non-coherent, so that each one is pointing in a slightly different direction and each is slightly ahead or behind its proper position with respect to the incoming wavefront.

The presentation of results here follows that in the previous memo, "first results from a crude image reconstruction computer program." Modifications to that program (CRUDE) now allow each telescope module to be tipped, tilted, and piston displaced. For each case, we show a contour diagram of the intensity in the focal plane, along with a cross-section through the focal-plane which includes the point of maximum intensity.

2. Tip-tilt correction. We start by blocking the beams from all but two of the telescopes. Taking these two to be adjacent, and square, we will initially see two sets of star images in the focal plane. The telescope can now be focussed so that each one produces images which are as small in diameter as is possible. If we look at a portion of this field of view, we will have a situation similar to that shown in Fig. 1a, where a single star appears double because the mirrors are tilted with respect to one another. We have offset the second wavefront* by one wavelength across its width for an angular tilt of λ/D, and also by the same angular amount in the perpendicular direction, for a net shift of $\sqrt{2}\ \lambda/D$, where D is the mirror dimension.

To combine the images, it is easy to see that a telescope operator can reduce the error to essentially zero along one axis without much difficulty, bringing us to the state shown in Fig. 1b. Here we see interference patterns developing in the overlap region. Successive tilts in the remaining direction produce the images shown in Figs. 1c, d, e, and f, going to tilts of (0.5, 0.25, 0.125, and 0.0) λ/D respectively.

---

*Throughout, we will refer to the state of the wavefront, rather than the state of the mirrors or other optical components. Thus a wavefront tilt of λ/D will be produced when the primary mirror is tilted by 0.5 λ/D, and likewise for piston errors.

3. Monochromatic piston correction. The telescopes in Fig. 1 had no piston displacement, i.e. we assumed coincident arrival of wavefronts in the focal plane. If there had been, say piston error of 0.5λ, then Fig. 1a would still fairly accurately describe the images since they do not yet overlap, but bringing the tip-tilt errors to zero will produce the result in Fig. 2a, rather than that in Fig. 1f. The "double image" in Fig. 2a is an artifact produced by the exact cancellation of amplitudes at the position where the star should ideally have been imaged. As we reduce the piston error to $(0.25, 0.125,$ and $0.0)\lambda$ we find that one of the images grows at the expense of the other, and that the peak intensity shifts toward the expected star position.

4. Combined tip-tilt and piston correction. The first two mirrors (or telescope modules) are now perfectly aligned. In general, of course, both tip-tilt and piston errors will be present together. However it is not necessary to demonstrate the simultaneous correction of both conditions because it is clear from Fig. 1a that we can immediately determine the tip-tilt error simply by measuring the offset between images and doing a one step correction, which takes us immediately to Fig. 2a.

5. Polychromatic piston correction. In monochromatic light the piston correction can only be made modulo one wavelength; but it is also reasonable to expect that if we use a wide spectral band we can reduce the error to at most a very few wavelengths, since we then have the combined leverage of the longest and shortest wavelengths to produce the sharpest possible image. As an example, suppose that the mechanical integrity and structural stability of the COSMIC array is such that we can assume each wavefront to be within a piston displacement $p \gg \lambda$ of the ideal position.

Then using a filter to generate monochromatic light, and following the correction steps shown in Figs. 1 and 2, we adjust the piston position of the second wavefront by an amount $< 1.0\lambda$. If we define $n = p/\lambda$, there are approximately $n \gg 1$ different positions where we will get about the same image quality, and these positions are spaced by λ. Suppose that the accuracy of positioning is $\varepsilon\lambda$, where $\varepsilon \ll 1.0$; comparison of Fig. 2c with 2d suggests that $\varepsilon \simeq 0.1$ is appropriate. This argument can also be used to show that the spectral purity of the nominally monochromatic beam does not have to be any better than $\Delta\lambda = \varepsilon\lambda$, which is easy to produce with an interference filter or a circular variable filter.

We now use a different filter to select a second wavelength λ_2, where λ_2 differs from the first wavelength λ by a fractional amount given by the quantity ε, so that $\lambda_2 \simeq \lambda(1.0 + \varepsilon)$. In general this will require a slightly different piston correction, again $< 1.0\,\lambda_2$. Now the number of possible positions where both λ and λ_2 give good images is reduced to approximately εn, spaced by $\lambda_2/\varepsilon \simeq \lambda/\varepsilon$.

If we repeat this process with a third wavelength $\lambda_3 \simeq \lambda\ (1.0 + 2\varepsilon)$, we will again increase the spacing between acceptable piston displacements to approximately λ/ε^2, i.e., another factor of $1/\varepsilon$. If we carry out this process a total of m times, we will increase the spacing between acceptable piston spacings to about $\lambda/\varepsilon^{m-1}$; we can stop when this quantity grows as large as the original positional uncertainty p, so we have $\lambda/\varepsilon^{m-1} = p$.

If we use the above estimate that $\varepsilon = 0.1$, and take $\lambda = 0.5$ micron and $p = 5$ mm (say), then we require $m = 5$. Thus we need 5 different filters centered at wavelengths 0.50, 0.55, 0.60, 0.65, 0.70 microns. Equivalently, it is likely to be true that we could simply use a single wide band ranging from 0.50 to 0.70 microns and sweep the mirror through the full adjustment range of 5 mm, searching for the minimum image width or brightest central peak.

6. Multi-mirror corrections. The procedures described above will bring two adjacent mirrors into essentially perfect alignment; remaining imperfections are clearly below the level of measurement, and are therefore unimportant. The other telescope mirrors can be aligned in succession. For example, the first mirror could be shuttered, and mirrors number two and three co-aligned, then three and four, etc. Uncovering all mirrors together should yield a well-aligned telescope array, with further minor adjustments needed only to eliminate any accumulated errors.

It may also be possible to devise even more automatic schemes whereby we perturb each mirror control element by a fixed amount, measure the image, and then calculate the complete correction needed, using a matrix inversion (for the linearized case) or an inverted image formation program (for the more general case). In the ideal case, of course, a single image measurement should suffice in order to generate the full correction needed, but this is not likely to be stable in the presence of noise. Nevertheless, these cases all deserve further investigation.

WAT:jv

Distribution:
- N. P. Carleton
- W. F. Davis
- H. Gursky, MRL
- M. Nein, MSFC
- R. Taylor

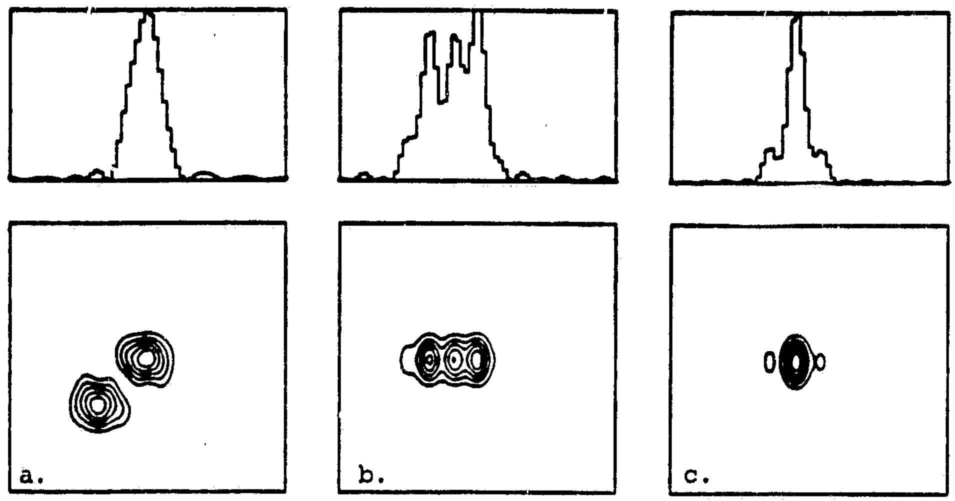

Fig. 1. Images from a single star, as formed by two adjacent telescope mirrors, each 7 by 7 elements in size, with second wavefront tipped and tilted with respect to the first mirror.

(a.) Tilt-tip from edge-to-edge of second wavefront is one wavelength (1.0λ) on each axis, so image splits in two parts, such that the first (reference) mirror's image remains centered.

(b.) Up-down tip on one axis restored to zero (0.0λ), with other axis tilt remaining at one wavelength (1.0λ).

(c.) Tilt reduced to 0.5λ.

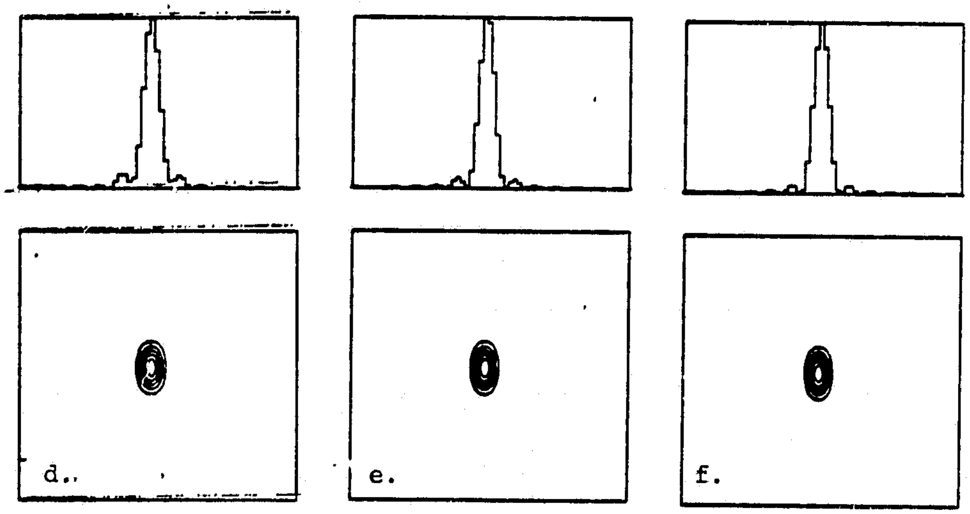

(d.) Tilt reduced to 0.25λ.

(e.) Tilt reduced to 0.125λ.

(f.) Tilt reduced to zero (0.0λ); note that, as may be expected, Figs. 1(e) and (f) are very similar.

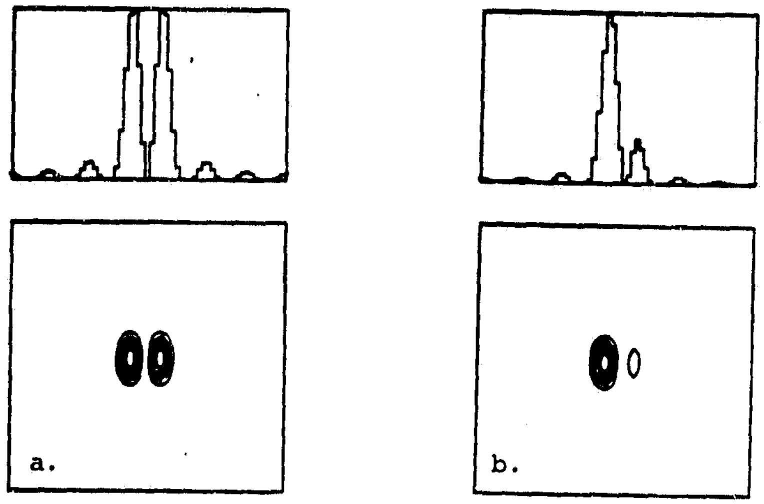

Fig. 2. Images from a single star, as formed by two adjacent telescope mirrors, each 7 by 7 elements in size, with second mirror displaced toward the star (i.e. a piston error) with respect to the first mirror.
(a.) Piston error of one-half wavelength (0.5λ) in the wavefront.
(b.) Piston error reduced to 0.25λ.

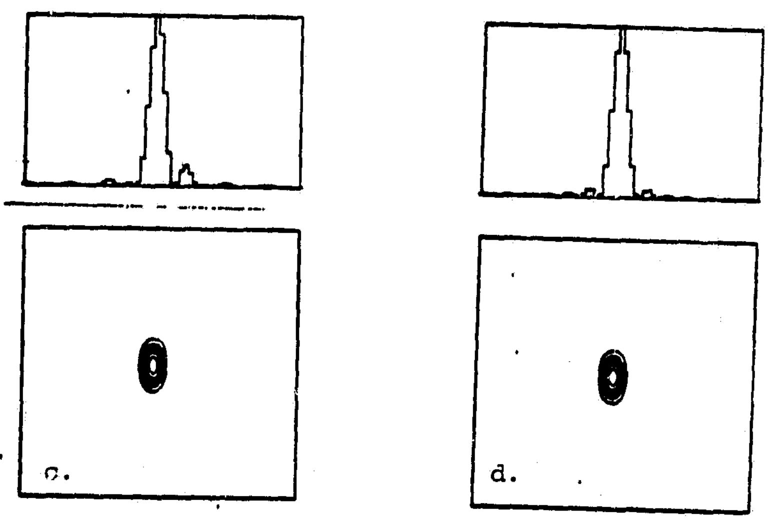

(c.) Piston error reduced to 0.125λ.
(d.) Piston error reduced to zero (0.0λ).

Memo

To: Distribution January 25, 1983

From: W. A. Traub

Subject: Lab demonstration of image reconstruction

This is a brief account of the first laboratory simulation of COSMIC, with computer reconstruction of the image. The work was done in August and September 1982, with Drs. J.Geary and N. P. Carleton in the lab and John Lavagnino at the computer.

Optics. The optical set-up is shown in Fig. 1. The light box, aperture slit, lens and CCD camera were clamped to a simple triangular-cross-section optical bench. The wood light box contains a low-wattage incandescent frosted bulb, run at 110 volts. The object mask is a 6 by 12 mm T-shaped slot milled in a thin sheet of brass, and backed by a piece of diffusing glass. The object mask and lens are separated by about 1067 mm. The aperture slit is from a lab monochromator, formed by evaporated metal jaws on glass; the width is 102 ± 2 μm and length is 534 ± 12 μm. The aperture slit mount can be rotated about the optical axis, and set by reference to an azimuth grid of polar coordinate paper taped to the mount. A blue-transmitting filter follows. The camera uses a multi-element f/5.6, 135 mm Componan Schneider-Kreuznach lens. The CCD is a thinned, back-illuminated RCA 320-by-512-element device, with 30 μm pixels, and essentially no dead space. The chip is located behind a window in an evacuated space, and is cooled by connection to an LN_2 reservoir to about 150 K.

Exposure. With the slit removed, the lens is first focussed at full aperture. With the slit inserted, the image is only slightly blurred in the 534 μm direction, but strongly blurred in the 102 μm direction. Eighteen frames are exposed at slit rotation increments of 10 degrees. Each frame consists of a short bias exposure and a long object exposure, in any order, summed on the CCD chip. The bias exposure is 1/30 sec, with the slit assembly removed, the object blocked, and the camera illuminated by dim room light scattered from a white surface; the bias level amounts to about 100 counts/pixel, and is needed because there is a loss of almost this amount in the camera readout. With the slit in place, the object exposure is 120 sec, giving a peak intensity of about 8000 counts/pixel. A flat field exposure is also made, like the bias exposure, but with a higher light level; the average intensity is 12000 counts/pixel. The conversion factor is 1 count $\simeq$ 30 electrons.

The 18 frames are spread over 2 days, since 5 of the original frames are contaminated by a ghost. A 15 degree tilt of the filter throws the ghost out of the field. The 18 useable frames are flat-fielded with standard Nova software. Readout defects affecting several columns outside the main image are removed by local averaging.

The centering is slightly different on the 2 days. From direct images without the slit, the first group appears to be centered at (row, column) = (208.5, 205(+)), and the second group is centered at (218(+), 204.5). A 256 by 256 pixel array is selected from each frame, centered at (208, 205) for the first group, and (218, 204) for the second group. There is thus some residual centering difference between the groups. The Nova images are recorded on tape for subsequent processing.

Reconstruction. The resulting clean, centered images are manipulated and displayed on the I^2S/VAX system. All images are first reduced to 128 by 128 pixels, by binning groups of 2 by 2; this is done to accommodate the finite storage space in the Array Processor.

The reconstruction algorithm needs to know the aperture shape, size, and orientation for each exposure. In our discrete Fourier transform approximation, with 128 points in each dimension, a rectangular function of width W pixels has a DFT which is a sinc^2 function having zeroes spaced at multiples of p_o = 128/W pixels. Thus the recorded image is (ideally) the convolution of this sinc^2 function with the geometric-optics image.

We determine W by measuring the relative positions of the 1st and 2nd secondary maxima in a selected image, where the object axes are conveniently aligned with the pixel axes. As sketched in Fig. 2, the diffraction pattern is

$$(\sin \pi p/p_o)^2/(\mu p/p_o)^2. \tag{1}$$

The first zero occurs at pixel

$$p_o = (\lambda/d)f \tag{2}$$

where f is the distance from the lens to the image:

$$f^{-1} + (1067)^{-1} = (135)^{-1}, \text{ or } f = 155 \text{ mm.} \tag{3}$$

From 7 measurements of various secondary maxima at positions

$$p(\max) = (\text{integer} + 1/2)p_o \tag{4}$$

we find

$$p_o = 23.90 \pm 0.76 \text{ pixel.} \tag{5}$$

Using equation (1) we calculate an effective wavelength

$$\lambda = 0.472 \pm 0.015\ \mu m. \quad (6)$$

The discrete equivalent aperture width is

$$W = 128/p_o = 5.36 \pm 0.17 \text{ pixel.} \quad (7)$$

Given the measured length to width ratio of the slit

$$535/102 = 5.24 \pm 0.16 \quad (8)$$

we calculate the discrete equivalent aperture length as

$$L = 5.24 \times 5.36 = 28.09 \pm 1.24 \text{ pixel.} \quad (9)$$

The reconstruction algorithm requires the autocorrelation function, which we usually generate from the DFT of the aperture transmission function. However since (L,W) are not whole integers, some approximation is needed. A modification to the program now allows non-integer aperture sizes, by adding a one-pixel fringe around the aperture with a fractional transmission instead of unity or zero transmission. The algorithm is also improved by a new aperture rotation scheme which searches out and eliminates gaps which occur as the aperture is numerically rotated on a discrete grid of points. However there still remains the effect that a numerically rotated aperture does not turn smoothly, but in discrete steps, generally producing a staircase profile where it should be smooth. Numerical simulations verified that the above modifications did indeed improve the quality of the reconstruction. Further simulations with a numerical point source also verified the two-dimensional analog of equation (1), as well as the fringe-pixel approximation which leads to

$$p_o W \simeq \text{const.} = 122 \text{ to } 129 \quad (10)$$

in the examples tested.

The mathematical procedure is described in Traub and Davis (1982), SPIE 332, 164-175. In Fig. 3 and 4 we show individual images at 0, 40, 90 degrees, and the final reconstructed image. Several variations of parameters were tried, none of which had any strong effect on the reconstructed image. First we tried 19 frames instead of 18, with only slight improvement. Next we tried filter 1 instead of filter 2, and it was worse, as expected. We tried various values of the cutoff parameter (ε) which prevents very small numbers from being divided by other, even smaller numbers; we found $\varepsilon = 0$ and 10^{-8} to be essentially identical, but 10^{-4} to be large enough to degrade the image noticeably. We tried changing the numerical aperture dimensions, finding +10 percent to give a slightly sharper image, and -10 percent to give a slightly poorer image. Finally we tried changing the initial offset angle of the aperture with respect to the pixel axes, and found -5 degrees to be a bit worse, +5 degrees to be a bit better, in agreement with independent estimates that +3 degrees or so would be most appropriate.

<u>Conclusion.</u> Our first laboratory demonstration of image reconstruction was remarkably successful. Many non-ideal factors entered into the process, amply demonstrating that the algorithm is immune to small perturbations. In the future, with an improved optical system, we can expect to do even better.

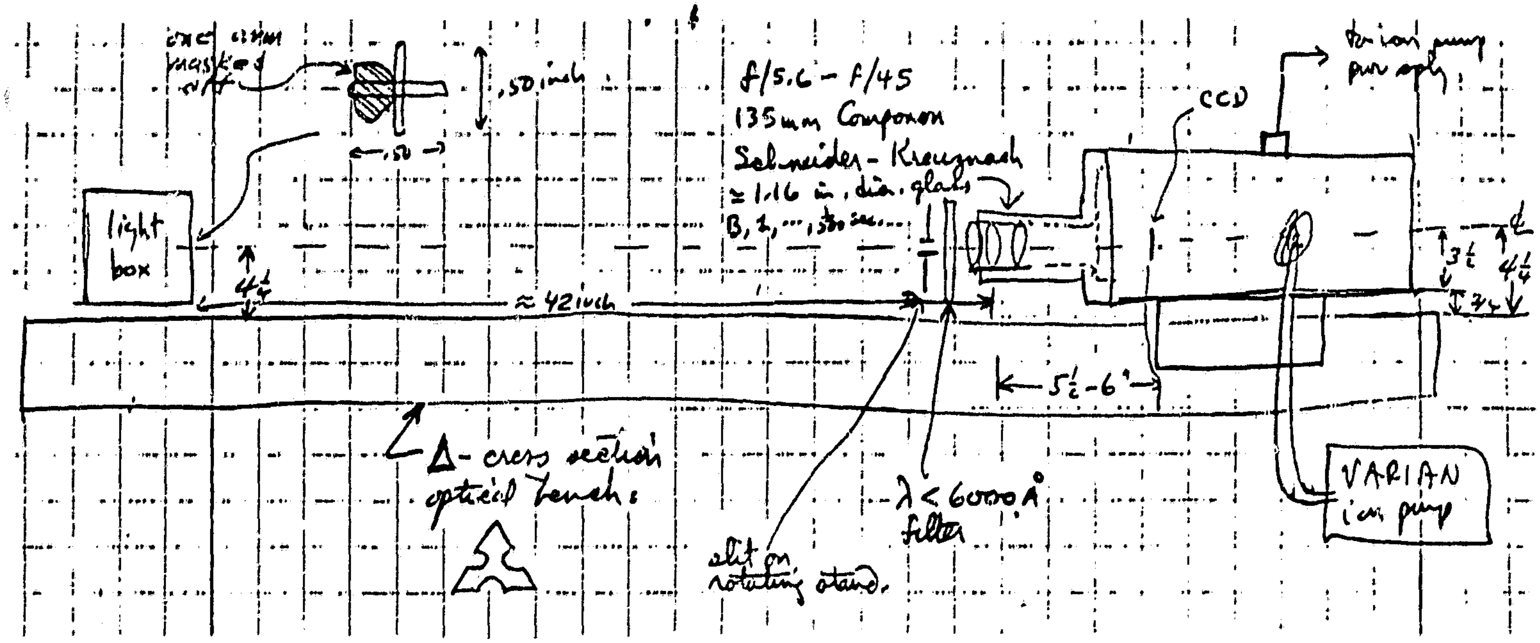

Figure 1. Optical arrangement. Starting from the back-illuminated object at the left, the light passes through the defining aperture slit, the blue filter, an imaging lens, a vacuum window, and finally falls on the CCD chip. Note that the aperture slit is not being used in strictly parallel light as would be required to simulate an astronomical telescope aperture. Also neither is the aperture coincident with the imaging lens, although it is as close as possible. Numerous glass-air surfaces in this system can contribute to ghosts, although the (untilted) filter-reflection ghost was the only major one noted.

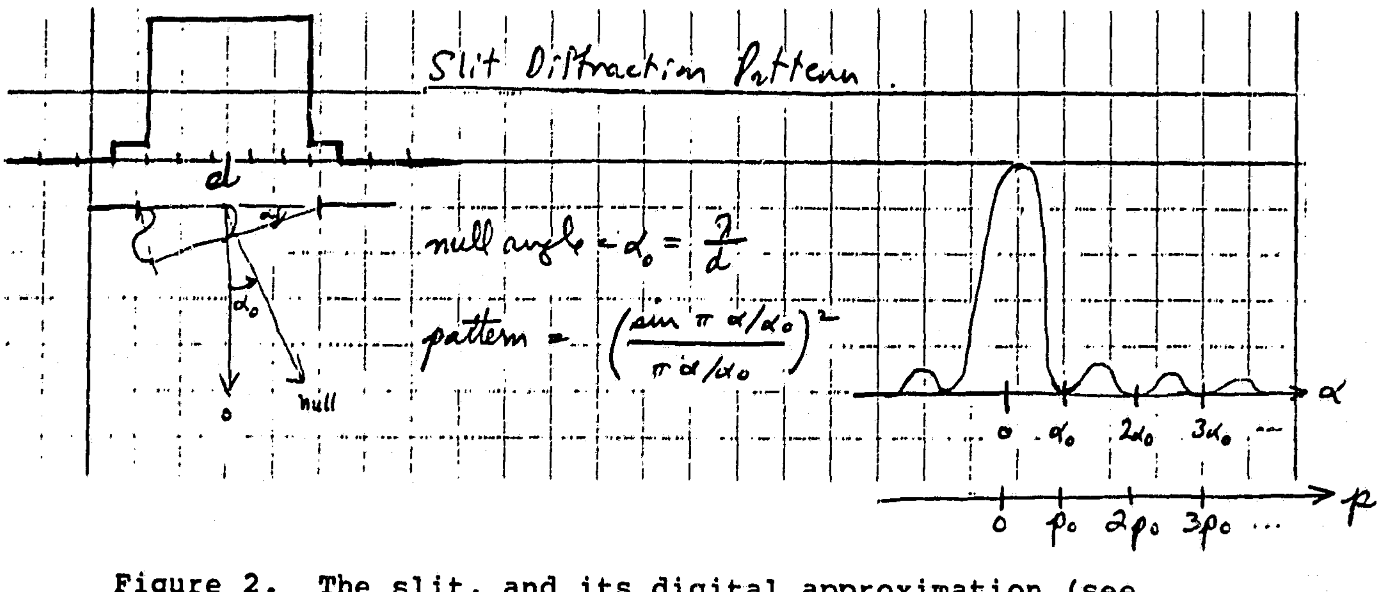

Figure 2. The slit, and its digital approximation (see text) are shown on the left. A schematic diffraction pattern with zero positions marked is shown on the right.

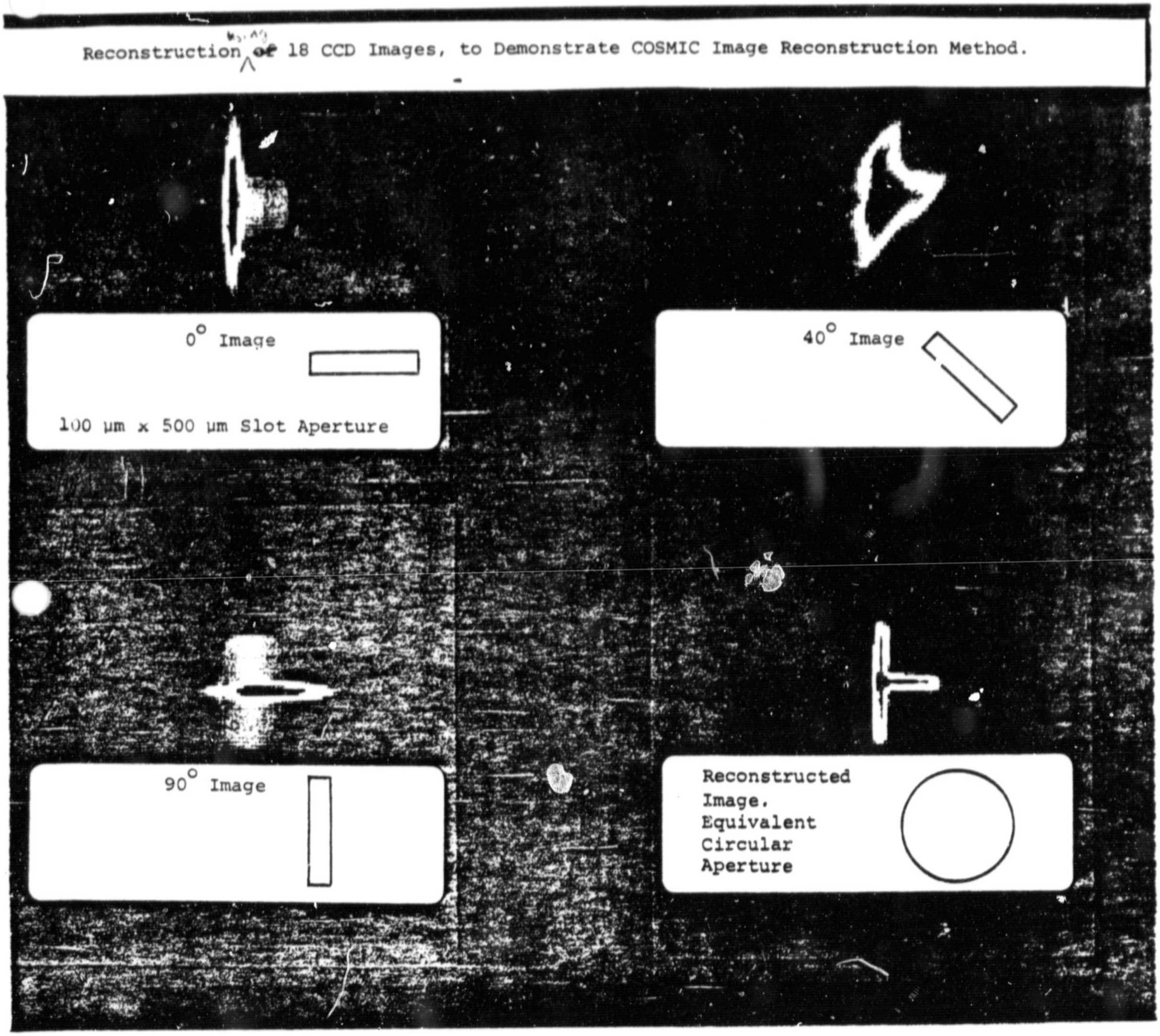

Figure 3. Images generated in the I^2S, originally rendered in false color on a transparency. The 0, 40, and 90 degree images are shown, along with the relative orientation of the aperture slit. The reconstructed image is shown at the lower right, along with the equivalent diameter circular aperture.

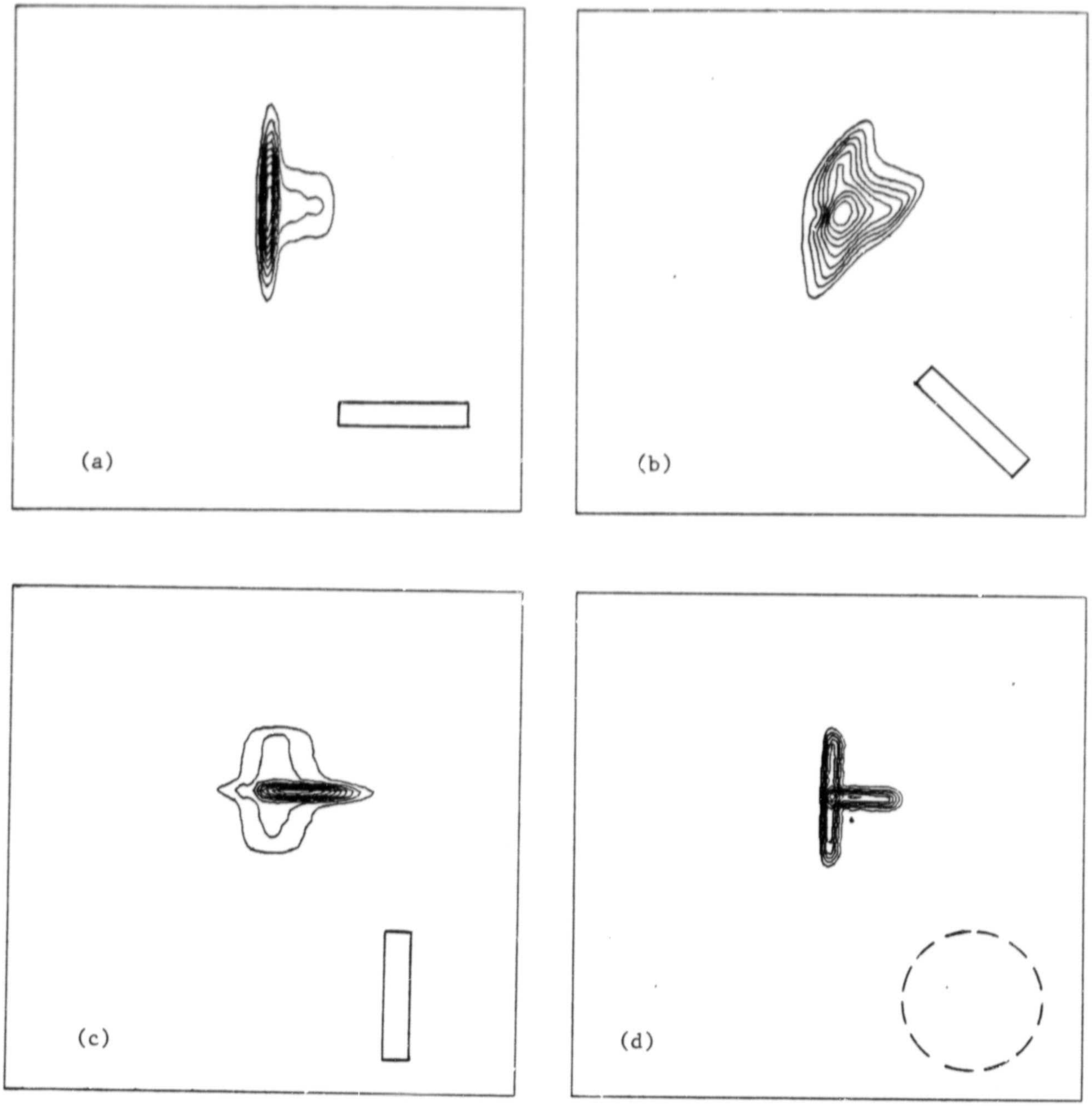

Figure 4. Contour diagrams of measured intensity are shown in (a)-(c) for the 0, 40, and 90 degree images. All contours are drawn at the 10, 20, 30,...80, 90 percent levels after subtraction of a weak background. The reconstructed image is (d), showing a small ghost feature at the 10 percent level near the inner edge of the arms.

DRAFT - NOT FOR CIRCULATION

SCIENTIFIC PROSPECTS WITH THE COSMIC TELESCOPE ARRAY

June 1982

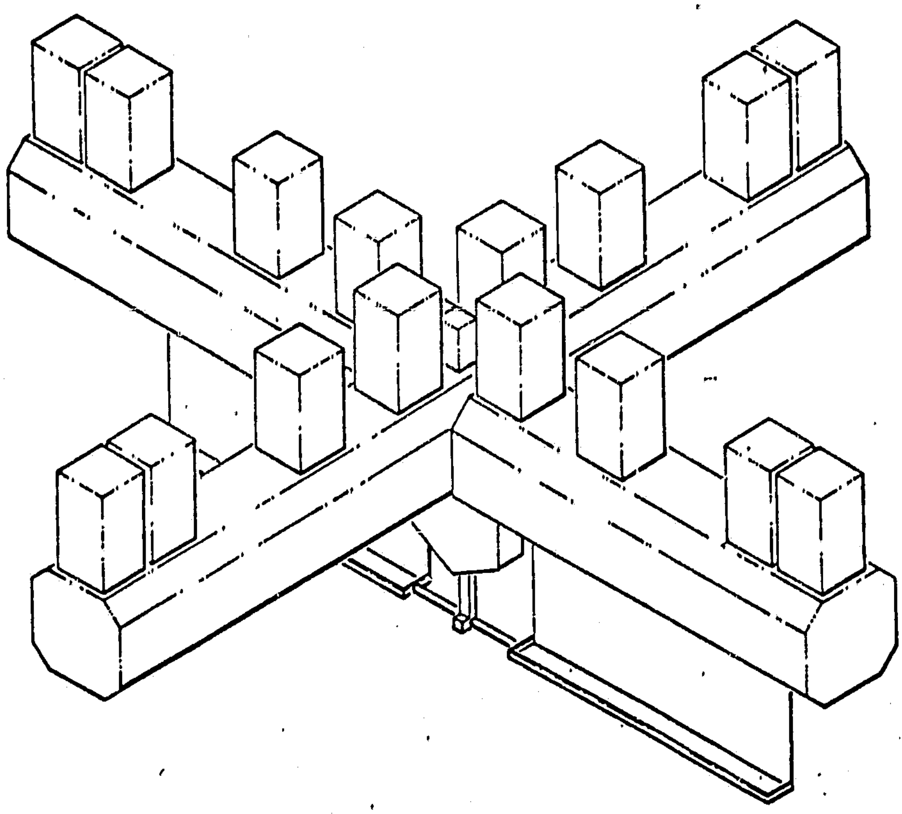

Center for Astrophysics
Harvard College Observatory and Smithsonian Astrophysical Observatory

ORIGINAL PAGE IS
OF POOR QUALITY

SCIENTIFIC PROSPECTS WITH THE COSMIC TELESCOPE ARRAY

Contributing Authors

N. P. Carleton
F. A. Franklin
M. Geller
J. E. Grindlay
J. P. Huchra
R. E. McCrosky
S. S. Murray
R. W. Noyes
M. J. Reid
R. Stachnik
L. P. van Speybroeck
M. V. Zombeck

Edited by W. A. Traub

Contents

Cover: General view of the full cruciform configuration of COSMIC, developed during the Marshall Space Flight Center engineering conceptual definition study (1981). Each of the four main arms is a telescope module which has been brought into orbit by the Space Shuttle. The fully-extended sunshades distributed along the upper surface of each telescope module are collapsed during launch. Also the downward projecting spacecraft and articulated solar panels are folded for launch. Each telescope module is sized to nearly fill the Shuttle bay (4.6 m diameter, 18.3 m length). The first telescope module to be placed in orbit will have an optical baseline of 14 m, and will be fully operational. The second telescope module will increase the optical baseline to 35 m. Third and fourth modules may be added to form a cruciform shape, although recent image reconstruction developments suggest that the cross arms may not be needed. Each telescope module is capable of supporting 7 collecting mirrors, each 1.8 m across (square as shown, or round); only 4 of the 7 possible telescopes in each module are shown, and these are arranged in a minimum redundancy configuration, although ideally of course all available positions will be utilized. A diffraction limited image of the sky is formed in a centrally located focal plane, which is instrumented with cameras and spectrometers analogous to those in Space Telescope.

SCIENTIFIC PROSPECTS WITH THE COSMIC TELESCOPE ARRAY

INTRODUCTION

In this paper we discuss for the first time a selected number of unique astronomical observations which would be possible with an orbiting telescope having both a large collecting area and an angular resolution in the milli-arc-second range. Most of these observations will allow us to study at firsthand phenomena for which we currently have little or no direct evidence. In many cases we will finally be able to resolve objects on an angular scale such that significant new features and new events can be seen, vastly enhancing the opportunity for discovery. In other cases we will be extending to a much greater distance our present capabilities for both isolating individual objects and making morphological measurements, so we will be able to study a significantly increased fraction of the universe at the same level that we can now with relatively nearby objects.

The COSMIC telescope array has been specifically designed to investigate the class of problems described in this paper. COSMIC stands for coherent optical system of modular imaging collectors. In particular we envision a linear array of orbiting telescopes held in a rigid framework which rotates about its line of sight, sweeping out an equivalent diameter circular aperture. All telescopes feed a common focal plane where a diffraction-limited image is formed when the optical path lengths are adjusted to be within a quarter wavelength. For resolvable stellar surfaces a narrow band filter or attenuator will be used to avoid detector saturation; otherwise broad-band imaging will be the normal mode of operation. The instantaneous diffraction-limited image of a point source is narrow along the array's major axis only, but by using an already demonstrated image reconstruction technique it will be easy to build up fully resolved images after a 180 degree rotation of the array, even in the presence of noise and optical imperfections. A 1981 conceptual definition study of COSMIC by engineering personnel at Marshall Space Flight Center established that the overall concept was viable using currently available or anticipated technology. Focal plane instrumentation could be similar to that now being built for Space Telescope in that both cameras and spectrometers can be provided, the latter taking advantage of the slit-like nature of the imaging point response function. Rapid read-out of the focal plane will ease spacecraft pointing requirements, now expected to be less stringent than for Space Telescope.

For concreteness, this report considers a COSMIC telescope array which is 35 m in length, brought up in two shorter sections by two Space Shuttle flights, although useful science can be done with only the first section in place. There are up to 14 collecting mirrors, each 1.8 m in diameter, feeding a central focal plane. The wavelength range is roughly 0.3 μm to 1.1 μm; at the short wavelength end this corresponds to an angular resolution λ/D = 1.8 milli-arc-sec, and in the visible the resolution is 3 milli-arc-sec. The array is a natural follow-on for Space Telescope, since it has about 28 times better angular resolution and 8 times greater collecting area. We expect that the limiting magnitude for COSMIC will be in the neighborhood of $m_v = 29$, for about 100 counts in a one hour observation.

The observing programs in this report were selected by the contributing authors from the perspective of their current research activities. Each of these programs has requirements in angular resolution and collecting area which go beyond the capabilities of Space Telescope. The only fundamental limitation is one which is common to all high angular resolution telescopes, including ST and VLBI, viz., the minimum detectable surface brightness increases as the angular resolution element decreases. Fortunately in the visible, as in the radio, there are a large number of classes of objects with intrinsically high surface brightness in the milli-arc-sec size range. The enhanced angular resolution of COSMIC will finally allow us to cross that boundary which separates our present status, where most astrophysical objects appear either as point sources or as hopelessly smeared images, from our potential future status, where a vast number of objects will become well enough resolved that we can begin to understand their true nature.

COMETS

Comet nuclei are thought to have diameters of from 1-10 km. Because of this small size and because of the difficulty in distinguishing between the solid nucleus and the bright, inner coma, there has not been a definitive, unambiguous measurement of a nucleus. Radar observation can give useful limits on the radar cross-section. Full scale COSMIC resolution capabilities should be adequate to resolve the nucleus of a comet passing within about 0.2 A.U. of Earth if the contrast between the nucleus and the coma - which will be fully developed at that heliocentric distance - is sufficiently high. COSMIC will also be able to detect and measure the velocities of comet nuclei which have split during perihelion passage.

COSMIC will permit detailed studies of the growth and activity of the inner coma. This includes: the formation, velocity and, possibly, the "hot spot" location of jets; the velocity field in the coma as displayed by any bright feature; and the evolution of the molecular species from the time gas is emitted from the surface until an equilibrium is reached.

ASTEROIDS

Radii of asteroids are normally obtained by a combination of visual and far-infrared photometry. Confirmation and/or calibration of these somewhat indirect results by direct measurement is important.

The COSMIC telescope will permit us to examine those asteroids for which there is some evidence of a bound companion.

Earth-bound observations of asteroids are limited to whole-disk measurements. Petrological or mineralogical differences between asteroids are apparent from narrow-band spectrophotometric measures. The periodic light variations seen in broad-band photoelectric photometry are probably due to irregular shapes rather than inhomogeneities in the surface composition but the two effects can not be separated in most asteroids by currently available observing procedures.

Assuming a mean perihelion distance of 2.5 A.U. for main belt asteroids and an albedo of 0.2 (measured albedos range from 0.05 to 0.4), the resolution element in the visible would be 3.2 km with a brightness of $m_V \approx 19$ per resolution element. Significant observations could be made on most of the numbered asteroids as displayed in the following table.

Perihelion magnitude	No. of cases	No. of resolution elements per diameter
15 - 16	672	25
14 - 15	666	60
13 - 14	364	160
<13	397	>270

Twelve of the asteroids included in the table are Amors with perihelion approaches to the earth of 0.2 A.U. or less and, in addition. there are 19 Apollos with still smaller approach distances. For these bodies, the resolution element will be in the range 100-400 meters. Apollos and Amors hold a special significance in that they, or still smaller bodies in similar orbits, are the source of meteorites. The question of their ultimate origin - asteroids, comets, or both - is unresolved. If, as believed by some, the Apollos include extinct cometary nuclei, the best hope for studying these lies in high resolution observations by COSMIC.

JUPITER

It would be possible with COSMIC to measure the shapes and rotation rates of the larger of the outer satellites J6 - J12. Time-dependent observations of Io and studies of Jupiter's atmosphere could also be carried out, since 1.8 milli-arc-sec at Jupiter corresponds to about 5 km resolution, which is comparable to some of the highest resolution images obtained by Voyager 2; for reference, the volcanic plumes on Io are about 100 km high.

SATURN

Two particular dynamical problems in the Saturnian system require high resolution astrometry.

(a) Positions of the two "co-orbital" satellites, 1980 S1 and 1980 S3. These two can be observed from the earth only at the time of ring plane passage (every 15 years). Accurate relative positions will provide the sum of the masses of the two bodies thanks to their unique "co-orbital" motion.

(b) Hyperion, S8, is a very irregular body whose long axis, apparently, points toward Saturn. This satellite moves in an orbit with an eccentricity of ~ 0.11 so that a libratron should occur. Measurement of this libratron provides a knowledge of the moment of inertia ratio of the body.

PLUTO

A detailed survey of the Pluto system would provide us with the planet's radius, rotation rate and axial orientation; it would also allow us to improve the orbit of, and possibly measure the radius of, its recently discovered satellite. Reliable values for these quantities are unobtainable by other means - i.e. although Voyager flights may provide such material for Uranus and Neptune, no encounters with Pluto are scheduled.

MAIN SEQUENCE STARS

A prototypical main sequence star, α Cen, has an angular diameter of about 10 milli-arc-sec, so one should be able to detect (using a narrow-band filter in the K-line, for instance) its rotation axis. It may be possible to obtain rough information on surface distribution of activity (whether, for example, emission is concentrated near the poles or the equator) and, over several years, follow crudely the "butterfly diagram" of latitude of activity versus phase in the activity cycle -- an experiment of importance for stellar dynamo theory. One might detect differential rotation (another parameter of great interest for dynamo theory) with precision sufficient to be extremely important. One could obtain information on size and shape of active regions or activity complexes. In a "magnetograph" mode, one could begin to map large-scale surface structure of magnetic fields. All of these would be extremely useful, when compared with solar behavior.

SUPERGIANTS

α Orionis has an angular diameter of 40 milli-arc-sec and reported diameters for o Cet range up to 100 milli-arc-sec. For o Cet, this implies as many as 30 resolution elements across the disk, in the visible. These M-type red giants possess very interesting and complex atmospheric structure. COSMIC may be able to answer some fundamental questions, such as whether the variability of these stars is primarily due to pulsation or temperature changes. Spectral-line VLBI observations of H_2O and SiO maser emission allow one to probe the extended photospheres of these stars in great detail. Very complex motions involving both expansion, contraction, and shocks are suggested by the data. The ability of COSMIC to obtain spectral information as a function of position on the stellar surface would greatly aid in the understanding of this class of objects. There are a wealth of features that should be searched for, including:

a) Brightness inhomogeneities on the disk due to large convective cells, predicted (Schwarzschild) to have sizes ~ 0.1 of the radius.
b) Velocity asymmetries on the disk due to the above convective motions.
c) Overall shape changes due to photospheric motions; these are already inferred from polarization studies by Daniel Hayes.
d) Chromospheric emission structure above the limb in strong lines like Ca II 8542, Hα, or others; already detections of this by speckle techniques are being reported (not yet in print).

e) Variable velocity outflow in expanding shell could be mapped using doppler-resolved imaging.

f) Radial and nonradial large-scale pulsation.

CIRCUMSTELLAR EMISSION

Emission from circumstellar material surrounding and enveloping interacting binaries is potentially a very rich field for investigation with narrow-band interferometry isolating excited lines like Hα, Ca II, O IV, etc. Much X-ray radio, UV and visual data suggest complex structure and motions. It would be extremely exciting to map this, for comparison with higher-energy data, including time development.

BINARY STARS

Although high resolution observations of binary stars may lack a certain glamour, they provide fundamental information on stellar masses. At the cost of a relatively small amount of observing time, a vast amount of fundamental information could be gathered.

GLOBULAR CLUSTERS

The milli-arc-sec angular resolution capability of COSMIC would be of special importance for studies of the highly condensed stellar cores of globular clusters. Centrally condensed globular clusters have central densities in the range $10^4 - 10^5$ stars/pc^3. Thus the typical stellar separations are only $\sim$ 0.01 parsec and would subtend an angle of 0.2 arcsec at typical cluster distances of 10 kpc. Star counts and stellar population studies can then be carried out in cluster cores with COSMIC. This could only be partially accomplished with ST because of both the more limited angular resolution and sensitivity. The extra factor of $\gtrsim$ 10 in angular resolution achieved with COSMIC will allow direct searches for visual binaries in cluster cores, since $\sim$ 2 AU separations are resolveable at

$\sim$ 1 kpc. This permits direct study of the frequency of binary systems in cluster cores. Compact binary systems are now known to exist in cluster cores since recent Einstein X-ray results have determined the mass of globular cluster X-ray sources to be $\sim 2\ M_\odot$, or consistent (only) with the sources being compact binary systems and not massive black holes. These binary systems have presumably evolved from a significant population of wider-separation binary systems formed by tidal capture, and it is these systems which COSMIC could study directly.

In addition to studying the binary problem in globular cluster cores with direct images, spatially resolved spectra (with long slits across the core) could extend the search greatly by allowing velocity variations to be measured for a large number of stars simultaneously. This is also of fundamental importance for measuring the velocity dispersions in the centers of globulars. Central velocity dispersions are now very poorly known (they are inferred from line profiles in the integrated cluster spectrum) and yet they are the most fundamental quantity of interest in describing the stellar dynamics of dense stellar systems. Again, the great improvements in both resolution and sensitivity over the ST capabilities allow much more detailed studies to be carried out, e.g., measurements of the degree of isotropy in the velocity dispersion vs. radius and velocity dispersions vs. stellar mass (i.e., spectral type) to explore the central potential.

Finally, the "classic" problem of searching for central cusps in the stellar density profile such as would arise from either a central black hole or a subcore of heavier, evolved stellar remnants (black holes, neutron stars or white dwarfs) can be carried out with COSMIC better than with any other instrument in the forseeable future. Present upper limits on the mass of central black holes in globulars (which are not, and need not, be X-ray sources) are $\lesssim 3000\ M_\odot$. COSMIC could measure the $r^{-7/4}$ density profile cusp expected around a central black hole for masses as small as $\sim$ 50-100 $M_\odot$, or significantly below the limits possible with ST. The existence of subcores in clusters, already suggested for the X-ray clusters M15 and NGC 6624, could similarly be explored and important constraints on stellar evolution and the initial mass functions of globulars derived.

ACTIVE GALACTIC NUCLEI

COSMIC is well suited for imaging of galactic nuclei (Seyferts, quasars, BL Lac objects). The structure of the central regions of AGN's - existence and possible variability of compact sources, accretion disk structure, etc. - is a topic of great current interest. Present descriptions of the source morphology are based primarily on radiative transfer modeling of spectroscopic emission line data, variability timescale arguments and poor resolution (1 arc-sec) imaging. Very few AGN are bright enough radio sources to be studied with VLBI, especially the closest objects (eg. NGC 4151 or NGC 1068) where the smallest spatial scales would be visible, so optical imaging may provide the key to understanding these objects.

Stratoscope observations (0.2 arc-sec resolution) coupled with lower resolution ground-based spectroscopy have placed some constraints on dynamical models of M31. However, models with M/L's from 0 to 50 can still be made to fit the data! Higher resolution observations ($\lesssim$ 0.05 arc-sec) can distinguish between the photometric profiles of the high and low M/L models. COSMIC can also be used to make high resolution observations of the nuclei of other nearby galaxies with a variety of morphologies.

To illustrate with a particular example, there would be great interest in studying the terminal results of emission flows onto active galactic nuclei. X-ray measurements on M87 and NGC 1275, which go down to a level of about 1 arcsecond, permit accretion flow studies down to distances of 100 to several hundred parsecs from the galactic nucleus. In this regime, there is considerable X-ray emission with temperatures falling down to a few million degrees. At closer distances, temperatures should continue to fall to the point where most of the emission is in the optical. Accreting gas would form bright filaments. It would be interesting to observe this structure on the scale of a few tenths of a parsec. Thus, the milli-arcsecond optical observations would provide a means of continuing the accretion flow studies that begins with X-rays at much larger distances.

SUPERNOVA REMNANTS

X-ray observations of galactic SNR indicate that several contain unusually bright knots that are not obviously associated with neutron stars or pulsars. The Vela SNR and MSH 15-52 are two examples containing bright knots (in addition to pulsars). It would be interesting to examine these bright knots to search for point-like components or for very fine filamentary structure that might show up in the optical.

JETS IN GALACTIC NUCLEI

Radio astronomers are now constructing images with an angular resolution from 0.0003 to 0.1 arcsec with VLBI techniques. These images have proven to be exciting and revolutionary and VLBI has become an unparalleled tool for studying the structure and origins of the great variety of bright sources in the Universe. At present, however, interpretation of VLBI images has been limited in part because high quality optical images with angular resolution better than 0.1 arcsec do not exist.

There are several cases where high resolution optical images would clearly show significant structure and greatly aid in the astrophysical understanding of the nature of the emitting objects. For example, radio jets are seen on scales from smaller than 0.001 to 10 arcseconds in objects such as QSO's, galaxies with active nuclei, and from the galactic "star" SS433. The mechanism for the radio emission is thought to be incoherent synchrotron emission. Extrapolating the synchrotron brightness to optical wavelengths suggests that many of these objects could be imaged with COSMIC. One of the most interesting extra-galactic sources, M87, appears to emit synchrotron radiation over nearly the entire electro-magnetic spectrum. It exhibits a striking radio/optical/X-ray jet emanating from the nucleus of the galaxy. VLBI images of the nucleus suggest that intensities of > 20 ergs/sec/cm**2/ sterad would be seen at optical wavelengths from a jet less than 0.01 wide and 0.2 arcseconds long; this intensity is nearly 10^4 times greater than the detection threshold for COSMIC, and should therefore be very easily detected.

SUPERMASSIVE GALACTIC CORES

Most of the problems outlined above for globular clusters can be carried out as well for the stellar clusters which are likely in galactic nuclei. A prime object for study, of course, is the nucleus of M31. Stars could be resolved if the density is as high as $\sim 4 \times 10^{7}$ pc^{-3} which is larger than required to fit the central surface brightness. In M87 stars could be resolved and counted into the nucleus at densities of $\sim 10^{4}$ pc^{-3}. This would allow measurements of the isotropy of the velocity dispersion to be made in regions where it should be anisotropic if the apparent central cusps in both density and velocity dispersion are _not_ due to a supermassive black hole. Thus COSMIC can directly probe the dynamical questions necessary to test whether active galactic nuclei and quasars are powered by supermassive ($\sim 10^{8} - 10^{9}$ $M_{\odot}$) black holes.

IDENTIFICATION OF FAINT X-RAY SOURCES

The most obvious use of the high optical resolution in conjunction with X-ray measurements is to find optical counterparts for X-ray sources which appear in deep surveys. For many X-ray sources, counterparts are too dim to be identified by present means. Very high resolution images, including color measurements (and high resolution spectroscopy, which should also be possible with COSMIC) might help us to find the counterpart or possibly to set very high lower limits on X-ray to optical luminosity and determine if the X-ray to optical ratio is evolving in the early universe. It is quite possible that the early universe contains X-ray sources with _no_ optical counterparts. In general, the X-ray positions would be very well known from AXAF or LAMAR measurements so that the small field of view of COSMIC should not be a problem. A limiting magnitude of 29 will be suitable and necessary for these observations. (Space Telescope is already needed for the Einstein deep surveys.)

EXTRAGALACTIC DISTANCE SCALE

The extension of galaxy distance measurements using Cepheids depends critically not only on light gathering power because the objects are faint ($M_V = -6$), but also on resolution because the objects are embedded in the parent galaxy. This is also true for the identification and photometry of globular cluster systems ($M_V = -10$) around other galaxies. COSMIC can be used to measure Cepheids in nearby galaxies and in galaxies as far as the Virgo and Pegasus clusters (distance modulii of 31 and 33 magnitudes respectively). It can also be used to identify and measure the globular cluster systems around galaxies as far away as the Coma cluster and possibly the Hercules cluster (100 Megaparsecs or a distance modulus of 35). Such measurements are important for studies of the large-scale dynamics of clusters of galaxies as well as for determination of the Hubble constant. Large-scale dynamical studies are a fundamental probe of the local mean mass density. Complete positional coordinates for galaxies in the flattened Local Supercluster are necessary for discrimination between the pancake and gravitational instability pictures for cluster formation.

DECELERATION PARAMETER

The morphology of the central regions of the brightest elliptical galaxies in clusters is interesting not only for the study of the dynamical evolution of such systems but also for the possible application of the angular size-redshift test to the determination of the cosmic deceleration parameter, q_o. If scale lengths in galaxies or clusters of galaxies can be used as "standard measuring rods," the determination of change in scale as a function of redshift relative to the expected Euclidean 1/r relation is a very powerful first order test of cosmological models. Brightest cluster galaxies have core-radii (Hubble profile) on the order of 1 kpc which is already smaller than 1 arc-sec at a redshift of only z = 0.1. To study galaxies at redshifts of 0.5, resolution well in excess of 0.05 arc-sec is required, so COSMIC is ideally matched to this type of observation.

ACKNOWLEDGEMENTS

We gratefully acknowledge the contribution of ideas and review comments by a number of individuals, including J. M. Moran, H. D. Tananbaum, W. H. Press, and G. B. Field. This work has been partially supported by NASA contract NAS8-33893 through Marshall Space Flight Center.

REFERENCES

The astronomical advantages of operating a large (but conventional) telescope in space have been presented in some detail in:

Longair, M. S., and Warner, J. W. 1979, editors, Scientific Research with the Space Telescope, IAU Colloquium No. 54, NASA publication CP-2111, 327 pp.

A discussion of the COSMIC telescope array may be found in:

Traub, W. A. and Gursky, H. 1980, "Coherent arrays for optical astronomy in space," in Optical and Infrared Telescopes for the 1990's, vol. I, ed. A. Hewitt, KPNO, pp. 250-262.

The mathematic basis of the image reconstruction algorithm, along with numerical demonstrations, is presented in:

Traub, W. A. and Davis, W. F. 1982, "The COSMIC telescope array: astronomical goals and preliminary image reconstruction results," in Advanced Technology Optical Telescopes, SPIE vol. to appear.

The engineering conceptual design study mentioned in the Introduction is found in:

Nein, M. E. and Davis, B. G. 1982, "Conceptual design of a coherent optical system of modular imaging collectors (COSMIC)," in Advanced Technology Optical Telescopes, SPIE vol. to appear.

Notes on Image Reconstruction for COSMIC

Part II (pp. 60-155)

Warren F. Davis

15 October 1982

Contents

WHICH, BY (155), CORRESPONDS TO $\lambda\alpha/2\pi A = 2.65 \times 10^{-6}$ RAD. INCLUDING $\theta_0 = 1 \times 10^{-6}$ RAD, THERE WILL BE AN IMAGE SAMPLE EVERY

$$\theta = 3.65 \times 10^{-6} \text{ RAD}/512 = 7.13 \times 10^{-9} \text{ RAD}.$$

THUS THE ACTUAL OVERSAMPLING FACTOR ALONG THE MAXIMUM RESOLUTION DIRECTION [$A = 15$ m] WILL BE

$$\eta = \frac{\lambda}{2\theta A} = 1.4 \quad .$$

IT WILL BE JUST POSSIBLE TO SEE THE DIFFRACTION PATTERN. THIS FACTOR IS, OF COURSE, JUST THE RATIO OF 512 ACTUAL SAMPLES TO THE 366 REQUIRED IN ν-SPACE.

ROTATION & AUTOCORRELATION OF THE APERTURE

IT IS NECESSARY TO COMPUTE THE AUTOCORRELATION OF THE APERTURE GIVEN BY (24) OR (26). IT IS ALSO NECESSARY TO DO SO FOR THE VARIOUS ANGULAR ORIENTATIONS OF THE APERTURE AS IT ROTATES ABOUT THE OPTICAL AXIS. FINALLY, FOR COMPUTATIONAL REASONS, IT IS NECESSARY TO WORK WITH DISCRETE VERSIONS OF THESE FUNCTIONS.

TO ROTATE THE AUTOCORRELATION, EITHER

a) THE APERTURE $a(\vec{r}_0)$ CAN BE ROTATED AND THEN THE FOURIER TRANSFORM OF THE SQUARED MODULUS OF THE TRANSFORM OF a [ROTATED] EVALUATED ACCORDING TO (25) AND (24)

OR,

b) THE FOURIER TRANSFORM OF $a(\vec{r}_0)$ CAN BE COMPUTED ONCE AND FOR ALL AND THE ROTATION ACHIEVED BY ROTATING FOURIER SPACE. AGAIN, THE AUTOCORRELATION [ROTATED] WILL BE THE FOURIER TRANSFORM OF THE SQUARED MODULUS OF THE [ROTATED] FOURIER TRANSFORM OF $a(\vec{r}_0)$ ACCORDING TO (24).

EITHER $a(\vec{r}_0)$ OR ITS FOURIER TRANSFORM $A(\vec{k})$ MUST BE ROTATED.

BECAUSE OF SAMPLING, BOTH APPROACHES WILL REQUIRE INTERPOLATION. WE WILL CONSIDER ROTATION [AND, THEREFORE, INTERPOLATION] IN FOURIER SPACE [CASE b)] BECAUSE THE FUNCTIONS TO BE INTERPOLATED THERE APPEAR TO BE SMOOTHER. HOWEVER, OVERALL THERE IS PROBABLY NO GREAT ADVANTAGE. WE WILL FORM THE AUTOCORRELATION USING FOURIER DOMAIN MULTIPLICATION IN ANY CASE AS THIS IS COMPUTATIONALLY MORE EFFICIENT. SINCE THIS REQUIRES COMPUTATION OF THE FT OF $a(\vec{r}_0)$, IT IS NOT UNREASONABLE TO CONSIDER ROTATION IN FOURIER SPACE.

THE FIRST QUESTION IS "ARE THE SAMPLING CONSTRAINTS ON $a(\vec{r}_0)$ IMPOSED BY ROTATION & AUTOCORRELATION USING FOURIER TECHNIQUES DIFFERENT FROM THOSE IMPOSED BY IMAGE RECONSTRUCTION GIVEN ABOVE AND, IF SO, WHY?"

CONSIDER A RECTANGULAR APERTURE IN ONE DIMENSION OF WIDTH A.

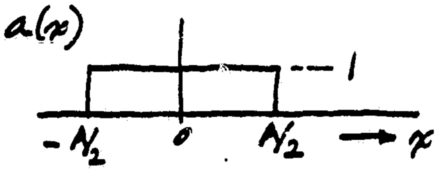

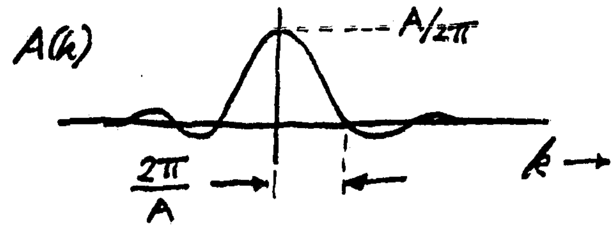

AT THE RIGHT IS SHOWN $A(k)$ WHICH, IN ONE DIMENSION IS, FROM (25),

$$A(k) = \frac{1}{2\pi}\int_{-\infty}^{\infty} a(x)\, e^{-ikx}\, dx = \tag{175}$$

$$= \frac{A}{2\pi}\;\frac{\sin\left(\frac{kA}{2}\right)}{\left(\frac{kA}{2}\right)}$$

NOTE THAT $A(k)$ DIFFERS FROM THE FT OF $a(x)$ BY THE FACTOR 2π WHICH DOES NOT APPEAR BEFORE k IN THE EXPONENTIAL [AS WELL AS BY THE OVERALL SCALE FACTOR OF $1/2\pi$].

SAMPLING OF $a(x)$ BY THE SERIES

$$\sum_{m=-\infty}^{\infty} \delta(x - mX) \tag{176}$$

IS EQUIVALENT TO CONVOLUTION OF $A(k)$ WITH

$$\frac{1}{X}\sum_{m=-\infty}^{\infty}\delta\left(k-\frac{2\pi m}{X}\right) \quad . \tag{177}$$

THAT IS, (177) IS THE TRANSFORM OF (176) WHERE THE TRANSFORM IS DEFINED BY (175). (177) IS A SERIES OF δ-FUNCTIONS AT INTERVALS $2\pi/X$ IN k.

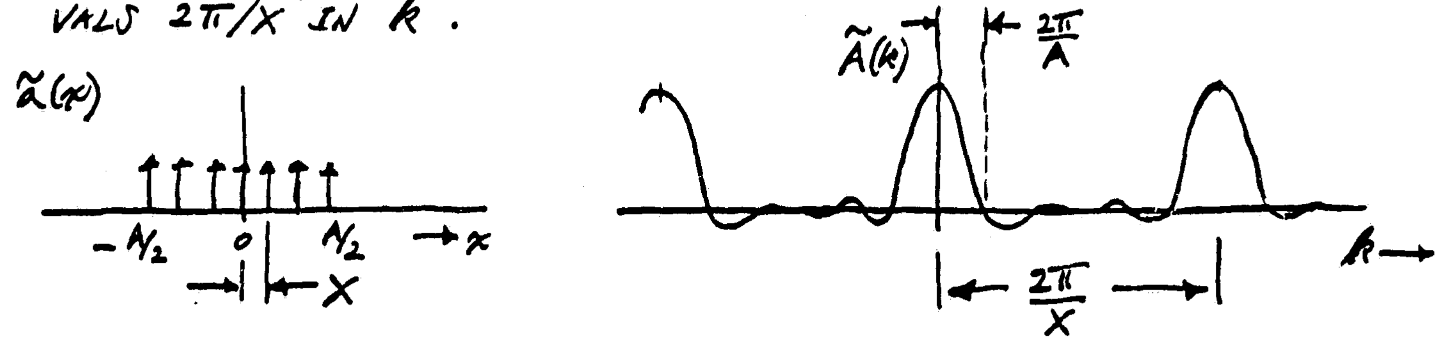

TO AVOID ALIASING IN k-SPACE WE WOULD LIKE THE ENVELOPE OF THE SINC FUNCTION (175) TO BE ATTENUATED BY SOME SUBSTANTIAL FACTOR α AT THE POINT AT WHICH SINC CAN BE TRUNCATED. THE TOTAL WIDTH OF THE [TRUNCATED] SINC FUNCTION, THAT IS TO SAY THE PERIODICITY IN k-SPACE, WILL BE TWICE THIS VALUE. WE REQUIRE THEN THAT

$$\frac{1}{\left(\frac{kA}{2}\right)} = \frac{1}{\alpha} \quad \text{OR,} \quad k = \frac{2\alpha}{A} \tag{178}$$

WHICH IS THE "ONE-SIDED" CHANGE IN k TO REACH THE $1/\alpha$ POINT OF THE ENVELOPE. THE TOTAL WIDTH WILL BE TWICE THIS VALUE

$$\frac{4\alpha}{A} = \frac{2\pi}{X} \quad \text{OR,} \quad X = \frac{\pi A}{2\alpha} \tag{179}$$

FOR $A = 1.8$ m AND $\alpha = 100$, $X = 2.82$ cm. THIS IS A MUCH CLOSER APERTURE SAMPLING INTERVAL THAN THAT DERIVED EARLIER BASED ON THE REQUIREMENTS OF IMAGE RECONSTRUCTION AND WE MUST INVESTIGATE WHY THIS IS SO.

CONSIDER (174) FOR X BASED ON IMAGE RECONSTRUCTION. IN PARTICULAR

CONSIDER THAT THE FIELD OF VIEW IS ALLOWED TO BE ZERO. I.E., $\theta_0 = 0$. THEN $X = 2\pi A/\alpha$ WHICH IS 4 TIMES THAT JUST DERIVED.

THIS FACTOR OF 4 COMES ABOUT FOR TWO REASONS, EACH OF WHICH CONTRIBUTES A FACTOR OF 2. BELOW IS REPRESENTED SCHEMATICALLY THE TWO PROCESSES INVOLVING THE APERTURE.

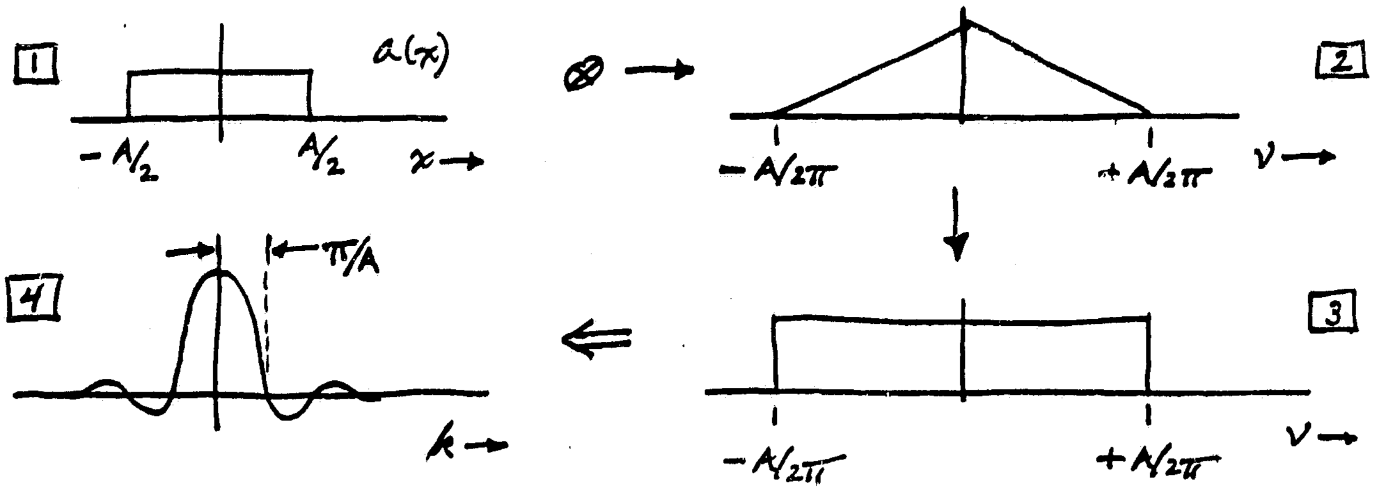

IMAGE RECONSTRUCTION

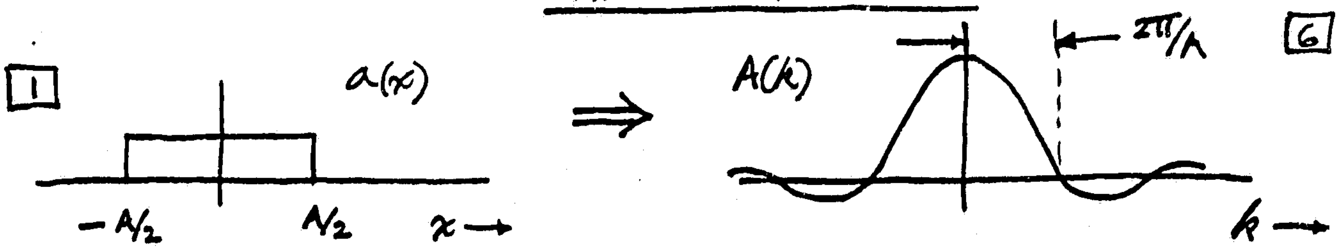

ROTATION/AUTOCORRELATION

IN THE FIRST CASE (IMAGE RECONSTRUCTION), AFTER FORMING THE AUTOCORRELATION $\boxed{2}$ THERE IS A DIVISION BY THE AUTOCORRELATION IN ν-SPACE WHICH EFFECTIVELY CREATES A RECTANGULAR WINDOW ON ν-SPACE OF WIDTH A/π $\boxed{3}$. THE FT OF $\boxed{3}$ HAS CHARACTERISTIC WIDTH π/A IN k-SPACE. THIS DIVISION STEP IS "UNPHYSICAL" AND RESULTS IN AN IMAGE-PLANE RESOLUTION TWICE THAT OBTAINED WITHOUT "RESTORATION" OF THE RECTANGULAR WINDOW IN ν-SPACE. ONE MEASURE OF THE "UNPHYSICALNESS" OF THE RESULTING IMAGE IS THAT IT, IN CONTRAST WITH THE ORIGINAL IMAGE, CONTAINS NEGATIVE [UNPHYSICAL] VALUES $\boxed{4}$. IF

THE TRANSFORM OF THE AUTOCORRELATION HAD INSTEAD BEEN TAKEN, THERE WOULD RESULT

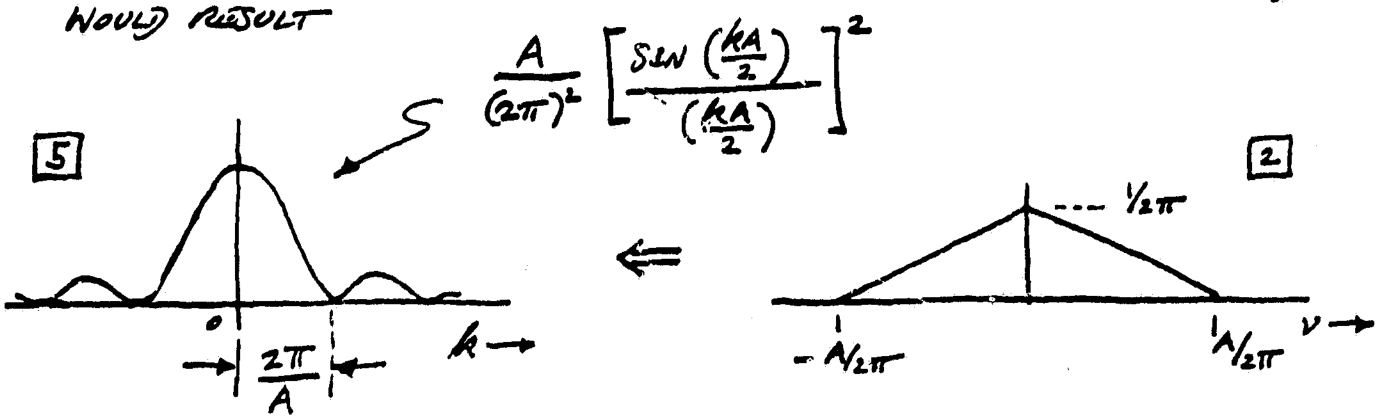

WITH RESOLUTION $2\pi/A$ AS COMPARED WITH π/A. WITHIN THE OVERALL FACTOR A THIS IS JUST THE SQUARE OF $A(k)$ (175) AND CONFIRMS (19) FOR A δ-FUNCTION IN $\mu(k)$.

$\boxed{5}$ IS THE ACTUAL [NON-NEGATIVE] IMAGE FORMED BY A POINT SOURCE. ITS TRANSFORM IS A CONSTANT FUNCTION MULTIPLIED BY THE AUTOCORRELATION OF THE APERTURE $\boxed{2}$. DIVISION BY $\boxed{2}$ IN ν-SPACE RESTORES [NEGLECTING NOISE] FULL WEIGHT TO THE CONSTANT FUNCTION OVER $-A/2\pi < \nu < +A/2\pi$ WHICH, IN TURN, RESULTS IN TWICE THE RESOLUTION IN THE IMAGE PLANE. WE HAVE RESTORED HIGH FREQUENCY INFORMATION ATTENUATED BY THE TAPERING AUTOCORRELATION.

THIS APPEARS TO BE A GENERAL RESULT WHICH COULD BE USED TO ENHANCE THE RESOLUTION OF ANY IMAGE GIVEN THE APERTURE FUNCTION.

COULD THIS ENHANCEMENT BE REPEATED ON THE ALREADY ENHANCED-RESOLUTION IMAGE $\boxed{4}$? THE ANSWER IS NO! WHEN WE STARTED WITH $\boxed{5}$ WE HAD TO DIVIDE IN ν-SPACE BY THE TRANSFORM OF $\boxed{5}$, $\boxed{2}$. THE TRANSFORM OF THE ALREADY ENHANCED IMAGE $\boxed{4}$ IS $\boxed{3}$, A CONSTANT OVER $-A/2\pi < \nu < +A/2\pi$. HENCE, NO NEW RELATIVE WEIGHTING OF THE ν-DOMAIN COMPONENTS OF THE IMAGE WILL RESULT, AND NO FURTHER IMPROVEMENT OF RESOLUTION.

IN THE SECOND CASE (ROTATION/AUTOCORRELATION) THE CHARACTERISTIC WIDTH OF THE FOURIER TRANSFORM OF THE APERTURE $\boxed{6}$ HAS TWICE THE VALUE IN k-SPACE AS THE RESOLUTION-ENHANCED IMAGE $\boxed{4}$. SAMPLING $a(x)$ AT INTERVALS X RESULTS, IN THE IMAGE RECONSTRUCTION CASE, IN SAMPLES IN ν-SPACE AT INTERVALS $X/2\pi$, WHICH IN TURN IMPLIES A

PERIODICITY IN THE IMAGE PLANE (k-SPACE) OF $2\pi/X$. LIKEWISE, SAMPLING $a(x)$ AT INTERVALS X RESULTS IN A PERIODICITY OF THE FOURIER REPRESENTATION OF $2\pi/X$. THE TWO PERIODICITIES ARE IDENTICAL. HOWEVER, THE LESSER WIDTH OF THE RESPONSE $\boxed{4}$ IN THE FORMER CASE MEANS THAT THE V-SPACE SAMPLING INTERVAL, AND ULTIMATELY THE SAMPLING OF $a(x)$, CAN BE INCREASED BY A FACTOR OF 2 RELATIVE TO THAT REQUIRED BY THE LATTER CASE. THIS ACCOUNTS FOR THE FIRST FACTOR OF 2 MENTIONED ABOVE.

THE SECOND FACTOR OF 2 IS EASIER TO SEE. THE WIDTH OF THE WINDOW IN k-SPACE, OUTSIDE OF WHICH IT IS ASSUMED THAT THE FT OF THE APERTURE IS NEGLIGIBLE, IS TWICE THE DISTANCE FROM THE PEAK OF THE SINC FUNCTION TO THE POINT AT WHICH THE ENVELOPE HAS FALLEN TO $1/\alpha$.

1^{ST} ZERO AT $2\pi/A$.

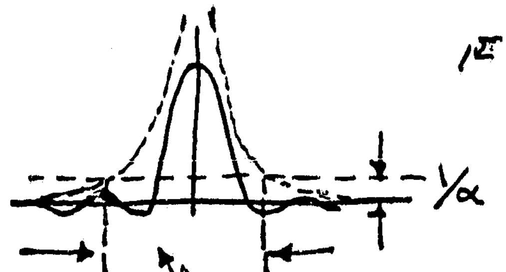

WINDOW = 2 X DISTANCE FROM PEAK TO $1/\alpha$ POINT OF ENVELOPE.

IN THE CASE OF IMAGE RECONSTRUCTION, HOWEVER, THE CRITERION IS THAT, AT ONE EDGE OF THE k-SPACE WINDOW, THE ENVELOPE ASSOCIATED WITH A POINT SOURCE AT THE OTHER WINDOW EDGE, REPLICATED DUE TO SAMPLING, BE ATTENUATED BY $1/\alpha$. ONLY THE ENVELOPE OF THE INTERFERING SOURCE IS CONSIDERED SO THAT ONLY <u>ONE</u> $1/\alpha$ DISTANCE IS INVOLVED.

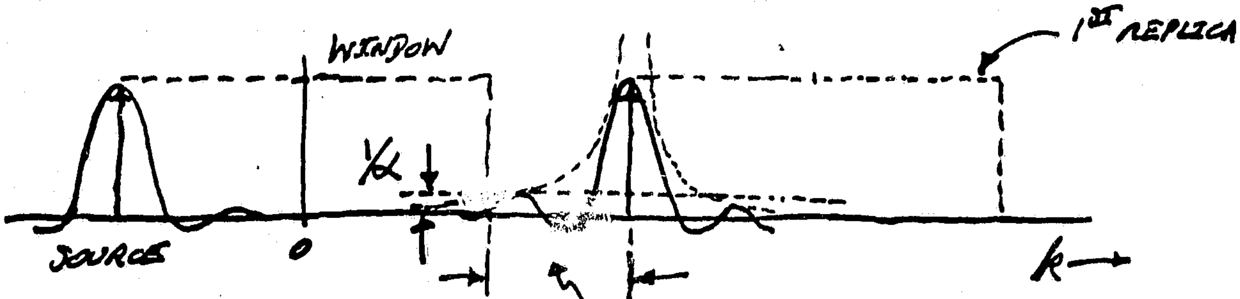

1 X DISTANCE FROM PEAK TO $1/\alpha$ POINT OF ENVELOPE.

1^{ST} ZERO AT π/A.

THIS RESULT IS SYMMETRICAL FOR A SOURCE AT EITHER WINDOW EDGE.

AGAIN, THE FACT THAT ONLY ONE $1/k$ - DISTANCE IS REQUIRED IN THE IMAGE RECONSTRUCTION CASE COMPARED WITH TWO FOR THE FOURIER REPRESENTATION ACCOUNTS FOR THE SECOND FACTOR OF 2 IN THE APERTURE SAMPLING INTERVAL.

IN FACT THE APERTURE SAMPLING INTERVAL $X = 2\pi A/\alpha$ BASED ON ZERO FIELD OF VIEW IS OBVIOUSLY UNREALISTIC. FOR $A = 1.8\,m$ AND $\alpha = 100$ THIS IS $X = 11.3$ cm. WHEN ALLOWANCE WAS MADE FOR A FIELD OF VIEW $\theta_0 = 0.2$ ARC SEC WE FOUND $X \leq 8.3$ cm. SINCE WE HAVE NOW FOUND THAT THE FOURIER REPRESENTATION OF $a(x)$ IMPOSES THE MOST SEVERE SAMPLING REQUIREMENT ($X = 2.82$ cm), LET US ASK WHAT FIELD OF VIEW THIS AFFORDS. WHEN WE COMBINE (179) AND (174) WE GET

$$K_0 = \frac{3\alpha}{A_{MIN}} \quad \text{OR,} \quad \theta_0 = \frac{3\lambda\alpha}{2\pi A_{MIN}} = \text{FIELD OF VIEW} \qquad (180)$$

FOR THE PARAMETERS WE HAVE BEEN USING WE FIND $\theta_0 = 7.96 \times 10^{-6}$ RAD = = 1.64 ARC SEC.

WITH ALL OF THESE CONSIDERATIONS IN MIND WE CAN NOW COLLECT TOGETHER A SET OF USEFUL RELATIONSHIPS PERTAINING TO SAMPLING. FROM (179) WE HAVE

$$X = \frac{\pi A_{MIN}}{2\alpha} = \text{SAMPLING INTERVAL ACROSS APERTURE} \qquad (181a)$$

$$m = \frac{A_{MAX}}{X} = \frac{A_{MAX}}{A_{MIN}}\,\frac{2\alpha}{\pi} = \text{NUMBER OF SAMPLES ACROSS MAXIMUM DIMENSION OF APERTURE.} \qquad (181b)$$

FROM (173) FOR THE GUARD ZONE, (155), AND (180), WE HAVE

$$\Phi = \theta_0 + \frac{\lambda\alpha}{2\pi A_{MIN}} = \frac{2\lambda\alpha}{\pi A_{MIN}} = \text{TOTAL ANGLE, FIELD OF VIEW PLUS GUARD ZONE} \qquad (181c)$$

IN TWO DIMENSIONS WE CAN PUT THE GUARD ZONE ENTIRELY AROUND THE

FIELD OF VIEW, OR ALONG TWO ORTHOGONAL EDGES.

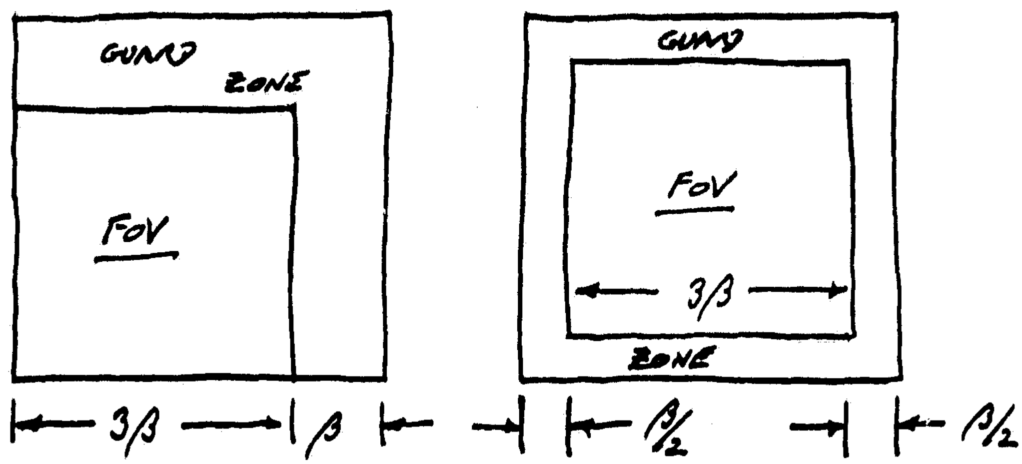

$$\beta = \frac{\lambda\alpha}{2\pi A_{MIN}}$$

THE NUMBER OF SAMPLES OF [NON-ZERO] APERTURE AUTOCORRELATION ALONG THE LONGER AXIS WILL BE $2m-1$, AN ODD NUMBER. AUTOCORRELATION USING FOURIER TECHNIQUES PRODUCES CIRCULAR, OR PERIODIC, CORRELATION. IF m POINTS ARE INPUT TO THE FOURIER PROCESS, m POINTS OF PERIODIC CORRELATION RESULT. THIS IS REPRESENTED SCHEMATICALLY BELOW FOR $m = 4$.

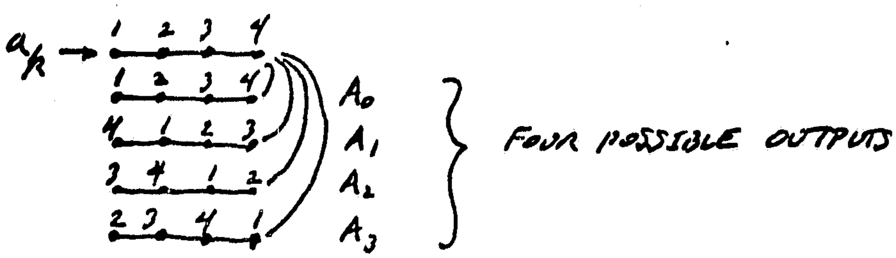

TO PRODUCE THE APERIODIC AUTOCORRELATION USING FOURIER TECHNIQUES IT IS NECESSARY TO PAD WITH AN EQUAL NUMBER OF ZEROS [m, RATHER THAN $m-1$, ZEROS MUST BE USED BECAUSE THE FFT REQUIRES m TO BE EVEN]. THIS WILL YIELD $2m$ AUTOCORRELATION POINTS, ONE OF WHICH WILL BE IDENTICALLY ZERO, BRINGING THE NUMBER OF MEANINGFUL POINTS TO $2m-1$. THE WAY THAT THIS COMES ABOUT IS ILLUSTRATED SCHEMATICALLY BELOW, AGAIN FOR $m = 4$.

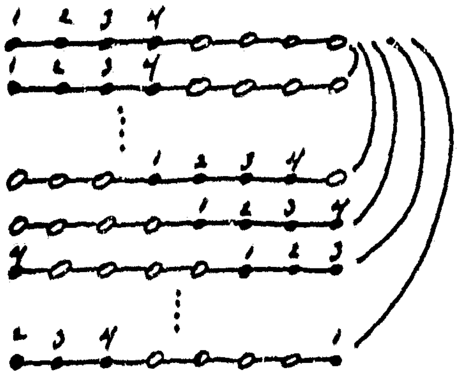

NOTE THAT THE CENTER POINT IS IDENTICALLY ZERO AND THAT THE RESULT IS SYMMETRIC ABOUT THIS POINT.

WE HAVE SEEN THAT THE NUMBER OF SAMPLES ACROSS THE APERTURE m (181b) LEADS TO $2m-1$, AN ODD NUMBER, SAMPLES IN ν-SPACE. WE HAVE ALSO SEEN THAT THE RECONSTRUCTED IMAGE INVOLVES THE INVERSE FT OF THE RESULT IN ν-SPACE AFTER DIVIDING OUT THE AUTOCORRELATION OF THE APERTURE. SINCE, ON A COMPUTER, WE MUST FORM DISCRETE FTS (DFT) AND IN PARTICULAR WILL WANT TO USE FFTS, THERE IS A QUESTION OF EXACTLY HOW TO HANDLE THE ODD SAMPLE NUMBER WHICH THE AUTOCORRELATION PRESENTS WHEN THE FFT REQUIRES EVEN SAMPLE NUMBERS AS INPUT AND OUTPUT.

LET US START WITH THE SAMPLED VERSION OF $U(\nu)$, $\tilde{U}(\nu)$, WHICH, AS A RESULT OF THE SAMPLED APERTURE AUTOCORRELATION, CONTAINS $2m-1$ SAMPLES CENTERED ON THE ν-SPACE ORIGIN AND HAS THE AUTO-CORRELATION SCALING EFFECT ALREADY DIVIDED OUT. THE RESULTING IMAGE WILL BE

$$\widetilde{|u(\vec{k})|^2} = \iint_{-\infty}^{\infty} d^2\vec{\nu}\, \tilde{U}(\vec{\nu})\, e^{+2\pi i \vec{k}\cdot\vec{\nu}} \tag{182}$$

WHERE

$$\tilde{U}(\vec{\nu}) = \sum_{l,s=-(m-1)}^{m-1} U(\vec{\nu})\, \delta\!\left(\nu_x - \frac{X}{2\pi} l\right) \delta\!\left(\nu_z - \frac{X}{2\pi} s\right) \tag{183}$$

(183) IN (182) GIVES

$$|\widetilde{\mu(\bar{k})}|^2 = \sum_{l,s=-(m-1)}^{m-1} U\left(\frac{X}{2\pi}l, \frac{X}{2\pi}s\right) e^{+2\pi i\left[k_x \frac{X}{2\pi} l + k_z \frac{X}{2\pi} s\right]} \quad . \tag{184}$$

TO EASE THE NOTATION, LET US CONSIDER ONLY ONE DIMENSION.

$$|\widetilde{\mu(k_x)}|^2 = \sum_{l=-(m-1)}^{m-1} U\left(\frac{X}{2\pi}l\right) e^{iXk_x l} \quad . \tag{185}$$

BREAK (185) INTO TWO SUMMATIONS AND CONCENTRATE ON THE SECOND.

$$|\widetilde{\mu(k_x)}|^2 = \sum_{l=0}^{m-1} U\left(\frac{X}{2\pi}l\right) e^{iXk_x l} + \sum_{l=-(m-1)}^{-1} U\left(\frac{X}{2\pi}l\right) e^{iXk_x l} \tag{186}$$

IN THE SECOND SUMMATION DEFINE $\mu = 2m + l = N + l$ WHERE

$$N = 2m \quad , \tag{187}$$

$$\sum_{l=-(m-1)}^{-1} U\left(\frac{X}{2\pi}l\right) e^{iXk_x l} = e^{-iXk_x(2m)} \sum_{\mu=m+1}^{N-1} U\left[\frac{X}{2\pi}(\mu - 2m)\right] e^{iXk_x \mu} \quad . \tag{188}$$

NOW LET US CHOOSE k_x SO THAT THE EXPONENTIAL MULTIPLYING THE SUMMATION ON THE RIGHT OF (188) IS UNITY. THAT IS,

$$Xk_x(2m) = 2\pi m \qquad (m = \text{INTEGER})$$

OR,

$$k_x = \frac{2\pi}{X}\frac{m}{N} \quad . \tag{189}$$

THEN (186) MAY BE WRITTEN

$$\left|\widetilde{\mu(k_x)}\right|^2_m = \sum_{l=0}^{m-1} U\left(\frac{X}{2\pi}l\right)e^{\frac{2\pi i m l}{N}} + \sum_{l=m+1}^{N-1} U\left[\frac{X}{2\pi}(l-N)\right]e^{\frac{2\pi i m l}{N}} . \qquad (190)$$

THE SAMPLES OF $U(\nu)$ FOR $\nu = \pm m \frac{X}{2\pi}$ ARE JUST OUTSIDE THE RANGE OF THE APERTURE AUTOCORRELATION AND SO HAVE VALUE ZERO. WE MAY WRITE THEREFORE THAT

$$\left|\widetilde{\mu(k_x)}\right|^2_m = \sum_{l=0}^{N-1} \hat{U}\left(\frac{X}{2\pi}l\right)e^{\frac{2\pi i m l}{N}} \equiv \mu^2_m \qquad (191)$$

$$(m = 0, 1, \ldots N-1)$$

WHERE:

$$\left.\begin{aligned} \hat{U}\left(\frac{X}{2\pi}l\right) &= U\left(\frac{X}{2\pi}l\right) \\ &= 0 \\ &= U\left[\frac{X}{2\pi}(l-N)\right] \end{aligned}\right\} \begin{aligned} &(l = 0, 1, 2, \ldots m-1) \\ &(l = \pm m) \\ &(l = m+1, m+2, \ldots N-1) \end{aligned}$$

μ^2_m (191) IS JUST THE DFT OF THE $N = 2m$ POINT SERIES $\hat{U}\left(\frac{X}{2\pi}l\right)$. THE PROBLEM WHICH AT FIRST INVOLVED AN <u>ODD</u> NUMBER OF POINTS DUE TO THE SAMPLED AUTOCORRELATION OF THE APERTURE NOW INVOLVES THE DFT OF AN <u>EVEN</u> NUMBER OF POINTS WHICH CAN BE IMPLEMENTED AS AN FFT. THE CORRESPONDING k-SPACE STEP SIZE IS, FROM (189),

$$K = \frac{1}{N}\frac{2\pi}{X} \qquad (N = 2m) \qquad (192)$$

$$= \frac{1}{N}\frac{4\alpha}{A_{MIN}}$$

WHERE WE HAVE USED ALSO (181a). THE ANGLE BETWEEN IMAGE SAMPLES IS FOUND FROM (192) BY MULTIPLYING BY $\lambda/2\pi$ ACCORDING TO (155) OR BY DIVIDING Φ FROM (181c) BY N.

$$\theta = \frac{2\lambda\alpha}{N\pi A_{MIN}} = \text{ANGLE BETWEEN IMAGE SAMPLES.} \qquad (181d)$$

CONSIDER NOW THE USE OF THE DFT TO COMPUTE THE AUTOCORRELATION OF A FUNCTION

$$g(x) = a(x) \quad (0 \le x \le A_{MAX}); \qquad = 0 \quad (A_{MAX} < x \le 2A_{MAX}) \tag{193}$$

SAMPLED AT N INTERVALS OVER THE RANGE $0 \le x < 2A_{MAX}$. THAT IS,

$$X = \frac{2A_{MAX}}{N} = \frac{A_{MAX}}{n} = \frac{\pi A_{MIN}}{2\alpha} \quad \text{(FROM (181a))} . \tag{194}$$

THE DFT OF $g(x)$ IS

$$G(k) = \sum_{m=0}^{N-1} g(mX)\, e^{-\frac{2\pi i m k}{N}} . \quad (k = 0, 1, 2, \ldots N-1) \tag{195}$$

COMPUTE THE DISCRETE FT OF $G^*(k)G(k)$.

$$\hat{a}(\ell) = \frac{1}{N}\sum_{k=0}^{N-1} G(k)G^*(k)\, e^{-\frac{2\pi i \ell k}{N}} =$$

$$= \frac{1}{N}\sum_{k=0}^{N-1}\sum_{m=0}^{N-1}\sum_{m=0}^{N-1} g(mX)\, g^*(mX)\, e^{-\frac{2\pi i m k}{N} + \frac{2\pi i m k}{N} - \frac{2\pi i \ell k}{N}} =$$

$$= \frac{1}{N}\sum_{m=0}^{N-1}\sum_{m=0}^{N-1} g(mX)\, g^*(mX) \underbrace{\sum_{k=0}^{N-1} e^{-\frac{2\pi i}{N}(m-m+\ell)k}}_{= N\delta_{m,(m+\ell)|_N} = N\delta_{m,(m-\ell)|_N}} =$$

$$= \sum_{m=0}^{N-1} g(mX)\, g^*((m+\ell)|_N X) = \sum_{m=0}^{N-1} g((m-\ell)|_N X)\, g^*(mX) \tag{196}$$

$$(\ell = 0, 1, 2, \ldots N-1)$$

WHERE $|_N$ MEANS "MODULO N". NOTE THAT WE HAVE TAKEN THE <u>FORWARD</u> TRANSFORM OF $G^*(k)G(k)$, NOT THE INVERSE TRANSFORM AS ONE WOULD ANTICIPATE. WE SEE THAT AS A RESULT (196) AGREES [EXCEPT FOR DIMENSIONALITY] WITH THE AUTOCORRELATION CONTAINED WITHIN (163). IT IS ALSO TO BE NOTED THAT (196) CONTAINS THE ADDITIONAL "MODULO N" NOTATION, WHICH ACCOUNTS FOR THE CIRCULAR OR PERIODIC NATURE OF THE DFT-BASED AUTOCORRELATION.

A CONSEQUENCE OF THIS AND THE ZERO PADDING GIVEN BY (193) IS THAT $\hat{a}(\ell)$ HAS THE CHARACTERISTICS OF $\hat{U}(\frac{X}{2\pi}\ell)$ GIVEN WITH (191). NAMELY,

$$\hat{a}(\ell) = \begin{cases} a\left(\frac{X}{2\pi}\ell\right) & (\ell = 0, 1, 2, \ldots m-1) \\ 0 & (\ell = \pm m) \\ a\left[\frac{X}{2\pi}(\ell - N)\right] & (\ell = m+1, m+2, \ldots N-1) \end{cases} \qquad (197)$$

SCHEMATICALLY, $\hat{a}(\ell)$ WILL LOOK LIKE:

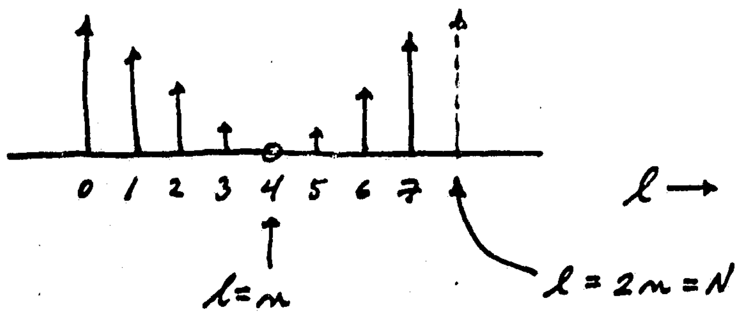

FROM (170) AND (181ℓ) THE OVERSAMPLING FACTOR ALONG THE MAXIMUM RESOLUTION DIRECTION WILL BE

$$\eta = \frac{A_{MIN}}{A_{MAX}} \frac{N\pi}{4\alpha} = \left[1, \text{ IF } m \text{ GIVEN BY } (181\ell)\right] \qquad (181$$

FOR EXAMPLE, IF $A_{MIN} = 1.8\,m$, $A_{MAX} = 12\,m$, $N = 1024 = 2^{10}$, $\alpha = 100$, THEN $\eta = 1.21$.

NOTE THAT THE k-SPACE STEP SIZE (192) WHICH CORRESPONDS TO MAKING

THE EXPONENTIAL FACTOR IN (188) ALWAYS UNITY LEADS TO A TOTAL SAMPLED WIDTH [OVER N SAMPLES] IN k-SPACE OF $2\pi/X$. THIS IS IDENTICALLY THE k-SPACE PERIODICITY DUE TO V-SPACE SAMPLING AT INTERVALS OF $X/2\pi$.

CONVERSELY, SAMPLING OF THE k-SPACE IMAGE AT INTERVALS (192) GENERATES A PERIODICITY, IN THE V-SPACE REPRESENTATION, OF $N(X/2\pi)$. AS CAN BE SEEN FROM (191) AND (197), THE BASIC V-SPACE INTERVAL IS $X/2\pi$ AND THERE ARE A TOTAL OF $N=2m$ SUCH SAMPLES OVER THE V-SPACE WINDOW. THIS PERIODICITY, AND THIS DISTRIBUTION OF SAMPLES, MEANS THAT THE N-POINT FFT OF THE $2\pi/X$ k-SPACE WINDOW YIELDS V-SPACE SAMPLES ALIGNED AND PROPERLY ORDERED FOR OPERATION WITH THE AUTOCORRELATION OF THE APERTURE, (196) AND (197), PRODUCED BY FFT TECHNIQUES.

A SUMMARY OF THE MAJOR STEPS INVOLVED, EXCLUDING NOISE AND APERTURE ROTATION, IS GIVEN BELOW. TECHNIQUES TO REDUCE THE OVERALL COMPUTATIONAL BURDEN WILL BE GIVEN LATER.

1) FORM m SAMPLES OF THE APERTURE FUNCTION ALONG ITS GREATEST DIMENSION AT INTERVALS $X \leq \pi A_{MIN}/2\alpha$. ADJUST X SO THAT m IS A POWER OF 2. SAMPLE THE APERTURE IN THE NORMAL DIRECTION AT THE SAME INTERVAL.

2) DOUBLE THE NUMBER OF SAMPLES ALONG THE GREATEST DIRECTION BY PADDING OUT WITH AN EQUAL NUMBER OF ZEROS. ALSO, PAD OUT THE SHORTER DIRECTION WITH ZEROS SO THAT AN $N \times N$ ARRAY RESULTS WITH $N=2m$.

3) USE RESULTS (195) AND (196) TO COMPUTE THE $N \times N$ APERIODIC AUTOCORRELATION OF THE APERTURE. THE DISTRIBUTION OF ZEROS IN THE RESULT WILL BE:

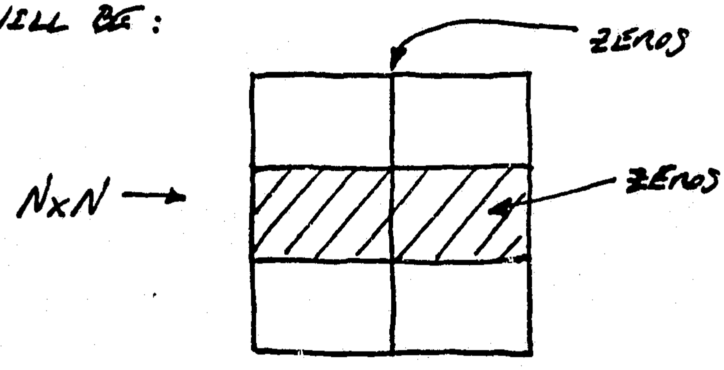

4) PREPARE AN IMAGE OF TOTAL WIDTH IN EACH DIRECTION OF $(2\lambda\alpha/\pi A_{MIN}) = \lambda/X$ RADIANS. 1/4 OF THIS SHOULD BE A GUARD ZONE OF ZEROS. FORM AN ARRAY OF $N \times N$ SAMPLES. TAKE THE $N \times N$ FFT.

5) "DIVIDE OUT" CORRESPONDING ELEMENTS OF THE IMAGE $N \times N$ TRANSFORM BY THE $N \times N$ AUTOCORRELATION.

6) TAKE THE INVERSE FFT TO GET THE ENHANCED IMAGE.

SOME NUMBERS FOR THE CASE:

$$\boxed{\begin{aligned} \lambda &= 3 \times 10^{-5}\ \text{cm} \\ \alpha &= 100 \\ A_{MIN} &= 180\ \text{cm} \\ A_{MAX} &= 1200\ \text{cm} \end{aligned}}$$

$\Rightarrow$ $X \leq 2.83$ cm,

$A_{MAX}/X = 424 \Rightarrow m = 512 = 2^9$,

$\Rightarrow \boxed{X = 2.34\ \text{cm}}$

$\Rightarrow$ $\boxed{N = 2m = 1024}$

TOTAL IMAGE WIDTH: $\boxed{1.28 \times 10^{-5}\ \text{RAD} = 2.64\ \text{ARC SEC}}$

ACTIVE IMAGE WIDTH: 1.98 ARC SEC

SAMPLE-SAMPLE ANGLE: 2.58×10^{-3} ARC SEC

OVERSAMPLING η: 1.206

RESOLUTION (BEST AXIS): 2.58×10^{-3} ARC SEC.

APERTURE SYNTHESIS

FOR A HIGH ASPECT RATIO, A_{MAX}/A_{MIN}, APERTURE THE PROCEDURE JUST OUTLINED IS INEFFICIENT IN TERMS OF COMPUTER STORAGE. THIS IS DUE TO THE LARGE NUMBER OF ZEROS IN THE APERTURE AND AUTO-CORRELATION PLANES WHEN $N \times N$ SQUARE SAMPLE ARRAYS ARE FORMED. THE NON-ZERO PART OF THE FINAL AUTOCORRELATION CAN BE FORMED BY SUITABLY COMBINING THE FFTS OF SMALLER CONTIGUOUS PORTIONS OF THE APERTURE. THIS IS COMPUTATIONALLY MORE CUMBERSOME BUT MAKES BETTER USE OF STORAGE.

AS USUAL WE WILL USE ONE-DIMENSIONAL ARGUMENTS TO SHOW THE NATURE OF RESULTS TO BE GENERALIZED TO TWO DIMENSIONS. IMPORTANT AMONG THESE WILL BE THE FOURIER SHIFT AND INTERPOLATION THEOREMS FOR THE DISCRETE CASE.

FOURIER SHIFT THEOREM

LET F_ℓ BE THE DISCRETE FOURIER TRANSFORM OF f_k.

$$F_\ell = \sum_{k=0}^{N-1} f_k \, e^{\frac{-2\pi i \ell k}{N}} \qquad (\ell = 0, 1, 2, \ldots N-1) \qquad (198)$$

LET THE DISCRETE FUNCTION f_k BE SHIFTED CYCLICALLY IN THE DIRECTION OF INCREASING k BY m SAMPLES

$$f_k \rightarrow f_{(k-m)|_N}$$

THE EFFECT ON THE TRANSFORM F_ℓ IS:

$$F_\ell \rightarrow \sum_{k=0}^{N-1} f_{(k-m)|_N} \, e^{\frac{-2\pi i \ell k}{N}} = \sum_{p=-m}^{N-1-m} f_{p|_N} \, e^{\frac{-2\pi i \ell (p+m)}{N}} =$$

$$= e^{\frac{-2\pi i \ell m}{N}} \sum_{p=-m}^{N-1-m} f_{p|_N} \, e^{\frac{-2\pi i \ell p}{N}}$$

BECAUSE $\exp(-2\pi i l p/N) = \exp(-2\pi i l p|_N /N)$, WE HAVE FINALLY,

$$F_l \rightarrow e^{-\frac{2\pi i l m}{N}} \sum_{p=0}^{N-1} f_p \, e^{-\frac{2\pi i l p}{N}} .$$

OR,

UNDER,

$$\boxed{\left.\begin{aligned} F_l &\rightarrow e^{-\frac{2\pi i l m}{N}} F_l \\ f_k &\rightarrow f_{(k-m)|_N} \end{aligned}\right\}} \quad \text{SHIFT THEOREM} \qquad (199)$$

THE ABOVE RULE SUGGESTS THAT A SHIFT OF THE SAMPLED FUNCTION f_k BY AN AMOUNT NOT EQUAL TO AN INTEGER NUMBER OF SAMPLES COULD BE AFFECTED BY MULTIPLYING IN THE TRANSFORM DOMAIN BY A NON-INTEGER m. THAT IS,

$$F_l \rightarrow e^{-\frac{2\pi i l x}{N X}} F_l \equiv G_l \qquad (200)$$

WHERE X IS THE SAMPLE INTERVAL AND x IS THE ARBITRARY SHIFT. THE DIFFICULTY COMES FROM THE FACT THAT SAMPLES OF f_k ARE NOT AVAILABLE FOR "NON-INTEGER m". WE MIGHT THEN ASK WHAT IS THE EFFECTIVE RESULT IN THE SAMPLE DOMAIN IF WE SIMPLY FORM (200) FOR x/X NON-INTEGER IN THE TRANSFORM DOMAIN. TO FIND OUT WE EVALUATE THE INVERSE TRANSFORM OF (200).

$$\hat{f}_k = \frac{1}{N} \sum_{l=0}^{N-1} G_l \, e^{\frac{+2\pi i l k}{N}} = \frac{1}{N} \sum_{l=0}^{N-1} F_l \, e^{\frac{+2\pi i l}{N}\left(k - \frac{x}{X}\right)} =$$

$$= \frac{1}{N} \sum_{m=0}^{N-1} f_m \sum_{l=0}^{N-1} e^{-\frac{2\pi i l}{N}\left(m - k + \frac{x}{X}\right)} \qquad (201)$$

$$(k = 0, 1, 2, \ldots N-1)$$

WHERE WE HAVE USED (198) AND INTERCHANGED THE ORDER OF SUMMATION.

CONSIDER THE SECOND SUMMATION IN (201) AND LET

$$\eta = e^{-\frac{2\pi i}{N}\left(m-k+\frac{x}{X}\right)} .$$

THEN,

$$\sum_{l=0}^{N-1} \eta^{l} = \sum_{l=0}^{\infty} \eta^{l} - \sum_{l=N}^{\infty} \eta^{l} = \sum_{l=0}^{\infty}\eta^{l} - \eta^{N}\sum_{l=0}^{\infty}\eta^{l} = (1-\eta^{N})\sum_{l=0}^{\infty}\eta^{l} =$$

$$= \frac{1-\eta^{N}}{1-\eta} ,$$

WHERE

$$\eta^{N} = e^{-2\pi i\left(m-k+\frac{x}{X}\right)} = e^{-2\pi i \frac{x}{X}} \qquad (k, m \text{ INTEGER}) .$$

WITH THE ABOVE RESULTS WE ARE ABLE TO EXPRESS (201) AS

$$\hat{f}_k = \frac{1}{N}\sum_{m=0}^{N-1} f_m \left\{ \frac{1-e^{-2\pi i \frac{x}{X}}}{1-e^{-\frac{2\pi i}{N}\left(m-k+\frac{x}{X}\right)}} \right\} . \qquad (202)$$

$$(k=0,1,2,\ldots N-1)$$

THE FACTOR IN BRACES IS AN INTERPOLATION FACTOR WHICH WEIGHTS MOST HEAVILY TERMS NEAR $m=k$. IF $x \to 0$, ONLY THE $m=k$ TERM SURVIVES AND

$$\hat{f}_k = f_k \qquad (x \to 0)$$

TO SEE THIS, CONSIDER THE MAGNITUDE OF THE TERM IN BRACES. MULTIPLYING BY THE CONJUGATE WE GET

$$\{\ldots\}\{\ldots\}^{*} = \frac{1-\cos\left(2\pi\frac{x}{X}\right)}{1-\cos\left[\frac{2\pi}{N}\left(m-k+\frac{x}{X}\right)\right]} = \frac{\sin^{2}\left(\pi\frac{x}{X}\right)}{\sin^{2}\left[\frac{\pi}{N}\left(m-k+\frac{x}{X}\right)\right]}$$

SO THAT THE MAGNITUDE OF THE COEFFICIENT OF f_m IN (202) IS

$$\left|\{\cdots\}\right| = \pm \frac{\sin\left(\pi \frac{x}{X}\right)}{\sin\left[\frac{\pi}{N}\left(m-k+\frac{x}{X}\right)\right]} \qquad (203)$$

SINCE INTEGER SHIFTS $x/X = m$ ARE HANDLED EXACTLY BY (199) IT IS NECESSARY ONLY TO CONSIDER

$$0 \le \frac{x}{X} < 1 \quad . \qquad (204)$$

THE NUMERATOR OF (203) IS NOT A FUNCTION OF m OR k. THE DENOMINATOR OF (203) IS SKETCHED BELOW AS A FUNCTION OF $m-k$.

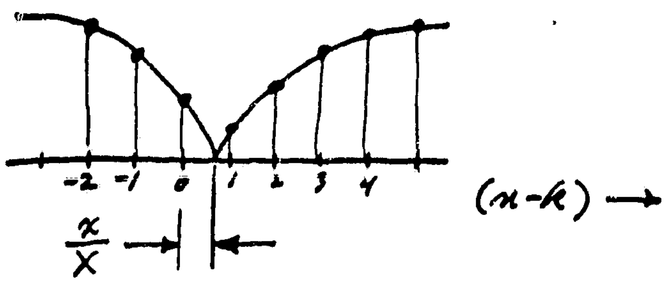

THE POSITIVE BRANCH ONLY IS SHOWN DUE TO THE $\pm$ SIGN ON (203). CLEARLY THE MAXIMUM VALUE OF (203) IS NEAR $m=k$ AND (203) GENERALLY TAPERS OFF AS m DEPARTS FROM k.

A SPECIAL CASE IS $x/X \to 0$. THEN

$$\sin\left[\frac{\pi}{N}\left(m-k+\frac{x}{X}\right)\right] = \sin\left[\frac{\pi}{N}(m-k)\right]\cos\left(\frac{\pi}{N}\frac{x}{X}\right) + \cos\left[\frac{\pi}{N}(m-k)\right]\sin\left(\frac{\pi}{N}\frac{x}{X}\right)$$

$$\xrightarrow[x\to 0]{} \sin\left[\frac{\pi}{N}(m-k)\right] + \frac{\pi}{N}\frac{x}{X}\cos\left[\frac{\pi}{N}(m-k)\right] \qquad (205)$$

CONSIDER FURTHER THAT $m=k$. THEN FROM (203) AND (205),

$$\left|\{\cdots\}\right| = \pm N \frac{\sin\left(\pi\frac{x}{X}\right)}{\left(\pi\frac{x}{X}\right)} \qquad (x\to 0,\ k=m) \qquad (206)$$

IN THE LIMIT THAT $x \to 0$, (206) EQUALS N. BECAUSE OF $\sin\left(\pi \frac{x}{X}\right)$ IN THE NUMERATOR OF (203), (203) IS ZERO FOR $m \neq k$ AND $x = 0$. THEREFORE ONLY THE $m = k$ TERM SURVIVES IN (202) WHEN $x \to 0$, GIVING

$$\hat{f}_k = f_k$$

AS CLAIMED.

WE SUMMARIZE THE SHIFT THEOREM AS FOLLOWS.

$$\boxed{\begin{aligned} &F_l \to e^{\frac{-2\pi i l x}{NX}} F_l \\ &f_k \to f_{\left(k - \frac{x}{X}\right)}\Big|_N \end{aligned}}$$

(207a)

SHIFT THEOREM

(207b)

THE RELATIONSHIP BETWEEN f_k AND F_l IS DEFINED BY (198). THE SENSE OF (207b) IS THAT THE RESULT IS EXACT FOR x/X INTEGER, AND AN APPROXIMATION BY INTERPOLATION WHEN x/X IS NOT INTEGER.

WE HAVE JUST DISCUSSED INTERPOLATION IN THE SAMPLE DOMAIN INDUCED BY A PHASE FUNCTION IN THE TRANSFORM DOMAIN. A SIMILAR RESULT OBTAINS WITH THE DOMAINS REVERSED. CONSIDER A SPECIAL CASE IN WHICH THE SAMPLE DOMAIN CONTAINS A LONG [CYCLICALLY] CONTIGUOUS STRING OF ZEROS. FOR SIMPLICITY, LET IT BE ASSUMED THAT THE SHIFT THEOREM HAS FIRST BEEN APPLIED TO BRING THE NON-ZERO SAMPLE SEQUENCE INTO REGISTER WITH THE LEFT EDGE OF THE SAMPLE WINDOW. I.E., SAMPLE NUMBERS $\phi, 1, 2, \ldots$.

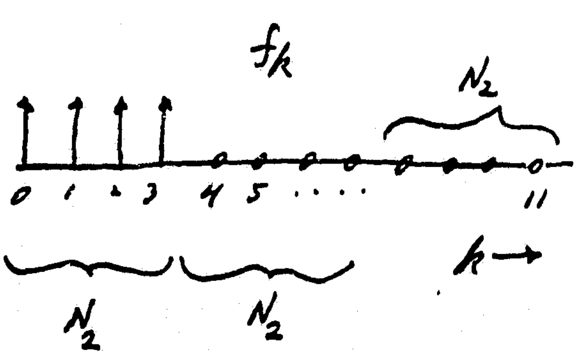

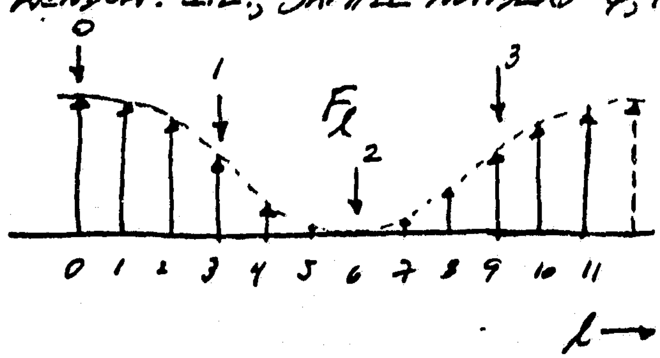

$N = 12$

ASSUME THAT THE SAMPLE NUMBER N IS

$$N = N_1 N_2 \qquad (208)$$

SO THAT THE INPUT SAMPLE SEQUENCE CAN BE CONSIDERED AS N_1 GROUPS OF N_2 SAMPLES EACH. LET US RESTRICT ATTENTION TO A SUBSET OF THE POSSIBLE F_λ GIVEN BY

$$\hat{F}_m \equiv F_{mN_1} \quad . \qquad (m=0,1,2,\ldots N_2-1) \quad (209)$$

SUBSTITUTION INTO (198) GIVES

$$\hat{F}_m = \sum_{k=0}^{N-1} f_k e^{\frac{-2\pi i k m N_1}{N_1 N_2}} = \sum_{k=0}^{N-1} f_k e^{\frac{-2\pi i m k}{N_2}} \quad . \qquad (210)$$

NOW, IF IT HAPPENS THAT THE f_k ARE ZERO FOR $k \geq N_2$, THEN

$$\hat{F}_m = \sum_{k=0}^{N_2-1} f_k e^{\frac{-2\pi i m k}{N_2}} \qquad (m=0,1,2,\ldots N_2-1) \quad (211)$$

THIS IS JUST THE N_2-POINT DISCRETE FOURIER TRANSFORM OF THE SEQUENCE f_k FOR $k=0,1,2,\ldots N_2-1$. IN WORDS, WE HAVE SHOWN THAT IF $N=N_1N_2$, WE CAN COMPUTE EVERY N_1-TH POINT OF THE DFT OF f_k BY FORMING THE N_2-POINT DFT OF f_k PROVIDED THAT THE f_k OUTSIDE THE RANGE $k=0,1,2,\ldots N_2-1$ ARE ALL ZERO. WE HAVE ILLUSTRATED ABOVE THE CASE $N=12$ WITH $N_2=4$, $N_1=3$. NOTE THAT THE SAMPLES IN THE LEFT-MOST GROUP OF f_k DO NOT HAVE TO BE ALL NON-ZERO; BUT ALL THE OTHER f_k MUST BE ZERO.

NOW, SUPPOSE THAT WE WOULD LIKE INSTEAD TO CALCULATE SOME OTHER N_2-POINT SUBSET OF THE N POSSIBLE F_λ VALUES.

$$\hat{F}_{m,\mu} \equiv F_{mN_1+\mu} = \sum_{k=0}^{N-1} f_k e^{\frac{-2\pi i k(mN_1+\mu)}{N_1 N_2}} =$$

$$= \sum_{k=0}^{N-1} \left[f_k e^{\frac{-2\pi i k \mu}{N}} \right] e^{-\frac{2\pi i m k}{N_2}}$$

$$(\mu = 0, 1, 2, \ldots N_1 - 1)$$
$$(m = 0, 1, 2, \ldots N_2 - 1)$$

AGAIN, IF $f_k = 0$ FOR $k \geq N_2$, THEN

$$\hat{F}_{m,\mu} = \sum_{k=0}^{N_2-1} \left[f_k e^{\frac{-2\pi i k \mu}{N}} \right] e^{-\frac{2\pi i m k}{N_2}} \qquad (212)$$

$$(\mu = 0, 1, 2, \ldots N_1 - 1)$$
$$(m = 0, 1, 2, \ldots N_2 - 1)$$

WHICH IS JUST THE N_2-POINT DFT OF PART OF THE ORIGINAL SEQUENCE OF f_k'S CONDITIONED BY THE PHASE FACTOR $\exp(-2\pi i k \mu / N)$.

CONVERSELY, THE EFFECT OF TAKING THE N_2-POINT INVERSE DFT OF AN N_2-POINT SUBSET [E.G., $\ell = 0, 3, 6, 9$ OR $\ell = 1, 4, 7, 10$ FOR $N = 12$] OF F_ℓ IS f_k IN THE RANGE $k = 0, 1, 2, \ldots N_2 - 1$ WITH A PHASE FACTOR APPLIED.

WE ARE NOW IN A POSITION TO SPECIFY THE STEPS REQUIRED TO SYNTHESIZE THE APERTURE AUTOCORRELATION FROM THE DFT'S OF THE SMALLER SUB-APERTURES.

LET US ILLUSTRATE IN ONE DIMENSION FIRST. LET $N = N_1 N_2$ WHERE

N_1 = NUMBER OF GROUPS OF SAMPLES,

N_2 = NUMBER OF SAMPLES/GROUP.

ASSUME THERE ARE R SUB-APERTURES $a_k^{(r)}$ WHERE $r = 1, 2, 3, \ldots R$ AND $k = 0, 1, 2, \ldots N-1$. ASSUME FURTHER THAT EACH SUB-APERTURE IS DEFINED SO THAT ITS NON-ZERO SAMPLES OCCUPY THE LOWEST k INDICES AND THAT

$$a_k^{(r)} = 0 \qquad \text{FOR } k \geq N_2 \text{, ALL } r. \qquad (213)$$

THE ℓ-TH POINT OF THE DFT OF THE r-TH SUB-APERTURE IS

$$A_\ell^{(r)} = \sum_{\mu=0}^{N-1} a_\mu^{(r)} e^{\frac{-2\pi i \ell \mu}{N}} \qquad (214)$$

WE CAN ALSO EXPRESS $\overset{(\lambda)}{A}_{\ell}$ AS

$$\overset{(\lambda)}{A}_{\ell} = \overset{(\lambda)}{\hat{A}}_{m,p} = \sum_{k=0}^{N_2-1}\left[\overset{(\lambda)}{a}_k e^{-\frac{2\pi i k p}{N}}\right] e^{-\frac{2\pi i m k}{N_2}} \qquad (\ell = 0,1,2,\ldots N-1) \tag{215}$$

FROM (212) WHERE

$$p = \ell \bmod N_1 \equiv \ell\big|_{N_1} \tag{216a}$$

$$m = \mathrm{int}(\ell/N_1) \equiv \left[\!\left[\frac{\ell}{N_1}\right]\!\right] \tag{216b}$$

AND (215) IS JUST AN APPLICATION OF (212).

FROM (207), THE DFT OF THE λ-TH APERTURE AFTER TRANSLATION A DISTANCE x_λ IS

$$\overset{(\lambda)}{A}{}'_{\ell} = e^{-\frac{2\pi i \ell}{N}\frac{x_\lambda}{X}} \overset{(\lambda)}{A}_{\ell} \tag{217}$$

WHERE X IS THE SAMPLE INTERVAL OVER THE APERTURE. BECAUSE OF THE LINEARITY OF THE DFT, THE DFT OF SEVERAL APERTURES IS THE SUM

$$A_\ell = \sum_{\lambda=1}^{R} \overset{(\lambda)}{A}{}'_{\ell} = \sum_{\lambda=1}^{R} e^{-\frac{2\pi i \ell}{N}\frac{x_\lambda}{X}} \overset{(\lambda)}{A}_{\ell} \tag{218}$$

FROM (196), THE m-TH POINT OF THE APERTURE AUTOCORRELATION IS

$$a_m = \frac{1}{N}\sum_{\ell=0}^{N-1} A_\ell A_\ell^* e^{-\frac{2\pi i \ell m}{N}} =$$

$$= \frac{1}{N}\sum_{\lambda=1}^{R}\sum_{\mu=1}^{R}\sum_{\ell=0}^{N-1} \overset{(\lambda)}{A}_{\ell} \overset{(\mu)}{A}{}^*_{\ell}\, e^{-\frac{2\pi i \ell}{N}\left(\frac{x_\lambda - x_\mu}{X} + m\right)} \tag{219}$$

$$(m = 0,1,2,\ldots N-1)$$

THE INNER SUMMATION ON l OVER THE RANGE $0 \le l < N$ CAN BE EQUATED TO SUMS OVER N_1 AND N_2 BY UTILIZING

$$\sum_{l=0}^{N-1} f_l = \sum_{m=0}^{N_2-1}\sum_{\mu=0}^{N_1-1} f_{mN_1+\mu} = \sum_{m=0}^{N_2-1}\sum_{\mu=0}^{N_1-1} \hat{\hat{f}}_{m,\mu} \tag{220}$$

WHERE m AND μ ARE DEFINED BY (216a, b) AND $\hat{\hat{f}}_{m,\mu}$ IS JUST $f_{mN_1+\mu}$. CONSEQUENTLY, (219) CAN BE WRITTEN AS

$$\boxed{a_{\mathfrak{m}} = \frac{1}{N}\sum_{r=1}^{R}\sum_{s=1}^{R}\sum_{m=0}^{N_2-1}\sum_{\mu=0}^{N_1-1} \hat{\hat{A}}^{(r)}_{m,\mu}\,\hat{\hat{A}}^{(s)*}_{m,\mu}\, e^{-\frac{2\pi i(mN_1+\mu)}{N}\left(\frac{x_r-x_s}{X}+\mathfrak{m}\right)}} . \tag{221}$$

$$(\mathfrak{m}=0,1,2,\ldots N-1)$$

FROM (215) WE SEE THAT $\hat{\hat{A}}^{(r)}_{m,\mu}$ IS AN N_2-POINT DFT, SO THAT (221) EXPRESSES THE $\mathfrak{m}$-TH POINT OF THE APERTURE AUTOCORRELATION IN TERMS OF DFT'S OF SMALLER SEGMENTS OF THE OVERALL APERTURE.

NOTE THAT, BY (215), FORMATION OF $\hat{\hat{A}}^{(r)}_{m,\mu}$ INVOLVES MULTIPLICATION OF $a^{(r)}_k$ BY A PHASOR DEPENDING ON μ. SUBSEQUENTLY (221) APPLIES ANOTHER PHASOR DEPENDING ON μ. IT IS POSSIBLE TO COMBINE THE OPERATIONS INVOLVING μ SO THAT A SIMPLER EXPRESSION RESULTS WITH THE SUMMATION ON μ DONE, AS WELL AS THAT ON m. INTRODUCE (215) INTO (221) TO GET

$$a_{\mathfrak{m}} = \frac{1}{N}\sum_{r=1}^{R}\sum_{s=1}^{R}\sum_{m=0}^{N_2-1}\sum_{\mu=0}^{N_1-1}\sum_{k=0}^{N_2-1}\sum_{l=0}^{N_2-1} a^{(r)}_k\, a^{(s)*}_l\, e^{-\frac{2\pi i}{N}(k\mu-l\mu)}\, e^{-\frac{2\pi i}{N_2}(mk-ml)} \times$$

$$\times\, e^{-\frac{2\pi i}{N}(mN_1+\mu)\left(\frac{x_r-x_s}{X}+\mathfrak{m}\right)} =$$

$$= \frac{1}{N}\sum_{r=1}^{R}\sum_{s=1}^{R}\sum_{k=0}^{N_2-1}\sum_{l=0}^{N_2-1} a^{(r)}_k\, a^{(s)*}_l \sum_{m=0}^{N_2-1} e^{-\frac{2\pi i}{N_2}\left(k-l+\frac{x_r-x_s}{X}+\mathfrak{m}\right)m} \times$$

$$\times \sum_{\mu=0}^{N_1-1} e^{-\frac{2\pi i}{N}\left(k-l+\frac{x_r-x_s}{X}+\mathfrak{m}\right)\mu} \tag{222}$$

THE SUMMATIONS ON μ AND p CAN BE DONE USING

$$\sum_{l=0}^{N-1} \eta^{l} = \frac{1-\eta^{N}}{1-\eta}$$

TO GET

$$\sum_{\mu=0}^{N_2-1} e^{-\frac{2\pi i}{N_2}\left(k-l+\frac{x_r-x_s}{X}+m\right)\mu} = \frac{1-e^{-2\pi i\left(k-l+m+\frac{x_r-x_s}{X}\right)}}{1-e^{-\frac{2\pi i}{N_2}\left(k-l+m+\frac{x_r-x_s}{X}\right)}}$$

AND,

$$\sum_{p=0}^{N_1-1} e^{-\frac{2\pi i}{N}\left(k-l+\frac{x_r-x_s}{X}+m\right)p} = \frac{1-e^{-\frac{2\pi i}{N_2}\left(k-l+m+\frac{x_r-x_s}{X}\right)}}{1-e^{-\frac{2\pi i}{N}\left(k-l+m+\frac{x_r-x_s}{X}\right)}}$$

NOTE THAT THE DENOMINATOR OF THE FIRST CANCELS THE NUMERATOR OF THE SECOND WHEN THE PRODUCT IS FORMED. NOTE ALSO THAT

$$e^{-2\pi i(k-l+m)} = 1 \qquad (k, l, m \text{ INTEGER})$$

SO THAT (222) BECOMES EQUIVALENTLY

$$\boxed{a_m = \frac{1}{N}\sum_{r=1}^{R}\sum_{s=1}^{R}\left(1-e^{-2\pi i\frac{x_r-x_s}{X}}\right)\sum_{k=0}^{N_2-1}\sum_{l=0}^{N_2-1}\frac{a_k^{(r)}\,a_l^{(s)*}}{1-e^{-\frac{2\pi i}{N}\left(k-l+m+\frac{x_r-x_s}{X}\right)}}} \tag{223}$$

$$(m = 0, 1, 2, \ldots N-1)$$

THIS MAY BE PUT INTO ANOTHER POSSIBLY USEFUL FORM BY SUBSTITUTING THE DISCRETE FOURIER REPRESENTATION [N_2-POINT] OF $a_k^{(r)}$. EQN. (211) IMPLIES THAT

$$a_k^{(r)} = \frac{1}{N}\sum_{m=0}^{N_2-1} \hat{A}_m^{(r)} e^{+\frac{2\pi i m k}{N_2}} \tag{224}$$

WHERE

$$\hat{A}_m^{(\lambda)} = \sum_{k=0}^{N_2-1} a_k^{(\lambda)} e^{-\frac{2\pi i m k}{N_2}} \tag{225}$$

WITH (224) a_m BECOMES

$$\boxed{a_m = \frac{1}{N^3} \sum_{\lambda=1}^{R} \sum_{\mu=1}^{R} \left(1 - e^{-2\pi i \frac{x_\lambda - x_\mu}{X}}\right) \sum_{m=0}^{N_2-1} \sum_{j=0}^{N_2-1} \hat{A}_m^{(\lambda)} \hat{A}_j^{(\mu)*} \times \times \sum_{k=0}^{N_2-1} \sum_{l=0}^{N_2-1} \frac{e^{\frac{+2\pi i}{N_2}(mk - jl)}}{1 - e^{-\frac{2\pi i}{N}\left(k - l + m + \frac{x_\lambda - x_\mu}{X}\right)}}} \tag{226}$$

THE RIGHT-MOST DOUBLE SUMMATION IS INDEPENDENT OF THE APERTURE AND IS ESSENTIALLY THE 2-DIMENSIONAL DFT OF THE FUNCTION

$$f_{kl} \equiv \left[1 - e^{-\frac{2\pi i}{N}\left(k - l + m + \frac{x_\lambda - x_\mu}{X}\right)}\right]^{-1}$$

POISSON PHOTON STATISTICS

TO GET A RECONSTRUCTION PROCEDURE WHICH APPLIES TO NOISY SIGNALS OF A MORE REALISTIC NATURE, LET US CONSIDER THAT THE ARRIVAL OF PHOTONS AT THE TELESCOPE IS POISSON DISTRIBUTED. THERE ARE AT LEAST 3 STAGES FOR WHICH WE WOULD LIKE EXPRESSIONS OF A STATISTICAL NATURE:

- ϕ) RAW IN-COMING SIGNAL.
- 1) SIGNAL AFTER INFLUENCE OF APERTURE.
- 2) FOURIER TRANSFORM OF POST-APERTURE SIGNAL.

WE WILL USE SUBSCRIPTS ϕ, 1, AND 2 ACCORDINGLY.

REVIEW OF POISSON STATISTICS

LET:

$p_0(\vec{k})$ = PROBABILITY PER UNIT TIME OF ARRIVAL OF A PHOTON AT THE TELESCOPE FROM DIRECTION $\vec{k}$.

T = TOTAL OBSERVING TIME WITH APERTURE IN A GIVEN ORIENTATION.

DIVIDE THE OBSERVING TIME T INTO ℓ INTERVALS OF LENGTH $\tau = \frac{T}{\ell}$.

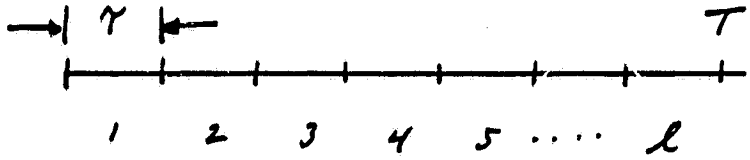

PROBABILITY OF PHOTON ARRIVING IN ANY ONE OF THE INTERVALS OF LENGTH τ IS $p_0\tau$. PROBABILITY OF NO PHOTON ARRIVING IN THE INTERVAL τ IS $1-p_0\tau$. MULTIPLE ARRIVALS ASSUMED NEGLIGIBLE. PROBABILITY OF EXACTLY m PHOTONS ARRIVING IN THE ℓ INTERVALS IS

$$P_0(m,T,\vec{k}) = \binom{\ell}{m}(p_0\tau)^m(1-p_0\tau)^{\ell-m} = \tag{227}$$

$$= \frac{\ell!}{m!\,(\ell-m)!}\left(\frac{p_0\tau}{1-p_0\tau}\right)^m(1-p_0\tau)^\ell .$$

LET THE NUMBER OF INTERVALS ℓ GO TO ∞. THEN

$$\lim_{\ell\to\infty}\left(\frac{p_0\tau}{1-p_0\tau}\right)^m = \lim_{\ell\to\infty}\left(\frac{1}{\frac{\ell}{p_0T}-1}\right)^m \simeq \left(\frac{p_0T}{\ell}\right)^m \tag{228}$$

AND,

$$\frac{\ell!}{(\ell-m)!}\xrightarrow[\ell\to\infty]{} O\left[\ell^m\right] \tag{229}$$

WHERE $O[\ ]$ MEANS "OF THE ORDER OF".

AND,

$$(1-p_0\tau)^{\ell} = \sum_{j=0}^{\ell} \binom{\ell}{j}(-p_0\tau)^{j} = \sum_{j=0}^{\ell} \frac{\ell!}{j!\,(\ell-j)!}\;\frac{(-p_0T)^{j}}{\ell^{j}} \qquad (230)$$

NOW APPLY (229) TO $\ell!/(\ell-j)!$ IN (230) AS $\ell \to \infty$

$$\frac{\ell!}{(\ell-j)!} \xrightarrow[\ell\to\infty]{} O[\ell^{j}] \quad .$$

THUS,

$$\lim_{\ell\to\infty} (1-p_0\tau)^{\ell} = \sum_{j=0}^{\infty} \frac{(-p_0T)^{j}}{j!} = e^{-p_0T} \quad . \qquad (231)$$

RESULTS (228), (229), AND (231) IN (227) GIVE

$$\boxed{P_0(m,T,\vec{k}) = e^{-p_0(\vec{k})T}\,\frac{\left[p_0(\vec{k})T\right]^{m}}{m!}} \qquad (232)$$

FOR THE PROBABILITY OF m PHOTONS ARRIVING AT THE TELESCOPE IN A FINITE MACRO-TIME T FROM THE DIRECTION $\vec{k}$.

WE NOW ASK WHAT IS THE EXPECTED NUMBER OF PHOTONS ARRIVING AT THE TELESCOPE IN TIME T FROM DIRECTION $\vec{k}$.

$$E_0\{m\} = \sum_{m=0}^{\infty} m\,P_0(m,T,\vec{k}) = e^{-p_0T}\sum_{m=0}^{\infty} m\,\frac{(p_0T)^{m}}{m!} =$$

$$= e^{-p_0T}\sum_{m=1}^{\infty}\frac{(p_0T)^{m}}{(m-1)!} = e^{-p_0T}(p_0T)\sum_{m=1}^{\infty}\frac{(p_0T)^{m-1}}{(m-1)!} =$$

$$= e^{-p_0T}\,(p_0T)\,e^{+p_0T}$$

or,

$$\boxed{E_0\{m\} = \rho_0(\vec{k})T} \qquad (233)$$

WHAT IS THE VARIANCE OF THE PHOTON NUMBER IN TIME T ABOUT THE MEAN VALUE (233)?

$$E_0\{(m-\rho_0 T)^2\} = E_0\{m^2 - 2m\rho_0 T + (\rho_0 T)^2\} =$$

$$= E_0\{m^2\} - 2\rho_0 T E_0\{m\} + (\rho_0 T)^2 = E_0\{m^2\} - (\rho_0 T)^2 \qquad (234)$$

$$E_0\{m^2\} = \sum_{m=0}^{\infty} m^2 P_0(m,T,\vec{k}) = e^{-\rho_0 T}\sum_{m=0}^{\infty} m^2 \frac{(\rho_0 T)^m}{m!} =$$

$$= \rho_0 T\, e^{-\rho_0 T}\sum_{m=1}^{\infty} m \frac{(\rho_0 T)^{m-1}}{(m-1)!} = \rho_0 T\, e^{-\rho_0 T}\sum_{m=0}^{\infty}(m+1)\frac{(\rho_0 T)^m}{m!} =$$

$$= \rho_0 T\, e^{-\rho_0 T}\left\{\sum_{m=0}^{\infty} m \frac{(\rho_0 T)^m}{m!} + e^{+\rho_0 T}\right\} =$$

$$= \rho_0 T\, e^{-\rho_0 T}\left\{\rho_0 T\, e^{+\rho_0 T} + e^{+\rho_0 T}\right\} = (\rho_0 T)^2 + (\rho_0 T) \qquad (235)$$

RESULT (235) IN (234) GIVES

$$\boxed{E_0\{(m-\rho_0 T)^2\} = \rho_0(\vec{k})T = E_0\{m\}} \qquad (236)$$

WE ASSUME THAT $\rho_0(\vec{k})$ IS PROPORTIONAL TO THE INCOMING INTENSITY.

$$\rho_0(\vec{k}) = \kappa\,|u(\vec{k})|^2 \qquad (237)$$

POST-APERTURE STATISTICS

BECAUSE OF (237) AND THE LINEARITY OF (19), THE PROBABILITY PER UNIT TIME OF DEPARTURE OF A PHOTON FROM THE TELESCOPE APERTURE IN DIRECTION $\vec{k}'$ IS

$$p_1(\vec{k}') = \kappa \langle I(\vec{k}',t)\rangle = \kappa \iint_{-\infty}^{\infty} dk_x\, dk_z\, |u(\vec{k})|^2 \left|A\left[(k_x'-k_x),(k_z'-k_z)\right]\right|^2 = \tag{238}$$

$$= \kappa I(\vec{k}') = \iint_{-\infty}^{\infty} dk_x\, dk_z\, p_0(\vec{k}) \left|A\left[(k_x'-k_x),(k_z'-k_z)\right]\right|^2 .$$

WE CAN WRITE DOWN IMMEDIATELY THAT

$$\boxed{\begin{aligned} E_1\{n\} &= p_1(\vec{k}')T && (239a)\\ E_1\{(n-p_1T)^2\} &= p_1(\vec{k}')T = E_1\{n\} && (239b)\\ P_1(n,T,\vec{k}') &= e^{-p_1(\vec{k}')T}\,\frac{[p_1(\vec{k}')T]^n}{n!} && (239c)\end{aligned}}$$

FOR PHOTONS TRAVELLING AWAY FROM THE APERTURE IN THE DIRECTION $\vec{k}'$.

FOURIER DOMAIN STATISTICS

AS DEFINED ABOVE, THE INTENSITY PRE OR POST-APERTURE IS A MEASURE OF THE PROBABILITY PER UNIT TIME OF COUNTING A PHOTON MOVING IN A GIVEN DIRECTION. EQUATION (21) REQUIRES US TO KNOW THE INTENSITY FUNCTION $I(\vec{k})$. STRICTLY, WE DO NOT KNOW $I(\vec{k})$ OR, WHAT IS THE SAME THING, THE PROBABILITY PER UNIT TIME OF A PHOTON. WHAT WE DO IS TO COUNT, FOR EACH $\vec{k}$, FOR A TIME T THE NUMBER OF PHOTONS. THAT IS, WE FORM A FUNCTION

$$N(T,\vec{k})$$

WHICH CONSISTS OF SAMPLES FROM THE DISTRIBUTION (239c). FOR EXAMPLE,

$$E\{N(T,\vec{k})\} = \sum_{m=0}^{\infty} m\, P_1(m,T,\vec{k}) \equiv E_1\{m\} = \mu_1(\vec{k})T = \kappa T\, I(\vec{k}) \quad . \qquad (240)$$

THUS THE EXPECTED VALUE OF $N(T,\vec{k})$ IS PROPORTIONAL TO THE FUNCTION WE WOULD LIKE TO KNOW EXACTLY, $I(\vec{k})$. BUT, IT IS $N(T,\vec{k})$ WHICH WE ACTUALLY MEASURE AND TAKE THE FOURIER TRANSFORM OF ACCORDING TO (21). THAT IS, WE FORM

$$\tilde{\mathcal{I}}(\vec{\nu}) = \iint_{-\infty}^{\infty} dk_x\, dk_z\, N(T,\vec{k})\, e^{-2\pi i \vec{k}\cdot\vec{\nu}} \quad . \qquad (241)$$

OVER AN ENSEMBLE, WHAT IS THE MEAN AND VARIANCE OF (241)?

$$\boxed{E_2\{\tilde{\mathcal{I}}(\vec{\nu})\} = \iint_{-\infty}^{\infty} dk_x\, dk_z\, E\{N(T,\vec{k})\}\, e^{-2\pi i \vec{k}\cdot\vec{\nu}} = \kappa T\, \mathcal{I}(\vec{\nu})} \qquad (242)$$

USING (240) AND (21). IN WORDS, THE EXPECTED VALUE AT A POINT $\vec{\nu}$ IN THE FOURIER DOMAIN IS PROPORTIONAL TO THE OBSERVING TIME T AND TO THE NOISELESS IMAGE TRANSFORM $\mathcal{I}(\vec{\nu})$.

THE VARIANCE IS FOUND FROM

$$E_2\{|\tilde{\mathcal{I}}(\vec{\nu}) - \kappa T\, \mathcal{I}(\vec{\nu})|^2\} =$$

$$= E_2\left\{\iint_{-\infty}^{\infty} d\vec{k}_1 \iint_{-\infty}^{\infty} d\vec{k}_2 \left[N(T,\vec{k}_1) - \kappa T\, I(\vec{k}_1)\right]\left[N(T,\vec{k}_2) - \kappa T\, I(\vec{k}_2)\right] e^{-2\pi i \vec{\nu}\cdot(\vec{k}_1-\vec{k}_2)}\right\} =$$

$$= \iint_{-\infty}^{\infty} d\vec{k}_1 \iint_{-\infty}^{\infty} d\vec{k}_2\, e^{-2\pi i \vec{\nu}\cdot(\vec{k}_1-\vec{k}_2)}\, E_1\left\{\left[N(T,\vec{k}_1) - \kappa T\, I(\vec{k}_1)\right]\left[N(T,\vec{k}_2) - \kappa T\, I(\vec{k}_2)\right]\right\} \qquad (243)$$

IF WE ASSUME THAT PHOTONS TRAVELLING IN DIRECTIONS $\vec{k}_1$ AND $\vec{k}_2$ ARE UNCORRELATED IF $\vec{k}_1 \neq \vec{k}_2$, THEN

$$E_1\{[N(T,\vec{k}_1)-\kappa T I(\vec{k}_1)][N(T,\vec{k}_2)-\kappa T I(\vec{k}_2)]\}=$$
$$= \delta(\vec{k}_1-\vec{k}_2)\, E_1\{[N(T,\vec{k}_1)-\kappa T I(\vec{k}_1)]^2\} =$$
$$= \delta(\vec{k}_1-\vec{k}_2)\, \kappa T\, I(\vec{k}_1) \tag{244}$$

THIS RESULT IN (243) GIVES

$$\boxed{E_2\{|\tilde{J}(\vec{v})-\kappa T \sigma(\vec{v})|^2\} = \kappa T \iint_{-\infty}^{\infty} d\vec{k}\; I(\vec{k}) = \iint_{-\infty}^{\infty} d\vec{k}\; E\{N(T,\vec{k})\}} \tag{245}$$

JUSTIFICATION FOR (244) MAY BE SEEN FROM THE QUANTUM MECHANICAL INTERPRETATION OF THE EFFECT OF THE TELESCOPE APERTURE ON THE INCOMING PHOTONS. SPECIFICALLY, THE APERTURE IS VIEWED IN THE PARTICLE PICTURE AS A SCATTERER OF THE INCOMING PHOTONS. PHOTONS FROM A GIVEN DIRECTION, WHICH ARE ASSUMED TO ARRIVE AT RANDOM AND UNCORRELATED WITH EACH OTHER, ARE SCATTERED INTO A "CONE" OF ANGLES WITH A PROBABILITY DISTRIBUTION GIVEN BY THE DIFFRACTION PATTERN OF THE WAVE PICTURE.

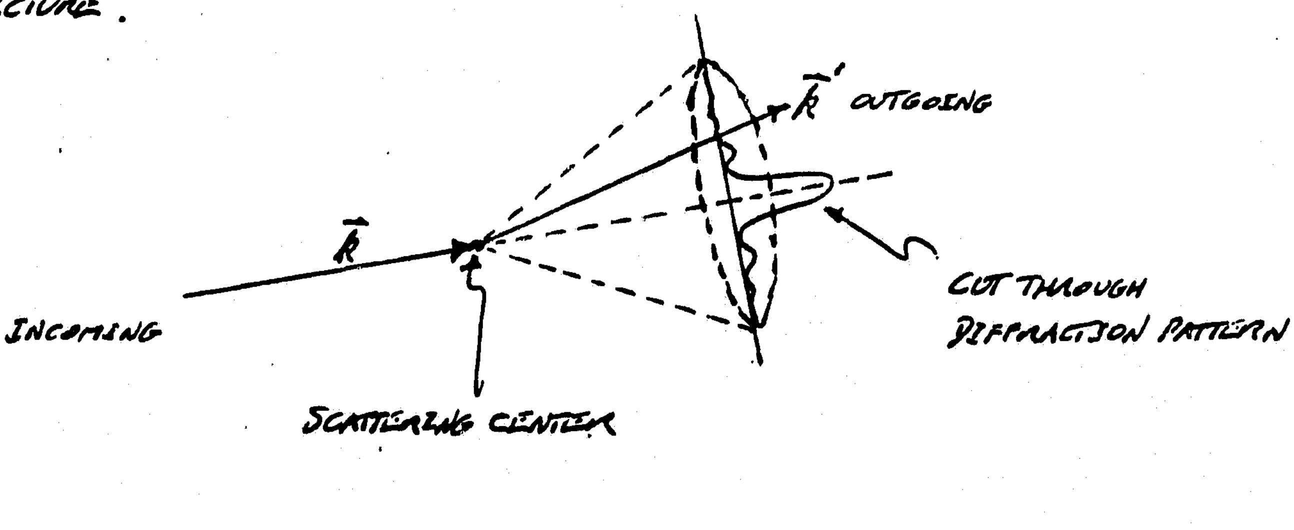

CONSIDER TWO DIFFERENT OUTGOING DIRECTIONS $\vec{k}_1'$ AND $\vec{k}_2'$ AND AN ENSEMBLE OF EXPERIMENTS RUN FOR A TIME T. OVER THE ENSEMBLE THE NUMBERS OF PHOTONS COUNTED OUTGOING ALONG $\vec{k}_1'$ AND $\vec{k}_2'$ WILL BE RANDOMLY DISTRIBUTED ABOUT TWO, GENERALLY DIFFERENT, MEAN VALUES.

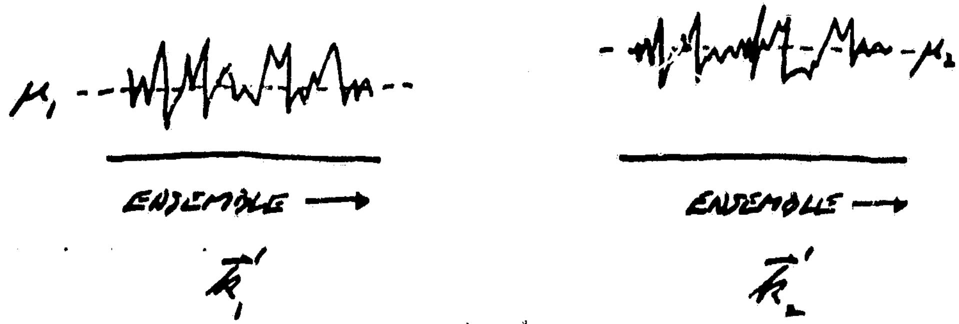

$\mu_1 \neq \mu_2$

WHEN THE APPROPRIATE MEANS ARE SUBTRACTED, AS IN (244), THERE IS NO CORRELATION OF THE VARIATION OF PHOTON COUNTS AT $\vec{k}_1'$ AND $\vec{k}_2'$ OVER THE ENSEMBLE, UNLESS THERE IS CORRELATION WITHIN EACH ENSEMBLE MEMBER.

CONSIDER THE SAME EXPERIMENT RUN MANY TIMES ON A SINGLE MEMBER OF THE ENSEMBLE. WE COUNT PHOTONS FOR INTERVALS T AT EACH OF THE TWO OUTGOING DIRECTIONS, $\vec{k}_1'$ AND $\vec{k}_2'$. AGAIN, OVER THE MANY INTERVALS, THE COUNTS WILL BE DISTRIBUTED RANDOMLY AROUND THE RESPECTIVE MEAN VALUES μ_1 AND μ_2. WILL THE RESIDUALS AFTER SUBTRACTING THE RESPECTIVE MEAN VALUES BE CORRELATED BETWEEN $\vec{k}_1'$ AND $\vec{k}_2'$ FOR $\vec{k}_1' \neq \vec{k}_2'$? THAT IS, WILL A COUNT ABOVE OR BELOW THE AVERAGE AT $\vec{k}_1'$ HAVE ANY PREDICTIVE VALUE FOR THE COUNT BEING ABOVE OR BELOW THE AVERAGE AT $\vec{k}_2'$ IN THE INTERVAL T? IT WOULD APPEAR FROM THE QUANTUM MECHANICAL VIEW THAT THE ANSWER MUST BE NO. AFTER ONE PHOTON HAS INTERACTED WITH THE APERTURE AND BEEN SCATTERED IT IS PRESUMED NOT TO CONDITION THE APPARATUS IN ANY WAY WHICH THE NEXT PHOTON COULD USE TO DECIDE TO WHERE IT WOULD PREFERENTIALLY LIKE TO SCATTER. IF SUCCESSIVE PHOTONS CAN NOT INFLUENCE EACH OTHER THROUGH THE INTERMEDIARY OF THE APERTURE, THEN THE RANDOMNESS BETWEEN $\vec{k}_1'$ AND $\vec{k}_2'$ MUST BE UNCORRELATED.

THIS LINE OF REASONING MUST BE TEMPERED BY THE FOLLOWING. THE WAVE FUNCTION IN QUANTUM MECHANICS MAKES STATISTICAL PREDICTIONS IN THE <u>ENSEMBLE AVERAGE SENSE ONLY</u>. ESSENTIALLY ALL OF THE APPARENT PARADOXES OF Q.M. COME FROM ATTEMPTING TO APPLY THESE PREDICTIONS TO A SINGLE MEMBER OF THE ENSEMBLE. A BETTER APPROACH IS TO SHOW THE RESULT IN THE ENSEMBLE SENSE AND THEN TO JUSTIFY THE ERGODIC ASSUMPTION.

IN WORDS, RESULTS (242) AND (245) STATE THAT:

a) THE AVERAGE VALUE AT A POINT $\vec{\nu}$ OF THE FOURIER TRANSFORM OF A REAL IMAGE MADE FROM POISSON-DISTRIBUTED PHOTONS IS PROPORTIONAL TO THE FOURIER TRANSFORM OF THE IDEAL NOISELESS IMAGE.

b) THE VARIANCE OF THE FOURIER TRANSFORM OF SUCH A REAL IMAGE IS INDEPENDENT OF $\vec{\nu}$ AND IS PROPORTIONAL TO THE TOTAL INTEGRATED INTENSITY OF THE IMAGE.

NOTE THAT:

a) THE FIRST RESULT ABOVE IS TRUE INDEPENDENT OF THE SPECIFIC NATURE OF THE PHOTON PROBABILITY DISTRIBUTION [BECAUSE THE EXPECTED VALUE OF THE TRANSFORM IS EQUAL TO THE TRANSFORM OF THE EXPECTED VALUE].

b) THE SECOND RESULT IS SPECIFIC TO THE POISSON NATURE OF THE PHOTON DISTRIBUTION; IN PARTICULAR THE FACT THAT THE VARIANCE AND MEAN OF A POISSON DISTRIBUTED VARIABLE ARE NUMERICALLY EQUAL. SEE (236) AND (239).

RESULT (245) FOR THE FOURIER-DOMAIN VARIANCE MAY BE EXPRESSED ALSO IN TERMS OF $\mathcal{I}(\vec{\nu})$. BY INSPECTION, IF WE SET $\vec{\nu}=0$ IN (21)

$$\mathcal{I}(\vec{\nu}=0) = \iint_{-\infty}^{\infty} d\vec{k}\, I(\vec{k})\, e^{0} = \iint_{-\infty}^{\infty} d\vec{k}\, I(\vec{k})$$

SO THAT

$$\boxed{E_2\left\{\left|\tilde{\mathcal{I}}(\vec{\nu}) - KT\mathcal{I}(\vec{\nu})\right|^2\right\} = KT\iint_{-\infty}^{\infty} d\vec{k}\, I(\vec{k}) = KT\,\mathcal{I}(\vec{\nu}=0)} \qquad (246)$$

THIS RESULT CAN BE OBTAINED ALSO BY SUBSTITUTING THE INVERSE FOURIER TRANSFORM OF $\mathcal{I}(\vec{\nu})$ FOR $I(\vec{k})$ IN (245) AND USING THE VECTOR FORM OF

THE DEFINITION OF THE DIRAC DELTA-FUNCTION (8).

OTHER SOURCES OF NOISE

BESIDES THE POISSON DISTRIBUTED PHOTONS FROM THE IMAGE [SKY] ITSELF, WE CONSIDER TWO OTHER NOISE SOURCES; PHOTONS EMITTED RANDOMLY [POISSON] FROM THE SKY INTO THE APERTURE AND COUNTS INDUCED AT RANDOM OVER THE CCD ARRAY IN THE POST-APERTURE IMAGE PLANE DUE TO COSMIC RAYS, ETC.

BACKGROUND PHOTONS FROM THE SKY APPEAR TO THE INSTRUMENT TO BE PART OF THE "IMAGE" AND ARE REFLECTED IN THE VALUE OF $\mu_0(\vec{k})$ AND, HENCE, OF $\mu_1(\vec{k})$. SEE (239). THERE IS NO WAY A PRIORI THAT THESE BACKGROUND PHOTONS CAN BE DISTINGUISHED FROM THE "TRUE" IMAGE.

CAN THE COUNTS INDUCED RANDOMLY OVER THE CCD ARRAY, BUT WHICH HAVE NOT BEEN THROUGH THE APERTURE, BE DISTINGUISHED AND, HENCE, COMPENSATED FOR IN ANY WAY? IN PARTICULAR, IS THERE ANY STATISTICAL PARAMETER [E.G., A HIGHER-ORDER MOMENT] WHICH MIGHT BE USED TO DISTINGUISH THIS SOURCE OF NOISE?

THE ANSWER IS EVIDENTLY NO. IF SUCH COUNTS ARE ASSUMED TO BE POISSON DISTRIBUTED, THEIR SUM WITH THE POISSON DISTRIBUTED PHOTONS WHICH HAVE BEEN THROUGH THE APERTURE IS ALSO POISSON. HENCE, NO HIGHER MOMENT CAN BE USED TO SEPARATE THE TWO SOURCES OF VARIABILITY AT A GIVEN POINT IN THE IMAGE PLANE. TO SHOW THIS LET THE TWO SOURCES COME FROM, OR BE REPRESENTED BY, POISSON DISTRIBUTIONS P_1 AND P_2.

$$P_1(m) = e^{-\mu_1 T}\frac{(\mu_1 T)^m}{m!} \quad , \quad P_2(m) = e^{-\mu_2 T}\frac{(\mu_2 T)^m}{m!} \qquad (247)$$

IF m COUNTS ARE RECEIVED FROM THE TWO DISTRIBUTIONS, THAT IS, A TOTAL OF m COUNTS IS RECEIVED AT A GIVEN POINT OF THE IMAGE PLANE, WHAT IS THE PROBABILITY IN TIME T OF SUCH A RESULT? THE m COUNTS CAN BE DUE TO ZERO COUNTS FROM P_1 AND m FROM P_2; ONE FROM P_1 AND $m-1$ FROM P_2, ETC. CONSIDERING ALL THE WAYS THAT m TOTAL COUNTS CAN RESULT FROM TWO DISTRIBUTIONS SUMMED, THE PROBABILITY OF THE RESULT m IS

$$P(n) = \sum_{l=0}^{n} P_1(l)\, P_2(n-l) = \sum_{l=0}^{n} e^{-\mu_1 T} \frac{(\mu_1 T)^l}{l!} e^{-\mu_2 T} \frac{(\mu_2 T)^{n-l}}{(n-l)!} =$$

$$= e^{-(\mu_1+\mu_2)T} \sum_{l=0}^{n} \frac{(\mu_1 T)^l (\mu_2 T)^{n-l}}{l!\,(n-l)!} =$$

$$= e^{-(\mu_1+\mu_2)T} \frac{1}{n!} \sum_{l=0}^{n} \frac{n!}{l!\,(n-l)!} (\mu_1 T)^l (\mu_2 T)^{n-l}$$

THE COEFFICIENT UNDER THE SUMMATION IS

$$\frac{n!}{l!\,(n-l)!} = \binom{n}{l}$$

AND THE ENTIRE SUMMATION WILL BE RECOGNIZED AS $(\mu_1 T + \mu_2 T)^n$ SO THAT

$$P(n) = e^{-(\mu_1+\mu_2)T} \frac{[(\mu_1+\mu_2)T]^n}{n!} \quad . \tag{248}$$

THUS, THE DISTRIBUTION OF THE SUM OF SAMPLES FROM POISSON DISTRIBUTIONS IS AGAIN POISSON DISTRIBUTED. BY INDUCTION, IF THERE ARE m POISSON DISTRIBUTIONS, THE DISTRIBUTION OF THE SUM WILL BE

$$P(n) = e^{-\lambda T} \frac{(\lambda T)^n}{n!} \tag{249a}$$

WHERE:

$$\lambda = \sum_{l=1}^{m} \mu_l \tag{249b}$$

SINCE THE SUM DISTRIBUTION IS AGAIN POISSON, THERE IS NO RELATIONSHIP INVOLVING HIGHER MOMENTS WHICH WILL DISTINGUISH THE TWO [OR SEVERAL POISSON-DISTRIBUTED] SOURCES OF COUNTS.

IT IS TO BE EMPHASIZED THAT THESE RESULTS APPLY TO THE STATISTICS AT

A GIVEN POINT IN THE IMAGE PLANE AND, HENCE, RELATE TO THE OPTIMUM COMBINATION OF OVERLAPPING IMAGES. THIS IS DISTINCT FROM THE SUBSEQUENT FILTERING PROCESS WHICH MAKES ESTIMATES ON THE BASIS OF INFORMATION IN A REGION OF THE PLANE, IMAGE AND/OR FOURIER. WHEN REGIONAL INFORMATION IS TAKEN INTO ACCOUNT, AS IN FILTERING, THEN THERE ARE DIFFERENCES BETWEEN PHOTON COUNTS IMAGED BY THE APERTURE AND IMAGE-PLANE-ONLY COUNTS. THE FORMER GROUP IN THE IMAGE PLANE IN CLUSTERS CHARACTERISTIC OF THE DIFFRACTION PATTERN OF THE INSTRUMENT; THE LATTER DO NOT. THIS DIFFERENCE CAN BE USEFUL ON A REGIONAL BASIS, BUT DOES NOT ENTER INTO THE QUESTION OF THE OPTIMUM COMBINATION OF OVERLAPPED IMAGES.

NOISE FILTER WITH POISSON STATISTICS

EARLIER WE DEVELOPED SOME TECHNIQUES FOR NOISE FILTERING [WEIGHTED MULTIPLE REGRESSION] ON THE ASSUMPTION OF GAUSSIAN STATISTICS IN THE $\vec{\nu}$-PLANE AFTER THE IMAGE COMBINATION STEP. WE NOW WANT TO LOOK MORE CLOSELY AT THIS PROBLEM, KEEPING IN MIND THAT THE STATISTICS IN THE ORIGINAL IMAGE DOMAIN ARE POISSON. WE ARE ESPECIALLY INTERESTED IN TECHNIQUES APPLICABLE TO LOW LIGHT-LEVELS WHEN THE DIFFERENCE BETWEEN POISSON AND GAUSSIAN STATISTICS IS MOST PRONOUNCED. AS THE LIGHT LEVEL IS INCREASED, THIS DIFFERENCE DE-CREASES, SO THAT WE ANTICIPATE THAT RESULTS DERIVED FOR THE POISSON CASE WILL GO OVER TO THE RESULTS DERIVED EARLIER FOR THE GAUSSIAN CASE. THIS WILL BE SO, OF COURSE, ONLY IF IT CAN BE SHOWN THAT THE $\vec{\nu}$-PLANE STATISTICS BECOME GAUSSIAN AT HIGH LIGHT LEVELS.

THE FIRST QUESTION TO BE ASKED IS "WHAT ARE THE $\vec{\nu}$-PLANE STATISTICS IF THE IMAGE PLANE STATISTICS ARE POISSON"? WE HAVE ALREADY RELATED THE MEAN AND VARIANCE IN THE $\vec{\nu}$-PLANE [FIRST AND SECOND STATISTICAL MOMENTS] TO THE STATISTICS OF THE IMAGE PLANE, BUT HAVE NOT GIVEN A RESULT FOR THE $\vec{\nu}$-PLANE DISTRIBUTION FUNCTION. RECALL THAT THE REGRESSION APPROACHED DEPENDED ON KNOWING THE PROBABILITY DENSITY FUNCTION, NOT JUST TWO MOMENTS.

THE DISCRETE FOURIER TRANSFORM WHICH PRODUCES THE $\vec{\nu}$-PLANE FROM THE ORIGINAL IMAGE PLANE GREATLY COMPLICATES DETERMINATION OF THE $\vec{\nu}$-PLANE DENSITY FUNCTION. EACH POINT IN THE $\vec{\nu}$-PLANE IS A

LINEAR COMBINATION OF THE POINTS OF THE IMAGE PLANE. EACH POINT OF THE LATTER IS A SAMPLE FROM A POISSON DISTRIBUTION, WHICH DISTRIBUTION IS A FUNCTION OF POSITION IN THE IMAGE PLANE. FURTHER, THE WEIGHTS OF THE LINEAR COMBINATION ARE COMPLEX TRANSCENDENTALS. CONSEQUENTLY, THE MOST OBVIOUS WAY OF GETTING AN EXPRESSION FOR THE $\vec{v}$-PLANE DENSITY FUNCTION BECOMES PROHIBITIVELY COMPLICATED.

TO BE SPECIFIC, IF THE WEIGHTS ARE ALL UNITY AND THE POSSIBLE SAMPLE VALUES n_i INTEGERS

$$n_i = 0, 1, 2, 3, \ldots \; ,$$

AND IF $p_i(n)$ IS THE PROBABILITY THAT THE i-TH SAMPLE HAS THE VALUE n, THEN THE PROBABILITY OF GETTING THE RESULT m FROM THE SUM OF TWO SAMPLES INVOLVES FINDING ALL THE WAYS $n_1 + n_2$ CAN EQUAL m. THAT IS, IF THE p_i ARE INDEPENDENT,

$$p(m) = \sum_{n=0}^{m} p_1(n)\, p_2(m-n) =$$

$$= p_1(n_1=0)\, p_2(n_2=m) + p_1(n_1=1)\, p_2(n_2=m-1) + \ldots$$

$$+ \; p_1(n_1=m)\, p_2(n_2=0)$$

THE DIFFICULTY WITH THIS APPROACH TO FINDING THE PROBABILITY DENSITY IN THE FOURIER DOMAIN COMES BECAUSE THE FOURIER WEIGHTS ARE TRANSCENDENTAL, THOUGH THE SAMPLE VALUES, BEING PHOTON COUNTS, ARE SIMPLE INTEGERS 0, 1, 2, 3, ... CONSIDER THE SUM OF JUST TWO SAMPLES

$$s = a_1 n_1 + a_2 n_2 \qquad (n_i = 0, 1, 2, \ldots)$$

WHERE THE WEIGHTS a_i ARE IRRATIONAL. BECAUSE THE a_i ARE IRRATIONAL, EVERY UNIQUE COMBINATION OF VALUES $\{n_i\}$ GIVES A <u>UNIQUE</u> VALUE FOR THE WEIGHTED SUM s. THE TRICK WHICH LEADS TO THE SUMMATION FORMULA ABOVE CAN NOT BE USED. MORE TO THE POINT, THE SUMMATION FORMULA MAY LEAD TO A CLOSED-FORM EXPRESSION FOR $p(m)$. THE BEST WE CAN SAY FOR $p(s)$ IS THAT

$$p(r) = p_1(n_1)\, p_2(n_2)$$

WHERE n_1 AND n_2 CAN NOT BE DETERMINED IN CLOSED-FORM FROM r.

AN APPARENT WAY OUT OF THE PROBLEM, AT LEAST TO THE POINT THAT AN INTEGRAL REPRESENTATION CAN BE FOUND FOR THE PROBABILITY DENSITY IN THE FOURIER DOMAIN, IS TO WORK WITH THE MOMENT-GENERATING FUNCTION (MGF) OF THE POISSON DISTRIBUTION. IF ONE KNOWS ALL MOMENTS OF A PROBABILITY DISTRIBUTION, ONE KNOWS THE DISTRIBUTION UNIQUELY. SINCE THE MGF SPECIFIES ALL MOMENTS, IT IS, IN A SENSE, EQUIVALENT TO THE DENSITY FUNCTION ITSELF.

WE WILL DISCUSS SOME RELEVANT PROPERTIES OF MGF'S BELOW BEFORE APPLYING THE RESULTS TO THE IMAGE PROBLEM AT HAND. ALSO, TO HELP CONVEY THE IDEAS, WE WILL WORK IN ONLY ONE DIMENSION INITIALLY.

THE r-TH MOMENT OF THE DISCRETE DISTRIBUTION $p(n)$ IS

$$\mu_r = \sum_{n=0}^{\infty} n^r\, p(n) \qquad . \qquad (250)$$

CONSIDER INSTEAD THE FUNCTION

$$M(\theta) = \sum_{n=0}^{\infty} e^{n\theta}\, p(n) \qquad . \qquad (251)$$

θ IS A CONTINUOUS VARIABLE. BY EXPANDING $e^{n\theta}$ WE GET

$$M(\theta) = \sum_{n=0}^{\infty} p(n) + \sum_{n=0}^{\infty} (n\theta)\, p(n) + \sum_{n=0}^{\infty} \frac{(n\theta)^2}{2!}\, p(n) + \cdots\cdots =$$

$$= \mu_0 + \theta\mu_1 + \frac{\theta^2}{2!}\mu_2 + \frac{\theta^3}{3!}\mu_3 + \cdots + \frac{\theta^m}{m!}\mu_m + \cdots \qquad (252)$$

WE SEE THAT WE CAN "PICK OFF" AN ARBITRARY MOMENT μ_r FROM THE SERIES (252) BY EVALUATING

$$\boxed{\mu_r = \left.\frac{d^r M(\theta)}{d\theta^r}\right|_{\theta=0}} \tag{253}$$

$M(\theta)$ IS THE MOMENT GENERATING FUNCTION (MGF) FOR $p(n)$.

FOR THE PARTICULAR CASE OF THE POISSON DISTRIBUTION

$$p(n) = e^{-\lambda T}\frac{(\lambda T)^n}{n!} = e^{-\beta}\frac{\beta^n}{n!}, \quad (\beta \equiv \lambda T) \tag{254}$$

$$M(\theta) = e^{-\beta}\sum_{n=0}^{\infty} e^{n\theta}\frac{\beta^n}{n!} = e^{-\beta}\sum_{n=0}^{\infty}\frac{(e^\theta\beta)^n}{n!} =$$

$$= e^{-\beta}e^{\beta e^\theta} = e^{\beta[e^\theta - 1]} \quad \text{(POISSON MGF)} \tag{255}$$

THE MOMENTS DEFINED BY (250) ARE ALL ABOUT THE ORIGIN. CONSIDER THE MOMENTS ABOUT A POINT a, NOT NECESSARILY INTEGER.

$$\tilde{\mu}_r = \sum_{n=0}^{\infty}(n-a)^r p(n) \tag{256}$$

CONSIDER LIKEWISE

$$\sum_{n=0}^{\infty} e^{(n-a)\theta} p(n) = e^{-a\theta} M(\theta) =$$

$$= \sum_{n=0}^{\infty} p(n) + \sum_{n=0}^{\infty}[(n-a)\theta]\,p(n) + \sum_{n=0}^{\infty}\frac{1}{2!}[(n-a)\theta]^2 p(n) + \cdots =$$

$$= \tilde{\mu}_0 + \theta\tilde{\mu}_1 + \frac{\theta^2}{2!}\tilde{\mu}_2 + \frac{\theta^3}{3!}\tilde{\mu}_3 + \cdots + \frac{\theta^m}{m!}\tilde{\mu}_m + \cdots \tag{257}$$

THUS, THE r-TH MOMENT OF $p(n)$ ABOUT a IS GIVEN BY

$$\boxed{\tilde{\mu}_r = \left. \frac{d^r \tilde{M}(\theta)}{d\theta^r} \right|_{\theta=0}} \tag{258}$$

WHERE $\tilde{M}(\theta)$ IS THE MGF FOR $p(n)$ ABOUT a,

$$\boxed{\tilde{M}(\theta) = e^{-a\theta} \cdot M(\theta)} \tag{259}$$

SUPPOSE THAT SAMPLES FROM THE DISCRETE DISTRIBUTION $p(n)$ ARE MULTIPLIED BY A FACTOR α TO FORM A NEW DISTRIBUTION $p'(n\alpha)$. SAMPLES FROM THE ORIGINAL DISTRIBUTION HAVE VALUES 0, 1, 2, 3, ...

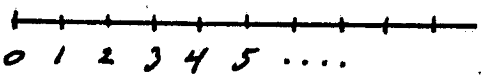

ORIGINAL SAMPLE VALUES

SAMPLES FROM THE NEW DISTRIBUTION HAVE VALUES 0, α, 2α, 3α, ...

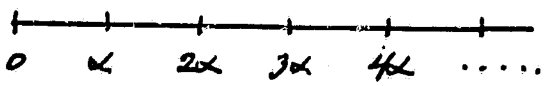

NEW SAMPLE VALUES

CLEARLY

$$p'(n\alpha) = p(n) \quad . \tag{260}$$

THE r-TH MOMENT OF THE NEW DISTRIBUTION ABOUT THE ORIGIN IS

$$\mu_r' = \sum_{n=0}^{\infty} (n\alpha)^r p'(n\alpha) = \alpha^r \sum_{n=0}^{\infty} n^r p(n)$$

OR,

$$\boxed{\mu_r' = \alpha^r \mu_r} \quad . \tag{261}$$

NOTE THAT α CAN BE COMPLEX.

THE MOMENT GENERATING FUNCTION APPROPRIATE TO THE NEW DISTRIBUTION IS FOUND BY CONSIDERING

$$\sum_{m=0}^{\infty} e^{m\alpha\theta} p'(m\alpha) = \sum_{m=0}^{\infty} e^{m\alpha\theta} p(m) =$$

$$= \sum_{m=0}^{\infty} p(m) + \sum_{m=0}^{\infty} (m\alpha\theta)\, p(m) + \frac{1}{2!}\sum_{m=0}^{\infty} (m\alpha)^2\theta^2 p(m) + \cdots =$$

$$= \mu_0' + \theta\mu_1' + \frac{\theta^2}{2!}\mu_2' + \cdots + \frac{\theta^m}{m!}\mu_m' + \cdots \tag{262}$$

WHERE μ_r' IS GIVEN BY (261). CONSEQUENTLY, THE r-TH MOMENT ABOUT THE ORIGIN OF A DISCRETE DISTRIBUTION WHOSE SAMPLES ARE SCALED BY THE FACTOR α IS

$$\boxed{\mu_r' = \left.\frac{d^r M'(\theta)}{d\theta^r}\right|_{\theta=0}} \tag{263}$$

WHERE

$$\boxed{M'(\theta) = \sum_{m=0}^{\infty} e^{m\alpha\theta} p(m)} \tag{264}$$

FOR THE PARTICULAR CASE OF THE POISSON DISTRIBUTION (254),

$$M'(\theta) = e^{-\beta}\sum_{m=0}^{\infty} e^{m\alpha\theta}\frac{\beta^m}{m!} = e^{-\beta}\sum_{m=0}^{\infty}\frac{(\beta e^{\alpha\theta})^m}{m!} =$$

$$= e^{-\beta} e^{\beta e^{\alpha\theta}} = e^{\beta\left[e^{\alpha\theta}-1\right]} \tag{265}$$

(SCALED POISSON MGF)

CONSIDER NOW THE MOMENTS AND MGF OF THE SUM OF TWO SAMPLES FROM INDEPENDENT DISCRETE DISTRIBUTIONS. LET THE TWO DISTRIBUTIONS BE μ_1 AND μ_2 AND LET US ASSUME THAT THE SAMPLES FROM μ_1 AND μ_2 ARE SCALED BY α_1 AND α_2 RESPECTIVELY. IF n AND m ARE THE SPECIFIC VALUES OF THE SAMPLES FROM μ_1 AND μ_2, WE CAN SEE THAT

$$\bar{\mu}(\alpha_1 n + \alpha_2 m) = \mu_1(n)\,\mu_2(m) \qquad (266)$$

DUE TO THE INDEPENDENCE OF μ_1 AND μ_2. $\bar{\mu}$ IS THE JOINT PROBABILITY DISTRIBUTION FOR THE WEIGHTED SUM. THE r-TH MOMENT ABOUT THE ORIGIN OF $\bar{\mu}$ IS

$$\bar{\mu}_r = \sum_{n=0}^{\infty}\sum_{m=0}^{\infty}(\alpha_1 n + \alpha_2 m)^r \mu_1(n)\,\mu_2(m) \quad . \qquad (267)$$

AS BEFORE, CONSIDER THE FUNCTION

$$\bar{M}(\theta) = \sum_{n=0}^{\infty}\sum_{m=0}^{\infty} e^{(\alpha_1 n + \alpha_2 m)\theta}\mu_1(n)\,\mu_2(m) = \sum_{n=0}^{\infty} e^{n\alpha_1\theta}\mu_1(n)\sum_{m=0}^{\infty} e^{m\alpha_2\theta}\mu_2(m) =$$

$$= M_1'(\theta)\,M_2'(\theta) \qquad (268)$$

WHERE

$$M_i'(\theta) \equiv \sum_{n=0}^{\infty} e^{n\alpha_i\theta}\mu_i(n) \quad . \qquad (269)$$

IT IS CLEAR FROM THE SAME REASONING USED EARLIER THAT

$$\boxed{\bar{\mu}_r = \left.\frac{d^r \bar{M}(\theta)}{d\theta^r}\right|_{\theta=0}} \quad , \qquad (270)$$

WITH

$$\bar{M}(\theta) = M_1'(\theta)\,M_2'(\theta) \quad .$$

THE RESULTS CLEARLY EXTEND TO THE SUM OF N SAMPLES FROM N INDEPENDENT DISTRIBUTIONS WITH WEIGHTS.

$$\bar{p}\left(\sum_{i=1}^{N} \alpha_i n_i\right) = \prod_{i=1}^{N} p_i(n_i) \tag{271}$$

$$\bar{M}(\theta) = \prod_{i=1}^{N} M_i'(\theta) \tag{272}$$

$$M_i'(\theta) \equiv \sum_{n_i=0}^{\infty} e^{n_i \alpha_i \theta}\, p_i(n_i) \qquad (i=1,2,\ldots N) \tag{273}$$

WITH (270) STILL APPLYING.

IN THE SPECIFIC CASE OF N POISSON DISTRIBUTIONS

$$p_i(n_i) = e^{-\beta_i} \frac{\beta_i^{n_i}}{(n_i)!} \qquad \begin{matrix}(\beta_i = \lambda_i T) \\ (i=1,2,\ldots N)\end{matrix} \tag{274}$$

WE KNOW FROM (265) THAT

$$M_i'(\theta) = e^{\beta_i\left[e^{\alpha_i \theta} - 1\right]} \tag{275}$$

SO THAT

$$\bar{M}(\theta) = \prod_{i=1}^{N} e^{\beta_i\left[e^{\alpha_i\theta}-1\right]} = e^{\sum_{i=1}^{N}\beta_i\left[e^{\alpha_i\theta}-1\right]} . \tag{276}$$

(MGF FOR SUM OF SCALED POISSON SAMPLES)

FOR COMPARISON WITH EARLIER RESULTS WE REQUIRE MOMENTS WITH RESPECT

TO THE MEAN. FROM (270) AND (276) WE FIND THAT THE MEAN OF THE SUM OF WEIGHTED POISSON SAMPLES IS

$$\bar{\mu}_1 = \frac{d\bar{M}(\theta)}{d\theta} = e^{-\sum_{i=1}^{N}\beta_i} \frac{d}{d\theta}\left\{e^{\sum_{i=1}^{N}\beta_i e^{\alpha_i\theta}}\right\} =$$

$$= e^{-\sum_{i=1}^{N}\beta_i} e^{\sum_{i=1}^{N}\beta_i e^{\alpha_i\theta}} \frac{d}{d\theta}\left\{\sum_{i=1}^{N}\beta_i e^{\alpha_i\theta}\right\} =$$

$$= e^{-\sum_{i=1}^{N}\beta_i} e^{\sum_{i=1}^{N}\beta_i e^{\alpha_i\theta}} \sum_{i=1}^{N}\beta_i\alpha_i e^{\alpha_i\theta}$$

EVALUATED AT $\theta = 0$ TO GIVE

$$\bar{\mu}_1 = \sum_{i=1}^{N}\beta_i\alpha_i \qquad \text{(MEAN OF WEIGHTED POISSON SAMPLES)} \qquad (277)$$

THIS RESULT IN ONE DIMENSION IS EQUIVALENT TO RESULT (242) EXPRESSED IN a) AT THE TOP OF PAGE 93. RESULT (259) PERMITS US TO WRITE, USING ALSO (276), THE MGF W.R.T. THE MEAN

$$\tilde{M}(\theta) = e^{-\bar{\mu}_1\theta}\bar{M}(\theta) = e^{\sum_{i=1}^{N}\beta_i\left[e^{\alpha_i\theta} - \alpha_i\theta - 1\right]} \qquad (278)$$

(MGF W.R.T. MEAN FOR SUM OF SCALED POISSON SAMPLES)

THIS RESULT FOLLOWS ALSO FROM (275). THAT IS, (275) GIVES FOR THE i-TH INDIVIDUAL MEAN $\beta_i\alpha_i$ SO THAT

$$M_i'(\theta) \rightarrow e^{\beta_i\left[e^{\alpha_i\theta} - \alpha_i\theta - 1\right]}. \qquad \text{(W.R.T. } i\text{-TH MEAN)}$$

SUBSTITUTION OF THIS INTO (272) THEN GIVES US IMMEDIATELY (278).

WE HAVE PROPOSED EARLIER TO FORM A WEIGHTED SUM OF THE FOURIER TRANSFORMS OF THE FOCAL PLANE DATA AND HAVE DEVELOPED AN EXPRESSION (62) FOR THE OPTIMUM WEIGHTS.

CONSIDER FIRST THE DFT OF A SINGLE IMAGE BEFORE WEIGHTING AND COMBINATION WITH THE TRANSFORMS OF THE OTHER IMAGES. LET THE SAMPLES OF THE IMAGE BE

$$\mu_{jk} \qquad (j,k = 0,1,2,\ldots N-1).$$

EACH SAMPLE jk COMES FROM A POISSON DISTRIBUTION

$$p_{jk}(n_{jk}) = e^{-\beta_{jk}} \cdot \frac{(\beta_{jk})^{n_{jk}}}{(n_{jk})!} \tag{279}$$

$$\beta_{jk} = \lambda_{jk} T = \text{MEAN} = \text{VARIANCE} \tag{280}$$

THE DFT OF μ_{jk} WILL BE

$$\mathcal{M}_{lm} = \sum_{j=0}^{N-1} \sum_{k=0}^{N-1} \mu_{jk} e^{\frac{-2\pi i (lj+mk)}{N}} = \tag{281}$$

$$= \sum_{j=0}^{N-1} \sum_{k=0}^{N-1} \mu_{jk} W^{lj} W^{mk} \qquad (l,m = 0,1,2,\ldots N-1)$$

$$W \equiv e^{-\frac{2\pi i}{N}} \tag{282}$$

THUS, THE $\mathcal{M}_{lm}$ CONSIST OF SUMS OF WEIGHTED SAMPLES FROM POISSON DISTRIBUTIONS. WE CAN EXTEND (278) TO READ THEN

$$\tilde{M}_{lm}(\theta) = e^{\sum_{j=0}^{N-1} \sum_{k=0}^{N-1} \beta_{jk} \left[e^{\theta W^{lj} W^{mk}} - \theta W^{lj} W^{mk} - 1 \right]} \tag{283}$$

$$(l,m = 0,1,2,\ldots N-1)$$

FOR THE MGF-ABOUT-THE-MEAN AT THE POINT lm OF THE DFT OF THE SINGLE IMAGE [POISSON STATISTICS] μ_{jk} BEFORE WEIGHTED IMAGE COMBI-

NATION.

TO BE ABLE TO APPLY THE REGRESSION TECHNIQUE TO THE FOURIER DOMAIN WE NEED AN EXPRESSION FOR THE PROBABILITY OF A GIVEN VALUE x AT EACH POINT IN THAT DOMAIN. LET US GO BACK TO (271-3) WHICH ARE NOT SPECIFIC TO THE CASE OF POISSON STATISTICS.

$$\bar{M}(\theta) = \prod_{i=1}^{N} \sum_{m_i=0}^{\infty} e^{m_i \alpha_i \theta} p_i(m_i) =$$

$$= \sum_{m_1=0}^{\infty} \sum_{m_2=0}^{\infty} \cdots \sum_{m_N=0}^{\infty} e^{(\alpha_1 m_1 + \alpha_2 m_2 + \cdots \alpha_N m_N)\theta} p_1(m_1) p_2(m_2) \cdots p_N(m_N) =$$

$$= \sum_{m_1=0}^{\infty} \sum_{m_2=0}^{\infty} \cdots \sum_{m_N=0}^{\infty} \left\{ e^{\theta \sum_{j=1}^{N} \alpha_j m_j} \right\} \left\{ \prod_{j=1}^{N} p_j(m_j) \right\} \qquad (284)$$

LET US REPLACE θ BY $i\omega$ AND FORM

$$\lim_{Q \to \infty} \frac{1}{2Q} \int_{-Q}^{Q} \bar{M}(i\omega) e^{-i\omega x} d\omega \qquad (285)$$

WE GET FROM (284)

$$\sum_{m_1=0}^{\infty} \sum_{m_2=0}^{\infty} \cdots \sum_{m_N=0}^{\infty} \left\{ \prod_{j=1}^{N} p_j(m_j) \right\} \left\{ \lim_{Q \to \infty} \frac{1}{2Q} \int_{-Q}^{Q} e^{-i\omega \left[x - \sum_{j=1}^{N} \alpha_j m_j \right]} d\omega \right\} \qquad (286)$$

WE CLAIM THAT THE SECOND EXPRESSION IN { } HAS THE VALUE

$$\begin{cases} 1, & \text{IF } \quad x = \sum_{j=1}^{N} \alpha_j m_j \\ 0, & \text{OTHERWISE.} \end{cases} \tag{287}$$

TO CONFIRM THIS, CONSIDER

$$\lim_{Q\to\infty} \frac{1}{2Q}\int_{-Q}^{Q} e^{-i\omega z}\,d\omega = \lim_{Q\to\infty}\frac{1}{2Q}\int_{-Q}^{Q}\left[\cos\omega z - i\sin\omega z\right] d\omega =$$

$$= \lim_{Q\to\infty}\frac{1}{Q}\int_{0}^{Q}\cos\omega z\,d\omega = \lim_{Q\to\infty}\frac{1}{Qz}\int_{0}^{Qz}\cos\omega\,d\omega =$$

$$= \lim_{Q\to\infty}\frac{1}{Qz}\Big[+\sin\omega\Big]_{0}^{Qz} = \lim_{Q\to\infty}\left\{\frac{\sin Qz}{Qz}\right\} =$$

$$= \begin{cases} 1 & \text{IF } z = 0 \\ 0 & \text{IF } z \neq 0 \end{cases} \tag{288}$$

AS CLAIMED.

LET US ASSUME, AS NOTED BEFORE, THAT THE WEIGHTS α_j ARE IRRATIONAL. IF $x = \sum \alpha_j m_j$ THERE IS THEN A UNIQUE SET OF VALUES m_j FOR WHICH THIS IS TRUE. ACCORDING TO (287), ALL OF THE TERMS OF (286) MUST BE ZERO EXCEPT FOR THE ONE UNIQUE SET OF VALUES IMPLIED BY x. IF x CAN NOT BE EXPRESSED BY ANY $\{m_j\}$, ALL TERMS OF (286) ARE ZERO. WE CONCLUDE THEN THAT

$$\lim_{Q\to\infty}\frac{1}{2Q}\int_{-Q}^{Q}\overline{M}(i\omega)e^{-i\omega x}\,d\omega \equiv \bar{\mu}(x) = \begin{cases} \bar{\mu}\left(\sum_{j=1}^{N}\alpha_j m_j\right) = \prod_{j=1}^{N} p_j(m_j) & (289a) \\ 0 & (289b) \end{cases}$$

CASE (289a) IS TRUE WHEN x* HAS A VALUE SUCH THAT A SET $\{m_j\}$ EXIST SATISFYING

$$x = \sum_{j=1}^{N} \alpha_j m_j \qquad (m_j \text{ INTEGER})$$

CASE (289b) IS TRUE OTHERWISE.

THUS, (285) IS A PRESCRIPTION FOR AN INTEGRAL REPRESENTATION OF THE PROBABILITY DISTRIBUTION IN THE FOURIER PLANE. THE MGF IN THE FOURIER PLANE WHICH GIVES MOMENTS ABOUT THE ORIGIN* IS

$$\bar{M}_{lm}(\theta) = e^{\sum_{j=0}^{N-1} \sum_{k=0}^{N-1} \beta_{jk} \left[e^{\theta W^{lj} W^{mk}} - 1 \right]} \qquad (l, m = 0, 1, 2, \ldots N-1) \tag{290}$$

AND THE INTEGRAL REPRESENTATION OF THE PROBABILITY DISTRIBUTION AT POINT lm IN THE DISCRETE FOURIER PLANE OF A SINGLE IMAGE IS

$$\boxed{\bar{p}_{lm}(x) = \lim_{Q \to \infty} \frac{1}{2Q} \int_{-Q}^{+Q} e^{\sum_{j=0}^{N-1} \sum_{k=0}^{N-1} \beta_{jk} \left[e^{i\omega W^{lj} W^{mk}} - 1 \right] - i\omega x} \, d\omega} \tag{291}$$

SOME MOMENTS IN THE FOURIER PLANE

BY COMPARING (276) AND (278) IT IS OBVIOUS THAT THE MGF AT A POINT lm OF THE DISCRETE FOURIER PLANE W.R.T. ZERO IS GIVEN BY (283) WITH THE SECOND TERM IN [ ] REMOVED. THIS IS JUST (290) ABOVE. BY COMPARING THE FORM OF (276) AND (290), AND CONSIDERING THE STEPS LEADING TO (277) IT IS CLEAR THAT

$$(\bar{\mu}_1)_{lm} = \sum_{j=0}^{N-1} \sum_{k=0}^{N-1} \beta_{jk} W^{lj} W^{mk} \tag{292}$$

THIS IS JUST THE DFT OF THE MEAN OF THE SIGNAL IN THE IMAGE PLANE AND

---

* "ORIGIN" HERE MEANS ZERO SAMPLE VALUE, NOT THE SPATIAL ORIGIN.

CONFIRMS (242) AND a) AT THE TOP OF PAGE 93.

FOR THE HIGHER MOMENTS W.R.T. THE MEAN, LET US WORK WITH THE FORM

$$M'(\theta) = e^{\beta\left[e^{\alpha\theta} - \alpha\theta - 1\right]} \tag{293}$$

FOR THE PURPOSES OF GETTING THE FORM OF THE DERIVATIVES. WE MAY LATER MAKE THE OBVIOUS CHANGES REFLECTING THE 2-D FT OF THE IMAGE.

$$\frac{dM'}{d\theta} = e^{-\beta} \frac{d}{d\theta}\left\{e^{\beta e^{\alpha\theta} - \beta\alpha\theta}\right\} = e^{-\beta}\left\{e^{\beta e^{\alpha\theta} - \beta\alpha\theta}\right\}\frac{d}{d\theta}\left\{\beta e^{\alpha\theta} - \beta\alpha\theta\right\} =$$

$$= e^{-\beta}\left\{e^{\beta e^{\alpha\theta} - \beta\alpha\theta}\right\}\left\{\beta\alpha e^{\alpha\theta} - \beta\alpha\right\} \tag{294}$$

AT $\theta = 0$,

$$\mu_1' = \left.\frac{dM'}{d\theta}\right|_{\theta=0} = \alpha(\beta - \beta) = 0 \tag{295}$$

AS IT SHOULD SINCE THE MEAN W.R.T. THE MEAN MUST BE ZERO.

$$\frac{d^2M'}{d\theta^2} = e^{-\beta}\left\{\left[e^{\beta e^{\alpha\theta} - \beta\alpha\theta}\right]\left[\beta\alpha e^{\alpha\theta} - \beta\alpha\right]^2 + \right.$$

$$\left. + \left[e^{\beta e^{\alpha\theta} - \beta\alpha\theta}\right]\left[\beta\alpha^2 e^{\alpha\theta}\right]\right\} \tag{296}$$

AT $\theta = 0$,

$$\mu_2' = \left.\frac{d^2M'}{d\theta^2}\right|_{\theta=0} = e^{-\beta}\left\{e^{\beta}(\beta\alpha - \beta\alpha)^2 + e^{\beta}\beta\alpha^2\right\} = \beta\alpha^2 \tag{297}$$

IN TERMS OF THE DFT OF THE IMAGE WE HAVE THEN THAT

$$(\mu_2')_{\ell m} = \sum_{j=0}^{N-1}\sum_{k=0}^{N-1}\beta_{jk}\left(W^{\ell j^*}W^{mk}\right)^2 = \text{VARIANCE ABOUT MEAN AT } \ell m \text{ IN THE FOURIER PLANE} \quad (298)$$

THIS IS NOT EQUIVALENT TO (245) AS EXPRESSED BY b) AT THE TOP OF PAGE 93 BECAUSE WE HAVE, IN SETTING UP THE MGF, USED THE COMPLEX MOMENT ARM, RATHER THAN THE MAGNITUDE OF THE MOMENT ARM AS WAS USED FOR (245). NO DOUBT A DERIVATION OF THE MGF FOR THE MOMENTS OF THE MAGNITUDES OF THE "ARMS" WOULD RESULT IN AN EXPRESSION SIMILAR TO (298) BUT WITH THE SQUARE REPLACED BY THE SQUARED MAGNITUDE. SINCE, BY (282), THE W'S ARE PHASORS OF MAGNITUDE 1, THERE WOULD THEN RESULT

$$\sum_{j=0}^{N-1}\sum_{k=0}^{N-1}\beta_{jk} \;.$$

THIS IS INDEPENDENT OF ℓm AND IS PROPORTIONAL TO THE TOTAL INTEGRATED INTENSITY OF THE IMAGE [SINCE β_{jk} IS PROPORTIONAL TO THE INTENSITY] AS REQUIRED IN b) AT THE TOP OF PAGE 93. WE WILL NOT GO INTO THIS FURTHER AS THE MGF WITH WHICH WE WANT TO WORK IS THE ONE DEFINED IN TERMS OF COMPLEX MOMENT ARMS BECAUSE IT IS THAT MGF WHICH LEADS TO THE PROBABILITY DENSITY ACCORDING TO (289).

WE COULD LOOK, AT THIS POINT, AT THE HIGHER MOMENTS IN THE FOURIER PLANE TO SEE UNDER WHAT CONDITIONS, IF ANY, THEY GO OVER TO MOMENTS OF GAUSSIAN DISTRIBUTIONS. IF THEY DID WE COULD THEN SPECIFY UNDER WHAT CIRCUMSTANCES THE REGRESSION ANALYSIS BEGUN EARLIER WAS APPLICABLE. HOWEVER, WE HAVE JUST SEEN THAT THE MGF (290) IS NOT THE APPROPRIATE ONE FOR THIS ANALYSIS AND WE WILL, THEREFORE, POSTPONE EXAMINATION OF THIS QUESTION.

OPTIMIZATION IN FOURIER PLANE

HAVING DEVELOPED AN EXPRESSION FOR THE PROBABILITY DISTRIBUTION IN THE FOURIER PLANE (291), IT IS TEMPTING TO TRY TO WORK OUT A MORE READILY USEFUL FORM. THIS TURNS OUT TO BE NOT THE MOST PRODUCTIVE APPROACH, BUT IT IS WORTHWHILE NEVERTHELESS TO TOUCH ON SOME OF THE MORE OBVIOUS CONSIDERATIONS BECAUSE THEY REVEAL THE CHARACTER OF (291).

THE FIRST POINT TO BE MADE IS THAT, WITH THE EXCEPTION OF THE FACTOR OF $1/2Q$, (291) IS, IN THE LIMIT $Q \to \infty$, THE FOURIER INTEGRAL TRANSFORM OF THE MOMENT GENERATING FUNCTION (290) WITH AN IMAGINARY ARGUMENT $\overline{M}_{\ell m}(i\theta)$. $\overline{M}_{\ell m}(i\theta)$ IS AN ENTIRE FUNCTION OF θ. THAT IS, $\overline{M}_{\ell m}(i\theta)$ IS ANALYTIC EVERYWHERE IN THE FINITE θ PLANE. BY LIOUVILLE'S THEOREM, SINCE IT IS NOT A CONSTANT, IT MUST EXHIBIT SINGULAR BEHAVIOR AT INFINITY. THIS IS EASILY CONFIRMED BY LETTING $\theta \to \infty$.

BEING AN ENTIRE FUNCTION IT IS NATURAL TO ASK IF $\overline{M}_{\ell m}(i\theta)$ HAS AN INFINITE PRODUCT REPRESENTATION. THIS IS OBTAINED BY CONSIDERING THE LOGARITHMIC DERIVATIVE OF $\overline{M}_{\ell m}(i\theta)$

$$\overline{M}'_{\ell m}(i\theta) = \frac{d}{d\theta}\overline{M}_{\ell m}(i\theta) = \overline{M}_{\ell m}(i\theta)\left\{ i \sum_{j=0}^{N-1}\sum_{k=0}^{N-1} \beta_{jk}\, e^{i\theta W^{\ell_j} W^{-mk}}\, W^{\ell_j} W^{-mk} \right\}$$

OR

$$\frac{d}{d\theta}\ln\left\{\overline{M}_{\ell m}(i\theta)\right\} = \frac{\overline{M}'_{\ell m}(i\theta)}{\overline{M}_{\ell m}(i\theta)} = i \sum_{j=0}^{N-1}\sum_{k=0}^{N-1} \beta_{jk}\, e^{i\theta W^{\ell_j} W^{-mk}}\, W^{\ell_j} W^{mk} \qquad (299)$$

SINCE THE LOGARITHMIC DERIVATIVE HAS NO ISOLATED SINGULARITIES IN THE FINITE θ PLANE, AND HAS AN ESSENTIAL SINGULARITY AT ∞, NO INFINITE PRODUCT REPRESENTATION IS POSSIBLE. IN PARTICULAR, THE ESSENTIAL SINGULARITY AT ∞ PROHIBITS INTRODUCTION OF ANY FINITE POWERS OF θ WHICH WILL, IN A SERIES EXPANSION OF (299), PERMIT (299) TO BE BOUNDED AS $\theta \to \infty$.

WE ARE AT LIBERTY TO MAKE A CHANGE OF INTEGRATION VARIABLE IN (291). THE ESSENTIAL SINGULARITY OF THE LOGARITHMIC DERIVATIVE OF $\overline{M}_{\ell m}(i\theta)$ AT ∞ SUGGESTS THE CHANGE OF VARIABLE

$$z = e^{\omega}$$

$$\Rightarrow dz = e^{\omega}\, d\omega \qquad \text{OR,} \qquad d\omega = \frac{dz}{z} \qquad (300)$$

WITH THIS CHANGE (291) BECOMES

$$\bar{\pi}_{lm}(x) = \lim_{Q\to\infty} \frac{1}{2Q} \int_{e^{-Q}}^{e^{+Q}} e^{\sum_{j=0}^{N-1}\sum_{k=0}^{N-1} \beta_{jk}\left[z^{iW^{lj}W^{mk}} - 1\right]} z^{-ix-1}\, dz \qquad (301)$$

IN THE LIMIT $Q \to \infty$, $e^{-Q} \to 0$ AND $e^{+Q} \to \infty$. THEREFORE, THE INTEGRAL IN (301) IN THE LIMIT $Q\to\infty$ BECOMES THE MELLIN TRANSFORM OF

$$f(z) = e^{\sum_{j=0}^{N-1}\sum_{k=0}^{N-1} \beta_{jk}\left[z^{iW^{lj}W^{mk}} - 1\right]} \qquad (302)$$

FOR THE ARGUMENT $S = -ix$. THE MELLIN TRANSFORM OF $f(z)$ IS DEFINED TO BE

$$F(S) = \int_0^\infty f(z)\, z^{S-1}\, dz \qquad (303)$$

THE MELLIN TRANSFORM POSSESSES A CONVOLUTION THEOREM ANALOGOUS TO THAT OF THE FOURIER TRANSFORM. SINCE $f(z)$ (302) CAN BE WRITTEN AS A FINITE PRODUCT

$$f(z) = \prod_{j=0}^{N-1}\prod_{k=0}^{N-1} e^{\beta_{jk}\left[z^{iW^{lj}W^{mk}} - 1\right]}, \qquad (304)$$

IT IS ESSENTIAL ONLY TO BE ABLE TO EVALUATE THE FORM

$$\lim_{Q\to\infty} \int_{e^{-Q}}^{e^{+Q}} e^{\beta\left[z^{iW} - 1\right]} z^{S-1}\, dz \qquad (305)$$

AN ANALOGOUS OBSERVATION IS, OF COURSE, TRUE FOR THE FOURIER INTEGRAL

(291).

CONSIDER THE LOGARITHMIC DERIVATIVE OF $f(z)$ (302).

$$\frac{d}{dz} \ln f(z) = \frac{f'(z)}{f(z)} = i \sum_{j=0}^{N-1} \sum_{k=0}^{N-1} \beta_{jk} W^{\ell j} W^{mk} z^{iW^{\ell j} W^{mk} - 1} \tag{306}$$

THIS HAS BRANCH POINTS AT $z=0$ AND $z=\infty$. CONSEQUENTLY, WE MUST MAKE A BRANCH CUT BETWEEN 0 AND ∞. AGAIN, AN INFINITE PRODUCT REPRESENTATION IS NOT POSSIBLE BECAUSE OF THE NEED TO INTEGRATE ACROSS THE BRANCH CUT.

THE REASON FOR TRYING TO FIND INFINITE PRODUCT REPRESENTATIONS OF $\overline{M}_{\ell m}(i\theta)$ AND $f(z)$ (302) IS THE POSSIBILITY OF THEREBY IDENTIFYING A FACTOR OF THE INTEGRAND WHICH, TOGETHER WITH $Q \to \infty$ AND THE FACTOR $1/2Q$ OUTSIDE THE INTEGRAL, WILL ACCOUNT FOR THE SELECTION OF DISCRETE VALUES OF THE ARGUMENT OF $\overline{\mu}_{\ell m}(x)$ FOR WHICH $\overline{\mu}_{\ell m}(x)$ IS NON-ZERO. WE KNOW THIS MUST BE THE NATURE OF $\overline{\mu}_{\ell m}(x)$ FROM THE DISCRETE NATURE OF THE PHOTON COUNTS IN THE ORIGINAL IMAGE PLANE. IF THE [IMPROPER] FUNCTION WHICH SELECTS THE ALLOWED ARGUMENTS CAN BE IDENTIFIED, AS FOR EXAMPLE IN (287) AND (288), IT MAY THEN BE POSSIBLE TO IDENTIFY THE FUNCTION FROM WHICH THE SELECTION IS MADE. AS SHOWN BY (289a), THIS FUNCTION WILL BE

$$P = \prod_{j=0}^{N-1} \prod_{k=0}^{N-1} \mu_{jk}(n_{jk}) \tag{307}$$

OF COURSE, THE DIFFICULTY WITH THE FORM (307) IS THAT POINTS IN THE FOURIER PLANE TAKE ON VALUES WHICH ARE DETERMINED BY THE n_{jk}. VALUES ARE "ORDERED" BY n_{jk}. BUT TO DO MEANINGFUL PROBABILITY COMPUTATIONS IN THE FOURIER PLANE WE NEED "NATURALLY" ORDERED VALUES. THAT IS, WE MUST GET AROUND THE PROBLEM OF HAVING TO DETERMINE THE n_{jk} WHICH PRODUCE A GIVEN COMPLEX VALUE AT ℓm IN THE FOURIER PLANE IN ORDER, VIA (307), TO COMPUTE THE PROBABILITY OF THAT COMPLEX VALUE AT ℓm. WE HOPE THEN THAT THE EXERCISE OF EVALUATING (291) OR (301) WILL RESULT IN A PROBABILITY EXPRESSED, NOT IN TERMS OF n_{jk}, BUT DIRECTLY IN TERMS OF THE COMPLEX VALUE AT POINT ℓm. THE TASK MAY BE, HOWEVER, INHERENTLY IMPOSSIBLE

AS IT WOULD AMOUNT TO A PROCEDURE IN CLOSED FORM FOR FINDING THE SET $\{n_{jk}\}$ IMPLIED BY A GIVEN COMPLEX VALUE.

WE KNOW THAT THE COMPLEX VALUE x AT THE POINT ℓm IN THE FOURIER PLANE WILL BE

$$x_{\ell m} = \sum_{j=0}^{N-1}\sum_{k=0}^{N-1} n_{jk} W^{\ell j} W^{mk} \qquad (308)$$

AND, THEREFORE, THAT

$$n_{jk} = \frac{1}{N^2}\sum_{\ell=0}^{N-1}\sum_{m=0}^{N-1} x_{\ell m} W^{-j\ell} W^{-km} \equiv z_{jk} . \qquad (309)$$

THUS, TO DETERMINE THE SET $\{n_{jk}\}$ REQUIRES ALL POINTS IN THE FOURIER PLANE $\{x_{\ell m}\}$. ONE INTERESTING PROPERTY OF (309) IS THAT THE n_{jk} ARE MATHEMATICALLY CONTINUOUS FUNCTIONS OF THE $x_{\ell m}$. ONE MIGHT THEN ATTEMPT TO EVALUATE

$$P = \prod_{j=0}^{N-1}\prod_{k=0}^{N-1} p_{jk}\left[\frac{1}{N^2}\sum_{\ell=0}^{N-1}\sum_{m=0}^{N-1} x_{\ell m} W^{-j\ell} W^{-km}\right] \qquad (310)$$

AS AN EXPRESSION OF THE PROBABILITY OF A GIVEN $\{x_{\ell m}\}$ OVER THE FOURIER PLANE. TWO ROUTES SHOULD BE POSSIBLE. EITHER DIRECT USE OF (310) TOGETHER WITH (279), OR CONTINUATION OF THE ATTEMPT TO EVALUATE (291) OR (301) WITH USE OF THE TRANSFORMATION (309) IF REQUIRED.

IF (310) IS TO BE EVALUATED IT WILL BE NECESSARY TO REPLACE THE FACTORIAL IN (279) WITH THE GAMMA FUNCTION.

$$z! = \Gamma(z+1) \qquad (311)$$

SO THAT

$$p_{jk}(z_{jk}) \equiv e^{-\beta_{jk}} \frac{(\beta_{jk})^{z_{jk}}}{\Gamma(z_{jk}+1)} \qquad (312)$$

THEN,

$$P = \prod_{j=0}^{N-1} \prod_{k=0}^{N-1} e^{-\beta_{jk}} \frac{(\beta_{jk})^{\frac{1}{N^2}\sum_{l=0}^{N-1}\sum_{m=0}^{N-1} x_{lm} W^{-jl} W^{-km}}}{\Gamma\left\{\frac{1}{N^2}\sum_{l=0}^{N-1}\sum_{m=0}^{N-1} x_{lm} W^{-jl} W^{-km} + 1\right\}} =$$

$$= e^{-\sum_{j=0}^{N-1}\sum_{k=0}^{N-1}\beta_{jk}} \frac{\left[\prod_{j=0}^{N-1}\prod_{k=0}^{N-1} (\beta_{jk})^{\sum_{l=0}^{N-1}\sum_{m=0}^{N-1} x_{lm} W^{-jl} W^{-km}}\right]^{\frac{1}{N^2}}}{\prod_{j=0}^{N-1}\prod_{k=0}^{N-1} \Gamma\left\{\frac{1}{N^2}\sum_{l=0}^{N-1}\sum_{m=0}^{N-1} x_{lm} W^{-jl} W^{-km} + 1\right\}} \tag{313}$$

EQUATION (313) IS USEFUL IN THE MOST GENERAL CASE IN WHICH VALUES IN THE FOURIER PLANE, x_{lm}, DO NOT CORRESPOND, VIA (309), TO INTEGER PHOTON COUNTS m_{jk} IN THE IMAGE PLANE. THIS MIGHT BE THE CASE, FOR EXAMPLE, AFTER THE SUB-IMAGE COMBINATION STEP DISCUSSED EARLIER.

BUT, TO GET A HANDLE ON AN APPROACH TO THE PROBLEM USING (307), LET US CONSIDER FIRST THE PROBLEM OF FILTERING JUST ONE SUB-IMAGE. IN THIS CASE THE z_{jk} GIVEN BY (309) ARE INTEGERS AND WE CAN WRITE FROM (279) AND (307) THAT

$$P = \prod_{j=0}^{N-1}\prod_{k=0}^{N-1} e^{-\beta_{jk}} \frac{(\beta_{jk})^{m_{jk}}}{(m_{jk})!} = e^{-\sum_{j=0}^{N-1}\sum_{k=0}^{N-1}\beta_{jk}} \frac{\prod_{j=0}^{N-1}\prod_{k=0}^{N-1}(\beta_{jk})^{m_{jk}}}{\prod_{j=0}^{N-1}\prod_{k=0}^{N-1}(m_{jk})!} =$$

$$= A e^{-\sum_{j=0}^{N-1}\sum_{k=0}^{N-1}\beta_{jk}} \prod_{j=0}^{N-1}\prod_{k=0}^{N-1}(\beta_{jk})^{m_{jk}} \tag{314}$$

THE OBJECTIVE IS TO APPROXIMATE, IN SOME WAY WHICH ACCOMPLISHES SMOOTHING, THE β_{jk} WHILE MAXIMIZING P. SINCE WE ARE CONTEMPLATING IMPLEMENTATION IN THE FOURIER PLANE LET THE APPROXIMATE β_{jk} BE

$$\tilde{\beta}_{jk} = \frac{1}{N^2} \sum_{\ell=0}^{M-1} \sum_{m=0}^{M-1} B_{\ell m} W^{-j\ell} W^{-km} \qquad (M \leq N) \tag{315}$$

WHERE, FOR $M=N$,

$$B_{\ell m} = \sum_{j=0}^{N-1} \sum_{k=0}^{N-1} \beta_{jk} W^{\ell j} W^{mk} \tag{316}$$

WE MUST NOW VARY THE AVAILABLE $B_{\ell m}$ $(\ell, m < M \leq N)$ SO AS TO MAXIMIZE P. THIS REQUIRES PARTIAL DERIVATIVES OF THE TWO FACTORS OF (314) INVOLVING β_{jk}.

$$\frac{\partial}{\partial B_{rs}} \left\{ e^{-\sum_{j=0}^{N-1} \sum_{k=0}^{N-1} \tilde{\beta}_{jk}} \right\} = -e^{-\sum_{j=0}^{N-1} \sum_{k=0}^{N-1} \tilde{\beta}_{jk}} \sum_{j=0}^{N-1} \sum_{k=0}^{N-1} \frac{\partial \tilde{\beta}_{jk}}{\partial B_{rs}} \tag{317}$$

FROM (315),

$$\frac{\partial \tilde{\beta}_{jk}}{\partial B_{rs}} = \frac{1}{N^2} \sum_{\ell=0}^{M-1} \sum_{m=0}^{M-1} W^{-j\ell} W^{-km} \frac{\partial B_{\ell m}}{\partial B_{rs}} = \frac{1}{N^2} \sum_{\ell=0}^{M-1} \sum_{m=0}^{M-1} W^{-j\ell} W^{-km} \delta_{\ell r} \delta_{ms} =$$

$$= \frac{1}{N^2} W^{-jr} W^{-ks} \epsilon_{Mr} \epsilon_{Ms} \tag{318}$$

WHERE

$$\left. \begin{aligned} \epsilon_{mn} &\equiv 1 \\ &\equiv 0 \end{aligned} \right\} \quad \begin{aligned} n &< m \\ n &\geq m \end{aligned} \tag{319}$$

THEREFORE, (317) BECOMES

$$\frac{\partial}{\partial \mathcal{B}_{mn}}\left\{e^{-\sum_{j=0}^{N-1}\sum_{k=0}^{N-1}\tilde{\beta}_{jk}}\right\} = -\frac{1}{N^2}\, e^{-\sum_{j=0}^{N-1}\sum_{k=0}^{N-1}\tilde{\beta}_{jk}}\, \epsilon_{mn}\epsilon_{mn} \underbrace{\sum_{j=0}^{N-1}\sum_{k=0}^{N-1} W^{-jm} W^{-kn}}_{N^2\delta_{0m}\,\delta_{0n}} =$$

$$= -\,\delta_{0m}\delta_{0n}\; e^{-\sum_{j=0}^{N-1}\sum_{k=0}^{N-1}\tilde{\beta}_{jk}} \tag{320}$$

WHERE

$$\epsilon_{mn}\epsilon_{mn}\,\delta_{0m}\delta_{0n} = \delta_{0m}\,\delta_{0n} \,. \tag{321}$$

WE REQUIRE ALSO,

$$\frac{\partial}{\partial \mathcal{B}_{mn}}\left\{\prod_{j=0}^{N-1}\prod_{k=0}^{N-1}(\tilde{\beta}_{jk})^{m_{jk}}\right\} = \sum_{r=0}^{N-1}\sum_{s=0}^{N-1}\prod_{\substack{j=0\\ j\neq r}}^{N-1}\prod_{\substack{k=0\\ k\neq s}}^{N-1}\tilde{\beta}_{jk}^{\,m_{jk}}\;\frac{\partial}{\partial \mathcal{B}_{mn}}\left\{\tilde{\beta}_{rs}^{\,m_{rs}}\right\} =$$

$$= \sum_{r=0}^{N-1}\sum_{s=0}^{N-1} m_{rs}\,\tilde{\beta}_{rs}^{\,m_{rs}-1}\;\frac{\partial\tilde{\beta}_{rs}}{\partial \mathcal{B}_{mn}}\prod_{\substack{j=0\\ j\neq r}}^{N-1}\prod_{\substack{k=0\\ k\neq s}}^{N-1}\tilde{\beta}_{jk}^{\,m_{jk}} =$$

$$= \frac{1}{N^2}\,\epsilon_{mn}\epsilon_{mn}\sum_{r=0}^{N-1}\sum_{s=0}^{N-1} m_{rs}\,\tilde{\beta}_{rs}^{\,m_{rs}-1}\, W^{-rm}\, W^{-sn}\prod_{\substack{j=0\\ j\neq r}}^{N-1}\prod_{\substack{k=0\\ k\neq s}}^{N-1}\tilde{\beta}_{jk}^{\,m_{jk}} =$$

$$= \frac{\epsilon_{mn}\epsilon_{mn}}{N^2}\sum_{r=0}^{N-1}\sum_{s=0}^{N-1}\left(\frac{m_{rs}}{\tilde{\beta}_{rs}}\right) W^{-rm}\, W^{-sn}\prod_{j=0}^{N-1}\prod_{k=0}^{N-1}\tilde{\beta}_{jk}^{\,m_{jk}} \tag{322}$$

RESULTS (320) AND (322) IN $\partial P/\partial B_{rs}$ FROM (314) GIVE,

$$\boxed{\frac{\partial P}{\partial B_{rs}} = P\left\{N^{-2}\epsilon_{Mr}\epsilon_{Ms}\sum_{j=0}^{N-1}\sum_{k=0}^{N-1}\left(\frac{m_{jk}}{\tilde{\beta}_{jk}}\right)W^{-jr}W^{-ks} - \delta_{or}\delta_{os}\right\} = 0} \tag{323}$$

WHERE $\tilde{\beta}_{jk}$ IS DEFINED BY (315).

AS A CHECK OF (323), IF $M=N$, $\tilde{\beta}_{jk} = \beta_{jk}$. (323) IS THEN SOLVED BY

$$\tilde{\beta}_{jk} = m_{jk} = \beta_{jk}$$

FOR

$$m_{jk}/\tilde{\beta}_{jk} = 1$$

AND

$$\sum_{j=0}^{N-1}\sum_{k=0}^{N-1} W^{-jr}W^{-ks} = N^2\delta_{or}\delta_{os} \quad .$$

USING ALSO (321) WE SEE THAT, FOR $M=N$, (323) IS SATISFIED BY $\tilde{\beta}_{jk} = m_{jk}$, AS IT SHOULD.

IN TERMS OF THE COEFFICIENTS B_{lm}, (323) IS EQUIVALENTLY, USING (315),

$$\frac{\partial P}{\partial B_{rs}} = P\left\{\epsilon_{Mr}\epsilon_{Ms}\sum_{j=0}^{N-1}\sum_{k=0}^{N-1}\left[\frac{m_{jk}W^{-jr}W^{-ks}}{\sum_{l=0}^{M-1}\sum_{m=0}^{M-1}B_{lm}W^{-jl}W^{-km}}\right] - \delta_{or}\delta_{os}\right\} = 0 \tag{324}$$

AS A FURTHER CHECK, CONSIDER THE SPECIAL CASE $M=1$. THUS, r AND $s < M \Rightarrow r = s = 0$. THE $\{\}$ IN (324) GIVE THEN

$$\sum_{j=0}^{N-1}\sum_{k=0}^{N-1} m_{jk} = B_{oo} \tag{325}$$

WHICH, WHEN PUT INTO (315), GIVES

$$\tilde{\beta}_{jk} = \frac{1}{N^2} B_{00} = \frac{1}{N^2} \sum_{j=0}^{N-1} \sum_{k=0}^{N-1} m_{jk} \quad . \tag{326}$$

THIS SAYS, QUITE REASONABLY, THAT IF THE APPROXIMATION OF THE IMAGE IS LIMITED TO A CONSTANT ($M=1$), THEN THE BEST GUESS ONE CAN MAKE ASSIGNS THE AVERAGE SAMPLE VALUE OVER THE IMAGE TO THAT CONSTANT.

THE FIRST STEP IN SOLVING THE GENERAL CASE OF (324) IS TO PUT THE FIRST TERM OVER A COMMON DENOMINATOR. CONSIDER THE INNER SUMMATION ON k FOR FIXED j AND LET

$$a_k \equiv m_{jk} W^{-jr} W^{-kn} \tag{327a}$$

$$b_k = \sum_{l=0}^{M-1} \sum_{m=0}^{M-1} B_{lm} W^{-jl} W^{-km} \equiv \gamma_{jk} \tag{327b}$$

TO DO THE SUM ON k WE USE

$$S_j = \sum_{k=0}^{N-1} \frac{a_k}{b_k} = \frac{\sum_{k=0}^{N-1} a_k \prod_{\substack{n=0 \\ n \neq k}}^{N-1} b_n}{\prod_{k=0}^{N-1} b_k} = \frac{A_j}{B_j} \tag{328}$$

WHERE

$$A_j = \sum_{k=0}^{N-1} m_{jk} W^{-jr} W^{-kn} \prod_{\substack{n=0 \\ n \neq k}}^{N-1} \gamma_{jn} \tag{329a}$$

$$B_j = \prod_{k=0}^{N-1} \gamma_{jk} \tag{329b}$$

THE OUTER SUMMATION ON j IS

$$S = \sum_{j=0}^{N-1} \frac{A_j}{B_j} = \sum_{j=0}^{N-1} S_j$$

FOR WHICH WE CAN AGAIN USE THE FORM (328) TO GET

$$S = \frac{\sum_{j=0}^{N-1} \left\{ \sum_{k=0}^{N-1} m_{jk} W^{-jn} W^{-ka} \prod_{\substack{v=0 \\ v \neq k}}^{N-1} \gamma_{jv} \right\} \prod_{\substack{u=0 \\ u \neq j}}^{N-1} \left\{ \prod_{\kappa=0}^{N-1} \gamma_{u\kappa} \right\}}{\prod_{j=0}^{N-1} \left\{ \prod_{k=0}^{N-1} \gamma_{jk} \right\}} \equiv S_{na} \qquad (330)$$

WHERE γ_{jk} IS GIVEN BY (327b).

WHILE S, WHICH IS EQUIVALENT TO THE FIRST TERM OF (324), CAN BE USED TO CLEAR (324) OF FRACTIONS, THE RESULT IS CLEARLY VERY COMPLICATED AND, THEREFORE, DOES NOT APPEAR TO BE A FRUITFUL WAY TO SOLVE FOR THE OPTIMUM B_{lm}. A BETTER APPROACH APPEARS TO BE TO FORM

$$\sum_{n=0}^{N-1} \sum_{a=0}^{N-1} \frac{\partial P}{\partial B_{na}} W^{vn} W^{ua} =$$

$$= P \left\{ \sum_{j=0}^{N-1} \sum_{k=0}^{N-1} \frac{m_{jk} \sum_{n=0}^{N-1} \sum_{a=0}^{N-1} \epsilon_{Mn} \epsilon_{Ma} W^{n(v-j)} W^{a(u-k)}}{\sum_{l=0}^{M-1} \sum_{m=0}^{M-1} B_{lm} W^{-jl} W^{-km}} - \right.$$

$$\left. - \sum_{n=0}^{N-1} \sum_{a=0}^{N-1} \delta_{0n} \delta_{0a} W^{vn} W^{ua} \right\} \qquad (331)$$

THE SECOND TERM IS JUST UNITY.

THE NUMERATOR OF THE FIRST TERM IS

$$\sum_{r=0}^{M-1}\sum_{s=0}^{M-1} W^{r(n-j)}\, W^{s(m-k)} \quad = \text{ DOUBLE GEOMETRIC SERIES.}$$

THOUGH WE HAVE SHOWN HOW TO EVALUATE SUCH A SERIES BEFORE [PAGE 77], THERE IS ANOTHER VERY SIMPLE WAY WHICH IS WORTH SHOWING.

LET

$$T = \sum_{m=0}^{N-1} a^m = 1 + a + a^2 + a^3 + \dots + a^{N-1} \qquad (332)$$

THEN

$$aT = a + a^2 + a^3 + \dots + a^N$$

AND

$$T - aT = T(1-a) = 1 - a^N$$

OR

$$T = \frac{1-a^N}{1-a} \qquad (333)$$

THEREFORE

$$\sum_{r=0}^{M-1}\sum_{s=0}^{M-1} W^{r(n-j)}\, W^{s(m-k)} = \frac{1-W^{M(n-j)}}{1-W^{n-j}}\;\frac{1-W^{M(m-k)}}{1-W^{m-k}} \qquad (334)$$

SINCE THE OPTIMUM CONDITION IS, BY (323), WHEN $\partial P/\partial B_{rs} = 0$ FOR ALL $\{r,s\}$, (331) AND (334) LEAD TO

$$\boxed{\sum_{j=0}^{N-1}\sum_{k=0}^{N-1} m_{jk} \frac{\dfrac{1-W^{M(n-j)}}{1-W^{n-j}}\;\dfrac{1-W^{M(m-k)}}{1-W^{m-k}}}{\displaystyle\sum_{l=0}^{M-1}\sum_{m=0}^{M-1} B_{lm} W^{-jl} W^{-km}} = 1} \qquad (335)$$

CONSIDER THE SPECIAL CASE $M = N$. THEN THE DOUBLE GEOMETRIC SERIES BECOMES

$$N^2 \delta_{0,(n-j) \bmod N}\, \delta_{0,(m-k) \bmod N}$$

AND (335) GOES OVER TO

$$N^2 m_{nw} = \sum_{l=0}^{N-1} \sum_{m=0}^{N-1} B_{lm} W^{-nl} W^{-wm} \qquad (M=N) \tag{336a}$$

OR

$$B_{lm} = \sum_{n=0}^{N-1} \sum_{w=0}^{N-1} m_{nw} W^{ln} W^{mw} \qquad (M=N) \tag{336b}$$

AS ONE WOULD SUSPECT SINCE $M=N$ ENABLES $\tilde{\beta}_{ij} = m_{ij} \Rightarrow$ MAXIMUM PROBABILITY FOR THE SAMPLE VALUES m_{ij}.

ANOTHER SPECIAL CASE WE CAN TEST IN (335) IS $M=1$. THEN THE DOUBLE GEOMETRIC SERIES IN THE NUMERATOR BECOMES 1 AND

$$B_{00} = \sum_{j=0}^{N-1} \sum_{k=0}^{N-1} m_{jk} \tag{337}$$

IN AGREEMENT WITH (326).

WHILE IT IS POSSIBLE TO USE (335) OR (324) TO SOLVE FOR THE B_{lm} IN THE SPECIAL CASES $M=1$ AND $M=N$, IT IS NOT OBVIOUS HOW TO PROCEED IN THE GENERAL CASE. THIS IS BECAUSE THE PROBLEM IS INHERENTLY NON-LINEAR DUE TO THE FACT THAT THE B_{lm} APPEAR IN THE DENOMINATOR OF THE OPTIMIZING CONDITIONS (324) OR (335).

AN ALTERNATE APPROACH IS TO FIND A LINEAR APPROXIMATION, WHICH PRESUMABLY CAN BE SOLVED, AND TO ITERATE TO THE VALUES OF THE B_{lm}. FOR EXAMPLE, CONSIDER THE CASE $M=N-1$. FOR $M=N$ WE KNOW THE EXACT B_{lm} FROM (336b). FOR $M=N-1$ WE MIGHT TAKE AS A REASONABLE STARTING GUESS THE B_{lm} GIVEN BY (336b) FOR $M=N$ WITH l AND m, OF COURSE, LIMITED TO $0, 1, \ldots, N-2$ [$N-1$ VALUES].

TO DEVELOP THE TECHNIQUE, LET US ASSUME THAT

$$B_{lm} = A_{lm} + a_{lm} \qquad \{l, m = 0, 1, 2, \ldots M-1\} \tag{338}$$

WHERE $a_{\ell m}$ IS "SMALL" AND WHERE IT IS ASSUMED THAT WE HAVE SOME WAY OF GETTING REASONABLE STARTING VALUES FOR THE $A_{\ell m}$. AFTER THE FIRST ITERATION THE $A_{\ell m}$ ARE THE OLD $A_{\ell m}$ WITH THE CORRECTIONS $a_{\ell m}$ APPLIED.

EQN. (338) GIVES FOR THE DENOMINATOR IN (324) [OR IN (335)]

$$\sum_{\ell=0}^{M-1}\sum_{m=0}^{M-1} A_{\ell m} W^{-j\ell} W^{-km} + \sum_{\ell=0}^{M-1}\sum_{m=0}^{M-1} a_{\ell m} W^{-j\ell} W^{-km} \quad . \tag{339}$$

TO EASE THE NOTATION LET US DEFINE

$$\alpha_{jk} \equiv \sum_{\ell=0}^{M-1}\sum_{m=0}^{M-1} A_{\ell m} W^{-j\ell} W^{-km} \tag{340}$$

AND LET US APPROXIMATE

$$\frac{1}{\sum_{\ell=0}^{M-1}\sum_{m=0}^{M-1} B_{\ell m} W^{-j\ell} W^{-km}} = \frac{1}{\alpha_{jk} + \sum_{\ell=0}^{M-1}\sum_{m=0}^{M-1} a_{\ell m} W^{-j\ell} W^{-km}} \approx$$

$$\approx \frac{1}{\alpha_{jk}}\left[1 - \frac{1}{\alpha_{jk}} \sum_{\ell=0}^{M-1}\sum_{m=0}^{M-1} a_{\ell m} W^{-j\ell} W^{-km}\right] \quad . \tag{341}$$

RESULT (341) ALLOWS US TO APPROXIMATE FROM (324) THAT

$$\boxed{\begin{aligned} &-\epsilon_{Mr}\epsilon_{Ms} \sum_{\ell=0}^{M-1}\sum_{m=0}^{M-1} a_{\ell m} \sum_{j=0}^{N-1}\sum_{k=0}^{N-1} \frac{n_{jk}}{(\alpha_{jk})^2} W^{-j(r+\ell)} W^{-k(s+m)} \approx \\ &\approx \delta_{0r}\delta_{0s} - \epsilon_{Mr}\epsilon_{Ms} \sum_{j=0}^{N-1}\sum_{k=0}^{N-1} \frac{n_{jk}}{\alpha_{jk}} W^{-jr} W^{-ks} \equiv b_{rs} \end{aligned}} \tag{342}$$

RESULT (342), WHICH IS LINEAR IN THE CORRECTIONS TO $B_{\ell m}$, $a_{\ell m}$, IS THE BASIS OF THE ITERATIVE SCHEME. GIVEN AN INITIAL GUESS FOR THE $A_{\ell m}$, THE α_{jk} ARE DETERMINED BY (340). THE m_{jk} ARE KNOWN SINCE THEY ARE THE RAW IMAGE DATA. CONSEQUENTLY, EVERYTHING REQUIRED IN (342) CAN BE EVALUATED SO THAT THE CORRECTIONS $a_{\ell m}$ CAN BE SOLVED FOR.

LET US DEFINE

$$Q_{r\ell s m} = \sum_{j=0}^{N-1} \sum_{k=0}^{N-1} \frac{m_{jk}}{(\alpha_{jk})^2} W^{-j(r+\ell)} W^{-k(s+m)} . \qquad (343)$$

IF WE LIMIT r AND s IN (342) TO $\{0,1,2,\ldots M-1\}$, (342) MAY BE WRITTEN

$$\sum_{\ell=0}^{M-1} \sum_{m=0}^{M-1} a_{\ell m} Q_{r\ell s m} = -b_{rs} . \qquad (344)$$

IN THIS FORM IT IS EASY TO SEE THAT THE CORRECTIONS $a_{\ell m}$ ARE PART OF A [2-DIMENSIONAL] VECTOR – [4-DIMENSIONAL] MATRIX PRODUCT AND THAT THEY COULD BE SOLVED FOR EXPLICITLY IF WE COULD FIND THE INVERSE OF $Q_{r\ell s m}$. FROM (343) WE SEE THAT THERE IS A HIGH DEGREE OF SYMMETRY WITHIN THE ELEMENTS OF $Q_{r\ell s m}$. IN FACT THERE ARE ONLY $(2M-1)^2$ UNIQUE ELEMENT VALUES IN $Q_{r\ell s m}$ WHICH SUGGESTS THAT A VERY EFFICIENT INVERSION TECHNIQUE MAY EXIST.

WE DIGRESS TO ILLUSTRATE ONE POSSIBLE METHOD OF INVERTING $Q_{r\ell s m}$. FOR CLARITY WE SUPPRESS ONE DIMENSION OF $a_{\ell m}$ AND b_{rs} SO THAT WE CONSIDER THE FORM

$$\sum_{\ell=0}^{M-1} a_\ell Q_{r\ell} = -b_r . \qquad (345)$$

THE MATRIX $Q_{r\ell}$ HAS THE FOLLOWING SYMMETRY,

$$[Q] = \begin{bmatrix} q_0 & q_1 & q_2 & q_3 & \cdots\cdots & q_{M-1} \\ q_1 & q_2 & q_3 & q_4 & \cdots\cdots & q_M \\ q_2 & q_3 & q_4 & q_5 & \cdots\cdots & q_{M+1} \\ \vdots & & & & & \\ q_{M-2} & q_{M-1} & q_M & q_{M+1} & \cdots\cdots & q_{2M-3} \\ q_{M-1} & q_M & q_{M+1} & q_{M+2} & \cdots\cdots & q_{2M-2} \end{bmatrix} \qquad (346)$$

NOTE THAT $[Q]$ IS SYMMETRIC AND, IN ADDITION, VALUES ALONG DIAGONALS PARALLEL TO THE MINOR DIAGONAL ARE EQUAL.

LET US ASSUME THAT WE KNOW THE INVERSE OF $[Q]$ OF M-TH ORDER AND WOULD LIKE TO KNOW THE INVERSE OF THE MATRIX $[Q]$ OF (M+1)-TH ORDER. SUCH A RELATIONSHIP WOULD PERMIT INVERSION OF $[Q]$ OF ANY SIZE BY ITERATION FROM THE KNOWN INVERSE OF A SMALLER UPPER-LEFT SQUARE OF $[Q]$. IN FACT ONE COULD START WITH THE 2X2 SQUARE WHOSE INVERSE IS

$$[\overset{2}{Q}]^{-1} = \frac{\begin{bmatrix} q_2 & -q_1 \\ -q_1 & q_0 \end{bmatrix}}{q_0 q_2 - q_1^2} \qquad (347)$$

LET THE (M+1)-TH ORDER MATRIX BE PARTITIONED AS FOLLOWS

$$\underbrace{\left[\begin{array}{c|c} \overset{M}{(Q)} & \alpha \\ \hline \alpha & \beta \end{array}\right]}_{[Q] = [\overset{M+1}{Q}]} \overbrace{\left[\begin{array}{c|c} \overset{M}{(Q')} & \gamma \\ \hline \gamma & \delta \end{array}\right]}^{[Q]^{-1}} = \left[\begin{array}{c|c} \overset{M}{(I)} & \begin{matrix} 0 \\ 0 \\ 0 \\ 0 \end{matrix} \\ \hline 0 \; 0 \; 0 \; 0 & 1 \end{array}\right] \qquad (348)$$

CAPITAL LETTERS IN BRACKETS WILL INDICATE MATRICES. THE ORDER WILL BE INDICATED ABOVE THE MATRIX WHEN REQUIRED. GREEK LETTERS WILL INDICATE VECTORS AS FOLLOWS:

$$[\alpha] = \text{COLUMN VECTOR, M-TH ORDER}$$

$$\underline{\overline{\alpha}} = \text{ROW VECTOR, M-TH ORDER}$$

$\overset{M}{[I]}$ DENOTES THE M-TH ORDER UNIT MATRIX.

IN (348) WE HAVE SHOWN THE PARTITIONED PRODUCT OF $\overset{M+1}{[Q]}$ WITH ITS INVERSE $\overset{M+1}{[Q]}^{-1}$ TO GIVE THE (M+1)TH ORDER UNIT MATRIX. FROM (348) WE CAN WRITE

$$\overset{M}{[Q]}\overset{M}{[Q']} + [\alpha]\underline{\overline{\gamma}} = \overset{M}{[I]} \tag{349a}$$

$$\underline{\overline{\alpha}}\overset{M}{[Q']} + \beta\underline{\overline{\gamma}} = \underline{\overline{0}} \tag{349b}$$

$$\overset{M}{[Q]}[\gamma] + \delta[\alpha] = [0] \tag{349c}$$

$$\underline{\overline{\alpha}}[\gamma] + \beta\delta = 1 \tag{349d}$$

THE FORM $[\alpha]\underline{\overline{\gamma}}$ REPRESENTS THE VECTOR OUTER PRODUCT OF M-TH ORDER. FOR EXAMPLE, IF

$$[\alpha] = \begin{bmatrix} \alpha_0 \\ \alpha_1 \\ \alpha_2 \end{bmatrix} \quad \text{AND,} \quad \underline{\overline{\gamma}} = \underline{\overline{\gamma_0 \quad \gamma_1 \quad \gamma_2}} \tag{350}$$

THEN

$$[\alpha]\underline{\overline{\gamma}} = \begin{bmatrix} \alpha_0\gamma_0 & \alpha_0\gamma_1 & \alpha_0\gamma_2 \\ \alpha_1\gamma_0 & \alpha_1\gamma_1 & \alpha_1\gamma_2 \\ \alpha_2\gamma_0 & \alpha_2\gamma_1 & \alpha_2\gamma_2 \end{bmatrix}. \tag{351}$$

THE FORM $\underline{\overline{\gamma}}[\alpha]$ REPRESENTS THE VECTOR INNER PRODUCT OF M-TH ORDER.

WITH THE DEFINITIONS (350) THEN,

$$\underline{\Upsilon}\,[\alpha] = \gamma_0\alpha_0 + \gamma_1\alpha_1 + \gamma_2\alpha_2 \quad . \tag{352}$$

NOW LET $[Q']$, WHICH IS TO BE DETERMINED, BE

$$[Q'] = [Q]^{-1} + [R] \tag{353}$$

SO THAT $[R]$ NOW MUST BE DETERMINED. EQN. (349a) BECOMES

$$[Q]\left\{[Q]^{-1} + [R]\right\} + [\alpha]\,\underline{\Upsilon} = [I] + [Q][R] + [\alpha]\,\underline{\Upsilon} =$$
$$= [I]$$

WE CAN ELIMINATE $[I]$ FROM BOTH SIDES AND PREMULTIPLY BY $[Q]^{-1}$ TO GET

$$[R] = -[Q]^{-1}[\alpha]\,\underline{\Upsilon} \tag{354}$$

BY PREMULTIPLYING (349c) BY $[Q]^{-1}$ WE CAN SOLVE FOR $[\Upsilon]$.

$$[\Upsilon] = -\delta\,[Q]^{-1}[\alpha] \tag{355}$$

SINCE THE INVERSE OF A SYMMETRIC MATRIX IS SYMMETRIC, THE TRANSPOSE OF (355) IS

$$\underline{\Upsilon} = -\delta\,\underline{\alpha}\,[Q]^{-1} \quad . \tag{356}$$

THIS IN (354) GIVES

$$[R] = \delta\,[Q]^{-1}[N][Q]^{-1} \tag{357}$$

WHERE THE MATRIX $[N]$ IS DEFINED TO BE THE OUTER PRODUCT

$$[N] \equiv [\alpha]\underline{\alpha} \tag{358}$$

SINCE $[\alpha]$ IS KNOWN, $[N]$ IS KNOWN. $[Q]^{-1}$ IS ASSUMED KNOWN, SO THAT WE NEED ONLY FIND δ IN ORDER TO BE ABLE TO EVALUATE $[R]$.

LET US USE (353) IN (349 b) AND PREMULTIPLY BY $[\alpha]$ TO GET

$$[\alpha]\underline{\alpha}\left\{[Q]^{-1}+[R]\right\} = -\beta\,[\alpha]\underline{\Upsilon} = \tag{359}$$
$$= \beta\delta\,[\alpha]\underline{\alpha}\,[Q]^{-1}$$

WHERE WE HAVE USED (356). USING THE DEFINITION (358), (359) BECOMES

$$[N][R] = (\beta\delta-1)[N][Q]^{-1} . \tag{360}$$

IF WE NOW SUBSTITUTE (357) FOR $[R]$ IN (360) WE GET

$$\delta\,[N][Q]^{-1}[N][Q]^{-1} = (\beta\delta-1)[N][Q]^{-1} . \tag{361}$$

SINCE β IS KNOWN, THIS MAY BE SOLVED (BY COMPARING ELEMENTS ON BOTH SIDES) FOR δ IN THE FORM

$$\left\{[N][Q]^{-1}\right\}^2 = \left(\beta-\frac{1}{\delta}\right)\left\{[N][Q]^{-1}\right\} \tag{362}$$

IN WHICH CASE $[N][Q]^{-1}$ PLAYS A CENTRAL ROLE. OR, (361) MAY BE POST MULTIPLIED BY $[Q]$ TO GIVE

$$[N][Q]^{-1}[N] = \left(\beta-\frac{1}{\delta}\right)[N] \tag{363}$$

WHICH CAN ALSO BE SOLVED FOR δ, BUT IN WHICH $[N][Q]^{-1}$ DOES NOT PLAY SUCH A FUNDAMENTAL ROLE.

WHEN δ IS KNOWN, $[R]$ CAN BE DETERMINED FROM (357) WHICH ALSO CONTAINS $[N][Q]^{-1}$.

IN FACT, GETTING δ FROM (362) DOES NOT REQUIRE THAT $[N][Q]^{-1}$ BE SQUARED. ONLY ONE ELEMENT OF THE SQUARE NEED BE EVALUATED. FOR EXAMPLE, THE DOT PRODUCT (INNER PRODUCT) OF THE FIRST ROW OF $[N][Q]^{-1}$ WITH THE FIRST COLUMN WILL SUFFICE. THIS SHOULD EQUAL $(\beta - 1/\delta)$ TIMES THE UPPER LEFT ELEMENT OF $[N][Q]^{-1}$, SO THAT δ IS VERY READILY DETERMINED.

THE STEPS OF THE INVERSION ARE THEN (GIVEN $[\overset{M}{Q}]^{-1}$):

1. FORM THE MXM MATRIX $[N]$

$$[\overset{M}{N}] = [\alpha]\,\underline{\overline{\alpha}} \quad .$$

2. FORM THE MATRIX

$$[N][Q]^{-1} \quad .$$

3. TAKE THE INNER PRODUCT OF THE FIRST ROW AND COLUMN OF $[N][Q]^{-1}$. CALL IT, ψ. EVALUATE δ FROM THE UPPER LEFT ELEMENT OF $[N][Q]^{-1}$

$$\psi = \left(\beta - \frac{1}{\delta}\right)\left\{[N][Q]^{-1}\right\}_{00}$$

OR,

$$\delta = \frac{\left\{[N][Q]^{-1}\right\}_{00}}{\beta\left\{[N][Q]^{-1}\right\}_{00} - \psi}$$

THERE IS EVIDENTLY NO INVERSE IF $\psi = \beta\left\{[N][Q]^{-1}\right\}_{00}$.

4. EVALUATE $[R]$ FROM

$$[R] = \delta\,[Q]^{-1}\left\{[N][Q]^{-1}\right\} \quad .$$

5. EVALUATE $[\gamma]$ FROM

$$[\gamma] = -\delta\,[Q]^{-1}[\alpha]$$

6. EVALUATE $[Q']$ FROM

$$[Q'] = [Q]^{-1} + [\Lambda]$$

IN THIS WAY ALL OF THE ELEMENTS OF THE $(M+1)$-TH ORDER INVERSE CAN BE DETERMINED FROM THE M-TH ORDER INVERSE. OBVIOUSLY THIS CAN BE ITERATED TO THE FINAL ORDER.

A SOMEWHAT BETTER APPROACH INVOLVES A MORE DIRECT WAY TO GET δ.

FROM (349d) AND (355) WE HAVE THAT

$$1 - \beta\delta = \overline{\underline{\alpha}}\,[\gamma] = -\delta\,\overline{\underline{\alpha}}\,[Q]^{-1}[\alpha] \tag{364}$$

WHICH GIVES FOR δ,

$$\delta = \frac{1}{\beta - \overline{\underline{\alpha}}\,[Q]^{-1}[\alpha]} \tag{365}$$

WE SEE THAT IN THIS FORMULATION THERE IS NO SOLUTION WHEN

$$\beta = \overline{\underline{\alpha}}\,[Q]^{-1}[\alpha] \qquad \text{(NO SOLUTION)} \tag{366}$$

WE NOW REPEAT THE STEPS OF THE INVERSION, IN A DIFFERENT FORM, STARTING WITH $[Q]^{-1}$ KNOWN.

1. FORM THE COLUMN VECTOR $[\eta] = [Q]^{-1}[\alpha]$.

2. COMPUTE δ FROM $\delta = \{\beta - \overline{\underline{\alpha}}\,[\eta]\}^{-1}$.

3. COMPUTE $[\gamma]$ FROM $[\gamma]^t = -\delta[\eta]$.

4. COMPUTE $[q]'$ FROM $[q]' = [q]^{-1} + \delta [\eta] \boxed{\eta}$.

AS BEFORE, THIS CAN BE ITERATED FROM THE 2X2 (OR EVEN 1X1) UPPER-LEFT CORNER OUT TO THE INVERSE OF THE FULL MXM MATRIX (346).

IT SHOULD BE NOTED THAT $[\eta]\boxed{\eta}$ IS SYMMETRIC [AS IS $[q]^{-1}$] SO THAT THE FULL MATRIX NEED NOT BE EVALUATED BY MULTIPLICATION. ALSO, OF COURSE, $\boxed{\gamma}$ IS IMPLIED WITHOUT FURTHER COMPUTATION FROM $[\gamma]$.

THE DERIVATION JUST GIVEN IS VALID FOR THE INVERSION OF ANY SYMMETRIC MATRIX. IT DOES NOT TAKE ADVANTAGE OF THE SPECIAL SYMMETRY THAT VALUES ALONG PARALLELS TO THE MINOR DIAGONAL ARE EQUAL, AS EXHIBITED IN (346). THIS SPECIAL KIND OF MATRIX IS CALLED "PERSYMMETRIC".

ATTENTION SHOULD BE GIVEN TO FINDING AN EFFICIENT ALGORITHM FOR SOLVING FOR THE a_{lm} WHICH TAKES FULL ADVANTAGE OF ALL SYMMETRIES. IN PARTICULAR, IT SHOULD BE NOTED THAT, THOUGH $Q_{\lambda l \lambda m}$ AS DEFINED BY (343) IS 4-DIMENSIONAL WITH M^4 ELEMENTS, THERE ARE ACTUALLY ONLY ON THE ORDER OF M^2 UNIQUE ELEMENTS IN $Q_{\lambda l \lambda m}$. THUS, SOLUTION FOR THE a_{lm}, IF DONE EFFICIENTLY, SHOULD BE ABOUT AS COMPUTATIONALLY DIFFICULT AS A 2-DIMENSIONAL PROBLEM: NOT A 4-DIMENSIONAL ONE. ALSO, IT IS GENERALLY ADVANTAGEOUS TO FIND AN ALGORITHM FOR THE UNKNOWNS, a_{lm} IN THIS CASE, DIRECTLY RATHER THAN TO INVERT THE SYSTEM MATRIX, $Q_{\lambda l \lambda m}$ IN THIS CASE, IN ORDER TO COMPUTE THE a_{lm}.

WE POSTPONE FURTHER DISCUSSION OF METHODS OF SOLVING FOR THE a_{lm} UNTIL WE HAVE FINISHED TREATING THE PROBLEM OF WEIGHTED COMBINED IMAGES.

COMBINED IMAGES

WE NOW EXTEND THE IDEAS DEVELOPED FOR A SINGLE SUB-IMAGE TO THE COMBINATION OF IMAGES WITH THE APERTURE AT DIFFERENT ORIENTATIONS.

MUCH EARLIER WE SHOWED HOW TO WEIGHT THE FOURIER TRANSFORMS OF SUB-IMAGES, IN THE CASE OF ADDITIVE NOISE, TO MINIMIZE THE VARIANCE AT EACH POINT IN THE ν-PLANE [FOURIER SPACE]. THIS SUGGESTS THAT, SINCE THE WEIGHTING WAS DONE IN THE FOURIER DOMAIN, WE TRY TO RELATE IMAGE PROBABILITY TO VALUES IN ν-SPACE AFTER THE FT IS TAKEN. TO FIND THE PROBABILITY OF A GIVEN SUB-IMAGE IN TERMS OF THE ELEMENTS OF ITS FOURIER TRANSFORM, IT IS TEMPTING TO FORM THE PRODUCT, OVER ALL ELEMENTS lm, OF $\bar{p}_{lm}(x)$ GIVEN BY (291). BUT THIS IS A VALID RECIPE FOR THE JOINT PROBABILITY DISTRIBUTION OF THE SUB-IMAGE ONLY IF THE $\bar{p}_{lm}(x)$ ARE STATISTICALLY INDEPENDENT. GENERALLY THEY ARE NOT, EVEN THOUGH THE ELEMENTS IN THE ORIGINAL IMAGE DOMAIN, $p_{jk}(n_{jk})$ GIVEN BY (279), ARE INDEPENDENT. THAT IS,

$$\overset{(j)}{P} \neq \prod_{l=0}^{N-1} \prod_{m=0}^{N-1} \overset{(j)}{\bar{p}}_{lm}(x_{lm}) \qquad \text{(IN GENERAL)} \qquad (367)$$

HERE, AND IN WHAT FOLLOWS, A SUPERSCRIPT IN PARENTHESES WILL DESIGNATE A PARTICULAR SUB-IMAGE.

WE SHOW FIRST THAT (367) IS TRUE BY SHOWING THAT, IN GENERAL, LINEAR COMBINATIONS OF SAMPLES FROM STATISTICALLY INDEPENDENT DISTRIBUTIONS DO NOT COME FROM STATISTICALLY INDEPENDENT DISTRIBUTIONS. THE DEFINITION OF STATISTICAL INDEPENDENCE IS THAT THE JOINT PROBABILITY DISTRIBUTION IS GIVEN BY THE PRODUCT OF THE INDIVIDUAL DISTRIBUTIONS.

$$p(x_1, x_2, x_3 \ldots) = p_1(x_1)\, p_2(x_2)\, p_3(x_3) \cdots \qquad (368)$$

ASSUME THAT THE $p_i(x_i)$ ARE STATISTICALLY INDEPENDENT, SO THAT (368) APPLIES, AND THAT NEW VARIABLES z_j ARE FORMED FROM LINEAR COMBINATIONS OF THE x_i.

$$z_j = \sum_i \alpha_{ji} x_i \tag{369}$$

ASSUME FURTHER THAT THE MAPPING HAS A UNIQUE INVERSE; THAT IS, THAT THE SYSTEM MATRIX α_{ji} HAS AN INVERSE. THAT IS,

$$x_i = \sum_j (\alpha^{-1})_{ij} z_j \tag{370}$$

SO THAT A SET OF z_j'S IMPLIES A UNIQUE AND DEFINITE SET OF x_i'S. IF WE SUBSTITUTE (370) INTO THE LEFT SIDE OF (368) WE GET AN EXPRESSION FOR THE JOINT PROBABILITY DISTRIBUTION FOR THE z_i'S BECAUSE OF THE UNIQUENESS OF THE IMPLIED x_i'S.

$$\tilde{p}(z_1, z_2, z_3 \ldots) = p_1(f_1(z_i))\, p_2(f_2(z_i))\, p_3(f_3(z_i)) \ldots \tag{371}$$

BUT, GENERALLY, THE FUNCTIONAL DEPENDENCE ON THE z_i'S ON THE RIGHT DOES NOT FACTOR, OR IS NOT SEPARABLE, AS REQUIRED FOR STATISTICAL INDEPENDENCE.

IN GENERAL, THEN, LINEAR COMBINATIONS OF SAMPLES FROM INDEPENDENT DISTRIBUTIONS ARE <u>NOT</u> REPRESENTED BY INDEPENDENT DISTRIBUTIONS.

SINCE THE FOURIER TRANSFORM HAS AN UNAMBIGUOUS INVERSE AND IS JUST A LINEAR COMBINATION [OR, ACTUALLY, COMBINATIONS] OF INPUTS, STATEMENT (367) FOR THE JOINT PROBABILITY DISTRIBUTION IN TERMS OF THE PROBABILITY $\bar{p}_{lm}(x_{lm})$ OF THE FOURIER ELEMENTS IS TRUE. WE CAN <u>NOT</u> SIMPLY MULTIPLY THE $\bar{p}_{lm}$ GIVEN BY (291).

THIS LINE OF REASONING BRINGS UP AN INTERESTING AND FUNDAMENTAL QUESTION.

AT THE OUTSET WE ASSUMED THAT PHOTONS ARRIVING AT THE SAMPLE POINTS OF THE IMAGE PLANE CAME FROM INDEPENDENT DISTRIBUTIONS. THESE SAMPLES ARE THE [INDEPENDENT] INPUTS TO THE FOURIER TRANSFORM JUST DISCUSSED. THEIR ASSUMED INDEPENDENCE JUSTIFIED STEPS SUCH AS (271). BUT, IN FACT, THESE SAMPLES ARE OF THE CONVOLUTION OF THE TRUE SKY [DIRECTIONAL] DISTRIBUTION WITH THE SO-CALLED INSTRUMENT FUNCTION. A CONVOLUTION IS A LINEAR COMBINATION, OR SEQUENCE OF LINEAR COMBINATIONS, SO THAT, BY THE ARGUMENTS JUST GIVEN, CAN WE ASSUME SAMPLE INDEPENDENCE IN THE STATISTICAL SENSE? NOTE THAT IT IS NOT ENOUGH TO ARGUE THAT THE SAMPLES ARE UNCORRELATED TO ESTABLISH STATISTICAL INDEPENDENCE.

THE ANSWER SEEMS TO COME BACK TO THE INTERPRETATION OF THE QUANTUM MECHANICS OF THE PHOTON/APERTURE INTERACTION.

STATEMENT (367) IS TRUE BECAUSE ONE HAS FORMED LINEAR COMBINATIONS OF <u>SAMPLES</u> FROM INDEPENDENT DISTRIBUTIONS. IN THE CASE OF PHOTONS INTERACTING WITH THE APERTURE, ACTUAL <u>SAMPLES</u> WOULD APPEAR TO BE THE <u>PHOTONS</u> <u>THEMSELVES</u>. IF THE INSTRUMENT FUNCTION IS CONVOLVED WITH THE PHOTONS, THEN, WE HAVE ARGUED, THE IMAGE-PLANE SAMPLES ARE NOT, IN GENERAL, STATISTICALLY INDEPENDENT. IF, ON THE OTHER HAND, THE CONVOLUTION OF THE INSTRUMENT FUNCTION IS WITH THE <u>INCOMING</u> <u>PROBABILITY</u> <u>DISTRIBUTION</u>, AND NOT WITH THE PHOTONS THEMSELVES, THEN IT <u>IS</u> REASONABLE TO ASSUME STATISTICAL INDEPENDENCE OF SAMPLES IN THE IMAGE PLANE. WE TAKE THE LATTER VIEW, SO THAT NOT ONLY ARE SAMPLE COUNTS UNCORRELATED AS ARGUED ON PAGES 91 AND 92, BUT THEY ARE STATISTICALLY INDEPENDENT.

THESE TWO INTERPRETATIONS SEEM TO BE CLOSELY RELATED TO THE LONG-STANDING DUAL INTERPRETATION OF THE WAVE FUNCTION IN QUANTUM MECHANICS. I.E., IS IT A FUNCTION WHICH REPRESENTS ONLY PROBABILITY [IN THE ENSEMBLE AVERAGE SENSE], OR DOES IT REPRESENT THE STATE AND EXTENT OF THE UNDERLYING PARTICLES THEMSELVES? STATISTICAL INDEPENDENCE OF SAMPLES IN THE IMAGE PLANE WOULD SEEM TO SUGGEST THE FORMER VIEW.

THE FACT THAT (367) IS TRUE IN THE FOURIER DOMAIN MEANS THAT WE CAN NOT USE (291) DIRECTLY TO COMPUTE THE JOINT PROBABILITY DISTRIBUTION FOR A GIVEN SET OF VALUES IN THE FOURIER PLANE. WE MUST GO BACK TO THE IMAGE-PLANE SAMPLES AND EXTEND THE TECHNIQUE USED FOR A SINGLE IMAGE. IN SO DOING, WE WILL NOT ASSUME A PRIORI THAT ONE OF THE OPERATIONS TO BE IMPLEMENTED OR DESCRIBED IN THE FOURIER PLANE IS WEIGHTED AVERAGING OF THE FTS OF SUB-IMAGES. RATHER, WE SHALL SIMPLY TRY TO FIND AN APPROXIMATION TO THE INCOMING SKY DISTRIBUTION WHICH MAXIMIZES THE GRAND JOINT PROBABILITY DISTRIBUTION FOR THE ENTIRE SET OF SUB-IMAGES. THIS MAY OR MAY NOT SHOW WEIGHTED FOURIER-DOMAIN AVERAGING TO BE A JUSTIFIED STEP.

LET

U_{lm} = FOURIER TRANSFORM OF THE SKY (DISCRETE)

$w^{(n)}_{lm}$ = APERTURE AUTOCORRELATION FOR THE n-TH APERTURE ORIENTATION.

$\beta^{(n)}_{jk}$ = MEAN NUMBER OF PHOTONS ARRIVING AT POINT jk OF SUB-IMAGE n IN TIME T.

$$\beta^{(n)}_{jk} = \lambda^{(n)}_{jk} T^{(n)} \tag{372}$$

$\lambda^{(n)}_{jk}$ = PROBABILITY PER UNIT TIME OF ARRIVAL OF PHOTONS AT POINT jk OF n-TH SUB-IMAGE.

$T^{(n)}$ = TIME OF OBSERVATION WITH APERTURE AT n-TH ORIENTATION.

FROM (242), AND EARLIER RESULTS WITH NO ADDITIVE NOISE, WE FIND THAT

$$K T^{(n)} U_{lm} w^{(n)}_{lm} = \sum_{j=0}^{N-1} \sum_{k=0}^{N-1} \beta^{(n)}_{jk} W^{jl} W^{km} \tag{373}$$

WHERE K IS A UNIVERSAL CONSTANT OF PROPORTIONALITY.

THEREFORE

$$\overset{(m)}{\beta}_{jk} = \frac{1}{N^2} K \overset{(m)}{T} \sum_{l=0}^{N-1} \sum_{m=0}^{N-1} U_{lm} \overset{(m)}{w}_{lm} W^{-lj} W^{-mk} \tag{374}$$

NOW, BECAUSE OF THE INDEPENDENCE OF IMAGE-DOMAIN SAMPLES, THE JOINT PROBABILITY OF THE m-TH SUB-IMAGE IS

$$\overset{(m)}{P} = \prod_{j=0}^{N-1} \prod_{k=0}^{N-1} e^{-\overset{(m)}{\beta}_{jk}} \frac{\left[\overset{(m)}{\beta}_{jk}\right]^{\overset{(m)}{n}_{jk}}}{\left[\overset{(m)}{n}_{jk}\right]!} \tag{375}$$

WHERE $\overset{(m)}{n}_{jk}$ IS THE ACTUAL PHOTON COUNT AT POINT jk OF THE m-TH IMAGE. TO ACTUALLY EVALUATE (375) WE MUST SOMEHOW KNOW $\overset{(m)}{\beta}_{jk}$. THE OBJECT IS TO MODEL THE SKY AS REPRESENTED BY U_{lm}, AND MODIFIED BY THE APERTURE $\overset{(m)}{w}_{lm}$, IN SUCH A WAY THAT THE $\overset{(m)}{\beta}_{jk}$ IMPLIED BY (374) MAXIMIZES THE OVERALL OR GRAND JOINT PROBABILITY DENSITY

$$P = \prod_{m=0}^{q-1} \overset{(m)}{P} = \text{MAXIMUM} \tag{376}$$

WHERE q IS THE NUMBER OF SUB-IMAGES TO BE COMBINED.

$\overset{(m)}{P}$ MAY BE WRITTEN ALSO AS

$$\overset{(m)}{P} = e^{-\sum_{j=0}^{N-1}\sum_{k=0}^{N-1} \overset{(m)}{\beta}_{jk}} \frac{\prod_{j=0}^{N-1}\prod_{k=0}^{N-1} \left[\overset{(m)}{\beta}_{jk}\right]^{\overset{(m)}{n}_{jk}}}{\prod_{j=0}^{N-1}\prod_{k=0}^{N-1} \left[\overset{(m)}{n}_{jk}\right]!} \tag{377}$$

LET US MODEL THE SKY BY TAKING M TERMS, $M \leq N$, OF THE FOURIER

TRANSFORM (373) OF THE [AS YET UNSPECIFIED] MEAN PHOTON COUNTS $\overset{(m)}{\beta}_{jk}$. THEN

$$\overset{(m)}{\tilde{\beta}}_{jk} = \frac{\overset{(m)}{KT}}{N^2} \sum_{l=0}^{M-1} \sum_{m=0}^{M-1} U_{lm} \overset{(m)}{w}_{lm} W^{-lj} W^{-mk} \quad . \tag{378}$$

TO OPTIMIZE P W.R.T. THE U_{lm} WE NEED TO FORM

$$\frac{\partial P}{\partial U_{rs}} = \sum_{j=0}^{Q-1} \frac{\partial \overset{(j)}{P}}{\partial U_{rs}} \prod_{\substack{m=0 \\ m \neq j}}^{Q-1} \overset{(m)}{P} = 0 \quad , \qquad \{r,s = 0,1,\ldots M-1\} \tag{379}$$

AND TO EVALUATE $\partial \overset{(j)}{P} / \partial U_{rs}$ WE NEED $\partial \overset{(m)}{\tilde{\beta}}_{jk} / \partial U_{rs}$ AND

$$\frac{\partial}{\partial U_{rs}} \prod_{j=0}^{N-1} \prod_{k=0}^{N-1} \left[\overset{(m)}{\tilde{\beta}}_{jk} \right]^{\overset{(m)}{n}_{jk}} .$$

FROM (378) WE FIND THAT

$$\frac{\partial \overset{(m)}{\tilde{\beta}}_{jk}}{\partial U_{rs}} = \frac{\overset{(m)}{KT}}{N^2} \sum_{l=0}^{M-1} \sum_{m=0}^{M-1} \overset{(m)}{w}_{lm} W^{-lj} W^{-mk} \delta_{lr} \delta_{ms} =$$

$$= \epsilon_{Mr} \epsilon_{Ms} \frac{\overset{(m)}{KT}}{N^2} \overset{(m)}{w}_{rs} W^{-rj} W^{-sk} \tag{380}$$

WHERE ϵ_{Mr} IS DEFINED BY (319). THEREFORE

$$\frac{\partial}{\partial U_{rs}} \left\{ e^{-\sum_{j=0}^{N-1} \sum_{k=0}^{N-1} \overset{(m)}{\tilde{\beta}}_{jk}} \right\} = -\epsilon_{Mr} \epsilon_{Ms} \frac{\overset{(m)}{KT}}{N^2} \overset{(m)}{w}_{rs} e^{-\sum_{j=0}^{N-1} \sum_{k=0}^{N-1} \overset{(m)}{\tilde{\beta}}_{jk}} \underbrace{\sum_{j=0}^{N-1} \sum_{k=0}^{N-1} W^{-rj} W^{-sk}}_{N^2 \delta_{r0} \delta_{s0}}$$

OR

$$\frac{\partial}{\partial U_{rs}}\left\{ e^{-\sum_{j=0}^{N-1}\sum_{k=0}^{N-1}\overset{(m)}{\tilde{\beta}}_{jk}} \right\} = -\delta_{r0}\delta_{s0}\, k\overset{(m)}{T}\,\overset{(m)}{w}_{rs}\, e^{-\sum_{j=0}^{N-1}\sum_{k=0}^{N-1}\tilde{\beta}_{jk}} \quad . \tag{381}$$

LIKEWISE, FROM (372) AND (380)

$$\frac{\partial}{\partial U_{rs}}\left\{ \prod_{j=0}^{N-1}\prod_{k=0}^{N-1}\left[\overset{(m)}{\tilde{\beta}}_{jk}\right]^{\overset{(m)}{n}_{jk}} \right\} =$$

$$= \sum_{\mu=0}^{N-1}\sum_{\nu=0}^{N-1} \overset{(m)}{n}_{\mu\nu}\, \overset{(m)}{\tilde{\beta}}_{\mu\nu}^{\left[\overset{(m)}{n}_{\mu\nu}-1\right]} \frac{\partial \overset{(m)}{\tilde{\beta}}_{\mu\nu}}{\partial U_{rs}} \prod_{\substack{j=0\\ j\neq\mu}}^{N-1}\prod_{\substack{k=0\\ k\neq\nu}}^{N-1} \overset{(m)}{\tilde{\beta}}_{jk}^{\;\overset{(m)}{n}_{jk}} =$$

$$= \frac{k\overset{(m)}{T}}{N^2}\epsilon_{Mr}\epsilon_{Ms}\overset{(m)}{w}_{rs} \sum_{\mu=0}^{N-1}\sum_{\nu=0}^{N-1} \overset{(m)}{n}_{\mu\nu}\, \overset{(m)}{\tilde{\beta}}_{\mu\nu}^{\left[\overset{(m)}{n}_{\mu\nu}-1\right]} W^{-r\mu}W^{-s\nu} \prod_{\substack{j=0\\ j\neq\mu}}^{N-1}\prod_{\substack{k=0\\ k\neq\nu}}^{N-1} \overset{(m)}{\tilde{\beta}}_{jk}^{\;\overset{(m)}{n}_{jk}} =$$

$$= \frac{k\overset{(m)}{T}}{N^2}\epsilon_{Mr}\epsilon_{Ms}\overset{(m)}{w}_{rs} \sum_{\mu=0}^{N-1}\sum_{\nu=0}^{N-1} \left\{ \frac{\overset{(m)}{n}_{\mu\nu}}{\overset{(m)}{\tilde{\beta}}_{\mu\nu}} \right\} W^{-r\mu}W^{-s\nu} \prod_{j=0}^{N-1}\prod_{k=0}^{N-1} \overset{(m)}{\tilde{\beta}}_{jk}^{\;\overset{(m)}{n}_{jk}} \tag{382}$$

RESULTS (381) AND (382) MAY BE COMBINED WITH (377) TO GIVE

$$\frac{\partial \overset{(m)}{P}}{\partial U_{rs}} = \overset{(m)}{P}\left\{ \frac{\epsilon_{Mr}\epsilon_{Ms}}{N^2}\sum_{j=0}^{N-1}\sum_{k=0}^{N-1}\left\{ \frac{\overset{(m)}{n}_{jk}}{\overset{(m)}{\tilde{\beta}}_{jk}} \right\} W^{-rj}W^{-sk} - \delta_{r0}\delta_{s0} \right\} k\overset{(m)}{T}\,\overset{(m)}{w}_{rs} \tag{383}$$

AND (383) IN (379) GIVES

ORIGINAL PAGE IS
OF POOR QUALITY

$$\boxed{\frac{\partial P}{\partial U_{rs}} = PK\left\{\sum_{\ell=0}^{Q-1} \overset{(\ell)}{T}\, \overset{(\ell)}{w}_{rs}\left[\frac{\epsilon_{Mr}\epsilon_{Ms}}{N^2}\sum_{j=0}^{N-1}\sum_{k=0}^{N-1}\left\{\frac{\overset{(\ell)}{m}_{jk}}{\overset{(\ell)}{\tilde{\beta}}_{jk}}\right\} W^{-rj}W^{-sk} - \delta_{r0}\delta_{s0}\right]\right\} = 0}$$ (384)

SINCE P AND K ARE NON-ZERO, THE CONDITION TO BE SATISFIED TO MAXIMIZE THE GRAND JOINT PROBABILITY FOR THE GIVEN OBSERVATIONS $\overset{(\ell)}{m}_{jk}$ IS

$$\boxed{\sum_{\ell=0}^{Q-1} \overset{(\ell)}{T}\, \overset{(\ell)}{w}_{rs}\left[\frac{\epsilon_{Mr}\epsilon_{Ms}}{N^2}\sum_{j=0}^{N-1}\sum_{k=0}^{N-1}\left\{\frac{\overset{(\ell)}{m}_{jk}}{\overset{(\ell)}{\tilde{\beta}}_{jk}}\right\} W^{-rj}W^{-sk} - \delta_{r0}\delta_{s0}\right] = 0} \qquad (385)$$

$\epsilon_{Mr}\epsilon_{Ms}$ CAN BE ELIMINATED IF $\{r, s = 0, 1, 2, \ldots M-1\}$.

ONE FEATURE WE CAN SEE IMMEDIATELY FROM (385) IS THAT SUB-IMAGES WITH LONGER INTEGRATION TIMES $\overset{(\ell)}{T}$, AND POINTS r, s WITHIN THE FOURIER DOMAIN OF THE SUB-IMAGE AT WHICH THE APERTURE AUTOCORRELATION $\overset{(\ell)}{w}_{rs}$ IS RELATIVELY LARGE, HAVE GREATER INFLUENCE OVER DETERMINATION OF $\overset{(\ell)}{\beta}_{jk}$ THAN DO THOSE WITH SHORTER INTEGRATION TIMES OR AT POINTS OF LOW RELATIVE AUTOCORRELATION VALUE. THIS IS AS IT SHOULD BE IN TERMS OF PLACING GREATEST WEIGHT WHERE INFORMATION IS LEAST UNCERTAIN.

THE RESULT (385) MAY BE DERIVED IN ANOTHER, MORE EFFICIENT, WAY. RELATIONSHIP (376) IS EQUIVALENT TO

$$\ln P = \ln \prod_{m=0}^{Q-1} \overset{(m)}{P} = \sum_{m=0}^{Q-1} \ln \overset{(m)}{P} = \text{MAXIMUM} \qquad (386)$$

NOW, FROM (375) WE FIND THAT

$$\ln \overset{(m)}{P} = \sum_{j=0}^{N-1}\sum_{k=0}^{N-1}\left\{-\overset{(m)}{\beta}_{jk} + \overset{(m)}{m}_{jk}\ln \overset{(m)}{\beta}_{jk} - \ln\left[\left(\overset{(m)}{m}_{jk}\right)!\right]\right\} \qquad (387)$$

LET US NOW USE (378) $\tilde{\beta}^{(m)}_{jk}$ FOR $\beta^{(m)}_{jk}$ IN (387) AND TAKE $\partial/\partial U_{rs}$.

$$\frac{\partial \ln P^{(m)}}{\partial U_{rs}} = \sum_{j=0}^{N-1}\sum_{k=0}^{N-1}\left\{-\frac{\partial \tilde{\beta}^{(m)}_{jk}}{\partial U_{rs}} + \frac{m^{(m)}_{jk}}{\tilde{\beta}^{(m)}_{jk}}\frac{\partial \tilde{\beta}^{(m)}_{jk}}{\partial U_{rs}}\right\} =$$

$$= \sum_{j=0}^{N-1}\sum_{k=0}^{N-1}\left\{\frac{m^{(m)}_{jk}}{\tilde{\beta}^{(m)}_{jk}} - 1\right\}\frac{\partial \tilde{\beta}^{(m)}_{jk}}{\partial U_{rs}} \qquad (388)$$

WE KNOW $\partial\tilde{\beta}^{(m)}_{jk}/\partial U_{rs}$ FROM (380). TO MAXIMIZE (386) WE FORM

$$\frac{\partial \ln P}{\partial U_{rs}} = \sum_{m=0}^{Q-1}\frac{\partial \ln P^{(m)}}{\partial U_{rs}} = 0 \qquad (389)$$

USING (388) AND (380) WE FIND THAT

$$\sum_{m=0}^{Q-1}\epsilon_{mr}\epsilon_{ms}\frac{KT^{(m)}}{N^2}w^{(m)}_{rs}\sum_{j=0}^{N-1}\sum_{k=0}^{N-1}\left\{\frac{m^{(m)}_{jk}}{\tilde{\beta}^{(m)}_{jk}} - 1\right\}W^{-rj}W^{-sk} = 0 \qquad (390)$$

IF $r,s = 0,1,2,\ldots M-1$ THEN WE MAY WRITE (390) AS

$$\boxed{\sum_{m=0}^{Q-1}T^{(m)}w^{(m)}_{rs}\sum_{j=0}^{N-1}\sum_{k=0}^{N-1}\left\{\frac{m^{(m)}_{jk}}{\tilde{\beta}^{(m)}_{jk}} - 1\right\}W^{-rj}W^{-sk} = 0} \qquad (391)$$

THIS IS EQUIVALENT TO (385), BUT IS SLIGHTLY MORE COMPACT.

ITERATIVE SOLUTION

LET US ASSUME THAT

$$U_{lm} = A_{lm} + a_{lm} \qquad (392)$$

WHERE a_{lm} IS "SMALL" RELATIVE TO A_{lm}. THEN, FROM (378),

$$\overset{(n)}{\beta}_{jk} = \overset{(n)}{\gamma}_{jk} + \frac{k\overset{(n)}{T}}{N^2}\sum_{l=0}^{M-1}\sum_{m=0}^{M-1} a_{lm}\overset{(n)}{w}_{lm} W^{-lj} W^{-mk} \qquad (393)$$

WHERE

$$\overset{(n)}{\gamma}_{jk} \equiv \frac{k\overset{(n)}{T}}{N^2}\sum_{l=0}^{M-1}\sum_{m=0}^{M-1} A_{lm}\overset{(n)}{w}_{lm} W^{-lj} W^{-mk} . \qquad (394)$$

THE SECOND TERM OF (393) IS ASSUMED, LIKEWISE, TO BE SMALL RELATIVE TO $\overset{(n)}{\gamma}_{jk}$.

EQUATION (391) MAY NOW BE WRITTEN, APPROXIMATELY,

$$\sum_{n=0}^{Q-1}\overset{(n)}{T}\overset{(n)}{w}_{rs}\sum_{j=0}^{N-1}\sum_{k=0}^{N-1}\left\{\frac{\overset{(n)}{m}_{jk}}{\overset{(n)}{\gamma}_{jk}}\left[1-\frac{kT}{N^2\overset{(n)}{\gamma}_{jk}}\sum_{l=0}^{M-1}\sum_{m=0}^{M-1} a_{lm}\overset{(n)}{w}_{lm} W^{-lj} W^{-mk}\right]-1\right\}\times$$

$$\times W^{-rj} W^{-sk} = 0$$

OR,

$$\sum_{n=0}^{Q-1}\overset{(n)}{T}\overset{(n)}{w}_{rs}\sum_{j=0}^{N-1}\sum_{k=0}^{N-1}\left\{\frac{\overset{(n)}{m}_{jk}}{\overset{(n)}{\gamma}_{jk}}-1\right\}W^{-rj}W^{-sk} =$$

$$= \sum_{n=0}^{Q-1}\overset{(n)}{T}\overset{(n)}{w}_{rs}\sum_{j=0}^{N-1}\sum_{k=0}^{N-1}\frac{\overset{(n)}{m}_{jk}k\overset{(n)}{T}}{\overset{(n)}{\gamma}{}^2_{jk}N^2}\sum_{l=0}^{M-1}\sum_{m=0}^{M-1} a_{lm}\overset{(n)}{w}_{lm} W^{-j(l+r)} W^{-k(m+s)}$$

ORIGINAL PAGE IS
OF POOR QUALITY

OR,

$$\frac{N^2}{K}\sum_{n=0}^{Q-1} T^{(n)} w^{(n)}_{rs} \sum_{j=0}^{N-1}\sum_{k=0}^{N-1}\left\{\frac{m^{(n)}_{jk}}{\gamma^{(n)}_{jk}}-1\right\} W^{-rj} W^{-sk} = \tag{395}$$

$$= \sum_{l=0}^{M-1}\sum_{m=0}^{M-1} a_{lm}\left\{\sum_{n=0}^{Q-1} T^{(n)2}\sum_{j=0}^{N-1}\sum_{k=0}^{N-1}\frac{m^{(n)}_{jk}}{\gamma^{(n)2}_{jk}}\, w^{(n)}_{rs}\, w^{(n)}_{lm}\, W^{-j(l+r)}\, W^{-k(m+s)}\right\}$$

THIS IS IN THE FORM OF A "MATRIX-VECTOR" EQUATION

$$a'_{rs} = G_{rs\,lm}\, a_{lm} \qquad \text{(SUM OVER } l, m) \tag{396}$$

WITH

$$a'_{rs} \equiv \frac{N^2}{K}\sum_{n=0}^{Q-1} T^{(n)} w^{(n)}_{rs} \sum_{j=0}^{N-1}\sum_{k=0}^{N-1}\left\{\frac{m^{(n)}_{jk}}{\gamma^{(n)}_{jk}}-1\right\} W^{-rj} W^{-sk} \tag{397}$$

AND

$$G_{rs\,lm} \equiv \sum_{n=0}^{Q-1} T^{(n)2}\sum_{j=0}^{N-1}\sum_{k=0}^{N-1}\frac{m^{(n)}_{jk}}{\gamma^{(n)2}_{jk}}\, w^{(n)}_{rs}\, w^{(n)}_{lm}\, W^{-j(l+r)}\, W^{-k(m+s)} \tag{398}$$

IN PRINCIPLE WE CAN SOLVE FOR THE a_{lm} BY INVERTING $G_{rs\,lm}$ OR BY ANY COMPUTER METHOD WHICH MAY NOT NECESSARILY INVOLVE EXPLICIT COMPUTATION OF THE INVERSE.

Hill Climbing Solution

THE DIFFICULTY WITH THE ITERATIVE SOLUTION IS THAT IT INVOLVES MANIPULATIONS WITH A 4-DIMENSIONAL MATRIX. IF $N = 256 = 2^8$, $N^4 = 2^{32} \approx 10^9$. THE NUMBER OF OPERATIONS AND STORAGE POTENTIALLY REQUIRED ARE PROHIBITIVE. THIS APPROACH WOULD BE PRACTICABLE IF GOOD USE

COULD BE MADE OF THE HIGH DEGREE OF STRUCTURE INVOLVED IN THE DEFINITION OF G_{gnalm} (398). I.E., THERE IS ACTUALLY A GREAT DEAL LESS THAN 10^{9} UNIQUE ELEMENTS OF INFORMATION IN G_{nalm} SO THAT INVERSION MAY BE POSSIBLE IN AN EFFICIENT MANNER. THIS MAY BE WORTH COMING BACK TO FOR MORE STUDY.

AN ALTERNATE APPROACH, WHICH REMAINS INHERENTLY A 2-DIMENSIONAL PROBLEM THROUGHOUT, IS TO "HILL CLIMB" ON U_{na} UNTIL THE PEAK VALUE OF THE JOINT PROBABILITY P IS ATTAINED. LET US HILL CLIMB ON $\ln P$, RATHER THAN ON P. WE WILL REQUIRE $\partial \ln P / \partial U_{na}$ WHICH WE FIND FROM (388) AND (380) TO BE

$$\frac{\partial \ln P}{\partial U_{na}} = \frac{K}{N^2} \sum_{m=0}^{Q-1} T^{(m)} w^{(m)}_{na} \sum_{j=0}^{N-1} \sum_{k=0}^{N-1} \left\{ \frac{m^{(m)}_{jk}}{\beta^{(m)}_{jk}} - 1 \right\} W^{-nj} W^{-ak} = 0 \qquad (399)$$

WHERE $\{n, a = 0, 1, \ldots M-1\}$, $M = N$, AND $\tilde{\beta}^{(m)}_{jk} \rightarrow \beta^{(m)}_{jk}$. WE ARE CONSIDERING THE CASE $M=N$ SO THAT THE FINAL RESULT FOR U_{na} WILL REPRESENT THE OPTIMUM COMBINATION OF INFORMATION FROM THE Q SUB-IMAGES WITH NO FILTERING. AS BEFORE, WE WILL REGARD FILTERING AS A DISTINCT STEP WHICH FOLLOWS OPTIMUM COMBINATION.

THE STRATEGY IS TO REGARD (399) AS THE GRADIENT OF A FUNCTION [REAL, SCALAR] OF N^2 VARIABLES U_{na}. WE USE THE GRADIENT AT A POINT IN THIS N^2-DIMENSIONAL SPACE [WHICH POINT CORRESPONDS TO AN INITIAL GUESS AT THE SOLUTION U_{na}] TO DETERMINE WHICH DIRECTION IS "UP THE HILL". WE WILL ACCORDINGLY ADJUST U_{na} BY AN AMOUNT CORRESPONDING TO A REASONABLE GUESS AS TO HOW FAR FROM THE CURRENT POINT IS THE "TOP OF THE HILL". THIS PROCESS WILL BE ITERATED UNTIL SOME CRITERION, SUCH AS THE RELATIVE CHANGE OF P, FALLS BELOW A PREDETERMINED VALUE.

AN INTERESTING BY PRODUCT OF THIS PROCESS IS THE COMPUTATION OF P. FOR AN OBSERVATION WITH GOOD SIGNAL-TO-NOISE, P SHOULD APPROACH 1. IN ANYCASE, P COULD SERVE AS A MEASURE OF CONFIDENCE IN THE FINAL IMAGE AND MIGHT EVEN BE USEFUL FOR CONTROLING OBSERVATION TIME ON A GIVEN FIELD OF VIEW IN REAL TIME.

THE FOURIER TRANSFORM (374) OF $\overset{(m)}{\beta}_{jk}$ WHICH DEFINES $U_{\lambda\lambda}$ IS AN ANALYTIC FUNCTION OF THE $U_{\lambda\lambda}$. AS SUCH IT IS TOO GENERAL. PHYSICALLY VALID SOLUTIONS $U_{\lambda\lambda}$ ARE THOSE WHICH CAUSE $\overset{(m)}{\beta}_{jk}$ (372) TO BE REAL. WE MUST SOMEHOW BUILD THIS CONSTRAINT ON THE ACCEPTABLE $U_{\lambda\lambda}$ INTO THE HILL CLIMBING PROCESS. ONE WAY TO DO THIS IS TO SET DOWN THE CONDITIONS ON $U_{\lambda\lambda}$ WHICH ARE NECESSARY AND SUFFICIENT FOR $\overset{(m)}{\beta}_{jk}$ TO BE REAL.

SINCE WE HAVE TAKEN $M=N$, (374) APPLIES, AS DOES (373), FROM WHICH WE CAN WRITE

$$\overset{(m)}{\psi}_{\ell m} \equiv \overset{(m)}{U}_{\ell m} w_{\ell m} = \frac{1}{K\overset{(m)}{T}} \sum_{j=0}^{N-1} \sum_{k=0}^{N-1} \overset{(m)}{\beta}_{jk} W^{j\ell} W^{km} \tag{400}$$

LET $\ell = \frac{N}{2} \pm p$, $m = \frac{N}{2} \pm q$. THEN

$$\overset{(m)}{\psi}_{\frac{N}{2}\pm p, \frac{N}{2}\pm q} = \frac{1}{K\overset{(m)}{T}} \sum_{j=0}^{N-1} \sum_{k=0}^{N-1} \overset{(m)}{\beta}_{jk} W^{j\left(\frac{N}{2}\pm p\right)} W^{k\left(\frac{N}{2}\pm q\right)} \tag{401}$$

NOW,
$$W^{k\frac{N}{2}} = e^{-\frac{2\pi i}{N}\frac{N}{2}k} = \left(e^{-\pi i}\right)^k = (-1)^k = \text{REAL}. \tag{402}$$

THEREFORE, (401) CAN BE WRITTEN

$$\overset{(m)}{\psi}_{\frac{N}{2}\pm p, \frac{N}{2}\pm q} = \frac{1}{K\overset{(m)}{T}} \sum_{j=0}^{N-1} \sum_{k=0}^{N-1} \left[\overset{(m)}{\beta}_{jk} (-1)^{j+k}\right] W^{\pm jp} W^{\pm kq} \tag{403}$$

IF, AS REQUIRED, $\overset{(m)}{\beta}_{jk}$ IS REAL, (403) SHOWS THAT

$$\boxed{\overset{(m)}{\psi}_{\frac{N}{2}\pm p, \frac{N}{2}\pm q} = \overset{(m)}{\psi}{}^{*}_{\frac{N}{2}\mp p, \frac{N}{2}\mp q}} \tag{404}$$

$\{p, q = 0, 1, \ldots, \frac{N}{2}\}$

BECAUSE $\overset{(m)}{\psi}_{lm} = U_{lm}\overset{(m)}{w}_{lm}$ AND $\overset{(m)}{\beta}_{jk}$ CONSTITUTE FOURIER TRANSFORM PAIRS, (404) IS THE NECESSARY AND SUFFICIENT CONDITION THAT $\overset{(m)}{\beta}_{jk}$ BE REAL.

NOW, BY (32), $\overset{(m)}{w}_{lm}$ IS THE DISCRETE VERSION OF THE APERTURE AUTO-CORRELATION. BY (26), OR (24) USING THE ARGUMENT JUST GIVEN, $\overset{(m)}{w}_{lm}$ MUST EXHIBIT THE SAME CONJUGATE SYMMETRY

$$\boxed{\overset{(m)}{w}_{\frac{N}{2}\pm p,\frac{N}{2}\pm q} = \overset{(m)}{w}^{*}_{\frac{N}{2}\mp p,\frac{N}{2}\mp q}} \tag{405}$$

EVEN IF THE APERTURE FUNCTION ITSELF IS COMPLEX.

RESULT (405) IN (404), OR (23) AND THE ARGUMENT JUST GIVEN, SHOW THAT ALSO,

$$\boxed{U_{\frac{N}{2}\pm p,\frac{N}{2}\pm q} = U^{*}_{\frac{N}{2}\mp p,\frac{N}{2}\mp q}} \tag{406}$$

IF WE START OFF WITH AN INITIAL GUESS AT U_{lm} WHICH CORRESPONDS TO $\overset{(m)}{\beta}_{jk}$ REAL, AND MAKE ALL CORRECTIONS SUCH THAT CONDITION (406) IS PRESERVED, WE SHALL CONVERGE ON A [ACTUALLY, <u>THE</u> UNIQUE SOLUTION AS WE SHALL SHOW] PHYSICALLY MEANINGFUL U_{lm}. WE WILL, ACCORDING TO (406), VARY FREELY ONLY A SUB-SET OF THE U_{lm}. THE VALUES TAKEN UP BY THE REMAINING U_{lm} WILL BE CONSTRAINED BY (406) IN ORDER TO GUARANTEE A PHYSICAL RESULT.

THE DIFFERENTIAL OF $\ln P$, WHICH MUST BE REAL, IS

$$d\left[\ln P\right] = \sum_{l=0}^{N-1}\sum_{m=0}^{N-1} \frac{\partial \ln P}{\partial U_{lm}}\, dU_{lm} \,. \tag{407}$$

THIS MAY BE EXPANDED TO READ

$$d[\ln P] = \sum_{l=0}^{N-1}\left\{ \frac{\partial \ln P}{\partial U_{l0}} dU_{l0} + \frac{\partial \ln P}{\partial U_{l\frac{N}{2}}} dU_{l\frac{N}{2}} + \sum_{m=1}^{\frac{N}{2}-1} \frac{\partial \ln P}{\partial U_{lm}} dU_{lm} + \sum_{m=\frac{N}{2}+1}^{N-1} \frac{\partial \ln P}{\partial U_{lm}} dU_{lm} \right\} =$$

$$= \sum_{l=0}^{N-1}\left\{ \frac{\partial \ln P}{\partial U_{l0}} dU_{l0} + \frac{\partial \ln P}{\partial U_{l\frac{N}{2}}} dU_{l\frac{N}{2}} + \sum_{m=1}^{\frac{N}{2}-1} \frac{\partial \ln P}{\partial U_{l,\frac{N}{2}-m}} dU_{l,\frac{N}{2}-m} + \sum_{m=1}^{\frac{N}{2}-1} \frac{\partial \ln P}{\partial U_{l,\frac{N}{2}+m}} dU_{l,\frac{N}{2}+m} \right\} \quad (408)$$

A SIMILAR EXPANSION ON l GIVES,

$$d[\ln P] = \frac{\partial \ln P}{\partial U_{00}} dU_{00} + \frac{\partial \ln P}{\partial U_{\frac{N}{2}0}} dU_{\frac{N}{2}0} + \sum_{l=1}^{\frac{N}{2}-1}\left\{ \frac{\partial \ln P}{\partial U_{\frac{N}{2}+l,0}} dU_{\frac{N}{2}+l,0} + \frac{\partial \ln P}{\partial U_{\frac{N}{2}-l,0}} dU_{\frac{N}{2}-l,0} \right\} + \frac{\partial \ln P}{\partial U_{0\frac{N}{2}}} dU_{0\frac{N}{2}} + \frac{\partial \ln P}{\partial U_{\frac{N}{2}\frac{N}{2}}} dU_{\frac{N}{2}\frac{N}{2}} +$$

$$+ \sum_{l=1}^{\frac{N}{2}-1}\left\{ \frac{\partial \ln P}{\partial U_{\frac{N}{2}+l,\frac{N}{2}}} dU_{\frac{N}{2}+l,\frac{N}{2}} + \frac{\partial \ln P}{\partial U_{\frac{N}{2}-l,\frac{N}{2}}} dU_{\frac{N}{2}-l,\frac{N}{2}} \right\} + \sum_{m=1}^{\frac{N}{2}-1} \frac{\partial \ln P}{\partial U_{0,\frac{N}{2}-m}} dU_{0,\frac{N}{2}-m} +$$

$$+ \sum_{m=1}^{\frac{N}{2}-1} \frac{\partial \ln P}{\partial U_{\frac{N}{2},\frac{N}{2}-m}} dU_{\frac{N}{2},\frac{N}{2}-m} + \sum_{l=1}^{\frac{N}{2}-1}\sum_{m=1}^{\frac{N}{2}-1} \frac{\partial \ln P}{\partial U_{\frac{N}{2}+l,\frac{N}{2}-m}} dU_{\frac{N}{2}+l,\frac{N}{2}-m} + \quad (409)$$

$$+\sum_{l=1}^{\frac{N}{2}-1}\sum_{m=1}^{\frac{N}{2}-1}\frac{\partial \ln P}{\partial U_{\frac{N}{2}-l,\frac{N}{2}-m}}\,dU_{\frac{N}{2}-l,\frac{N}{2}-m}+\sum_{m=1}^{\frac{N}{2}-1}\frac{\partial \ln P}{\partial U_{0,\frac{N}{2}+m}}\,dU_{0,\frac{N}{2}+m}+$$

$$+\sum_{m=1}^{\frac{N}{2}-1}\frac{\partial \ln P}{\partial U_{\frac{N}{2},\frac{N}{2}+m}}\,dU_{\frac{N}{2},\frac{N}{2}+m}+\sum_{l=1}^{\frac{N}{2}-1}\sum_{m=1}^{\frac{N}{2}-1}\frac{\partial \ln P}{\partial U_{\frac{N}{2}+l,\frac{N}{2}+m}}\,dU_{\frac{N}{2}+l,\frac{N}{2}+m}+$$

$$+\sum_{l=1}^{\frac{N}{2}-1}\sum_{m=1}^{\frac{N}{2}-1}\frac{\partial \ln P}{\partial U_{\frac{N}{2}-l,\frac{N}{2}+m}}\,dU_{\frac{N}{2}-l,\frac{N}{2}+m} \qquad (409)$$

NOW, $$W^{-(\frac{N}{2}\pm p)j}\,W^{-(\frac{N}{2}\pm q)k}=(-1)^{j+k}\,W^{\mp pj}\,W^{\mp qk}=$$

$$=\left[W^{-(\frac{N}{2}\mp p)j}\,W^{-(\frac{N}{2}\mp q)k}\right]^{*} \qquad (410)$$

THIS RESULT, (405), AND $\beta_{jk}^{(n)}$ REAL IN (399) SHOWS THAT

$$\boxed{\frac{\partial \ln P}{\partial U_{\frac{N}{2}\pm p,\frac{N}{2}\pm q}}=\left[\frac{\partial \ln P}{\partial U_{\frac{N}{2}\mp p,\frac{N}{2}\mp q}}\right]^{*}} \qquad (411)$$

ONE FURTHER OBSERVATION IS REQUIRED REGARDING (404), (405), (406), AND (411). IF p OR q IS $N/2$, WE WILL HAVE A SUBSCRIPT ZERO ON ONE SIDE, AND N ON THE OTHER. SINCE

$$W^{N}=e^{\frac{-2\pi i}{N}N}=1=W^{0},$$

WE MAY REGARD THE SUBSCRIPT N AS THE SUBSCRIPT ZERO ALSO.

WITH THESE RESULTS IN MIND, WE MAY WRITE (409) AS

$$
\begin{aligned}
d[\ln P] = {} & \frac{\partial \ln P}{\partial U_{00}} dU_{00} + \frac{\partial \ln P}{\partial U_{\frac{N}{2},0}} dU_{\frac{N}{2},0} + \frac{\partial \ln P}{\partial U_{0,\frac{N}{2}}} dU_{0,\frac{N}{2}} + \frac{\partial \ln P}{\partial U_{\frac{N}{2},\frac{N}{2}}} dU_{\frac{N}{2},\frac{N}{2}} + \\
& + 2\sum_{l=1}^{\frac{N}{2}-1} Re\left[\frac{\partial \ln P}{\partial U_{\frac{N}{2}-l,0}} dU_{\frac{N}{2}-l,0}\right] + 2\sum_{l=1}^{\frac{N}{2}-1} Re\left[\frac{\partial \ln P}{\partial U_{\frac{N}{2}-l,\frac{N}{2}}} dU_{\frac{N}{2}-l,\frac{N}{2}}\right] + \\
& + 2\sum_{l=1}^{\frac{N}{2}-1} Re\left[\frac{\partial \ln P}{\partial U_{0,\frac{N}{2}-l}} dU_{0,\frac{N}{2}-l}\right] + 2\sum_{l=1}^{\frac{N}{2}-1} Re\left[\frac{\partial \ln P}{\partial U_{\frac{N}{2},\frac{N}{2}-l}} dU_{\frac{N}{2},\frac{N}{2}-l}\right] + \\
& + 2\sum_{l=1}^{\frac{N}{2}-1}\sum_{m=1}^{\frac{N}{2}-1} Re\left[\frac{\partial \ln P}{\partial U_{\frac{N}{2}+l,\frac{N}{2}-m}} dU_{\frac{N}{2}+l,\frac{N}{2}-m}\right] + 2\sum_{l=1}^{\frac{N}{2}-1}\sum_{m=1}^{\frac{N}{2}-1} Re\left[\frac{\partial \ln P}{\partial U_{\frac{N}{2}-l,\frac{N}{2}-m}} dU_{\frac{N}{2}-l,\frac{N}{2}-m}\right]
\end{aligned}
\tag{412}
$$

IT IS EASY TO SEE THAT THE FIRST 4 PARTIALS ARE REAL, SO THAT dU_{00}, $dU_{\frac{N}{2},0}$, $dU_{0,\frac{N}{2}}$, AND $dU_{\frac{N}{2},\frac{N}{2}}$ ARE REAL. THE REMAINING 6 ARE, IN GENERAL, COMPLEX. THE TERMS 5 THROUGH 8 ACCOUNT FOR $8\left(\frac{N}{2}-1\right)$ REAL DIFFERENTIALS. TERMS 9 AND 10 ACCOUNT FOR $4\left(\frac{N}{2}-1\right)^2$ REAL DIFFERENTIALS. THE TOTAL NUMBER IS

$$
4\left(\frac{N}{2}-1\right)^2 + 8\left(\frac{N}{2}-1\right) + 4 = 4\left[\left(\frac{N}{2}-1\right)^2 + 2\left(\frac{N}{2}-1\right) + 1\right] =
$$

$$
= 4\left[\left(\frac{N}{2}-1\right)+1\right]^2 = N^2
$$

WHICH IS THE SAME AS THE NUMBER OF REAL INPUT IMAGE SAMPLES. WE THUS REGARD THE HILL CLIMBING ON $\ln P$ AS TAKING PLACE IN AN N^2-DIMENSIONAL REAL SPACE. FROM THE RELATIONSHIP

$$
(\alpha + i\beta)(a + ib) = \alpha a - \beta b + i(\beta a + \alpha b)
$$

AND THE DEFINITION $dU_{lm} = dR_{lm} + i\, dI_{lm}$

WE CAN WRITE

$$d[\ln P] = Re\left[\frac{\partial \ln P}{\partial U_{00}}\right] dR_{00} + Re\left[\frac{\partial \ln P}{\partial U_{\frac{N}{2},0}}\right] dR_{\frac{N}{2},0} + Re\left[\frac{\partial \ln P}{\partial U_{0,\frac{N}{2}}}\right] dR_{0,\frac{N}{2}} +$$

$$+ Re\left[\frac{\partial \ln P}{\partial U_{\frac{N}{2},\frac{N}{2}}}\right] dR_{\frac{N}{2},\frac{N}{2}} + 2\sum_{l=1}^{\frac{N}{2}-1} Re\left[\frac{\partial \ln P}{\partial U_{\frac{N}{2}-l,0}}\right] dR_{\frac{N}{2}-l,0} - 2\sum_{l=1}^{\frac{N}{2}-1} Im\left[\frac{\partial \ln P}{\partial U_{\frac{N}{2}-l,0}}\right] dI_{\frac{N}{2}-l,0} +$$

$$+ 2\sum_{l=1}^{\frac{N}{2}-1} Re\left[\frac{\partial \ln P}{\partial U_{\frac{N}{2}-l,\frac{N}{2}}}\right] dR_{\frac{N}{2}-l,\frac{N}{2}} - 2\sum_{l=1}^{\frac{N}{2}-1} Im\left[\frac{\partial \ln P}{\partial U_{\frac{N}{2}-l,\frac{N}{2}}}\right] dI_{\frac{N}{2}-l,\frac{N}{2}} +$$

$$+ 2\sum_{l=1}^{\frac{N}{2}-1} Re\left[\frac{\partial \ln P}{\partial U_{0,\frac{N}{2}-l}}\right] dR_{0,\frac{N}{2}-l} - 2\sum_{l=1}^{\frac{N}{2}-1} Im\left[\frac{\partial \ln P}{\partial U_{0,\frac{N}{2}-l}}\right] dI_{0,\frac{N}{2}-l} +$$

$$+ 2\sum_{l=1}^{\frac{N}{2}-1} Re\left[\frac{\partial \ln P}{\partial U_{\frac{N}{2},\frac{N}{2}-l}}\right] dR_{\frac{N}{2},\frac{N}{2}-l} - 2\sum_{l=1}^{\frac{N}{2}-1} Im\left[\frac{\partial \ln P}{\partial U_{\frac{N}{2},\frac{N}{2}-l}}\right] dI_{\frac{N}{2},\frac{N}{2}-l} +$$

$$+ 2\sum_{l=1}^{\frac{N}{2}-1}\sum_{m=1}^{\frac{N}{2}-1} Re\left[\frac{\partial \ln P}{\partial U_{\frac{N}{2}+l,\frac{N}{2}-m}}\right] dR_{\frac{N}{2}+l,\frac{N}{2}-m} - 2\sum_{l=1}^{\frac{N}{2}-1}\sum_{m=1}^{\frac{N}{2}-1} Im\left[\frac{\partial \ln P}{\partial U_{\frac{N}{2}+l,\frac{N}{2}-m}}\right] dI_{\frac{N}{2}+l,\frac{N}{2}-m} +$$

$$+ 2\sum_{l=1}^{\frac{N}{2}-1}\sum_{m=1}^{\frac{N}{2}-1} Re\left[\frac{\partial \ln P}{\partial U_{\frac{N}{2}-l,\frac{N}{2}-m}}\right] dR_{\frac{N}{2}-l,\frac{N}{2}-m} - 2\sum_{l=1}^{\frac{N}{2}-1}\sum_{m=1}^{\frac{N}{2}-1} Im\left[\frac{\partial \ln P}{\partial U_{\frac{N}{2}-l,\frac{N}{2}-m}}\right] dI_{\frac{N}{2}-l,\frac{N}{2}-m} \qquad (413)$$

NOW, LET $\vec{\nabla} P$ BE A VECTOR OF THE COEFFICIENTS OF THE DIFFERENTIALS

IN (413), AND $d\vec{U}$ A VECTOR OF THE ORDERED DIFFERENTIALS, SO THAT WE CAN WRITE

$$d\,[\ln P] = \vec{\nabla} P \cdot d\vec{U} \qquad (414)$$

THE COMPONENTS OF $\vec{\nabla} P$ CAN BE PICKED OUT OF AN EVALUATION OF (399) USING (413). FOR AN APPROXIMATE COMPUTER EVALUATION THE DIFFERENTIALS IN (414), DEFINED BY (413), ARE REPLACED BY FINITE DIFFERENCES.

$$\begin{aligned} d\,[\ln P] &\rightarrow \Delta\,[\ln P] \\ d\vec{U} &\rightarrow \Delta\vec{U} \end{aligned} \qquad (415)$$

$$\Rightarrow \qquad \Delta\,[\ln P] = \vec{\nabla} P \cdot \Delta\vec{U} \qquad (416)$$

THE "UP HILL" DIRECTION IS GIVEN BY $-\vec{\nabla} P$. THE UNIT VECTOR IN THE UP HILL DIRECTION IS

$$\hat{u} = -\frac{\vec{\nabla} P}{|\vec{\nabla} P|} \qquad (417)$$

WHERE

$$|\vec{\nabla} P| = \sqrt{\sum_{l=0}^{N^2-1} (\vec{\nabla} P)_l^2} \qquad (418)$$

IT REMAINS TO PICK AN APPROPRIATE STEP SIZE ALONG $\hat{u}$.

LET US ASSUME WE HAVE MADE A VERTICAL CUT IN THE N^2-DIMENSIONAL SPACE OF THE FREE COMPONENTS OF U_{nk} ALONG THE DIRECTION $\hat{u}$.

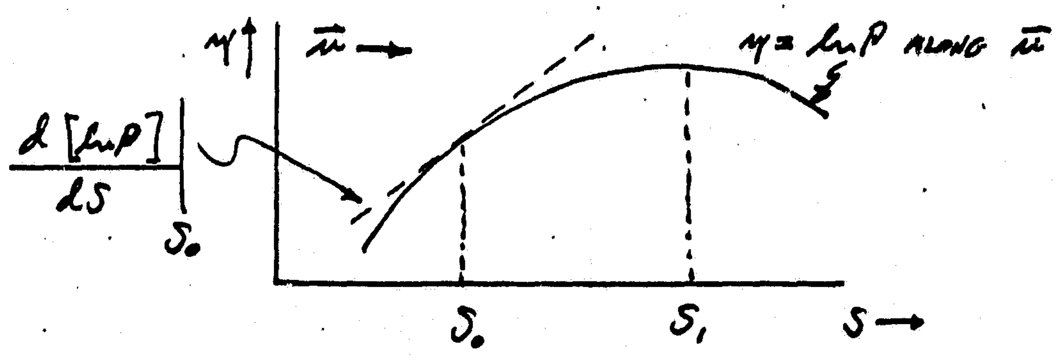

CLEARLY

$$\Delta\vec{U} = \Delta S\,\vec{u} \qquad (419)$$

SO THAT

$$\frac{d[\ln P]}{dS} \approx \frac{\Delta[\ln P]}{\Delta S} = \vec{\nabla}p\cdot\vec{u} = -\frac{\vec{\nabla}p\cdot\vec{\nabla}p}{|\vec{\nabla}p|} =$$

$$= -|\vec{\nabla}p| \qquad (420)$$

LET US ASSUME THAT LOCALLY y IS QUADRATIC IN S.

$$y = \ln P \text{ ALONG } \vec{u} = aS^2 + bS + c \qquad (421a)$$

THEN

$$\frac{dy}{dS} = 2aS + b \qquad (421b)$$

$$\frac{d^2y}{dS^2} = 2a \qquad (421c)$$

$dy/dS = 0$ AT THE EXTREMUM GIVES, FROM (421b),

$$S_1 = -\frac{b}{2a} \qquad (422)$$

FROM (421 b & c), IN GENERAL,

$$b = \frac{dy}{dS} - \frac{d^2y}{dS^2}S \qquad (423)$$

SO THAT FROM (422) AND (421c),

$$S_1 = \frac{-\frac{dy}{dS} + \frac{d^2y}{dS^2}S}{\frac{d^2y}{dS^2}} = S - \frac{dy/dS}{d^2y/dS^2}$$

OR,

$$\boxed{\Delta S = -\frac{dy/dS}{d^2y/dS^2} = -\frac{d[\ln P]/dS}{d^2[\ln P]/dS^2}} \qquad (424)$$

WE CAN EVALUATE THE NUMERATOR FROM (420). THE DENOMINATOR

REQUIRES THE DIRECTIONAL SECOND DERIVATIVE ALONG $\vec{\mu}$.

$$\frac{d^2[\ln P]}{dS^2} = (\vec{\mu}\cdot\vec{\nabla})^2[\ln P] =$$

$$= \vec{\mu}\cdot\vec{\nabla}\left\{\vec{\mu}\cdot\vec{\nabla}\ln P\right\} = \vec{\mu}\cdot\vec{\nabla}\left\{\vec{\mu}\cdot\vec{\nabla}P\right\} \tag{425}$$

IN THE NOTATION OF (414) IN WHICH $\vec{\nabla}P$ REPRESENTS (399).

$$\vec{\nabla}P \equiv \frac{\partial \ln P}{\partial U_{\mu\lambda}} \tag{426}$$

WHICH IS A COVARIANT N^2-DIMENSIONAL VECTOR.

$$dU_{\mu\lambda} = \mu_{\mu\lambda}\, dS \quad \text{OR,} \quad \mu_{\mu\lambda} = \frac{dU_{\mu\lambda}}{dS} \tag{427}$$

SO THAT (425) CAN BE WRITTEN

$$\frac{d^2[\ln P]}{dS^2} = \frac{\partial}{\partial U_{\alpha\beta}}\left\{\frac{\partial \ln P}{\partial U_{\gamma\delta}}\frac{dU_{\gamma\delta}}{dS}\right\}\frac{dU_{\alpha\beta}}{dS} =$$

$$= \frac{\partial}{\partial U_{\alpha\beta}}\left\{\frac{\partial \ln P}{\partial U_{\gamma\delta}}\mu_{\gamma\delta}\right\}\mu_{\alpha\beta} = \frac{\partial^2 \ln P}{\partial U_{\alpha\beta}\,\partial U_{\gamma\delta}}\mu_{\alpha\beta}\mu_{\gamma\delta} \tag{428}$$

[EINSTEIN SUMMATION CONVENTION ASSUMED]. IN THIS SAME NOTATION,

$$\frac{d[\ln P]}{dS} = (\vec{\mu}\cdot\vec{\nabla})[\ln P] = \frac{\partial \ln P}{\partial U_{\alpha\beta}}\mu_{\alpha\beta} =$$

$$= -\frac{1}{|\vec{\nabla}P|}\frac{\partial \ln P}{\partial U_{\alpha\beta}}\frac{\partial \ln P}{\partial U_{\alpha\beta}} = -|\vec{\nabla}P| \tag{429}$$

WHERE:

$$\mu_{\alpha\beta} = -\frac{1}{|\vec{\nabla} P|}\frac{\partial \ln P}{\partial U_{\alpha\beta}} \tag{430}$$

TO EVALUATE (428) WE REQUIRE

$$\frac{\partial^2 \ln P}{\partial U_{\alpha\beta}\,\partial U_{\gamma\delta}} = \frac{K}{N^2}\sum_{n=0}^{Q-1} \overset{(n)}{T}\,\overset{(n)}{w}_{\gamma\delta} \sum_{j=0}^{N-1}\sum_{k=0}^{N-1} \overset{(n)}{m}_{jk}\, W^{-\gamma j} W^{-\delta k}\, \frac{\partial \overset{(n)}{\beta}{}^{-1}_{jk}}{\partial U_{\alpha\beta}} \tag{431}$$

FROM (399). NOW

$$\frac{\partial \overset{(n)}{\beta}{}^{-1}_{jk}}{\partial U_{\alpha\beta}} = -\frac{1}{\overset{(n)}{\beta}{}^2_{jk}}\frac{\partial \overset{(n)}{\beta}_{jk}}{\partial U_{\alpha\beta}} = -\frac{1}{\overset{(n)}{\beta}{}^2_{jk}}\frac{K\overset{(n)}{T}}{N^2}\,\overset{(n)}{w}_{\alpha\beta}\, W^{-\alpha j} W^{-\beta k} \tag{432}$$

WHERE WE HAVE USED (374). THUS,

$$\boxed{\frac{\partial^2 \ln P}{\partial U_{\alpha\beta}\,\partial U_{\gamma\delta}} = -\frac{K^2}{N^4}\sum_{n=0}^{Q-1} \overset{(n)}{T}{}^2\,\overset{(n)}{w}_{\alpha\beta}\,\overset{(n)}{w}_{\gamma\delta} \sum_{j=0}^{N-1}\sum_{k=0}^{N-1} \frac{\overset{(n)}{m}_{jk}}{\overset{(n)}{\beta}{}^2_{jk}}\, W^{-j(\alpha+\gamma)}\, W^{-k(\beta+\delta)}} \tag{433}$$

NOW, WE HAVE ASSUMED THAT α, β, γ, AND δ IN (428) – (433) RANGE ONLY OVER THE INDICIES AND ELEMENTS IMPLIED BY (413). WHILE $d\ln P/dS$ REDUCES TO $-|\vec{\nabla} P|$ [SEE (420) AND (429)], IT IS NOT CLEAR THAT $d^2\ln P/dS^2$ REDUCES TO A SIMILARLY COMPACT RESULT. THUS, FROM A COMPUTATIONAL POINT OF VIEW, IT MAY BE WELL TO FORMULATE THE HILL CLIMBING PROBLEM IN A MORE GENERAL WAY.

THE DIRECTIONAL DERIVATIVE OF $\ln P$ ALONG THE DIRECTION GIVEN BY THE UNIT VECTOR $\vec{\mu}$ IS

$$\frac{d[\ln P]}{dS} = \frac{\partial \ln P}{\partial U_{\alpha\beta}}\,\mu_{\alpha\beta} \tag{434}$$

WHERE $\{\alpha,\beta\} = 0,1,2,\ldots N-1$. IF WE WISH TO CONSTRAIN $d\ln P/dS$ TO BE

REAL, WE MUST TAKE

$$\mu_{\alpha\beta} = -\left(\frac{\partial \ln P}{\partial U_{\alpha\beta}}\right)^* \Bigg/ \sqrt{\left(\frac{\partial \ln P}{\partial U_{\gamma\delta}}\right)\left(\frac{\partial \ln P}{\partial U_{\gamma\delta}}\right)^*} \tag{435}$$

[SUMMATION ON REPEATED INDICES]. THUS

$$\mu_{\alpha\beta}\,\mu^*_{\alpha\beta} = 1 \tag{436}$$

THE MINUS SIGN IN (435) GIVES THE "UP HILL" DIRECTION. IN AN ACTUAL COMPUTER EVALUATION OF (434) AND (435) ADVANTAGE CAN BE TAKEN OF THE SYMMETRY (411).

LIKEWISE THE SECOND DERIVATE IS

$$\frac{d^2[\ln P]}{dS^2} = \frac{\partial^2 \ln P}{\partial U_{\alpha\beta}\,\partial U_{\gamma\delta}}\,\mu_{\alpha\beta}\,\mu_{\gamma\delta} \tag{437}$$

WITH $\mu_{\alpha\beta}$ DEFINED BY (435) AND THE SECOND PARTIAL BY (433). ΔS IS FOUND FROM (424) AND THE CORRECTION TO $U_{\alpha\beta}$ FROM (419),

$$\Delta U_{\alpha\beta} = \Delta S\,\mu_{\alpha\beta} \tag{438}$$

AGAIN, COMPUTATIONAL ADVANTAGE MAY BE TAKEN OF THE SYMMETRY (411). RESULTS (399), (411), (424), AND (433) - (438) FORM THE BASIS OF A COMPUTER HILL-CLIMBING ROUTINE. EQN. (374) RELATES $\beta^{(m)}_{jk}$ TO $U_{\ell m}$, FOR WHICH THERE MUST BE AN INITIAL GUESS. ONCE $\partial \ln P/\partial U_{\ell m}$ IS COMPUTED FROM (399), $\mu_{\alpha\beta}$ CAN BE FOUND FROM (435). EVALUATION OF (434) AND (437) INVOLVES

$$\sum_{\alpha=0}^{N-1}\sum_{\beta=0}^{N-1} w^{(m)}_{\alpha\beta}\, W^{-j\alpha}\, W^{-k\beta}\,\mu_{\alpha\beta} \equiv Z^{(m)}_{jk} \tag{439}$$

SO THAT

$$\frac{d[\ln P]}{dS} = \frac{K}{N^2} \sum_{m=0}^{Q-1} \overset{(m)}{T} \sum_{j=0}^{N-1} \sum_{k=0}^{N-1} \left\{ \frac{\overset{(m)}{m}_{jk}}{\overset{(m)}{\beta}_{jk}} - 1 \right\} \overset{(m)}{Z}_{jk} \tag{440}$$

AND,

$$\frac{d^2[\ln P]}{dS^2} = -\frac{K^2}{N^4} \sum_{m=0}^{Q-1} \overset{(m)}{T}{}^2 \sum_{j=0}^{N-1} \sum_{k=0}^{N-1} \frac{\overset{(m)}{m}_{jk}}{\overset{(m)}{\beta}{}^2_{jk}} \overset{(m)}{Z}{}^2_{jk} \tag{441}$$

THOUGH (437) APPEARS TO REQUIRE AN N^4 SUMMATION, (439) AND (441) SHOW ONLY AN N^2 SUMMATION.

NOTE ALSO THAT (439) IS THE 2-D FT OF $\overset{(m)}{w}_{\alpha\beta}\, u_{\alpha\beta}$. $\overset{(m)}{w}_{\alpha\beta}$ HAS THE CONJUGATE SYMMETRY (405), AS DOES $u_{\alpha\beta}$ DUE TO (411). THEREFORE $\overset{(m)}{w}_{\alpha\beta}\, u_{\alpha\beta}$ HAS THE CONJUGATE SYMMETRY ALSO. THE FT OF A FUNCTION WITH SUCH SYMMETRY IS REAL [INDEED THIS IS HOW THE SYMMETRY WAS DEDUCED] SO THAT $\overset{(m)}{Z}_{jk}$ BY (439) MUST BE REAL. THUS $\overset{(m)}{Z}{}^2_{jk}$ IS NON-NEGATIVE IN (441). SINCE ALL THE OTHER FACTORS IN (441) ARE NON-NEGATIVE, THE SIGN OF (441) IS CONSTANT. AS A CONSEQUENCE, THE SENSE OF THE CONCAVITY OF THE FUNCTION $\ln P$ IS CONSTANT SO THAT AN EXTREMUM, IF FOUND, IS UNIQUE.

THE OVERALL STEPS OF THE HILL CLIMBING PROCESS ARE:

1. AFTER THE MEASUREMENTS $\overset{(m)}{m}_{jk}$ ARE MADE, FIND AN INITIAL U_{lm}. FOR EXAMPLE, TAKE FT OF EACH SUB-IMAGE AND WEIGHT AS FOR ADDITIVE NOISE [EQN. (63)]. THAT IS, IF $\overset{(m)}{\eta}_{lm}$ IS THE FT OF THE m-TH SUB-IMAGE

$$\overset{(m)}{\eta}_{lm} \equiv \sum_{j=0}^{N-1} \sum_{k=0}^{N-1} \overset{(m)}{m}_{jk}\, W^{jl}\, W^{km}, \tag{442}$$

FORM THE INITIAL GUESS

$$\hat{U}_{lm} = \frac{\sum_{m=0}^{Q-1} \overset{(m)}{w}{}^*_{lm}\, \overset{(m)}{\eta}_{lm}}{\sum_{m=0}^{Q-1} \left| \overset{(m)}{w}_{lm} \right|^2}. \tag{443}$$

Summary of Cosmic Image Reconstruction as of Dec. 15, 1982

Warren F. Davis

SUMMARY OF COSMIC IMAGE RECONSTRUCTION AS OF OCT. 15, 1982

WARREN F. DAVIS

LET

U_{lm} = DISCRETE FOURIER TRANSFORM OF THE SKY.

$\overset{(n)}{w}_{lm}$ = AUTOCORRELATION OF THE APERTURE IN THE n-TH ORIENTATION.

$\overset{(n)}{\beta}_{jk}$ = MEAN NUMBER OF PHOTONS ARRIVING AT POINT jk OF n-TH SUB-IMAGE IN TIME $\overset{(n)}{T}$.

$$\overset{(n)}{\beta}_{jk} = \overset{(n)}{\lambda}_{jk} \overset{(n)}{T} \tag{1}$$

$\overset{(n)}{\lambda}_{jk}$ = PROBABILITY PER UNIT TIME OF ARRIVAL OF PHOTONS AT POINT jk IN THE n-TH SUB-IMAGE.

$\overset{(n)}{T}$ = TIME OF OBSERVATION WITH THE APERTURE AT THE n-TH ORIENTATION.

N = SUB-IMAGE IMAGE SIZE IN PIXELS. I.E., IMAGE IS $N \times N$ PIXELS.

Q = NUMBER OF SUB-IMAGES

$W \equiv e^{-\frac{2\pi i}{N}}$

K = PROPORTIONALITY CONSTANT.

$\overset{(n)}{\beta}_{jk}$ [OR $\overset{(n)}{\lambda}_{jk}$] CAN BE REPRESENTED IN TERMS OF U_{lm} AND $\overset{(n)}{w}_{lm}$ AS

$$\overset{(n)}{\beta}_{jk} = \overset{(n)}{\lambda}_{jk} \overset{(n)}{T} = \frac{K\overset{(n)}{T}}{N^2} \sum_{l=0}^{N-1} \sum_{m=0}^{N-1} U_{lm} \overset{(n)}{w}_{lm} W^{-lj} W^{-mk} \tag{2}$$

WE ASSUME THAT THE PROBABILITY OF ARRIVAL OF $m_{jk}^{(m)}$ PHOTONS AT POINT jk IN THE m-TH SUB-IMAGE IN TIME $T^{(m)}$ IS POISSON DISTRIBUTED,

$$P_{jk}^{(m)} = e^{-\beta_{jk}^{(m)}} \frac{\left[\beta_{jk}^{(m)}\right]^{m_{jk}^{(m)}}}{\left[m_{jk}^{(m)}\right]!} , \qquad (3)$$

AND THAT PHOTONS AT DIFFERENT ARRIVAL LOCATIONS ARE INDEPENDENT. CONSEQUENTLY, IF WE KNOW $\lambda_{jk}^{(m)}$, WE CAN ASSIGN A PROBABILITY TO THE EVENT OF MEASURING THE SET OF COUNTS $m_{jk}^{(m)}$ COMPRISING AN ACTUAL SUB-IMAGE

$$P^{(m)} = \prod_{j=0}^{N-1} \prod_{k=0}^{N-1} P_{jk}^{(m)} . \qquad (4)$$

ASSUMING THAT SUB-IMAGE DATA ARE STATISTICALLY INDEPENDENT, WE CAN ASSIGN A PROBABILITY [GRAND JOINT PROBABILITY] TO THE EVENT OF HAVING MEASURED Q SETS OF COUNTS $m_{jk}^{(m)}$ OVER ALL APERTURE ORIENTATIONS.

$$P = \prod_{m=0}^{Q-1} P^{(m)} \qquad (5)$$

$\lambda_{jk}^{(m)}$, AND MORE FUNDAMENTALLY U_{lm} THROUGH (2), REPRESENTS THE ACTUAL SKY INTENSITY DISTRIBUTION. WE DO NOT KNOW U_{lm} [FROM WHICH $\lambda_{jk}^{(m)}$ CAN BE COMPUTED FROM (2)]. AND MUST BE CONTENT TO APPROXIMATE U_{lm} FROM OUR MEASUREMENTS $m_{jk}^{(m)}$. THE WAY WE HAVE CHOSEN TO DO THIS IS TO ASK WHAT U_{lm} MAXIMIZES THE P COMPUTED FROM THE SET OF MEASUREMENTS $m_{jk}^{(m)}$ ACTUALLY MADE. FOR REAL POSITIVE P THIS IS EQUIVALENT TO MAXIMIZING $\ln P$. FROM (4) AND (5) WE DEMAND

$$\ln P = \sum_{m=0}^{Q-1} \sum_{j=0}^{N-1} \sum_{k=0}^{N-1} \ln P_{jk}^{(m)} = \text{MAXIMUM} . \qquad (6)$$

FROM (3) WE FIND THAT

$$\ln \overset{(m)}{P}_{jk} = -\overset{(m)}{\beta}_{jk} + \overset{(m)}{n}_{jk} \ln \overset{(m)}{\beta}_{jk} - \ln\left[\left(\overset{(m)}{n}_{jk}\right)!\right] \quad . \tag{7}$$

THE CONDITION THAT $\ln P$ BE MAXIMIZED W.R.T. U_{rs} REQUIRES

$$\frac{\partial \ln P}{\partial U_{rs}} = 0 \quad [\text{AT MAX. } \ln P] \tag{8}$$

WHICH, BY (6), IN TURN REQUIRES THAT WE EVALUATE $\partial \ln \overset{(m)}{P}_{jk} / \partial U_{rs}$.
FROM (7) WE FIND THAT

$$\frac{\partial \ln \overset{(m)}{P}_{jk}}{\partial U_{rs}} = \left\{ \frac{\overset{(m)}{n}_{jk}}{\overset{(m)}{\beta}_{jk}} - 1 \right\} \frac{\partial \beta_{jk}}{\partial U_{rs}} \tag{9}$$

FROM (2) AND

$$\frac{\partial U_{lm}}{\partial U_{rs}} = \delta_{lr}\,\delta_{ms} \quad , \tag{10}$$

WE CONCLUDE THAT

$$\frac{\partial \overset{(m)}{\beta}_{jk}}{\partial U_{rs}} = \frac{K\overset{(m)}{T}}{N^2} \overset{(m)}{w}_{rs} W^{-rj} W^{-sk} \quad , \tag{11}$$

SO THAT

$$\frac{\partial \ln \overset{(m)}{P}_{jk}}{\partial U_{rs}} = \left\{ \frac{\overset{(m)}{n}_{jk}}{\overset{(m)}{\beta}_{jk}} - 1 \right\} \frac{K\overset{(m)}{T}}{N^2} \overset{(m)}{w}_{rs} W^{-rj} W^{-sk} \quad . \tag{12}$$

CONDITION (8), USING ALSO (6) AND (12), IS THEREFORE

$$\boxed{\sum_{m=0}^{Q-1} \overset{(m)}{T} \overset{(m)}{w}_{rs} \sum_{j=0}^{N-1} \sum_{k=0}^{N-1} \left\{ \frac{\overset{(m)}{n}_{jk}}{\overset{(m)}{\beta}_{jk}} - 1 \right\} W^{-rj} W^{-sk} = 0} \quad . \tag{13}$$

THIS IS THE CONDITION WHICH MUST BE SATISFIED BY $\overset{(m)}{U}_{\ell m}$, THROUGH (2), IN ORDER THAT A SET OF ACTUAL PHOTON COUNTS $\overset{(m)}{n}_{jk}$ HAVE THE MAXIMUM LIKELIHOOD. THAT IS, THE GUESS AT THE SKY PROVIDED BY THE $U_{\ell m}$ WHICH SATISFIES (13) IS THE ONE MOST LIKELY TO HAVE PRODUCED THE ACTUAL SET OF MEASUREMENTS $\overset{(m)}{n}_{jk}$. TO DISTINGUISH THAT GUESS FROM THE ACTUAL SKY TRANSFORM IN THE LIMIT OF NOISELESS SAMPLES, WE WILL USE

$$\hat{U}_{\ell m}$$

TO DENOTE THE [UNCERTAIN] SOLUTION OF (13) WHICH, WE HOPE, APPROXIMATES $U_{\ell m}$.

MORE GENERALLY, THE RESULTS SO FAR SHOW THAT

$$\frac{\partial \ln P}{\partial U_{rs}} = \frac{K}{N^2} \sum_{m=0}^{Q-1} \overset{(m)}{T} \overset{(m)}{w}_{rs} \sum_{j=0}^{N-1} \sum_{k=0}^{N-1} \left\{ \frac{\overset{(m)}{n}_{jk}}{\overset{(m)}{\beta}_{jk}} - 1 \right\} W^{-rj} W^{-sk} \tag{14}$$

WITH $\overset{(m)}{\beta}_{jk}$ GIVEN BY (2).

SINCE WE CAN NOT SOLVE FOR $\overset{(m)}{\beta}_{jk}$ [OR, EQUIVALENTLY, $U_{\ell m}$] IN (13) DIRECTLY, LET US FORMULATE THE SOLUTION OF (13) FOR $U_{\ell m}$ IN TERMS OF A HILL CLIMBING ON $\ln P$ IN WHICH $\ln P$ IS MAXIMIZED W.R.T. THE $U_{\ell m}$.

REGARD $\ln P$ AS A FUNCTION OF A COMPLEX N^2-DIMENSIONAL SPACE OF $U_{\ell m}$'S. THAT IS, A SET OF N^2 $U_{\ell m}$ VALUES DETERMINES A POINT IN THIS SPACE, AT WHICH POINT $\ln P$ TAKES ON A SPECIFIC VALUE. ASSUME THAT WE PICK A SET OF N^2 $U_{\ell m}$'S WHICH YIELD A "PHYSICAL" P. THAT IS, P IS REAL AND GREATER THAN ZERO, SO THAT $\ln P$ IS FINITE AND REAL. LET A PATH IN THIS SPACE BE PARAMETRIZED BY S AND LET US INVESTIGATE

$$\frac{d \ln P}{dS} = \frac{\partial \ln P}{\partial U_{\alpha\beta}} \frac{dU_{\alpha\beta}}{dS} = \frac{\partial \ln P}{\partial U_{\alpha\beta}} \mu_{\alpha\beta} \tag{15}$$

[EINSTEIN SUMMATION CONVENTION ON REPEATED INDICES].

ORIGINAL PAGE IS
OF POOR QUALITY

$u_{\alpha\beta} = dU_{\alpha\beta}/dS$ IS A "UNIT" VECTOR IN THE SENSE THAT

$$u_{\alpha\beta} u^*_{\alpha\beta} = \frac{dU_{\alpha\beta}}{dS} \frac{dU^*_{\alpha\beta}}{dS^*} = \frac{|dS|^2}{|dS|^2} = 1 \tag{16}$$

WHERE S IS SCALED SUCH THAT

$$dU_{\alpha\beta}\, dU^*_{\alpha\beta} = |dS|^2 \quad . \tag{17}$$

EQUATION (15) IS THE DIRECTIONAL DERIVATIVE OF $\ln P$ ALONG THE DIRECTION OF A UNIT VECTOR [DEFINED BY (16)] IN THE N^2 DIMENSIONAL SPACE OF U_{lm}'S. WE WISH TO CONSTRAIN (15) TO BE REAL. THAT IS, WE WISH TO FOLLOW PATHS IN THE SPACE SUCH THAT THE CHANGE IN $\ln P$, AND HENCE $\ln P$ IF IT IS INITIALLY REAL, IS REAL. THIS WILL BE SO IF WE PICK

$$u_{\alpha\beta} = -\left(\frac{\partial \ln P}{\partial U_{\alpha\beta}}\right)^* \Bigg/ \sqrt{\left(\frac{\partial \ln P}{\partial U_{\gamma\delta}}\right)\left(\frac{\partial \ln P}{\partial U_{\gamma\delta}}\right)^*} \quad . \tag{18}$$

CLEARLY, (18) SATISFIES (16). THE MINUS SIGN IS USED IN (18) TO GIVE THE "UP HILL" DIRECTION. ANY READJUSTMENTS OF THE U_{lm} ALONG $u_{\alpha\beta}$ WILL RESULT IN NEW VALUES OF $\ln P$ WHICH ARE AGAIN REAL.

IF WE MAKE A CUT IN THE SPACE ALONG $u_{\alpha\beta}$ GIVEN BY (18), AND ASSUME $\ln P$ TO BE LOCALLY QUADRATIC, WE CAN SHOW THAT AN ESTIMATE OF HOW FAR, AS MEASURED BY ΔS, WE MUST GO TO LOCATE THE PEAK OF THE QUADRATIC IS

$$\Delta S = -\frac{d[\ln P]/dS}{d^2[\ln P]/dS^2} \quad . \tag{19}$$

[SEE PAGES 150 AND 151 OF MAIN NOTES.] THE CORRESPONDING

CHANGES IN $U_{\alpha\beta}$ ARE

$$\Delta U_{\alpha\beta} = \mu_{\alpha\beta}\,\Delta S \quad . \tag{20}$$

OF COURSE, UNDER A FINITE STEP, $\ln P$ MAY NOT BE PURELY REAL AT $U_{\alpha\beta} + \Delta U_{\alpha\beta}$, BUT WILL BE NEARLY SO. ONE MAY NEED TO INCLUDE A "RENORMALIZATION" STEP IN THE COMPUTATIONS TO FIND THE POINT NEAR $U_{\alpha\beta} + \Delta U_{\alpha\beta}$ WHERE $\ln P$ IS AGAIN PURELY REAL.

FROM (14), (15), AND (18) WE CAN EVALUATE THE NUMERATOR OF (19). THE DENOMINATOR REQUIRES

$$\frac{d^2 \ln P}{dS^2} = \frac{d}{dS}\left[\frac{d \ln P}{dS}\right] = \frac{\partial}{\partial U_{\alpha\beta}}\left[\frac{\partial \ln P}{\partial U_{\gamma\delta}}\,\mu_{\gamma\delta}\right]\frac{dU_{\alpha\beta}}{dS} =$$

$$= \frac{\partial^2 \ln P}{\partial U_{\alpha\beta}\,\partial U_{\gamma\delta}}\,\mu_{\alpha\beta}\,\mu_{\gamma\delta} \quad . \tag{21}$$

THIS, IN TURN, REQUIRES $\partial^2 \ln P / \partial U_{\alpha\beta}\,\partial U_{\gamma\delta}$. FROM (14) WE FIND THAT

$$\frac{\partial^2 \ln P}{\partial U_{\alpha\beta}\,\partial U_{\gamma\delta}} = \frac{K}{N^2}\sum_{m=0}^{Q-1} \overset{(m)}{T}\,\overset{(m)}{w}_{\gamma\delta} \sum_{j=0}^{N-1}\sum_{k=0}^{N-1} \overset{(m)}{n}_{jk}\, W^{-\gamma j}\, W^{-\delta k}\, \frac{\partial \overset{(m)}{\beta}{}^{-1}_{jk}}{\partial U_{\alpha\beta}} \quad . \tag{22}$$

FROM (2) WE FIND THAT

$$\frac{\partial \overset{(m)}{\beta}{}^{-1}_{jk}}{\partial U_{\alpha\beta}} = -\frac{1}{\overset{(m)}{\beta}{}^{2}_{jk}}\,\frac{\partial \overset{(m)}{\beta}_{jk}}{\partial U_{\alpha\beta}} = -\frac{1}{\overset{(m)}{\beta}{}^{2}_{jk}}\,\frac{K\overset{(m)}{T}}{N^2}\,\overset{(m)}{w}_{\alpha\beta}\, W^{-\alpha j}\, W^{-\beta k} \tag{23}$$

SO THAT

$$\boxed{\frac{\partial^2 \ln P}{\partial U_{\alpha\beta}\,\partial U_{\gamma\delta}} = -\frac{K^2}{N^4}\sum_{m=0}^{Q-1} \overset{(m)}{T}{}^{2}\,\overset{(m)}{w}_{\alpha\beta}\,\overset{(m)}{w}_{\gamma\delta}\sum_{j=0}^{N-1}\sum_{k=0}^{N-1}\frac{\overset{(m)}{n}_{jk}}{\overset{(m)}{\beta}{}^{2}_{jk}}\, W^{-j(\alpha+\gamma)}\, W^{-k(\beta+\delta)}} \tag{24}$$

WHEN (14) AND (24) ARE USED TO EVALUATE (15) AND (21), RESPECTIVELY, ONE SEES THAT THE FUNCTION

$$\overset{(m)}{z}_{jk} = \sum_{\alpha=0}^{N-1} \sum_{\beta=0}^{N-1} \overset{(m)}{w}_{\alpha\beta}\, u_{\alpha\beta}\, W^{-\alpha j} W^{-\beta k} \tag{25}$$

OCCURS IN BOTH. IN TERMS OF $\overset{(m)}{z}_{jk}$, (15) AND (21) BECOME

$$\frac{d \ln P}{dS} = \frac{K}{N^2} \sum_{m=0}^{Q-1} \overset{(m)}{T} \sum_{j=0}^{N-1} \sum_{k=0}^{N-1} \left\{ \frac{\overset{(m)}{n}_{jk}}{\overset{(m)}{\beta}_{jk}} - 1 \right\} \overset{(m)}{z}_{jk} \tag{26}$$

AND,

$$\frac{d^2 \ln P}{dS^2} = -\frac{K^2}{N^4} \sum_{m=0}^{Q-1} \overset{(m)}{T}{}^2 \sum_{j=0}^{N-1} \sum_{k=0}^{N-1} \frac{\overset{(m)}{n}_{jk}}{\overset{(m)}{\beta}{}^2_{jk}} \overset{(m)}{z}{}^2_{jk} \tag{27}$$

IT CAN BE SHOWN [PAGE 155 OF MAIN NOTES] THAT

$$\overset{(m)}{w}_{\frac{N}{2}\pm p, \frac{N}{2}\pm q}\, u_{\frac{N}{2}\pm p, \frac{N}{2}\pm q} = \left[\overset{(m)}{w}_{\frac{N}{2}\mp p, \frac{N}{2}\mp q}\, u_{\frac{N}{2}\mp p, \frac{N}{2}\mp q} \right]^* . \tag{28}$$

AS A RESULT OF THIS SYMMETRY, $\overset{(m)}{z}_{jk}$ IS REAL AND $\overset{(m)}{z}{}^2_{jk}$ IS NON-NEGATIVE IN (27). IT IS ASSUMED THAT $\overset{(m)}{\beta}_{jk}$ IS REAL SO THAT $\overset{(m)}{\beta}{}^2_{jk}$ IS LIKEWISE NON-NEGATIVE. $\overset{(m)}{n}_{jk}$ ARE REAL, NON-NEGATIVE PHOTON COUNTS. CONSEQUENTLY, $d^2 \ln P / dS^2$ IS ALWAYS NEGATIVE. THEREFORE THERE IS BUT ONE UNIQUE SOLUTION TO (8) GIVING $\hat{U}_{\alpha\beta}$. EXCEPT UNDER PATHOLOGICAL CONDITIONS, SUCH AS ALL $\overset{(m)}{n}_{jk} = 0$, THERE ARE NO AMBIGUOUS INFLECTION POINTS IN THE SEARCH FOR $\hat{U}_{\alpha\beta}$.

WE NOW RECONSIDER THE POINT MADE EARLIER ABOUT "RENORMALIZATION" OF $U_{\alpha\beta} + \Delta U_{\alpha\beta}$ TO MAKE $\ln P$ PURE REAL UNDER A FINITE STEP SIZE. $u_{\alpha\beta}$ EXHIBITS THE SAME SYMMETRY AS (28) BECAUSE $\partial \ln P / \partial U_{\alpha\beta}$

DOES ALSO [SEE PAGE 147 OF MAIN NOTES] IF $\beta_{jk}^{(m)}$ IS REAL. IN CONSEQUENCE OF THIS, AND (20), $\Delta U_{\alpha\beta}$ EXHIBITS ALSO THE SYMMETRY OF (28). THIS MEANS IN TURN THAT $\beta_{jk}^{(m)}$ GIVEN BY (2) REMAINS REAL WHEN U_{lm} IS ADJUSTED BY ΔU_{lm}. SINCE THE $m_{jk}^{(m)}$ ARE REAL AND GREATER THAN OR EQUAL TO ZERO, (7) REVEALS THAT $\ln P_{jk}^{(m)}$ CAN HAVE AN IMAGINARY PART ONLY IF $\beta_{jk}^{(m)}$ IS NEGATIVE. SINCE NONE OF THE COUNTS $m_{jk}^{(m)}$ IS EVER NEGATIVE, THE SUMMATIONS IN (6) CAN NEVER RESULT IN CANCELLATION OF IMAGINARY PARTS OF TWO OR MORE $\ln P_{jk}^{(m)}$. THEREFORE, $\ln P$ WILL BE PURE REAL UNLESS AT LEAST ONE OF THE $\beta_{jk}^{(m)}$ IMPLIED BY (2) IS OR BECOMES NEGATIVE. THUS, $\ln P$ SHOULD REMAIN REAL UNDER ADJUSTMENT OF U_{lm} BY ΔU_{lm} UNLESS THE STEP SIZE IS TOO LARGE. IN THAT CASE $\ln P$ MUST HAVE GONE TO $-\infty$ SOMEWHERE IN THE STEP INTERVAL DUE TO THE BEHAVIOR OF THE TERM

$$m_{jk}^{(m)} \ln \beta_{jk}^{(m)}$$

IN (7) AS $\beta_{jk}^{(m)}$ GOES TO ZERO ON ITS WAY TO THE NEGATIVE VALUE WHICH GAVE RISE TO AN IMAGINARY COMPONENT OF $\ln P$. ONE CAN SEE FROM (14) THAT AS $\beta_{jk}^{(m)}$ GOES TO ZERO, $\partial \ln P / \partial U_{\lambda\lambda}$ BECOMES INFINITE. THERE IS THEREFORE A "WALL" WITHIN WHICH $\ln P$ REMAINS REAL AND WHICH SHOULD REPEL STRONGLY ANY TENDENCY TO GENERATE A STEP ACROSS.

THUS THE "RENORMALIZATION" MENTIONED EARLIER IS NOT A SUBTLE READJUSTMENT OF $U_{\alpha\beta}$. IF, AFTER RECOMPUTING $\ln P$ WITH THE NEW $U_{\alpha\beta}$, AN IMAGINARY COMPONENT IS FOUND, WE HAVE STEPPED OVER THE INFINITE WALL WHICH COULD ONLY HAPPEN IF THE STEP WAS IN THE WRONG DIRECTION OR GROSSLY TOO LARGE. IN FACT, (18) SHOULD HAVE PREVENTED THIS ALTOGETHER.

THIS POINTS OUT THE FURTHER CONCLUSION THAT SOLUTIONS OF (13) CORRESPOND TO "PHYSICAL" SKYS IN THAT NO $\beta_{jk}^{(m)}$ [OR $\Sigma_{jk}^{(m)}$ BY (1)] CAN BE NEGATIVE.

THE STEPS OF AN ITERATIVE HILL-CLIMBING SOLUTION OF (13) ARE GIVEN ON PAGES 155 AND 156 OF THE MAIN NOTES AND WILL NOT BE REPEATED HERE.

REMAINING CONSIDERATIONS

THE FINAL RESULT $\hat{U}_{lm}$ WILL EXHIBIT NON-UNIFORM VARIANCE ACROSS THE SPATIAL FREQUENCY PLANE. IT REMAINS TO

a) SHOW THAT $\hat{U}_{lm}$ CONVERGES IN THE ENSEMBLE SENSE TO THE MEAN VALUE U_{lm} [TRUE SKY TRANSFORM]

b) DERIVE AN EXPRESSION FOR THE ENSEMBLE VARIANCE OF $\hat{U}_{lm}$ OVER THE SPATIAL FREQUENCY PLANE

AND TO

c) SPECIFY A SUITABLE FILTERING ALGORITHM GIVEN KNOWLEDGE OF (b) BEFORE TRANSFORMING $\hat{U}_{lm}$ TO THE IMAGE DOMAIN. IT HAS ALREADY BEEN ARGUED THAT WEINER FILTERING MAY NOT BE APPROPRIATE AND A WEIGHTED RUNNING AVERAGE SUGGESTED INSTEAD [SEE PAGES 27 AND 28 OF THE MAIN NOTES]. MAXIMUM ENTROPY METHODS HAVE ALSO BEEN SUGGESTED [I.I. SHAPIRO, 10/8/82].

Appendix A

Relationship to Radio Interferometry

Warren F. Davis

APPENDIX A

RELATIONSHIP TO RADIO INTERFEROMETRY

RECIPROCITY

THE DEVELOPMENT SO FAR HAS BEEN IN TERMS OF IMAGES IN THE IMAGE PLANE. THE CENTRAL RELATIONSHIP (19)

$$I(\vec{k}') = \iint_{-\infty}^{\infty} dk_x\, dk_z \left|\mu(\vec{k})\right|^2 \left|A\left[(k_x'-k_x),(k_z'-k_z)\right]\right|^2 \qquad (A.1)$$

TELLS US THAT IF THE SOURCE $\mu(\vec{k})$ IS DISPLACED, THE IMAGE $I(\vec{k}')$ WILL BE DISPLACED CORRESPONDINGLY. IN THE IMAGE PLANE THE DIFFRACTION PATTERN IS "CARRIED ALONG WITH THE IMAGE". IN RADIO ASTRONOMY ONE THINKS OF A FIXED, DIFFRACTION-LIMITED BEAM PROJECTED ONTO THE SKY THROUGH WHICH THE OBSERVED OBJECT MAY MOVE. THE OBJECT DOES NOT DRAG ALONG ITS OWN DIFFRACTION PATTERN BUT RATHER MOVES THROUGH IT. HOW ARE THESE TWO INTERPRETATIONS RECONCILED?

IN RADIOASTRONOMY $\vec{k}'$ TAKES ON A FIXED VALUE DETERMINED BY THE GEOMETRY; IT IS NOT A VARIABLE AS IN THE CASE OF IMAGING. IF THE SKY REPRESENTED BY $\mu(\vec{k})$ IS DISPLACED BY

$$\vec{k} \rightarrow \vec{k}+\Delta\vec{k}$$

THEN

$$\iint_{-\infty}^{\infty} dk_x\, dk_z \left|\mu(\vec{k}+\Delta\vec{k})\right|^2 \left|A\left[(k_x'-k_x),(k_z'-k_z)\right]\right|^2 =$$

$$= \iint_{-\infty}^{\infty} dk_x\, dk_z \left|\mu(\vec{k})\right|^2 \left|A\left[(k_x'-(k_x-\Delta k_x)),(k_z'-(k_z-\Delta k_z))\right]\right|^2 =$$

$$= I(\vec{k}'+\Delta\vec{k}) \qquad (A.2)$$

THEREFORE, LETTING THE SKY MOVE WITH $\vec{k}'$ FIXED [RELATIVE TO THE RADIOTELESCOPE] GENERATES A VARIABLE OUTPUT WHICH IS EQUIVALENT

TO SAMPLING THE IMAGE OF A FIXED SKY AT A POINT DISPLACED IN THE IMAGE PLANE. IN EFFECT THE POINT DIFFRACTION PATTERN OF THE INSTRUMENT HAS BEEN PROJECTED ONTO THE SKY.

EQUIVALENCE OF MULTIPLE APERTURES

MULTIPLE APERTURES [RADIO TELESCOPES] ARE EMPLOYED IN RADIO ASTRONOMY. WHEN DATA ARE COMBINED FROM SUCH MULTIPLE APERTURES IN THE WAY CUSTOMARY IN RADIO ASTRONOMY, IS THE RESULT REALLY EQUIVALENT TO OUR VIEW OF IMAGING THROUGH MULTIPLE APERTURES?

TAKE THE IMAGING VIEW FIRST. LET THE APERTURE $a(x,z)$ CONSIST OF TWO COMPONENT APERTURES $a_m(x,z)$ AND $a_\ell(x,z)$. EQUATION (A.1) REQUIRES THE FT OF

$$a(x,z) = a_m(x,z) + a_\ell(x,z) \tag{A.3}$$

DEFINED FROM (9) TO BE

$$A(\vec{k}) = \frac{1}{(2\pi)^2}\iint_{-\infty}^{\infty} d^2\vec{r}\; a(\vec{r})\, e^{-i\vec{k}\cdot\vec{r}} \quad . \tag{A.4}$$

$\vec{k}$ AND $\vec{r}$ ARE CONFINED TO THE x,z-PLANE IN (A.4). BY THE LINEARITY OF (A.4), $A(\vec{k})$ WILL BE THE SUM OF THE TRANSFORMS OF a_m AND a_ℓ. LET a_m AND a_ℓ BE IDENTICAL EXCEPT THAT a_ℓ IS DISPLACED IN THE x,z-PLANE FROM a_m BY $\vec{b}$. THAT IS,

$$a_\ell(x,z) \equiv a_\ell(\vec{r}) = a_m(\vec{r}-\vec{b}) \quad . \tag{A.5}$$

THUS,

$$A_\ell(\vec{k}) = \frac{1}{(2\pi)^2}\iint_{-\infty}^{\infty} d^2\vec{r}\; a_m(\vec{r}-\vec{b})\, e^{-i\vec{k}\cdot\vec{r}} =$$

$$= \frac{1}{(2\pi)^2}\iint_{-\infty}^{\infty} d^2\vec{r}\; a_m(\vec{r})\, e^{-i\vec{k}\cdot(\vec{r}+\vec{b})}$$

OR,

$$A_l(\vec{k}) = e^{-i\vec{k}\cdot\vec{b}} A_m(\vec{k}) \tag{A.6}$$

SO THAT

$$A(\vec{k}) = A_m(\vec{k})\left[1 + e^{-i\vec{k}\cdot\vec{b}}\right] \quad . \tag{A.7}$$

TO EVALUATE (A.1) WE REQUIRE

$$|A(\vec{k})|^2 = |A_m(\vec{k})|^2 \left(1 + e^{-i\vec{k}\cdot\vec{b}}\right)\left(1 + e^{+i\vec{k}\cdot\vec{b}}\right) =$$

$$= 2|A_m(\vec{k})|^2 \left(1 + \cos(\vec{k}\cdot\vec{b})\right) ,$$

SO THAT $I(\vec{k}')$ BECOMES FOR TWO IDENTICAL SUB-APERTURES a_m SEPARATED IN THE x,z-PLANE BY $\vec{b}$,

$$\boxed{I(\vec{k}') = 2\iint_{-\infty}^{\infty} dk_x\, dk_z\, |u(\vec{k})|^2 \left|A_m(\vec{k}'-\vec{k})\right|^2 \left[1 + \cos((\vec{k}'-\vec{k})\cdot\vec{b})\right]} \tag{A.8}$$

WHERE IT IS TO BE UNDERSTOOD THAT A_m IS A FUNCTION ONLY OF THE x AND z COMPONENTS OF $\vec{k}$.

IS THIS RESULT REALLY EQUIVALENT TO THAT WHICH IS PRODUCED BY AN INTERFEROMETER IN RADIO ASTRONOMY? TO GET A HANDLE ON THIS WE NEED TO GO BACK TO THE EXPRESSION FOR THE INSTANTANEOUS OUTPUT [COMPLEX] OF A SINGLE APERTURE (11),

$$f(\vec{k}') = \iint_{-\infty}^{\infty} d^2\vec{k}\, u(\vec{k})\, \hat{e}(\vec{k})\, e^{-i\left[\omega t + \gamma(\vec{k},t)\right]} A(\vec{k}'-\vec{k}) \tag{A.9}$$

SEE THE EARLIER DISCUSSION FOR DEFINITION OF SYMBOLS.

CONSIDER TWO SUB-APERTURES AS BEFORE. LET EACH BE ALIGNED SO THAT $\vec{k}'$ IS THE SAME FOR EACH. FURTHER, LET THE SUM OF THE

TWO INSTANTANEOUS SUB-APERTURE OUTPUTS BE FORMED WITH AN ARBITRARY PHASE φ APPLIED TO ONE OF THEM. THAT IS, WE FORM

$$\iint_{-\infty}^{\infty} d^2\vec{k}\, \mu(\vec{k})\, \hat{e}(\vec{k})\, e^{-i[\omega t+\gamma(\vec{k},t)]} A_m(\vec{k}'-\vec{k}) + \tag{A.10}$$

$$+\, e^{-i\varphi}\iint_{-\infty}^{\infty} d^2\vec{k}''\, \mu(\vec{k}'')\, \hat{e}(\vec{k}'')\, e^{-i[\omega t+\gamma(\vec{k}'',t)]} A_\ell(\vec{k}'-\vec{k}'') = g(\vec{k}')$$

THE INTERFEROMETER OUTPUT IS PROPORTIONAL TO $|g(\vec{k}')|^2$. WHEN WE FORM THIS FROM (A.10) WE GET FOR THE DIRECT TERMS

$$\iint_{-\infty}^{\infty} d^2\vec{k}\, |\mu(\vec{k})|^2 |A_m(\vec{k}'-\vec{k})|^2 + \iint_{-\infty}^{\infty} d^2\vec{k}\, |\mu(\vec{k})|^2 |A_\ell(\vec{k}'-\vec{k})|^2 \tag{A.11}$$

AFTER TIME-AVERAGING. THE CROSS TERMS BEFORE TIME-AVERAGING ARE

$$e^{+i\varphi}\iint_{-\infty}^{\infty} d^2\vec{k}'' \iint_{-\infty}^{\infty} d^2\vec{k}\, \mu(\vec{k})\mu^*(\vec{k}'')\, [\hat{e}(\vec{k})\cdot\hat{e}(\vec{k}'')]\, e^{-i[\gamma(\vec{k},t)-\gamma(\vec{k}'',t)]} \times$$

$$\times A_m(\vec{k}'-\vec{k})\, A_\ell^*(\vec{k}'-\vec{k}'') + \text{c.c.} \tag{A.12}$$

WHERE C.C. MEANS "COMPLEX CONJUGATE". WHEN WE TIME-AVERAGE, THE EXPONENTIAL INVOLVING t BEHAVES LIKE A DIRAC DELTA FUNCTION IN $\vec{k}-\vec{k}''$. THEREFORE, AFTER TIME-AVERAGING AND INTEGRATION ON $\vec{k}''$, (A.12) GOES OVER TO

$$e^{+i\varphi}\iint_{-\infty}^{\infty} d^2\vec{k}\, |\mu(\vec{k})|^2 A_m(\vec{k}'-\vec{k}) A_\ell^*(\vec{k}'-\vec{k}) + \text{c.c.} \tag{A.13}$$

WHEN ALL THE RESULTS ARE COMBINED WE GET

$$I(\vec{k}') = \iint_{-\infty}^{\infty} d^2\vec{k}\, |\mu(\vec{k})|^2 \Big\{ |A_m(\vec{k}'-\vec{k})|^2 + |A_\ell(\vec{k}'-\vec{k})|^2 + e^{+i\varphi} A_m(\vec{k}'-\vec{k}) A_\ell^*(\vec{k}'-\vec{k}) + e^{-i\varphi} A_m^*(\vec{k}'-\vec{k}) A_\ell(\vec{k}'-\vec{k}) \Big\} \quad (A.14)$$

NOW ASSUME THAT a_m AND a_ℓ ARE IDENTICAL EXCEPT THAT a_ℓ IS DISPLACED FROM a_m BY $\vec{b}$ SO THAT (A.6) APPLIES. THE TERMS IN { } ABOVE BECOME

$$|A_m(\vec{k}'-\vec{k})|^2 + |A_m(\vec{k}'-\vec{k})|^2 + e^{i(\varphi+(\vec{k}'-\vec{k})\cdot\vec{b})} |A_m(\vec{k}'-\vec{k})|^2 + e^{-i(\varphi+(\vec{k}'-\vec{k})\cdot\vec{b})} |A_m(\vec{k}'-\vec{k})|^2 =$$

$$2\,|A_m(\vec{k}'-\vec{k})|^2 \left[1 + \cos[\varphi + (\vec{k}'-\vec{k})\cdot\vec{b}]\right] \quad (A.15)$$

SO THAT

$$\boxed{I(\vec{k}') = 2\iint_{-\infty}^{\infty} d^2\vec{k}\, |\mu(\vec{k})|^2 |A_m(\vec{k}'-\vec{k})|^2 \{1 + \cos[\varphi + (\vec{k}'-\vec{k})\cdot\vec{b}]\}} \quad (A.16)$$

COMPARE THIS WITH (A.8) FOR THE IMAGING CASE. THE RESULTS ARE IDENTICAL FOR $\varphi = 0$ OR MULTIPLES OF 2π.

SPECIAL CASE FOR RADIOINTERFEROMETRY

$\vec{k}'$ IS FIXED FOR RADIO ASTRONOMY. SUPPOSE $\mu(\vec{k})$ IS NON-ZERO FOR A LOCALIZED SET OF DIRECTIONS CENTERED ON $\vec{k}^0$. SUPPOSE THAT $|A_m(\vec{k})|^2$ IS MAXIMUM AT $\vec{k}=0$ AND IS VERY BROAD. THE SITUATION IS AS ILLUSTRATED BELOW,

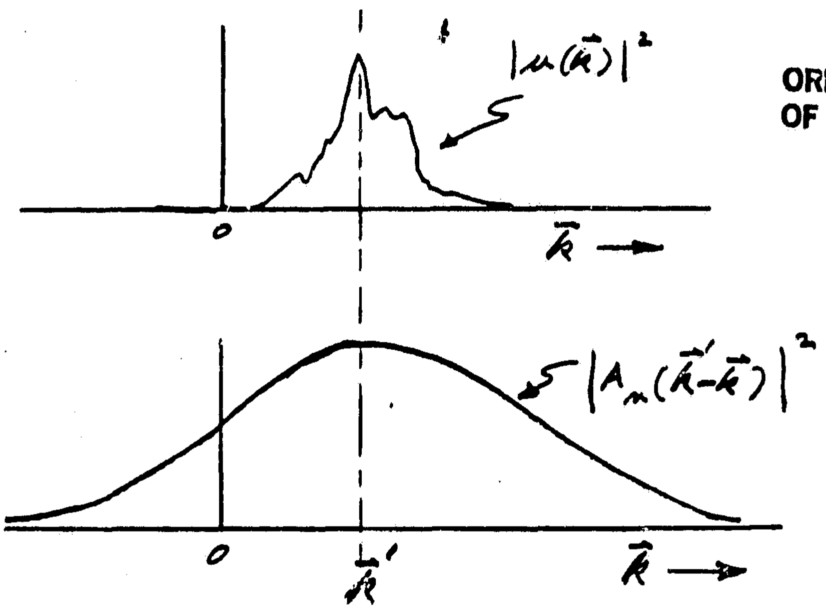

$|A_m(\vec{k}'-\vec{k})|^2$ IS THE ENVELOPE OF A SINGLE SUB-APERTURE DISPLACED TO $\vec{k}'$ AS ILLUSTRATED. THAT IS, THE TELESCOPE IS "POINTED" ALONG $\vec{k}'$.

IF $|u(\vec{k})|^2$ IS SUFFICIENTLY NARROW, $|A_m(\vec{k}'-\vec{k})|^2$ IS ESSENTIALLY CONSTANT OVER $|u(\vec{k})|^2$ AND CAN BE TAKEN OUT OF THE INTEGRAL (A.16).

$$I(\vec{k}') \simeq 2\left|A_m(\vec{k}=0)\right|^2 \iint_{-\infty}^{\infty} d^2\vec{k}\, |u(\vec{k})|^2 \left\{1+\cos\left[\varphi+(\vec{k}'-\vec{k})\cdot\vec{b}\right]\right\} =$$

$$= 2\left|A_m(\vec{k}=0)\right|^2 \iint_{-\infty}^{\infty} d^2\vec{k}\, |u(\vec{k})|^2 + \qquad \text{(A.17)}$$

$$+\, 2\left|A_m(\vec{k}=0)\right|^2 \iint_{-\infty}^{\infty} d^2\vec{k}\, |u(\vec{k})|^2 \cos\left[\varphi+(\vec{k}'-\vec{k})\cdot\vec{b}\right]$$

THE FIRST TERM IS A CONSTANT INDEPENDENT OF φ AND $\vec{b}$. THE SECOND TERM MAY BE WRITTEN

$$2\left|A_m(\vec{0})\right|^2 Re \left\{ \iint_{-\infty}^{\infty} d^2\vec{k}\, |u(\vec{k})|^2 e^{+i[\varphi+\vec{k}'\cdot\vec{b}]} e^{-i\vec{k}\cdot\vec{b}} \right\} =$$

$$= 2\left|A_m(\vec{0})\right|^2 \mathrm{Re}\left\{ e^{+i[\varphi+\vec{k}'\cdot\vec{b}]}\, U\!\left(\frac{\vec{b}}{2\pi}\right)\right\} \qquad (A.18)$$

WHERE U, THE FT OF THE SKY, IS DEFINED BY (23).

THE EFFECT OF $\exp[i(\varphi+\vec{k}'\cdot\vec{b})]$ IS TO ROTATE $U(\vec{b}/2\pi)$. BY VARYING φ, OR LETTING $\vec{k}'\cdot\vec{b}$ VARY, THE MAGNITUDE OF $U(\vec{b}/2\pi)$ CAN BE DEDUCED FROM THE PEAK-TO-PEAK EXCURSION OF $I(\vec{k}')$. IF $\vec{k}'\cdot\vec{b}$ IS KNOWN FROM THE GEOMETRY, OR AT LEAST HELD CONSTANT, AND φ IS SET TO SOME REFERENCE VALUE, SAY, 0, THE PHASE OF $U(\vec{b}/2\pi)$ CAN BE INFERRED. IN THIS WAY <u>ONE POINT</u> IN THE $\vec{\nu}$-PLANE, $\vec{\nu}=\vec{b}/2\pi$, OF THE FT OF THE IMAGE CAN BE ESTIMATED. WHEN $U(\vec{b}/2\pi)$ HAS BEEN ESTIMATED FOR MANY DIFFERENT $\vec{b}$, THE SKY FUNCTION $|\mu(\vec{k})|^2$ CAN BE ESTIMATED FROM THE INVERSE FT OF $U(\vec{b}/2\pi)$.

STRIP INTEGRATION

RADIOINTERFEROMETRY AND THE CAT ALGORITHM BOTH EMPLOY WHAT BRACEWELL REFERS TO AS STRIP INTEGRATION. THE MORE FAMILIAR CONCEPT OF LINE INTEGRATION CONSISTS IN INTEGRATING A FUNCTION ALONG A LINE. CONSIDER A FUNCTION $f(x,y)$.

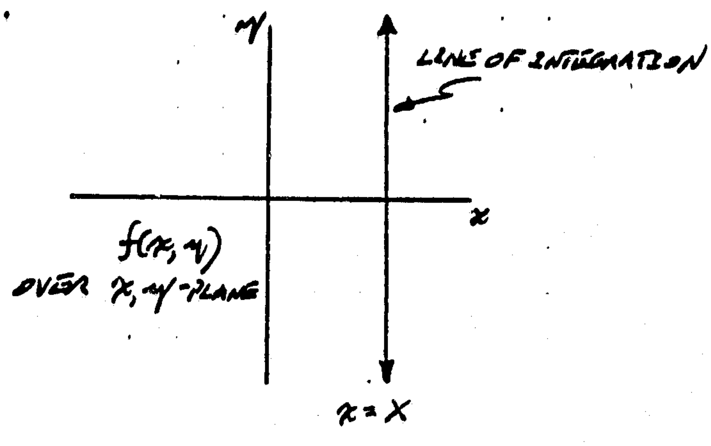

THE LINE INTEGRAL OF $f(x,y)$ ALONG A LINE $x = X$

$$g(X) = \int_{-\infty}^{\infty} f(X,y)\, dy$$

IS A ONE-DIMENSIONAL FUNCTION OF THE POSITION OF THE LINE X. THE DIMENSIONALITY OF THE ORIGINAL FUNCTION $f(x,y)$ HAS BEEN COLLAPSED FROM TWO TO ONE DIMENSION.

STRIP INTEGRATION CONSISTS IN A SIMILAR PROCESS WHEREIN THE INTEGRATION IS CARRIED OUT WITHIN A STRIP, RATHER THAN ALONG A LINE.

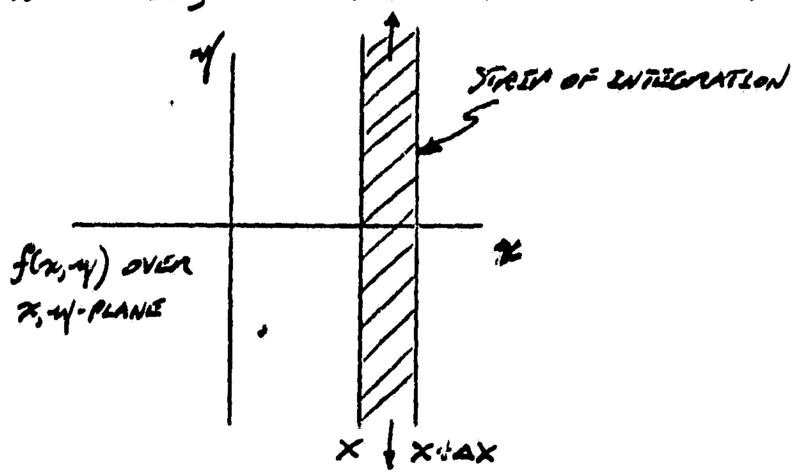

$$g(x) = \int_{x}^{x+\Delta x} dx \int_{-\infty}^{\infty} dy\, f(x,y)$$

ASSUMING Δx IS REGARDED AS A CONSTANT, $f(x,y)$ IS AGAIN COLLAPSED FROM A TWO TO A ONE-DIMENSIONAL FUNCTION BY THE INTEGRATION.

BOTH LINE AND STRIP INTEGRATION EXHIBIT THE PROPERTY THAT "FEATURES" OF $f(x,y)$ CAN BE DISPLACED ALONG y WITHOUT ALTERING THE RESULT. THERE IS "NO RESOLUTION" ALONG y.

IF THE CAT SCAN BEAM IS REGARDED AS VERY NARROW AND FREE FROM SCATTER, THE CAT DETECTOR MEASURES A LINE INTEGRAL THROUGH THE SUBJECT. IF THE BEAM IS FINITE IN WIDTH, THE DETECTOR MEASURES A STRIP INTEGRAL.

IN THE RADIOINTERFEROMETRY CASE WE NEED TO CONSIDER

$$U\left(\frac{\vec{b}}{2\pi}\right) = \iint_{-\infty}^{\infty} d^2\vec{k}\, \left|u(\vec{k})\right|^2 e^{-i\vec{k}\cdot\vec{b}} \qquad \text{(A.9)}$$

FROM (A.18). GIVEN CONSTANT $\vec{b} = \hat{e}_x b_x + \hat{e}_z b_z$, $\vec{k}\cdot\vec{b}$ WILL BE CONSTANT FOR ALL $\vec{k}$ WHICH HAVE THE SAME PROJECTION ONTO $\vec{b}$. THAT IS, $\exp(-i\vec{k}\cdot\vec{b})$ IS CONSTANT ALONG LINES NORMAL TO $\vec{b}$. IT IS ALSO PERIODIC IN ITS ARGUMENT. SCHEMATICALLY (A.19) IS AS SHOWN BELOW.

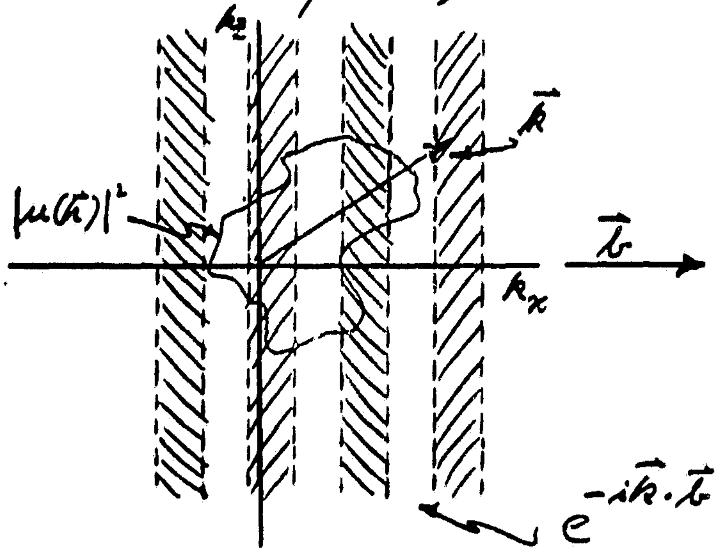

$\vec{b}$ IS SHOWN ALONG k_x, BUT ITS ORIENTATION IS ARBITRARY AND THE HATCHED STRIPS WOULD ROTATE ACCORDINGLY SO AS TO REMAIN NORMAL TO $\vec{b}$. THE SCHEMATIC NATURE OF THE DIAGRAM IS TO BE EMPHASIZED. IT IS NOT POSSIBLE TO SHOW THE COMPLEX NATURE OF THE OVERLYING EXPONENTIAL. NEVERTHELESS, THE INDEPENDENCE NORMAL TO $\vec{b}$ CAUSES (A.19) TO BE A GENERALIZATION OF THE CONCEPT OF A STRIP INTEGRATION GIVEN ABOVE.

AGAIN, AS ABOVE, $|\mu(\vec{k})|^2$ CAN BE DISPLACED NORMAL TO $\vec{b}$ WITHOUT CHANGING THE VALUE OF (A.19). GIVEN THE ORIENTATION OF $\vec{b}$, (A.19) IS A ONE-DIMENSIONAL FUNCTION OF $|\vec{b}|$, IN ANALOGY WITH THE REMARKS ON LINE AND STRIP INTEGRATION ABOVE. IF $\vec{b}$ IS FIXED FOR THE DURATION OF THE OBSERVATION, THEN ONLY ONE POINT IN THE $\vec{\nu}$-PLANE OVER WHICH $U(\vec{\nu})$ IS DEFINED CAN BE DETERMINED, NAMELY AT $\vec{\nu} = \vec{b}/2\pi$. [THE CONJUGATE POINT CORRESPONDING TO $-\vec{b}$ IS ALSO DETERMINED.]

ESSENTIAL DIFFERENCES

THE MOST OBVIOUS AND SIGNIFICANT WAY IN WHICH THE IMAGE RECONSTRUCTION ALGORITHM DERIVED HERE DIFFERS FROM BOTH THE CAT AND RADIO-INTERFEROMETRY ALGORITHMS IS IN THE NON-COLLAPSE OF THE DIMENSIONALITY OF THE PROBLEM. BOTH THE CAT AND THE RADIO ALGORITHMS DETERMINE $U(\vec{\nu})$ AT A POINT OR ALONG A LINE OF POINTS. THIS IS

BECAUSE THEY BOTH USE LINE OR STRIP INTEGRATION. THAT IS, THEY BOTH THROW AWAY OR, MORE PRECISELY, COMPRESS INFORMATION ALONG ONE DIMENSION. THIS IS NOT THE CASE WITH THE NEW ALGORITHM. THE NEW ALGORITH INHERENTLY GIVES INFORMATION ABOUT AREAS, RATHER THAN POINTS OR LINES, IN THE PLANE OF THE FT OF THE IMAGE. THIS MEANS IN TURN THAT SPECIAL CONSIDERATION MUST BE GIVEN TO WEIGHTING IMAGE TRANSFORMS WHEN SUMMED IN $\vec{V}$-SPACE BECAUSE OF OVERLAPPING AREAS. ALL THREE ALGORITHMS ARE ALIKE IN THAT THEY ATTEMPT TO BUILD UP THE FOURIER PLANE OF THE IMAGE. BUT, THE CAT AND RADIO CASES DO SO IN AN INHERENTLY ONE-DIMENSIONAL WAY, WHEREAS THE NEW ALGORITHM DOES SO IN A FULLY TWO-DIMENSIONAL MANNER. ONLY WHEN THE APERTURE OF THE TELESCOPE ITSELF BECOMES ONE DIMENSIONAL [A LINE] DOES THE NEW ALGORITHM BECOME DESCRIBABLE IN TERMS OF STRIP INTEGRALS IN WHICH ONE DIMENSION IS SUPPRESSED.